

THÈSE DE DOCTORAT EN COTUTELLE

**DÉVELOPPEMENT ET CARACTÉRISATION DE MATÉRIAUX ANTIMICROBIENS À BASE
DE CHITOSANE ET DE NANOPARTICULES D'ARGENT POUR DES APPLICATIONS DE
REVÊTEMENT SUR DES DISPOSITIFS MÉDICAUX**

**DEVELOPMENT AND CHARACTERIZATION OF CHITOSAN AND SILVER BASED
NANOPARTICLES ANTIMICROBIAL MATERIALS FOR COATING APPLICATIONS ON MEDICAL
DEVICES**

**THÈSE PRÉSENTÉE À
L'UNIVERSITÉ DU QUÉBEC À TROIS-RIVIÈRES
ET
L'UNIVERSIDADE FEDERAL DO PARANÁ
COMME EXIGENCE PARTIELLE DU
DOCTORAT EN DOCTORAT EN SCIENCES DE L'ÉNERGIE ET DES MATÉRIAUX**

**PAR
MARCOS ANTONIO POLINARSKI**

FÉVRIER 2025

Université du Québec à Trois-Rivières
Service de la bibliothèque

Avertissement

L'auteur de ce mémoire, de cette thèse ou de cet essai a autorisé l'Université du Québec à Trois-Rivières à diffuser, à des fins non lucratives, une copie de son mémoire, de sa thèse ou de son essai.

Cette diffusion n'entraîne pas une renonciation de la part de l'auteur à ses droits de propriété intellectuelle, incluant le droit d'auteur, sur ce mémoire, cette thèse ou cet essai. Notamment, la reproduction ou la publication de la totalité ou d'une partie importante de ce mémoire, de cette thèse et de son essai requiert son autorisation.

UNIVERSITÉ DU QUÉBEC À TROIS-RIVIÈRES
DOCTORAT EN SCIENCES DE L'ÉNERGIE ET DES MATÉRIAUX (PH. D.)

Direction de recherche:

Phuong Nguyen-Tri

Prénom et nom	Directeur de recherche
---------------	------------------------

Helton José Alves

Prénom et nom	Directeur de recherche
---------------	------------------------

Juliana Bernardi Wenzel

Prénom et nom	Co-Directrice de recherche
---------------	----------------------------

Jury d'évaluation:

Phuong Nguyen-Tri

Directeur de recherche

Prénom et nom	Fonction du membre de jury
---------------	----------------------------

Juliana Bernardi Wenzel

Co-Directrice de recherche

Prénom et nom	Fonction du membre de jury
---------------	----------------------------

Alireza Saidi

Président de jury

Prénom et nom	Fonction du membre de jury
---------------	----------------------------

Gláucia Medeiros Burin

Évaluateur externe

Prénom et nom	Fonction du membre de jury
---------------	----------------------------

Douglas Cardoso Dragunski

Évaluateur externe

Prénom et nom	Fonction du membre de jury
---------------	----------------------------

To my parents, Ervino and Lurdes Polinarski,
whose hard work in the fields made it
possible for me to achieve the education they
never had the opportunity to receive.

Aos meus pais, Ervino e Lurdes Polinarski,
cujo trabalho árduo no campo tornou possível
que eu alcançasse a educação que eles
próprios não tiveram a oportunidade de
receber.

À mes parents, Ervino et Lurdes Polinarski,
dont leur travail acharné dans les terres
agricoles m'a permis d'accéder à une
éducation que eux-mêmes n'ont jamais eu
l'opportunité de recevoir.

ACKNOWLEDGMENTS

My profound gratitude goes to God and Our Lady of Aparecida, who, in my deepest moments, guided me through faith.

I extend my deepest appreciation to my thesis supervisors, Prof. Dr. Helton José Alves and Prof. Dr. Phuong Nguyen-Tri, and my co-supervisor, Prof. Dr. Juliana Bernardi-Wenzel, for their constant supervision, guidance, and hard work in making this project possible. Throughout this PhD journey, I encountered many challenges in my personal life, and they always demonstrated understanding, humanity, and unwavering support. To them, I express my sincerest gratitude.

I am thankful to the Programa de Pós-Graduação em Engenharia e Tecnologia Ambiental (PPGETA), the Universidade Federal do Paraná (UFPR), the Programme de Doctorat en Sciences de l'Énergie et des Matériaux, and the Université du Québec à Trois-Rivières (UQTR) for making this cotutelle agreement a reality.

Special thanks to the Araucária Foundation, the State Secretariat of Science, Technology and Higher Education of Paraná, and BIOPARK Educação for their financial support through the Brazilian scholarship. I also acknowledge the Université du Québec à Trois-Rivières and Prof. Phuong Nguyen-Tri for their financial assistance through the Canadian scholarship.

I am grateful to Innofibre (Quebec, Canada) and Prof. Simon Barnabé for granting access to their laboratory facilities. I also thank my colleagues Lazaro José Gasparrini, Manuela Nepomuceno Ladeira, Safa Ladhari, Cédrik Boisvert, Nhu-Nang Vu, Rayssa Cristina Souza, and Kéziah Milette for their help in performing analyses and characterizations.

My heartfelt thanks to all my colleagues at LABMATER and the Nguyen-Tri Lab, especially my friends Bruna Machado, Lígia Oliveira, Bárbara Bulhões, Claire Stuppa, and Safa Ladhari, for the shared moments and for making this journey memorable.

I also express my gratitude to my lifelong friends: Gabriel Laivière, Caroline Tanaka, Jakeline Rojas, Bruna Machado, Mara Carnieli, Andressa Neves, Vinícius Leal, Vicky Alain, Sabrina Grenier, and Lauriane Thibault. To all my other friends—although I cannot name everyone here—please know that each of you holds a special place in my heart. Your support, kindness, and encouragement have been invaluable throughout this journey.

Finally, I owe my deepest gratitude to my parents, Lurdes and Ervino Polinarski, as well as my sisters, nephews, and nieces, for their endless love, prayers, and sacrifices.

ABSTRACT

Medical devices, such as catheters, probes, and wound dressings, are particularly vulnerable to microbial contamination and biofilm formation, especially by multidrug-resistant bacteria. In this way, nanomaterials with antimicrobial activity hold a promising solution to overcome this problem. Among these nanomaterials, nanoparticles (NPs) derived from natural sources, such as chitosan (CS), and metal-based nanoparticles, such as silver (Ag), are gaining significant attention in nanomedicine. CS can offer great potential as coating and antimicrobial agent, while AgNPs possess antimicrobial effects against different pathogens. Together, these materials can result in a powerful nanocomposite suitable for antimicrobial coatings with enhanced antimicrobial properties due to the combination of the unique properties of both components. This project focused on the development of new antimicrobial materials based on CS-Ag NPs and composite with high antimicrobial properties to be applied as coating in medical devices and it was divided into three parts. The first part investigated the use of various reducing agents, including CS, combined with different AgNO_3 proportions in the synthesis of AgNPs. The second part presented a facile and practical approach to preparing potent antimicrobial coatings based on CS-Ag composites, by simply stirring a CS solution with different amounts of AgNO_3 . The third part presented a two-step synthesis of AgNPs using CS and nanochitosan (NCS) as reducing agents, with varying AgNO_3 concentrations. The results showed significant differences in nanoparticle morphology and antimicrobial activity based on the choice of reducing agent and the AgNO_3 concentration, revealing CS as the best choice due to its dual role as a reducing and stabilizing agent. The CS-Ag composite demonstrated excellent photocatalytic and antimicrobial activity against *E. coli*, especially in the presence of light, with a bacterial reduction rate ranging from 75% to 100%. Morphological characterizations revealed the presence of Ag rods formed AgNPs embedded into a CS film. Ag^+ ions were reduced to Ag^0 during the coating process due to the electron-rich oxygen atoms in the polar hydroxyl and ether groups in the CS. Both CS and NCS effectively reduced Ag^+ to Ag^0 , enabling the formation of small, spherical, and potentially semicrystalline AgNPs. Antimicrobial testing revealed that AgNPs synthesized with CS showed a larger inhibition zone against *S. aureus*, while no significant differences were observed among samples tested against *E. coli*. The use of CS and NCS appeared to influence the stabilization and size regulation of AgNPs, with no direct relation. Additionally, both CS and NCS based AgNP coatings demonstrated antibiofilm activity, suggesting their great potential as antimicrobial coatings for medical device surfaces. The findings of this study offer promising solutions to combat biofilm

formation, highlighting synthesized materials as potential alternatives for applications in the biomedical field.

Keywords: Nanotechnology; Nanocomposites; Biofilm Formation; Antimicrobial Materials; Biopolymers.

RÉSUMÉ

Les dispositifs médicaux, tels que les cathéters, les sondes et les pansements, sont particulièrement vulnérables à la contamination microbienne et à la formation de biofilms, notamment par des bactéries multirésistantes. Dans ce contexte, les nanomatériaux dotés d'une activité antimicrobienne représentent une solution prometteuse pour lutter contre ce problème. Parmi ces nanomatériaux, les nanoparticules (NPs) issues de sources naturelles, comme le chitosane (CS), et les nanoparticules métalliques, telles que celles à base d'argent (Ag), suscitent un intérêt croissant, particulièrement en nanomédecine. Le CS présente un fort potentiel pour la création de revêtements antimicrobiens, tandis que les AgNPs possèdent des propriétés antimicrobiennes efficaces contre divers pathogènes. Ensemble, ces matériaux peuvent former un nanocomposite doté de propriétés antimicrobiennes élevées, idéal pour des revêtements destinés aux dispositifs médicaux. Ce projet visait à développer de nouveaux matériaux antimicrobiens à base de NPs de CS-Ag et de composites aux propriétés antimicrobiennes améliorées, destinés à être appliqués comme revêtements sur des dispositifs médicaux. Il a été divisé en trois parties. La première partie a examiné l'utilisation de divers agents réducteurs, y compris la CS, combinés à différentes proportions de AgNO_3 pour la synthèse des AgNPs. La deuxième partie a proposé une méthode simple et pratique pour préparer des revêtements antimicrobiens efficaces à base de composites CS-Ag, en mélangeant simplement une solution de CS avec différentes quantités de AgNO_3 . La troisième partie a exploré une synthèse en deux étapes des AgNPs, utilisant la CS et la nanochitosane (NCS) comme agents réducteurs, avec des concentrations variables de AgNO_3 . Les résultats ont montré des différences significatives dans la morphologie des NPs et dans l'activité antimicrobienne en fonction du choix de l'agent réducteur et de la concentration de AgNO_3 . La CS s'est révélée être le meilleur choix en raison de son double rôle d'agent réducteur et stabilisant. Le composite CS-Ag a démontré une excellente activité photocatalytique et antimicrobienne contre *E. coli*, notamment en présence de lumière, avec un taux de réduction bactérienne allant de 75 % à 100 %. Les caractérisations morphologiques ont révélé la présence de structures en forme de tiges d'Ag formées par des AgNPs intégrées dans un film de CS. Les ions Ag^+ ont été réduits en Ag^0 durant le processus de revêtement, grâce aux atomes d'oxygène riches en électrons des groupes hydroxyles de la CS. La CS et la NCS ont toutes deux efficacement réduit Ag^+ en Ag^0 , favorisant la formation de petites AgNPs sphériques et potentiellement semi-cristallines. Les tests antimicrobiens ont révélé que les AgNPs synthétisées avec la CS présentaient une zone d'inhibition plus large contre *S. aureus*, tandis

qu'aucune différence significative n'a été observée entre les échantillons testés contre *E. coli*. L'utilisation de la CS et de la NCS semble influencer la stabilisation et la régulation de la taille des AgNPs, bien que sans relation directe. De plus, les revêtements d'AgNPs à base de CS et de NCS ont tous deux démontré une activité antibiofilm, ce qui souligne leur fort potentiel en tant que revêtements antimicrobiens pour les surfaces des dispositifs médicaux. Les résultats de cette étude offrent des solutions prometteuses pour combattre la formation de biofilms, positionnant les matériaux synthétisés comme des alternatives potentielles pour des applications dans le domaine biomédical.

Mots-clés: Nanotechnologie; Nanocomposites; Formation de Biofilm; Matériaux Antimicrobiens; Biopolymères.

RESUMO

Dispositivos médicos, como cateteres, sondas e curativos, são particularmente vulneráveis à contaminação microbiana e à formação de biofilmes, especialmente por bactérias multirresistentes. Neste sentido, nanomateriais com atividade antimicrobiana representam uma solução promissora para combater esse problema. Entre esses nanomateriais, as nanopartículas (NPs) derivadas de fontes naturais, como a quitosana (CS), e as nanopartículas à base de metais, como a prata (Ag), estão ganhando cada vez mais atenção, especialmente na nanomedicina. A CS oferece um grande potencial para a criação de revestimentos e atividade antimicrobiana, enquanto as AgNPs possuem efeitos antimicrobianos contra diferentes patógenos. Juntos, esses materiais podem resultar em um nanocompósito com potencial de uso como revestimentos com propriedades antimicrobianas elevadas devido à combinação das propriedades únicas de ambos os materiais. Este projeto teve como objetivo o desenvolvimento de novos materiais antimicrobianos a base de NPs de CS-Ag e compósitos com altas propriedades antimicrobianas para serem aplicados como revestimento em dispositivos médicos e foi dividido em três partes. A primeira parte investigou o uso de vários agentes redutores, incluindo CS, combinados com diferentes proporções de AgNO_3 na síntese de AgNPs. A segunda parte apresentou uma abordagem fácil e prática para preparar revestimentos antimicrobianos potentes baseados em compósitos de CS-Ag, simplesmente misturando uma solução de CS com diferentes quantidades de AgNO_3 . A terceira parte apresentou uma síntese AgNPs em duas etapas usando CS e nanoquitosana (NCS) como agentes redutores, com concentrações variáveis de AgNO_3 . Os resultados mostraram diferenças significativas na morfologia das NPs e na atividade antimicrobiana com base na escolha do agente redutor e na concentração de AgNO_3 , com destaque para a CS como a melhor escolha devido ao seu papel duplo como agente redutor e estabilizante. O composto CS-Ag demonstrou excelente atividade fotocatalítica e antimicrobiana contra *E. coli*, especialmente na presença de luz, com uma taxa de redução bacteriana variando de 75% a 100%. As caracterizações morfológicas revelaram a presença de hastes de Ag formadas por AgNPs embutidas em um filme de CS. Os íons de Ag foram reduzidos a Ag^0 durante o processo de revestimento devido aos átomos de oxigênio ricos em elétrons nos grupos hidroxila da CS. Tanto a CS quanto a NCS reduziram efetivamente Ag^+ a Ag^0 , permitindo a formação de AgNPs pequenas, esféricas e potencialmente semicristalinas. Os testes antimicrobianos revelaram que as AgNPs sintetizadas com CS mostraram uma zona de inibição maior contra *S. aureus*, enquanto nenhuma diferença significativa foi observada entre as amostras testadas contra *E. coli*. O uso de CS e NCS pareceu influenciar a estabilização

e a regulação do tamanho das AgNPs, sem uma relação direta. Além disso, tanto os revestimentos de AgNPs a base de CS quanto de NCS demonstraram atividade antibiofilme, sugerindo seu grande potencial como revestimentos antimicrobianos para superfícies de dispositivos médicos. Os resultados deste estudo oferecem soluções promissoras para o combate contra a formação de biofilmes, destacando os materiais sintetizados como alternativas potenciais para aplicações no campo biomédico.

Palavras-chave: Nanotecnologia; Nanocompósitos; Formação de Biofilme; Materiais Antimicrobianos; Biopolímeros.

FOREWORD

The rise of bacterial infections, particularly those caused by multidrug-resistant strains, presents a critical challenge to healthcare systems, with millions of hospital-acquired infections annually and substantial economic burdens. In this context, nanotechnology offers a promising solution to develop advanced antimicrobial materials to be used as coating on medical devices. This doctoral thesis investigates the synergistic potential of silver nanoparticles and chitosan for antimicrobial applications. It highlights the advantages of chitosan as a reducing agent over plant-based green synthesis methods, providing superior control over nanoparticle size, stability, and antimicrobial efficacy. The proposed synthesis routes aim to create reproducible and efficient antimicrobial coatings to address this pressing issue.

In the first article (Chapter 3), different methods for synthesizing silver nanoparticles were explored, using reducing agents such as sodium borohydride, heparin, glucose, chitosan, and nanochitosan, based on adaptations of methodologies reported in the literature. Among the reducing agents and synthesis methods evaluated, chitosan stood out as the most effective, resulting in nanoparticles with superior antimicrobial properties. Among the synthesis methods using chitosan, two were particularly noteworthy: one conducted without the application of heat during synthesis and another involving heating to 100°C. It was observed that the use of temperature played a crucial role in the reduction of silver ions to metallic silver, leading to the formation of nanoparticles with high antimicrobial activity and significant potential to inhibit biofilm formation.

The second article (Chapter 4), based on the previous findings, focused on the synthesis of a silver-chitosan nanocomposite developed through a simple method, without the need for heating, aimed at antimicrobial coatings. Different proportions of silver ions (5%, 10%, 20%, and 50%) relative to the amount of chitosan were tested. The results demonstrated that the formulation containing 20% Ag^+ exhibited the most promising antimicrobial activity, eliminating up to 100% of bacteria within just 120 minutes of contact. Furthermore, this formulation effectively inhibited biofilm formation by *Escherichia coli* and *Staphylococcus epidermidis*.

The third article (Chapter 5) was built on the findings presented in the first article and used chitosan and nanochitosan as reducing agents for the synthesis of silver nanoparticles. Chitosan and nanochitosan were produced from shrimp shells and used in combination with different concentrations of AgNO_3 (75 mg, 37.5 mg, and 25 mg). All formulations demonstrated

satisfactory antimicrobial activity against *Escherichia coli* and *Staphylococcus aureus*. Furthermore, these formulations were applied as coating on the surface of central venous catheters, and subjected to biofilm formation tests, showing promising results in biofilm inhibition.

Overall, this thesis demonstrates that the combination of chitosan and silver nanoparticles represents a promising alternative for the development of antimicrobial coatings, with the potential to significantly reduce bacterial infections in patients relying on medical devices.

LIST OF FIGURES

Figure 1. Chemical methods preparing chitosan from seafood byproducts as compared to biological methods of fermentation.....	8
Figure 2. Schematic representation of the chemical and biological routes for producing chitosan.....	10
Figure 3. Different approaches for synthesizing AgNPs (Hasan et al., 2022).....	19
Figure 4. Correlation between physical and chemical characteristics of AgNPs and their antimicrobial effect.....	22
Figure 5. Main approaches to produce CS-AgNPs. Adapted from (Frank et al., 2020).....	29
Figure 6. Schematic model of the antimicrobial mechanism of Cs-AgNPs.....	32
Figure 7. Schematic representation of the different methods used for the synthesis of AgNPs. A) represents the procedures for the Chitosan-TPP mediated Synthesis; B) represents the Chitosan and Nanochitosan-based synthesis; C) represents the Heparin-mediated synthesis; D) represents the Chitosan/Nanochitosan-Glucose Synthesis; E) represents Sodium Borohydride Reduction Synthesis; F) represents the Synthesis of AgNPs with variation in the amount of chitosan and AgNO ₃	45
Figure 8. Particle size distribution of AgNPs synthesized using different methods measured by DLS in number distribution mode.	49
Figure 9. UV-Vis absorption spectra of AgNPs synthesized by various methods.	51
Figure 10. SEM images of samples: A) CS-TPP-Ag, B) CS-Ag, C) NCS-Ag, and D) CS-HP-Ag.	54
Figure 11. SEM images of samples: A) CS-Glc-Ag, B) NCS-Glc-Ag, C) NaBH ₄ -Ag 1:1, and D) NaBH ₄ -Ag 2:1.	55
Figure 12. SEM images of AgNPs synthesized with a fixed AgNO ₃ concentration (200 mg) and varying CS amounts: A) CS50-Ag200, B) CS100-Ag200, C) CS150-Ag200, D) CS200-Ag200, and E) CS250-Ag200.....	57
Figure 13. SEM images of AgNPs synthesized with a fixed CS concentration (150 mg) and varying AgNO ₃ amounts: A) CS150-Ag75, B) CS150-Ag150, C) CS150-Ag250, D) CS150-Ag500, E) CS150-Ag1000 and F) CS150-Ag1500.....	59
Figure 14. Inhibition Zone of all synthesized AgNPs solutions against <i>S. aureus</i>	62
Figure 15. SEM micrographs of CVC specimens under different conditions: (A) CVC without bacterial exposure, serving as a control; (B) CVC after five days of exposure to <i>S. aureus</i> bacterial suspension; (C) CVC exposed to <i>S. aureus</i> bacterial suspension for five days in the	

presence of the CS150-Ag75 solution; (D) CVC pre-treated by immersion in the CS150-Ag75 solution prior to five days of exposure to *S. aureus* bacterial suspension.65

Figure 16. Illustration of the applied coating methods on the surface of PS pieces using CS-Ag composite.71

Figure 17. Scanning Electron Microscopy micrographs of PS pieces coated with CS-Ag composite, where (A) corresponds to sample CS-Ag-5%, (B) to CS-Ag-10%, (C) to CS-Ag-20%, and (D) to CS-Ag-50%.....74

Figure 18. SEM and elemental mapping image (C, O, N, and Ag) of (A) CS-Ag-5%, (B) CS-Ag-10%, (C) CS-Ag-20%, and (D) CS-Ag-20%.....75

Figure 19. Inhibition Zone of uncoated PS pieces (Blank) and PS pieces coated with pure AgNO₃, Chitosan, and CS-Ag composite against *E. coli* and *S. epidermidis*.76

Figure 20. Scanning electron microscopy micrographs of samples prepared by the dip-coating technique, where (A-B) correspond to sample with 1 coating layer, (C-D) 2 coating layers, and (E-F) 3 coating layers.77

Figure 21. Scanning electron microscopy micrographs of CS-Ag-20% of the coating overview, silver rods and AgNPs, and EDS mapping of Ag, where (A) correspond to sample Drop-100 and (B) sample Dip-2L in different magnifications.78

Figure 22. XPS Survey for samples Drop-100 (A) and Dip-2L (B) showing the presence of C, N, O, and Ag. Ag3d spectra for samples Drop-100 (C) and Dip-2L (D).79

Figure 23. Water contact angle of pure PS sample (Blank) and samples Drop-50, Drop-75, Drop-100, Dip-1L, Dip-2L and Dip-3L.....80

Figure 24. Surface roughness and images of samples DROP-100 and DIP-2L.81

Figure 25. (A) FTIR spectra of uncoated PS, PS coated with chitosan, and samples Drop-100, and Dip-2L. (B) UV-vis spectra of uncoated PS, Drop-100 and Dip-2L.....82

Figure 26. Antibacterial activity against *E. coli* and *S. epidermidis* of CS-Ag-20% coated with different methods on PS surfaces (A). Antibacterial activity of sample DROP-100 against *E. coli* and *S. epidermidis* bacteria over time (B). Agar plates inoculated with *E. coli* (C) and *S. epidermidis* (D) bacterial suspension after contact with the PS samples coated with CS-Ag-20% under light and dark conditions.84

Figure 27. CS-Ag-20% coatings usability test. (A) Bacterial viability of *E. coli* after 1, 2, and 3 uses. (B) Bacterial viability of *S. epidermidis* after 1, 2, and 3 uses.87

Figure 28. SEM micrographs of uncoated PS and Drop-100 after five days in contact with a bacteria suspension of *E. coli* and *S. epidermidis*.89

Figure 29. Proposed mechanism of antimicrobial activity on prepared CS-Ag composite coatings.....	90
Figure 30. Scanning Electron Microscopy of chitosan at A) 1000x magnification; and B) 500x magnification; and nanochitosan at C) 1000x magnification and D) 500x magnification.	99
Figure 31. Particle size distribution of CS and NCS measured by DLS in number distribution mode.	100
Figure 32. UV-Vis spectra for AgNPs synthesized with (A) chitosan and (B) nanochitosan. Distribution size by dynamic light scattering for AgNPs synthesized with (C) chitosan and (D) nanochitosan.	101
Figure 33. TEM analysis of sample CS-Ag_2, where: (A) TEM micrograph; (B) particle size distribution histogram; (C) HRTEM; (D) SAED pattern.	104
Figure 34. TEM analysis of sample CS-Ag_4, where: (A) TEM micrograph; (B) particle size distribution histogram; (C) HRTEM; (D) SAED pattern.	105
Figure 35. TEM analysis of sample CS-Ag_6, where: (A) TEM micrograph; (B) particle size distribution histogram; (C) HRTEM; (D) SAED pattern.	106
Figure 36. TEM analysis of sample NCS-Ag_2, where: (A) TEM micrograph; (B) particle size distribution histogram; (C) HRTEM; (D) SAED pattern.	107
Figure 37. TEM analysis of sample NCS-Ag_4, where: (A) TEM micrograph; (B) particle size distribution histogram; (C) HRTEM; (D) SAED pattern.	108
Figure 38. TEM analysis of sample NCS-Ag_6, where: (A) TEM micrograph; (B) particle size distribution histogram; (C) HRTEM; (D) SAED pattern.	109
Figure 39. A) Morphology of CVC segment without coating. B) CVC coated with sample CS-Ag_2. C) CVC coated with sample NCS-Ag_4. D) CVC coated with sample NCS-Ag_6...	110
Figure 40. Energy-dispersive X-ray spectroscopy (EDS) analysis and elemental mapping of the surface of pure central venous catheter.....	111
Figure 41. EDS analysis and elemental mapping of the surface of CVC coated with sample CS-Ag_2.	111
Figure 42. SEM of CVC coated with sample NCS-Ag_2.	112
Figure 43. Inhibition Zone of the synthesized AgNPs against <i>S. aureus</i> and <i>E. coli</i>	113
Figure 44. SEM images of CVC segments with and without AgNP coatings (CS-AgNPs and NCS-AgNPs) after incubation with <i>S. aureus</i> and <i>E. coli</i> . Figures A to G represent the test against <i>S. aureus</i> , where A) uncoated CVC; B) CVC coated with CS-Ag_2; C) CS-Ag_4; D) CS-Ag_6; E) NCS-Ag_2; F) NCS-Ag_4; G) NCS-Ag_6. Figure H to N represent the test	

against *E. coli*, where H) uncoated CVC; I) CVC coated with CS-Ag_2; J) CS-Ag_4; K) CS-Ag_6; L) NCS-Ag_2; M) NCS-Ag_4; and N) NCS-Ag_6. 118

LIST OF TABLES

Table 1. Synthesis methods of chitosan NPs, characteristics, and antimicrobial activity.	16
Table 2. Synthesis methods of AgNPs, characteristics, and antimicrobial activity.....	25
Table 3. Synthesis methods of CS-AgNPs, characteristics, and antimicrobial activity.....	36
Table 4. Elemental composition (weight %) of different samples obtained by EDS analysis.	60
Table 5. Description of CS-Silver composites: CS and silver ions amount, and coating methodology.	70
Table 6. PS samples were coated with CS-Ag-20% composite using different coating methodologies.....	71
Table 7. Description of the synthesized AgNPs: samples, and amounts of chitosan, nanochitosan, and AgNO ₃	96
Table 8. ANOVA results for inhibition zones of AgNP samples against <i>S. aureus</i> and <i>E. coli</i>	113
Table 9. Ag concentration, average particle size (TEM), and antimicrobial activity, as determined by inhibition zone and minimum inhibitory concentration (MIC) against <i>S. aureus</i> and <i>E. coli</i>	115

ABBREVIATIONS

Ag – Silver

Ag⁺ – Silver Ion

Ag⁰ – Metallic Silver

AgNO₃ – Silver Nitrate

AgNPs – Silver Nanoparticles

CAUTIs - catheter-associated urinary tract infections

CDC – Center for Disease Control and Prevention

CEO - clove essential oil

CIN – cinnamaldehyde

CoNS - coagulase-negative *Staphylococci*

CRBSIs - Catheter-related bloodstream infections

CS – Chitosan

CS-Ag – Chitosan-Silver

CS-AgNPs – Chitosan-Silver Nanoparticles

CUR – Curcumin

CVC – Central Venous Catheter

DD - degree of deacetylation

DIC – diclofenac

DLS – Dynamic Light Scattering

EDS - energy-dispersive X-ray spectroscopy

ESBL – Extended-spectrum β -lactam

ESC - Extended-Spectrum Cephalosporins

FCC – Face-centered cubic

FTIR - Fourier transform infrared spectroscopy

Glc – Glucose

HAIs - hospital-acquired infections

HCl - Hydrochloric acid

HMw – Hight Molecular Weight

HP – Heparin

HRTEM - high-resolution Transmission electron microscopy

LMw – Low Molecular Weight

MDR – Multi-Drug Resistant

MH - Mueller-Hinton

MHB - Muller Hinton Broth

MIC – Minimum Inhibitory Concentration

MIV - minimum inhibitory volume

MMw – Medium molecular Weight

MRSA – Methicillin-resistant *S. aureus*

MRSE - methicillin-resistant *S. epidermidis*

MSSA - methicillin-sensitive *S. aureus*

Mw – Molecular Weight

NaBH₄ - Sodium borohydride

NADH - nicotinamide adenine dinucleotide

NaOH - sodium hydroxide

NCS – Nanochitosan

NCS-AgNPs – Nanochitosan-Silver Nanoparticles

NPs – Nanoparticles

OCNPs - oleoyl-chitosan nanoparticles

OECD – Organization for Economic Co-operation and Development

ROS – Reactive Oxygen Species

SAED - selected area electron diffraction

SEM - Scanning electron microscopy

SPR - surface plasmon resonance

TEM - transmission electron microscopy

TPP - Sodium tripolyphosphate

UTIs - urinary tract infections

VREF - vancomycin-resistant *E. faecalis*

VRSA – Vancomycin-resistant *S. aureus*

WHO – World Health Organization

XRD - X-ray diffraction

ZP – Zeta Potential

SUMMARY

ABSTRACT	i
RÉSUMÉ	iii
RESUMO	v
FOREWORD	vii
LIST OF FIGURES	ix
LIST OF TABLES	xiii
ABBREVIATIONS	xiv
CHAPTER 1 – INTRODUCTION	1
1.1 Objectives	3
1.1.1 General Objectives.....	3
1.1.2 Specific Objectives	4
CHAPTER 2 - LITERATURE REVIEW	6
2.1 Multidrug resistance and the use of NPs	6
2.2 Chitosan	8
2.2.1 Synthesis methods	9
2.2.2 Properties of chitosan	11
2.2.3 Antimicrobial activity	12
2.3 Silver Nanoparticles	18
2.3.1 AgNPs synthesis methods.....	18
2.3.2 Antimicrobial activity	21
2.4 Chitosan-Silver Nanoparticles	28
2.4.1 Synthesis methods	28
2.4.2 Antimicrobial activity	31
2.4.3 Toxicity of CS-AgNPs.....	39
CHAPTER 3: ARTICLE 1	41
Effect of chitosan and other reducing agents on the synthesis and antimicrobial activity of silver nanoparticles for antimicrobial coatings	41
3.1 Introduction	42
3.2 Material and Methods	44
3.2.1 Synthesis of Silver Nanoparticles (AgNPs).....	44
3.2.1.1 Chitosan-TPP mediated Synthesis.....	46
3.2.1.2 Chitosan and Nanochitosan-based synthesis	46
3.2.1.3 Heparin-mediated synthesis.....	46
3.2.1.4 Chitosan/Nanochitosan-Glucose Synthesis	46
3.2.1.5 Sodium Borohydride Reduction Synthesis.....	47

3.2.1.6 Synthesis of AgNPs with variation in the amount of chitosan	47
3.2.1.7 Synthesis of AgNPs with variation in the amount of AgNO ₃	47
3.2.2 Characterizations	47
3.2.3 Antimicrobial Assays.....	48
3.2.3.1 Agar diffusion method.....	48
3.2.3.2 Antibiofilm Activity Test	48
3.3 Results and Discussion	49
3.3.1 Particle Size Distribution	49
3.3.2 Optical Properties and Plasmonic Behavior	51
3.3.3 Morphological and Elemental Analysis.....	53
3.3.4 Antimicrobial Activity and Biofilm Inhibition of Synthesized AgNPs.....	62
3.4 Partial Conclusions	66
CHAPTER 4: ARTICLE 2.....	67
In-situ growth of Ag nanoparticles embedded in chitosan coating for potent antimicrobial activity.....	67
4.1 Introduction	68
4.2 Material and Methods	70
4.2.1 Materials	70
4.2.2 Synthesis of chitosan-silver composite.....	70
4.2.3 Preparation and coating of the plastic samples	70
4.2.4 Characterizations	72
4.2.5 Antibacterial assays	72
4.2.5.1 Agar diffusion method.....	72
4.2.5.2 Spread plate technique for colony counting	73
4.2.5.3 Evaluation of Biofilm Formation.....	73
4.3 Results and Discussion	73
4.3.1 Preliminary evaluation of chitosan-silver coatings.....	73
4.3.2 Characteristics.....	76
4.3.3 Antimicrobial Properties.....	83
4.3.3.1 Reusability test.....	86
4.3.3.2 Biofilm Formation	88
4.3.3.3 Proposed Antimicrobial Mechanism	89
4.4. Partial Conclusions	91
CHAPTER 5: ARTICLE 3	92
Chitosan and Nanochitosan as dual reducing-stabilizing agents in the synthesis of AgNPs for advanced biomedical applications.....	92
5.1 Introduction.....	93
5.2 Material and Methods	95

5.2.1 Procedures to obtain chitosan	95
5.2.2 Procedures to obtain nanochitosan	95
5.2.3 Synthesis of silver nanoparticles	95
5.2.4 Preparation of CS-Ag and NCS-Ag NP coatings	96
5.2.5 Materials Characterization	96
5.2.6 Antimicrobial Activity	97
5.2.6.1 Agar Disk Diffusion Method	97
5.2.6.2 Minimal Inhibitory Concentration	97
5.2.6.3 Antibiofilm Activity Test	98
5.3 Results and Discussion	98
5.3.1 Chitosan and Nanochitosan	98
5.3.2 Characterization of CS-AgNPs and NCS-AgNPs	100
5.3.2.1 Optical properties and dynamic light scattering of AgNPs	100
5.3.2.2 Structural and morphological analyses of AgNPs	103
5.3.3 Coating morphology	109
5.3.4 Antimicrobial Activity	113
5.3.4.1 Agar diffusion method	113
5.3.4.2 Minimal Inhibitory Concentration	115
5.3.4.3 Qualitative antibiofilm assays	117
5.4. Partial Conclusions	121
5.5 Future Perspectives	121
CHAPTER 6: CONCLUSIONS	123
BIBLIOGRAPHY	125

CHAPTER 1 – INTRODUCTION

The spread of bacterial infections, especially those caused by Multi-Drug Resistant (MDR) strains, has become a critical global issue, posing a severe threat to public health (Alavi & Moradi, 2022). Besides being life-threatening, MDR infections are also connected with economic issues (Fafliora et al., 2014). For example, it was estimated that about 1.7 million hospital-acquired infections in the United States each year involving biofilm infections promoted by MRS bacteria with an annual cost of \$94 billion in healthcare costs (Römling et al., 2014). In the United Kingdom, catheter-associated urinary tract infections cause an additional burden to healthcare systems in the range of £1–2.5 billion (Alves et al., 2020). In the face of this situation, there is an urgent need to develop new and effective materials capable of avoiding the growth of bacterial contamination (Anjugam et al., 2018; Sheridan et al., 2022).

Nanoparticles (NPs) are colloidal particles typically ranging from 1 to 100 nanometers, and they are categorized into organic and inorganic types, each with distinct advantages. Inorganic particles, such as silver (Ag) and golden nanoparticles are valued due to their tunable optical properties and physical and optical stability, while organic particles, polymers and biopolymers, are prized for their flexibility in applications that require biocompatibility and chemical versatility (Divya & Jisha, 2017; Öztürk et al., 2024). In the past few decades, nanotechnology has emerged as a promising field of science with significant applications across many fields, from industrial to biomedical domains, especially because nanoscale materials possess unique properties that differ significantly from their respective bulk materials (Öztürk et al., 2024). Their small size, high surface area, redox potential, optical scattering, and fluorescence make them highly suitable for diverse biomedical applications (Khan et al., 2024). The exceptional biological activity of NPs—particularly their antibacterial effects across a wide range of cells—has driven advancements in their manufacturing and surface modification to enhance their effectiveness as coating agents and antimicrobial agents (Fahim et al., 2024).

In this scenario, organic materials, and metallic particles, as chitosan (CS) and Ag, have been widely studied as an alternative to overcome microbial resistance, especially in the biomedical field, with numerous application possibilities, such as wound healing and drug delivery and antimicrobial coatings (Azadpour et al., 2022; Farhangi Ghaleh Joughi et al., 2022; Mishra et al., 2015; Pishbin et al., 2013; Teixeira-Santos et al., 2021; G. Xu et al., 2022; Yang et al., 2022).

Known for its optical, electrical, and catalytic properties, Ag is a metal with an oligodynamic effect. Because of that, it can affect the permeability of the microbial membrane and the synthesis of proteins and DNA, leading to oxidative damage and cell death (Abbasi et al., 2014; Antsiferova et al., 2018). In the form of salt (e.g., AgNO_3) or complex species, Ag is used to treat local infections, mental illness, epilepsy, burns, and chronic wounds (Joardar et al., 2021). In the form of nanoparticles, Ag is widely used in wound dressing, water disinfectants, in antiseptic sprays, and as coatings on medical devices (e.g., synthetic implants and catheters) to prevent infections (Chernousova & Epple, 2013; C. G. A. Das et al., 2020; Joardar et al., 2021; Logambal et al., 2023). Thus, the synthesis of silver nanoparticles (AgNPs) is advantageous due to a large surface area to volume ratio at the nanometric scale, which improves Ag ion (Ag^+) release and promotes efficient interactions with microbial cells. (Polinarski et al., 2021).

CS is a linear polysaccharide of 2-amino-2-deoxy-D-glucopyranose and 2-acetamido-2-deoxy-D-glucopyranose, obtained by N-deacetylation of chitin, the second most abundant biopolymer in nature, which are found in the exoskeletons of arthropods and the carapaces of crustaceans (Bach et al., 2022; Frank et al., 2020; B. Hu et al., 2021). This biopolymer is well known for its unique properties, such as processability, biodegradability, biocompatibility, and antimicrobial and biological activities, widely explored by the industry for environmental, food, and biomedical applications (Bernardi et al., 2018; Campana et al., 2018; Kumari et al., 2021; Q. Li et al., 2022; Panda et al., 2021; Rubini et al., 2021).

Regarding the antibacterial mechanism of CS, it is known that this biopolymer is most active on the cell surface of bacteria (J. Li & Zhuang, 2020). The interaction between them is mainly electrostatic, where the positive charge of the protonated amino group of CS interacts with the negative charge molecules on the bacterial cell surface, causing the leakage of intracellular substances and eventually leading to cell death (Costa et al., 2012; Krajewska et al., 2011; H. Liu et al., 2004; Raafat et al., 2008). Furthermore, the antimicrobial properties of CS are affected by many factors, such as molecular weight (Mw), deacetylation degree (DD), CS source, and type of microorganism (J. Li & Zhuang, 2020). Additionally, one of the options to improve the antibacterial activity of CS is by transforming it in nanochitosan (NCS) or combining it with other antibacterial materials, including metallic particles, such as Ag (Ansari-Asl et al., 2022; Q. Deng et al., 2022; Z. Liu et al., 2022; Mutlu et al., 2022; Samanta et al., 2022).

Due to its structure with unique functional groups, CS interacts with metal ions and metal NPs, conferring the ability to form composites with Ag or other metals in their ionic or

metallic forms (Zienkiewicz-Strzałka et al., 2020). In the last few years, chitosan-silver (CS-Ag) composite synthesized by different methods (chemical or physical) has been one of the strategies to improve the antimicrobial activity of CS because of its biocompatibility and biodegradability (Kumar-Krishnan et al., 2015; Mirajkar et al., 2021). The antimicrobial properties of CS-Ag composites were significantly enhanced compared to AgNPs or CS alone (Mirajkar et al., 2021).

Given these qualities, AgNPs stand out as highly effective antimicrobial agents due to their remarkable functionality, small size, ease of preparation, and surface plasmon resonance. Their broad-spectrum activity and ability to disrupt bacterial cell membranes make them especially suitable for infection control applications (Jiang et al., 2023). Conversely, CS, a natural biopolymer, offers additional advantages with its high biodegradability, biocompatibility, non-antigenicity, antimicrobial and antioxidant activities, and excellent film-forming capacity, positioning it as a promising alternative for delivery systems, wound healing, and antimicrobial applications where sustained release and low toxicity are essential (Guo et al., 2024). Together, the complementary properties of these inorganic and organic compounds create a synergistic effect, combining the antimicrobial potency of AgNPs with the biocompatibility and film-forming capabilities of CS. This combination holds promise for advanced medical coatings, dressings, and therapeutic delivery, expanding the potential applications of both materials in healthcare (Polinarski et al., 2021).

The objective of this work was to explore the use of chitosan and nanochitosan as reducing agents for the synthesis of AgNPs and their application in antimicrobial coatings for medical devices. These coatings aim to prevent bacterial proliferation and biofilm formation. The study was based on the hypothesis that chitosan, due to its reducing and stabilizing properties, is a promising agent for AgNP synthesis, enabling the development of effective antimicrobial coatings. The experimental work was divided into three research articles: (1) exploring different AgNP synthesis methods, (2) investigating chitosan and Ag⁺ for antimicrobial coatings, and (3) evaluating chitosan and nanochitosan as reducing agents in AgNP synthesis for coating central venous catheters.

1.1 Objectives

1.1.1 General Objectives

- I. To synthesize and evaluate AgNPs produced with different reducing agents, characterizing their physicochemical properties and antimicrobial activity to identify the most effective formulations for antimicrobial applications;
- II. To develop and characterize CS-Ag composite coatings with enhanced antimicrobial and antibiofilm properties, focusing on green synthesis, physicochemical properties, and antimicrobial mechanisms;
- III. To synthesize AgNPs using CS and NCS as reducing and stabilizing agent focusing on their antimicrobial and antibiofilm properties, with potential applications as coatings for medical devices to prevent biofilm formation;

1.1.2 Specific Objectives

- i. To synthesize AgNPs using various reducing agents, including CS, NCS, glucose, heparin, and tripolyphosphate, following methodologies adapted from the literature;
- ii. Compare the influence of different reducing agents on the physical and antimicrobial properties of AgNPs, identifying the most promising agent for antimicrobial applications;
- iii. To synthesize CS-Ag composites using a facile, eco-friendly, two-step method, and evaluate their application as antimicrobial coatings;
- iv. To investigate the in-situ formation of AgNPs within CS coatings;
- v. To characterize the physicochemical properties of the coatings and assess the antimicrobial performance of the CS-Ag composite coatings against *Escherichia coli* (*E. coli*) and *Staphylococcus epidermidis* (*S. epidermidis*) under different conditions;
- vi. To evaluate the potential of CS-Ag composite coatings to inhibit biofilm formation, investigate their reusability and long-term antimicrobial efficiency;
- vii. To propose the antimicrobial mechanisms of the coatings and the interaction of CS with bacterial cells;
- viii. To synthesize CS-AgNPs and NCS-AgNPs using CS and NCS as dual reducing and stabilizing agents, optimizing the synthesis through variations in AgNO₃ concentrations;
- ix. To characterize the physicochemical properties of CS and NCS AgNPs, including size, shape, crystallinity, using different techniques;

- x. To compare the antimicrobial efficacy of CS-AgNPs and NCS-AgNPs against *E. coli* and *Staphylococcus aureus* (*S. aureus*);
- xi. To evaluate the antibiofilm activity of CS and NCS AgNPs applied as coatings on medical devices and explore their potential mechanisms of action in preventing biofilm formation.

CHAPTER 2 - LITERATURE REVIEW

The content of this section has been previously published in *Particle & Particle System Characterization* (<https://doi.org/10.1002/ppsc.202100009>). For inclusion in this thesis, revisions and updates have been incorporated to enhance alignment with the current research scope and objectives.

2.1 Multidrug resistance and the use of NPs

Since the beginning of the antibiotics use with penicillin in the 1940s, bacterial resistance has been identified and expanded more rapidly, especially in the last two decades (Ventola, 2015). From an evolutionary perspective, bacteria has developed mechanisms of resistance to antibiotics by gene mutations and horizontal gene transfer (Fair & Tor, 2014; Munita & Arias, 2016). Bacterial resistance can occur to different classes of antibiotics, which in turn are classified according to the mechanism of action on the bacterial structure. The main modes of action of antibiotics are inhibition of cell wall synthesis (β -lactam, carbapenem), nucleic acids synthesis (quinolone, rifampicin), and metabolic pathways (sulfonamide, trimethoprim); damage of bacterial membrane structure (polymyxin); and modification of protein synthesis through interactions with polypeptide chains (glycopeptide) or ribosomes (aminoglycosides, macrolide) (Pham et al., 2019; Quinlivan et al., 2000; Schwarz et al., 2004; Tipper, 1985; Velkov et al., 2010).

Bacteria have developed resistance over the years for each class of antibiotics with specific mechanisms of action. The Organization for Economic Co-operation and Development (OECD) predicts that more than 2 million people in Europe, North America, and Australia will die from infections caused by resistant microorganisms until 2050, with an estimated cost of up to US\$3.5 billion per year. In developing countries, such as Brazil and Russia, with around 50% of infections caused by resistant microorganisms, bacterial resistance is expected to increase up to seven times faster than in the OECD member countries (Hofer, 2018).

The genetic basis for bacterial resistance to antibiotics comes from the transfer of plasmids containing antibiotic resistance genes, transposons, and integrons, including horizontal gene transfer by conjugation (with plasmids transfer), transformation (integration of free genetic material), and bacteriophages-mediated transduction (Sultan et al., 2018). These genetic changes can induce modifications in molecular structures and activate different mechanisms of antibiotic resistance in bacterial cells, including efflux pumps (antibiotic removal out of the cell), presence of an external membrane (as in gram-negative bacteria to control the entry of antibiotics), and porins (selective barrier for antibiotics) (Blair et al., 2014).

Other modifications allow the production of enzymes that inactivate antimicrobial molecules or active sites in different enzymes responsible for the antibiotic metabolism but remain functional for the bacteria, and small changes in bacterial ribosomal subunits to prevent the antibiotic action (Munita & Arias, 2016; Wright, 2011).

Multidrug-resistant bacteria are a class of bacteria resistant to different antibiotics. They include carbapenem-resistant *Acinetobacter baumannii*; β -lactams- and quinolones-resistant *Clostridium difficile*; carbapenem-resistant Enterobacteriaceae; multidrug-resistant (extended-spectrum cephalosporins (ESC), ceftriaxone, cefixime, azithromycin) *Neisseria gonorrhoeae*, which is listed as urgent threats by the Center for Disease Control and Prevention (CDC). Other bacterial strains listed as serious threats by CDC report are the methicillin-resistant *S. aureus* (MRSA); vancomycin-intermediate *S. aureus*; vancomycin-resistant *S. aureus* (VRSA); vancomycin-resistant *Enterococci*; β -lactams-, macrolides-, and quinolones-resistant *Streptococcus pneumoniae*; rifamycin-, quinolones-, aminoglycosides-resistant *Mycobacterium tuberculosis*; extended-spectrum β -lactam (ESBL)-producing Enterobacteriaceae; and multidrug-resistant (MDR) *P. aeruginosa* (Fair & Tor, 2014; Młynarczyk-Bonikowska et al., 2020; van Duin & Paterson, 2016; Ventola, 2015).

Multidrug resistance can be associated with the mentioned mechanisms of antibiotic resistance or bacterial organization, as in biofilms. In biofilms, bacterial cells are about 1000 times more resistant than individual cells because the exopolysaccharides matrix acts as a barrier, hindering the antimicrobial activity. Also, the reduced mobility favors the transformation and conjugation processes, resulting in resistance gene transfer (Dimopoulos et al., 2016; Rabin et al., 2015). The antimicrobial action after biofilm formation is difficult, especially in medical devices, which are commonly susceptible to biofilm formation. Therefore, new strategies to overcome multidrug-resistant bacteria need to be developed. In this sense, the use of NPs represents an advantageous measure to control multidrug resistance (Kandi & Kandi, 2015).

The physicochemical properties of these nanomaterials favor the design of new antimicrobials to treat infections caused by multidrug-resistant bacteria. The NPs can be used as therapeutic agents or carrier agents of antimicrobial compounds. The mechanism of action of NPs is explained by multiple pathways, including the bacterial membrane rupture, attachment to intracellular components (DNA, ribosomes, and enzymes), and interruption of metabolic functions that culminate with cell death before its adaptation (Gupta et al., 2019). Different studies report the antimicrobial action of CS, NCS and AgNPs against multidrug-resistant bacteria (F. Alqahtani et al., 2020; Lara et al., 2010).

2.2 Chitosan

Environmental clean-up has become a central aspect of the green economy, highlighting the urgent need for innovative solutions to address the toxicity and persistence of contaminants from both human and natural sources (Issahaku et al., 2023). In response to this demand, high-performance, eco-friendly materials like CS have become a major focus of research, particularly in the biomedical field and in the development of biobased polymers with antimicrobial properties (Geng et al., 2023; Guo et al., 2024; Meng et al., 2023).

CS is a natural polymer derived from chitin, the second most abundant biopolymer after cellulose. Chitin contains three reactive functional groups, an amino group at the C-2 position, as well as primary and secondary hydroxyl groups at the C-3 and C-6 positions, respectively (Kumar et al., 2020). Chitin is typically sourced from fungal cell walls and the exoskeletons of crustaceans and insects through processes of demineralization and deproteinization. In its natural state, chitin has limited solubility and reactivity, but its properties can be significantly improved by removing acetyl groups from the amine groups at the C-2 position on the glucan ring in a process called deacetylation (Teixeira-Santos et al., 2021). When chitin is deacetylated above 50%, it transforms into CS, a copolymer composed β -(1-4)-linked 2-amino-2-deoxy-D-glucopyranose (deacetylated units) and 2-acetamido-2-deoxy-D-glucopyranose (acetylated units) (Lupatini et al., 2018) (**Figure 1**).

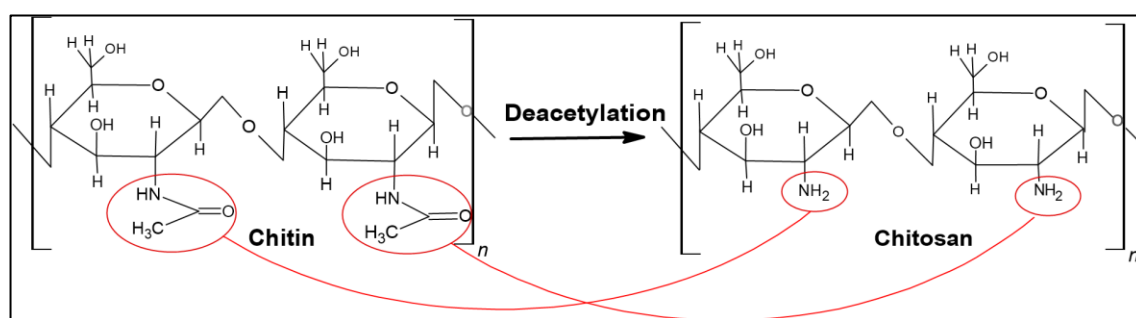


Figure 1. Chemical methods preparing chitosan from seafood byproducts as compared to biological methods of fermentation. Source: Alves et al. (2017) and Polinarski et al. (2021).

The seafood processing industry, a major contributor to CS production, generates large quantities of shell waste, particularly from shrimp, where approximately 45% of production results in non-edible waste composed of exoskeletons and cephalothoraxes (Huq et al., 2022). However, this discarded shell material is the primary source of chitin for commercial use, making it an excellent option for CS production. By converting this previously wasted material into valuable resources, the industry adds value to the circular economy (Engels & O’Born,

2022). This market, valued at over \$1.2 billion as of 2015, has an annual production capacity estimated between 10 and 100 million tons, illustrating the significant environmental and economic potential of CS (Teixeira-Santos et al., 2021).

CS has emerged as a promising, nature-derived biopolymer due to its abundance, reasonable price, and distinctive physicochemical properties, including biodegradability, biocompatibility, antimicrobial and antioxidant activities, low immunogenicity, and non-toxicity (Seidi et al., 2021). In this regard, CS has been widely studied, produced, and applied in different fields, such as pharmaceuticals, the food industry, agriculture, and the biomedical area (H. J. Alves et al., 2021). Its stable polycationic structure makes it suitable for diverse applications, ranging from food additives and wastewater treatment agents to live cell encapsulation, enzyme immobilization, and cholesterol-lowering agents. In biomedicine and pharmaceuticals, CS is frequently used in wound healing, drug delivery, and as a dressing material, thanks to its biocompatibility with various tissues, organs, and cells (Huq et al., 2022).

2.2.1 Synthesis methods

As previously mentioned, CS is derived from chitin, which is primarily extracted from marine invertebrates. Typically, the exoskeleton of crustaceans consists of 15–40% chitin, 20–40% protein, and 20–50% calcium and magnesium carbonates, along with other minor components (Antonino et al., 2017). Thus, in order to extract chitin from its raw material, the process of deproteinization and demineralization are essential. These processes can be performed through a chemical or biological route. On the chemical route, deproteinization is performed by treating chitinous feedstock with strong alkali solutions, such as sodium hydroxide (NaOH), to effectively remove proteins from the material. Conversely, demineralization is used performed with acids of mild concentration, such as hydrochloric (HCl) and acetic acids (Nwabike Amitaye et al., 2024). On the biological route, demineralization and deproteinization are performed using plant enzymes or microorganisms. Acid-producing bacteria, such as *Lactobacillus* and *Bacillus*, act as bio-demineralizers by removing mineral carbonates, while protease-producing bacteria, like *Serratia marcescens*, serve as bio-deproteinizers by breaking down proteins (Kou et al., 2021; Nwabike Amitaye et al., 2024). This eco-friendly approach preserves long molecular chains but is generally slower, costlier, and less efficient compared to chemical methods (Kou et al., 2021; Nwabike Amitaye et al., 2024). Once the chitin is extracted, the next step is deacetylation. This process can be performed through alkaline or enzymatic methods. In the alkaline method, chitin is treated with 40-50% NaOH, resulting in the conversion of N-acetyl-d-glucosamine units to d-glucosamine

units with exposed -NH_2 functional groups. In the enzymatic methods, the deacetylation is performed through chitin deacetylase, an enzyme responsible for hydrolyzing acetyl groups to produce CS (Kou et al., 2021). The process to obtain CS is illustrated in **Figure 2**.

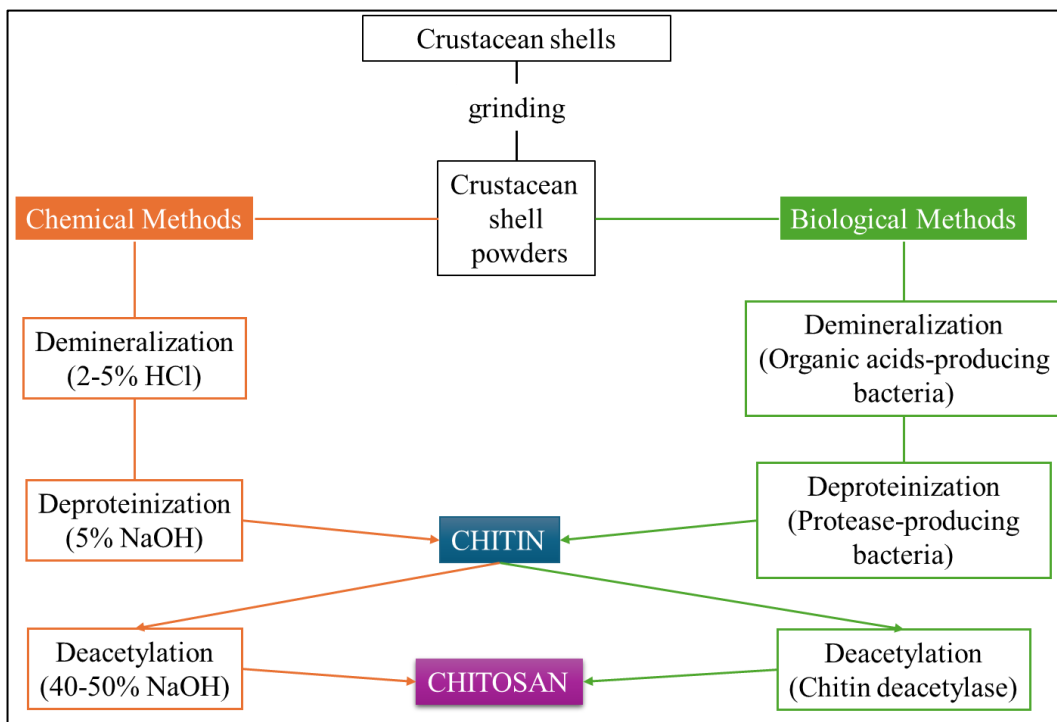


Figure 2. Schematic representation of the chemical and biological routes for producing chitosan.

Alternative physical methods have been reported in the literature to produce NCS, including gamma irradiation, ultraviolet (UV) irradiation, and thermal shock treatment (H. J. Alves et al., 2018, 2021; Yue et al., 2009; G. Zhang et al., 2019). Although some techniques result in high molecular weight (Mw) NCS with high particle diameter, the thermal shock treatment can reduce both the Mw (less than 21 kDa) and particle size (hydrodynamic diameter below 30 nm) (H. J. Alves et al., 2018). A study has shown the correlation between Mw and particle size, in which CSN with Mw less than 30 kDa are probably at the nanometer scale with average sizes below 100 nm (H. J. Alves et al., 2021).

Considering the synthesis of NCS, the ionic or ionotropic gelation is based on the ability of polyelectrolytes to crosslink in the presence of counter ions to form composites in nanometric scale (Patil et al., 2012). This method commonly uses sodium tripolyphosphate (TPP) solution as a crosslinker to produce NCS particles, but some studies report the use of essential oils and its derivatives, such as the cinnamaldehyde, for the same purpose (Costa et al., 2018; Gadkari et al., 2019).

2.2.2 Properties of chitosan

The versatility of CS as a biopolymer enables it to be processed into different forms, such as flakes, beads, powders, membranes, gels, and sponges, suitable for diverse applications (Huq et al., 2022). Among its characteristics, the degree of deacetylation (DD) and molecular weight (Mw) stand out as the most important ones that influence the resulting properties of CS (Arantes et al., 2015).

As a raw material, chitin is highly insoluble and exhibits low reactivity. However, its structure can be modified by removing acetyl groups, a process that results in CS, a deacetylated form with enhanced properties (Zargar et al., 2015). The glucosamine/N-acetyl glucosamine ratio rises as chitin is converted to CS, indicating the degree of deacetylation. When the portion of N-acetyl glucosamine exceeds that of glucosamine, the biopolymer is called chitin. In the meantime, the compound is called CS when the glucosamine portion exceeds that of N-acetyl glucosamine. Thus, when the DD of CS is 80%, the CS contains 80% D-glucosamine units and 20% N-acetyl-glucosamine units in the polymer chain (Kumar et al., 2020).

The DD represents the percentage of acetyl groups removed, and plays a crucial role in determining the physicochemical characteristics of CS. As higher the DD, the more hydrophilic and soluble in dilute acidic solutions (e.g., acetic, formic, succinic, lactic acids) CS becomes. This happens due to an increase in D-glucosamine groups, allowing the glucosamine units ($-NH_2$) to convert to their protonated, soluble form ($-NH_3^+$) (Kumar et al., 2020; Teixeira-Santos et al., 2021). Additionally, the DD directly influences the intermolecular interactions in CS, affecting the tendency to form aggregates in acidic conditions, even when fully protonated. This aggregation is associated with hydrogen bonds and hydrophobic interactions, determined by the polysaccharide backbone and the N-acetyl groups at the C₂ position (Issahaku et al., 2023). Generally, the conversion of $-NH_2$ groups into NH_3^+ groups make CS highly basic and polycationic. A higher DD enhances these qualities, improving CS's abilities as a metal chelator and increasing its solubility, microbial binding capacity, film-forming potential, viscosity, optical and structural characteristics (Issahaku et al., 2023; Teixeira-Santos et al., 2021). As a cationic polymer, CS has some characteristics, such as cell transfection, biological adhesion, anti-inflammatory, and anti-microbial properties, that can be enhanced when combined with other materials (Gao & Wu, 2022).

The molecular weight is also an important parameter to be considered because it influences CS's characteristics, such as its hydrophobicity, solubility, and viscosity (H. J. Alves et al., 2018; Arantes et al., 2015). The Mw of CS generally lies between 10 to 10³ kDa,

depending on the source from which it is extracted and the process applied for chitin deacetylation (H. J. Alves et al., 2021). CS with a molecular weight below 100 kDa is classified as low molecular weight (LMw). CS with a molecular weight between 100 kDa and 1000 kDa is considered medium molecular weight (MMw), while CS with a molecular weight above 1000 kDa is classified as high molecular weight (HMw) (Nwabike Amitaye et al., 2024). Another important parameter is the zeta potential (ZP) of CS, i.e. the surface charge measured in aqueous solution and represents the electrostatic repulsion between particles (Müller et al., 2001). CS with high positive ZP has a greater antimicrobial activity due to stronger interactions between the positive charges of CS with negative charges of microbial surface (Darabpour et al., 2016; Ing et al., 2012; N. C. Silva et al., 2015).

2.2.3 Antimicrobial activity

Nowadays, the search for new antimicrobial agents is widely increasing, mostly because of the existence of drug-resistant pathogens and the emerging problem of microbial infections (Matica et al., 2019). In this way, CS emerges as one of the most promising natural polymers known to possess antimicrobial properties. According to the literature, CS has a few main widely accepted mechanisms of action against microorganisms, such as electrostatic interactions, plasma membrane damage mechanism, interaction with microbial DNA, metal chelation capacity of CS, and deposition onto the microbial surface (Beck et al., 2019; Chien et al., 2016; Matica et al., 2019; Severino et al., 2015; Tao et al., 2011; K. Xing et al., 2015; Yuan et al., 2016).

Li et al. (2010) investigated the inhibition activity of CS of three Mw (1000, 50, and 3 kDa) against *E. coli*. They reported that CS demonstrated intense inhibition activity against the bacteria, but the inhibition activity varied according to the CS Mw. CS with a Mw of 50 kDa possessed the most potent inhibition activity in their case. In addition, ultrastructural analysis by transmission electron microscopy (TEM) revealed evidence that CS caused cytoplasmic membrane disruption and lysis in the bacteria (Li et al., 2010).

Xing et al. (2009) studied the interaction between oleoyl-chitosan nanoparticles (OCNPs) and bacteria (*E. coli*) and investigated the binding between OCNPs and DNA/RNA. The results showed that when the concentration of OCNP increases, the DNA inhibition starts, achieving the complete inhibition of the *E. coli* DNA and RNA migration with an OCNP concentration of 1000 mg/L. The interaction of OCNP with DNA/RNA was evidenced by the inhibition of OCNP on the electrophoretic mobility of bacterial genomic DNA or total RNA. The amino groups present in the CS possess positive charges that interact with the negatively

charged phosphate groups in the chain of nucleic acids, affecting pathogen activity (K. Xing et al., 2009).

Sheng et al. (2022) evaluated the antimicrobial activity of CS with different Mw against *S. aureus*, *E. coli*, and *Saccharomyces cerevisiae*. In this case, CS showed better antimicrobial activity against Gram-positive bacteria than for Gram-negative bacteria and fungi. Furthermore, the results showed that the antimicrobial effect of LMw CS was significantly higher than that HMw CS. The authors related this event to the fact that LMw CS can enter the cell through osmosis and adsorb anionic substances in the body due to the positive charge of the amino group. Meanwhile, HMw CS played a bacteriostatic effect, where it was adsorbed on the cell surface to form a polymer film to prevent the transportation of nutrients into the cell (Sheng et al., 2022).

Curcumin-loaded NCS with an average diameter of 134.37 ± 1.99 nm and a surface charge of 18.10 ± 0.82 mV were tested against polymicrobial biofilms of *Candida albicans* and *S. aureus*. The minimum inhibitory concentration (MIC) value was $400 \mu\text{g mL}^{-1}$ for both microorganisms. At the concentration of $200 \mu\text{g mL}^{-1}$, curcumin-loaded NCS inhibited almost all of the mono- and polymicrobial biofilms, evidencing their effectiveness against one microorganism as well as the combination of both strains (S. Ma et al., 2020). Infections related to polymicrobial biofilms have significantly higher mortality rates compared to infections caused by monomicrobial biofilms. This clinical problem has been widely studied because microbial cells in polymicrobial biofilms are more resistant to antimicrobial agents (Costerton et al., 1999; Flemming et al., 2016; Peters & Noverra, 2013).

CS with an average diameter of 226.6 ± 5.24 nm and surface charge of 27.1 ± 3.09 mV were tested against the antibiotic-resistant skin pathogens VRSA, vancomycin-resistant *E. faecalis* (VREF), *P. aeruginosa* reference strain, cefotaxime-resistant *P. aeruginosa* from clinical isolate, *Acinetobacter baumannii* reference strain, and multi-resistant *A. baumannii* (resistant to cefotaxime, cefepime, ciprofloxacin, and trimethoprim/sulfamethoxazole) from clinical isolate. The MIC of CS NPs was 2 mg mL^{-1} for VRSA, VREF, and *P. aeruginosa* from a clinical isolate and 1 mg mL^{-1} for the remaining strains. Considering that all tested microorganisms are resistant to several antibiotics, CS NPs inhibited their growth at relatively low MIC values (Costa et al., 2018).

In a similar study, CS with an average size of 244 ± 12 nm and charge of 17.3 ± 1.4 mV were tested against MRSA, methicillin-sensitive *S. aureus* (MSSA), and methicillin-resistant *S. epidermidis* (MRSE). CS inhibited the growth of all microorganisms ($\text{MIC} = 1.25 \text{ mg mL}^{-1}$) as well as their biofilm formation at concentrations of $\frac{1}{2}$ and $\frac{1}{4}$ of MIC. The biofilm formation

of MRSE strain was less susceptible to the CS than the biofilms of MSSA and MRSA. The biofilm inhibition was above 90% for MSSA and around 75% for MRSA (Costa et al., 2017). These values can be compared to the antibacterial activity of CS-cinnamaldehyde NPs, a size range of 80-150 nm, which were evaluated against non-resistant *S. aureus* and *E. coli* bacteria. The bacterial inhibition was 98% against *S. aureus* and 96% against *E. coli* with a MIC of 5 mg mL⁻¹ for both microorganisms (Gadkari et al., 2019).

Diclofenac-loaded CS NPs prepared from LMw and HMw CS had average diameters of 295 ± 3 and 336 ± 22 nm with a surface charge of 29.3 and 22.5 mV, respectively. The antibacterial activity against *S. aureus* and *Bacillus subtilis* was dependent on CS Mw. The MIC values against *S. aureus* ranged from 18 to 35 µg mL⁻¹ (HMw and LMw) and *B. subtilis* varied between 9 and 17.5 µg mL⁻¹ (HMw and LMw), respectively. Diclofenac-loaded CS NPs with LMw presented the same inhibition zone against *B. subtilis* compared to ampicillin (positive control) in agar diffusion assays (Alqahtani et al., 2019).

The antibacterial activity of CS NPs loaded with clove essential oil (CEO) was assessed against *S. aureus*, *Listeria monocytogenes*, *Salmonella typhi*, and *E. coli*. The CEO-loaded CS NPs were in the size range of 223 to 444 nm. The minimum inhibitory volume (MIV) of loaded CS NPs was 2 µL against the four bacteria. Pure CEO showed a MIV of 2 µL for *S. aureus*, *L. monocytogenes*, *S. typhi*, and 4 µL for *E. coli*. Unloaded CS NPs had a MIV of 8 µL against all the bacteria (Hadidi et al., 2020). Moreover, the antibacterial activity of CS NPs (LMw and HMw) loaded with polyphenols was evaluated against *B. cereus*, *E. coli*, *Listeria innocua*, *S. aureus*, *Salmonella typhimurium*, and *Yersinia enterocolitica*. The best encapsulation performance was obtained for NPs produced with LMw and the polyphenol rosmarinic acid with 355.9 ± 21.6 nm and surface charge of 28.0 ± 2.1 mV. The MIC value was 1.5 mg mL⁻¹ against *S. typhimurium*, *E. coli*, and *Y. enterocolitica*, and 1.0 mg mL⁻¹ against *L. innocua*, *S. aureus*, and *B. cereus* (Madureira et al., 2015). In both studies, the mechanism of NPs action was believed to be the adsorption to cell membranes, increasing their permeability along with the leakage of cytoplasmic constituents and cell death.

LMw CS inhibited *Staphylococcus xylosus* and *S. aureus* growth with MIC values of 100 and 800 µg mL⁻¹, respectively. Also, the inhibition capacity against *S. xylosus* and *S. aureus* biofilms at 100 µg mL⁻¹ was 83.9% and 51.7%, respectively. This result reinforces the antimicrobial action of CS against strains usually involved in chronic bovine mastitis (Felipe et al., 2019).

The antibacterial activity of NCS with an average diameter of 40 nm was tested against *E. coli*, *Salmonella choleraesuis*, *Salmonella typhimurium*, and *S. aureus* in distilled water (pH

6.5) and 0.25% acetic acid solution (pH 5.0). The MIC at both pH values was below $0.25 \mu\text{g mL}^{-1}$, but in acetic acid solution, the antimicrobial activity of CS NPs was higher (L. Qi et al., 2004). This result corroborates with other studies reporting the antimicrobial activity of NCS against strains of *Bacillus cereus*, *E. coli*, *S. aureus*, *Pseudomonas fluorescens*, and clinical isolates of *K. pneumoniae* and *E. coli* in urinary catheters. In general, the antimicrobial activity of NCS was more effective in acidic solutions against gram-negative bacteria (Campana et al., 2017; O'Callaghan & Kerry, 2016).

NCS in the size range of 50 to 250 nm and surface charge from 12 to 41 mV were effective against *S. aureus* and *E. coli* growth. The lowest MIC values were less than $75 \mu\text{g mL}^{-1}$ and $12.5 \mu\text{g mL}^{-1}$ against *E. coli* and *S. aureus*, respectively, for NPs with 111.4 nm and charge of 29.3 mV. In this case, the MIC value and zone inhibition assay showed that gram-positive bacteria were more susceptible to the antimicrobial activity of NCS due to their optimal size (Tyagi et al., 2014).

Table 1 summarizes the most common synthesis methods to produce CS NPs as well as their corresponding results of Mw, DD, particle size, and antimicrobial activity.

Table 1. Synthesis methods of chitosan NPs, characteristics, and antimicrobial activity.

Material*	Synthesis method**	Mw initial and after depolymerization (kDa)	DD (%)***	Average particle size (nm)****	Microorganisms and antimicrobial activity (MIC/MIV)*****	Reference
LMw CS	Depolymerization in dilute acetic acid solution with mineral adsorbent	410 to 60	>75	NE	NE	(Pandit et al., 2020)
LMw CS	Depolymerization by enzymatic hydrolysis (papain)	350 to 40	91	NE	NE	(Pan et al., 2016)
LMw CS	Depolymerization by enzymatic hydrolysis (amylase)	410 to 0.73	93	NE	NE	(Wu, 2011)
LMw CS	Oxidative route: H ₂ O ₂ 0.2%, 65 °C, 12 h Acid route: HCl 5.15 mol L ⁻¹ , 65 °C, 12 h	200 to 21.6 (oxidative) and 38.8 (acid)	73	NE	NE	(de Farias et al., 2019)
LMw CS	Acid route: HCl, 65 °C, 30 h	2038 to 73.8	75	NE	NE	(Kasaai et al., 2013)
LMw CS	Oxidative route: HCl 0.1 M, H ₂ O ₂ 15% v/v, 60 °C, 4 h	700 to 200	80	NE	NE	(Bezerra, 2011)
LMw CS	UV irradiation + O ₂	722 to 53.2	88	NE	NE	(Yue et al., 2009)
NC	Thermal shock	160 to 18	75	30	NE	(H. J. Alves et al., 2018)
NCS + CIN	Ionotropic gelation	50 - 190	90	80 - 150	<i>S. aureus</i> , <i>E. coli</i> MIC: 5 mg mL ⁻¹	(Gadkari et al., 2019)
NCS+ CUR	Ionotropic gelation	107	80	134	<i>S. aureus</i> , <i>C. albicans</i> MIC: 400 µg mL ⁻¹	(S. Ma et al., 2020)
NCS	Ionotropic gelation	107	80	226.6	VRSA, VREF, <i>P. aeruginosa</i> Ci MIC: 2 mg mL ⁻¹ <i>A. baumannii</i> R, <i>A. baumannii</i> Ci, <i>P. aeruginosa</i> R MIC: 1 mg mL ⁻¹ <i>S. aureus</i> MIC: 800 µg mL ⁻¹ <i>S. xylosus</i> MIC: 100 µg mL ⁻¹	(Costa et al., 2018)
LMw CS	Solubilized in acetic acid 2%	60 - 120	75	NE	<i>S. aureus</i> MIC: 18 and 35 µg mL ⁻¹ <i>B. subtilis</i>	(Felipe et al., 2019)
NCS + DIC	Ionotropic gelation	107 and 260	NE	295 and 336	<i>S. aureus</i> MIC: 18 and 35 µg mL ⁻¹ <i>B. subtilis</i>	(Alqahtani et al., 2019)

NCS	Ionotropic gelation	100	80	244	MIC: 9 and 17 $\mu\text{g mL}^{-1}$ <i>S. aureus</i> , <i>S. epidermidis</i> MIC: 1.25 mg mL^{-1} <i>S. aureus</i> , <i>L. monocytogenes</i> , <i>S. typhi</i>	(Costa et al., 2017)
NCS + CEO	Ionotropic gelation	50 - 190	75 - 85	223 - 444	MIV: 2 μL <i>E. coli</i> MIV: 4 μL <i>E. coli</i> , <i>S. choleraesuis</i> , <i>S. typhimurium</i> , <i>S. aureus</i>	(Hadidi et al., 2020)
NCS	Ionotropic gelation	220	85	40	MIC: <0.25 $\mu\text{g mL}^{-1}$ <i>S. typhimurium</i> , <i>E. coli</i> , <i>Y. enterocolitica</i>	(L. Qi et al., 2004)
NCS	Ionotropic gelation	107	75 - 85	355.9	MIC: 1.5 mg mL^{-1} <i>L. innocua</i> , <i>S. aureus</i> , <i>B. cereus</i> MIC: 1.0 mg mL^{-1} <i>E. coli</i>	(Madureira et al., 2015)
NCS	Ionotropic gelation	50	85	51.97 - 245.9	MIC: 75 - 150 $\mu\text{g mL}^{-1}$ <i>S. aureus</i> MIC: 12.5 - 50 $\mu\text{g mL}^{-1}$ Absorbance: <i>Escherichia coli</i> :0.27	(Tyagi et al., 2014)
CS	Deproteinization, desalination, decolorization followed by deacetylation (Chitin source: fly pupae)	42	88.29	NE	<i>Staphylococcus aureus</i> :0.1 <i>Saccharomyces cerevisiae</i> :0.2 Absorbance: <i>Escherichia coli</i> : 0.07	(Sheng et al., 2022)
NCS		4.8	91.35	NE	<i>Staphylococcus aureus</i> :0.02 <i>Saccharomyces cerevisiae</i> :0.02	

* LMw CS (low molecular weight chitosan), NCS (nanochitosan), CIN (cinnamaldehyde), CUR (Curcumin), DIC (diclofenac), CEO (clove essential oil).

**H₂O₂ (hydrogen peroxide), HCl (hydrochloric acid).

***DD (degree of deacetylation).

****NE (not evaluated).

*****MIC (minimum inhibitory concentration), MIV (minimum inhibitory volume), Ci (clinical isolate), R (reference).

2.3 Silver Nanoparticles

AgNPs have been the focus of many researchers due to their photocatalytic and antibacterial properties (Vorobyova et al., 2022). Ag is a metal known for its optical, electrical, and catalytic properties. Also, its oligodynamic effect can affect the permeability of the microbial membrane and the synthesis of proteins and DNA, causing oxidative damage and cell death (Abbasi et al., 2014; Durán et al., 2019; Markowska et al., 2013; Nurani et al., 2015). In the form of silver nitrate (AgNO_3), Ag has been used as an antimicrobial agent to treat burns and open wounds (Das et al., 2020). At the nanoscale, metallic silver (Ag^0) has been employed in the manufacture of cosmetics, sponges, gels, fibrous materials, and antimicrobial agents (Mohandas et al., 2018).

The synthesis of AgNPs is advantageous due to a large surface area to volume ratio at a nanometric scale enhancing the release of Ag^+ and promoting efficient interactions with microbial cells (Guggenbichler et al., 1999; Rojas-Andrade et al., 2015). In biomedical areas, AgNPs have been widely used as an alternative to treat infections caused by resistant bacteria (Mathur et al., 2018).

2.3.1 AgNPs synthesis methods

The literature proposes several different processing routes to synthesize AgNPs, divided into two main categories: Top-down and Bottom-up (**Figure 3**) (Hasan et al., 2022). In the top-down strategy, the bulk materials are chopped and trimmed to obtain nanostructures using chemical, physical, and biological energy sources. On the other hand, the bottom-up approach involves synthesizing NPs from tiny basic units (layered in atomic, molecular, or cluster forms), which then grow into a nanoscopic particle using various chemical, physical and biological techniques (Hasan et al., 2022; Malik et al., 2022; Rahman et al., 2022).

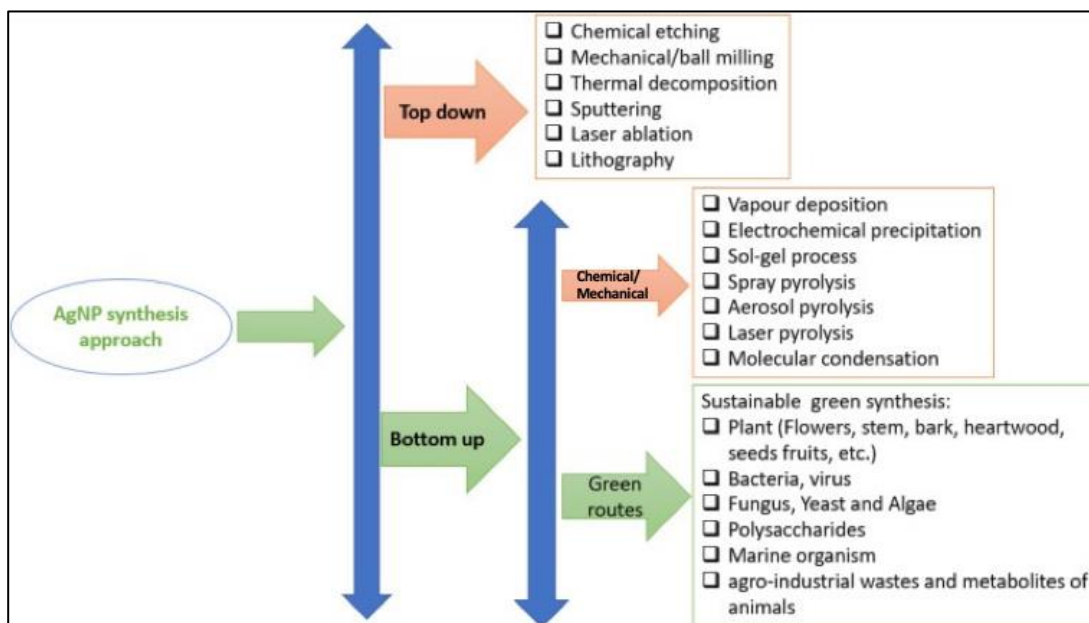


Figure 3. Different approaches for synthesizing AgNPs. Source: Hasan et al. (2022).

One of the most applied methods for the synthesis of AgNPs is the methodology proposed by Lee and Meisel (1982), based on studies of Turkevich, Stevenson, and Hillier (1951). These authors standardized the chemical synthesis by reducing the Ag^+ with sodium citrate and/or sodium borohydride in an aqueous solution to yield a colloidal and stable Ag dispersion (P. C. Lee & Meisel, 1982; Turkevich et al., 1951).

Currently, there is an increasing demand for green synthesis methods as an alternative to chemical and physical protocols. The green methods are considered efficient and environmentally friendly, also avoiding the use of high temperatures and energy (Sharma et al., 2009). These methodologies can employ polysaccharides (Biao et al., 2017), plant extracts (Sasidharan et al., 2020), or microorganisms (Devi & Joshi, 2015).

The synthesis of AgNPs with polysaccharides is accomplished by mixing soluble starch and AgNO_3 in an autoclave at 15 psi, 121 °C for 5 min (Vigneshwaran et al., 2006). The resulting yellow solution indicated the formation of nanoparticles, which was confirmed by UV-vis spectroscopy at 420 nm. This peak corresponds to the characteristic surface plasmon resonance (SPR) of AgNPs. The NPs presented different structures and shapes with an average diameter of 22.85 ± 12.94 nm, estimated by transmission electron microscopy (TEM). The iodometric titration and X-ray diffraction (XRD) spectrum confirmed the presence of AgNPs embedded in the amylose chain of soluble starch by the change color of UV-vis spectra at different intervals of iodometric titration and diffractions from the planes of face-centered cubic (FCC) Ag.

Biao et al. (2017) synthesized CS-functionalized Ag NPs. The synthesis was performed by mixing 10 mL of 0.7% CS solution with 25 mL of pure water and 1% AgNO₃ solution under pH 5.0. Then, the volume was adjusted to 40 mL, and the solution was kept in the dark for 40 min before being transferred into a Teflon-lined autoclave at 140°C for 4 hours. The UV-Vis absorption spectra indicated the presence of nanoparticles, mainly in a spherical shape. Fourier transform infrared spectroscopy (FTIR) analysis revealed that the primary amine and amide groups of CS have specific interactions with the surface of AgNPs. Furthermore, it found nanoparticles with an average diameter of 10 ± 5.4 nm, determined by TEM. (Biao et al., 2017).

AgNPs can also be synthesized by reducing a solution of AgNO₃ with the culture supernatants of *Aspergillus terreus* at room temperature (G. Li et al., 2012). The biosynthesis was an enzyme-mediated extracellular process evidenced by the supplement of reduced nicotinamide adenine dinucleotide (NADH) as a reducing agent. The authors verified that NADH alone was not sufficient for the redox reaction, suggesting that active molecules in the cell filtrate contributed to the reduction of Ag⁺ ions and stabilization of AgNPs. The formation of AgNPs was evidenced by a brown solution due to the SPR effect and reduction of AgNO₃, with a broad peak at 440 nm (SPR band) monitored by UV-vis spectroscopy. The AgNPs were spherical with sizes between 1 and 20 nm (obtained by TEM images). The XRD analysis showed characteristic peaks of crystalline planes from the FCC Ag.

In another study, AgNPs were synthesized by enzymatic reduction of AgNO₃ using the marine endophytic fungus *Penicillium polonicum*. (Neethu et al., 2020). Protein components and enzymes in the fungal extract reduced Ag⁺ ions and stabilized the AgNPs only in ambient light conditions, which may be attributed to the photosensitization of aromatic compounds in the fungal cell filtrate, culminating with the reduction of Ag⁺ ions. The optimum conditions were 8:2 ratio of AgNO₃:fungal extract, pH 7.0, and 60 minutes of reaction time. The AgNPs were spherical with sizes between 10 and 15 nm, determined by TEM micrographs, with an absorption peak at 430 nm measured by UV-vis spectroscopy. The AgNPs were impregnated in Central Venous Catheters (CVCs) to prevent biofilm formation and sepsis (generalized infection).

It is also possible to ascertain that some results and characterization techniques are complementary to each other, such as the XRD spectra and SPR bands in UV-vis spectroscopy. The XRD pattern of AgNPs generally presents peaks attributed to the (111), (200), (220), and (311) crystalline planes of the FCC structure (B. Das, Tripathy, et al., 2017; Neethu et al., 2020; Shameli et al., 2012). The UV-vis spectra of spherical AgNPs commonly show characteristic absorption peaks within the 420-450 nm range (J. Deng et al., 2015; Reicha et al., 2012). In the

case of faceted structures, such as Ag nanotriangles, typical absorption peaks can be found at ~342 nm, ~422 nm, and ~584 nm in the UV-vis spectra (G. Hu et al., 2018).

2.3.2 Antimicrobial activity

The antimicrobial activity and mechanism of action of AgNPs are generally attributed to the surface-binding to bacterial cells, ion release, and generation of oxidative stress that damage intracellular biomolecules and structures. The AgNPs catalyze the generation of free radicals and reactive oxygen species (ROS) that react with DNA components and cell membranes, thus hindering cell division and reproduction (Tang & Zheng, 2018).

Several studies report that the antimicrobial activity of AgNPs is dependent on their shape and size. The faceted structures, such as triangular and truncated triangular NPs, presented the strongest biocidal action compared to spherical and rod-shaped NPs due to the greater reactivity of the (111) lattice plane (Pal et al., 2007; Rojas-Andrade et al., 2015; Tak et al., 2015). AgNPs with less than 10 nm in size have demonstrated improved antibacterial effect because they are easily internalized within the cells, also possessing higher surface area (Agnihotri et al., 2014). Another parameter that improves the antibacterial action of AgNPs is the surface charge. Highly charged AgNPs (ZP ~ -40 mV) showed the highest antimicrobial activity against *C. albicans* and *S. aureus*. This system offers the advantage of a synergistic effect between these nanomaterials to enhance the resulting antimicrobial activity and biocompatibility (Bilal et al., 2017). In the case of AgNPs produced by electrochemical oxidation/complexation and UV irradiation reduction, higher processing and irradiation times led to an increase in the antibacterial activity against gram-positive *Bacillus thuringiensis* and gram-negative *P. aeruginosa* (Reicha et al., 2012). The correlation between AgNPs structures and antimicrobial properties is illustrated in **Figure 4**.

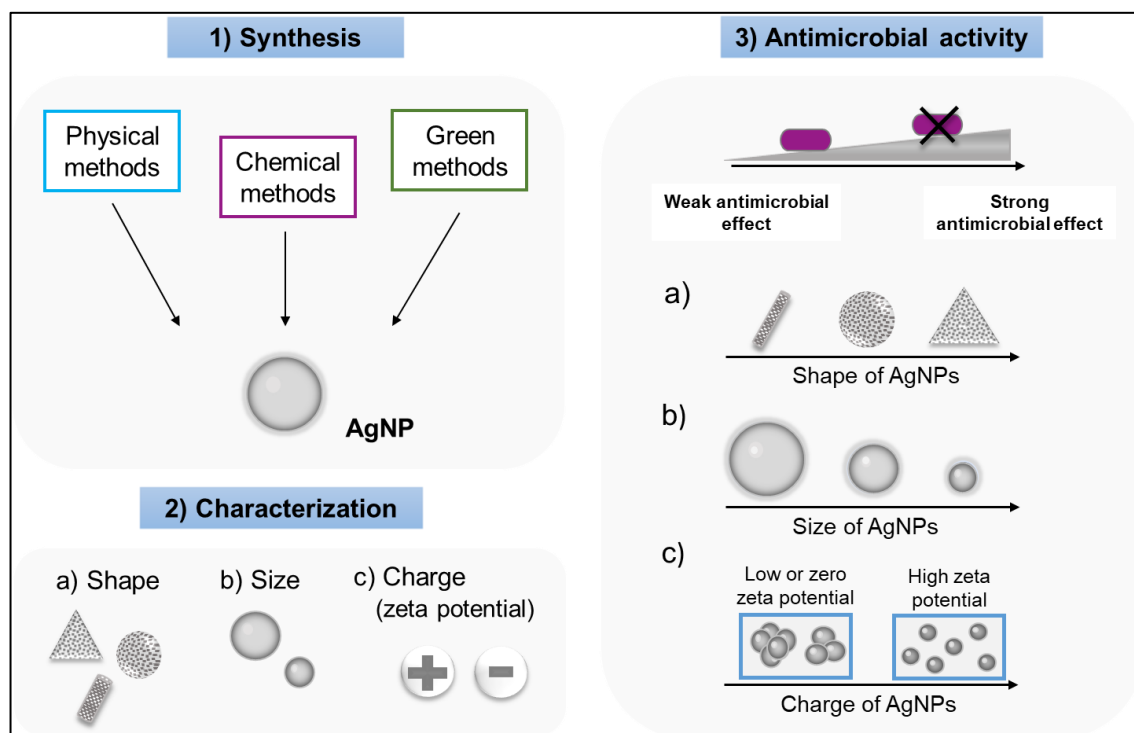


Figure 4. Correlation between physical and chemical characteristics of AgNPs and their antimicrobial effect. Source: Polinarski et al. (2021).

The antibiofilm and antibiotic potential of AgNPs combined to tetracycline, gentamicin, streptomycin, kanamycin, cephalosporin, and penicillin have been investigated against nosocomial microorganisms from standard strains and hospital isolates (Ebrahimi et al., 2018). The average MIC values were $3.1 \mu\text{g mL}^{-1}$ against *P. aeruginosa*, $6.25 \mu\text{g mL}^{-1}$ for *A. baumannii* and *E. faecalis*, and $12.5 \mu\text{g mL}^{-1}$ for *S. aureus*. The antimicrobial activity of AgNPs associated with antibiotics was enhanced against *P. aeruginosa* and *S. aureus*, suggesting a synergistic effect.

AgNPs were synthesized from a biological route using the endophytic fungus *A. terreus*, isolated from *Calotropis procera* (Rani et al., 2017). The AgNPs were oval and spherical with an average size of 16.54 nm. The antimicrobial activity was evaluated against twelve bacterial strains, including nine reference strains (*P. aeruginosa*, *Serratia marcescens*, *Shigella flexneri*, *S. typhi*, *E. coli*, *Proteus mirabilis*, *K. pneumoniae*, *E. faecalis*, and *S. aureus*) and three multi-resistant strains (*E. coli*, *K. pneumoniae*, and *P. aeruginosa*). For reference strains, inhibition zones in agar diffusion tests varied from 13.67 ± 0.58 to 16.67 ± 0.58 mm, while the MIC was in the range of 11.43 to 308 $\mu\text{g mL}^{-1}$. For multi-resistant strains, the inhibition zone varied from 13.33 ± 0.58 to 15.33 ± 0.58 mm, with MIC ranging between 34.2 and 308 $\mu\text{g mL}^{-1}$.

The antimicrobial activity and cytocompatibility of AgNPs were assessed on the surface of CVCs (Deng et al., 2015). Commercial CVCs were treated with a dopamine solution

(DCVCs) and immersed in different concentrations of AgNO_3 solution (1.0, 0.1, and 0.01 M) to produce AgNPs-coated DCVCs. The dopamine reduced Ag^+ ions without additional reducing agents and increased the hydrophilicity of DCVCs surface, promoting a uniform AgNPs adhesion. SEM images of the DCVCs surface showed spherical AgNPs with 30-50 nm size, evidencing the reduction of Ag^+ ions by polydopamine surface. The antimicrobial activity of AgNPs-coated DCVCs against *S. aureus* was dependent on the AgNPs concentration. Inhibition zones varied from 0.2 to 0.35 cm, even with the use of high bacterial concentration (10^8 CFU mL^{-1}). Cytocompatibility tests, assessed by water-soluble tetrazolium salts (WST-1) assays with MC3T3-E1 cells, showed that a higher density of AgNPs increased the cytotoxicity. The authors reported that DCVCs with the lowest AgNPs concentration (i.e., DCVCs treated with 0.01 M AgNO_3 solution) presented good antibacterial properties and biocompatibility.

Although many studies address the antimicrobial effect of AgNPs and highlight their potential use in medical devices, few studies report the AgNPs covering medical devices. Polydopamine was used to adhere the AgNPs to the CVC surface, and the antibiofilm action of these DCVC-AgNPs was tested against *A. baumannii* [131]. The antibacterial potential was confirmed by an inhibition zone of 23.9 ± 0.8 mm. Scanning electron microscopy (SEM) analysis revealed that in CVCs without AgNPs, a thick layer of biofilms was formed, while dispersion of biofilms and bacterial cell lysis was observed in DCVC-AgNPs at a minimum concentration of $32.2 \mu\text{g mL}^{-1}$.

A urinary catheter coated with AgNPs was tested against coagulase-negative *Staphylococci* (CoNS) (R. Thomas et al., 2015). The AgNPs were synthesized using AgNO_3 and microbial biomass from *Bacillus* sp. as a reducing agent. The urinary catheter was immersed into AgNPs suspension ($20 \mu\text{g mL}^{-1}$) for 24 h. Surface characterization of the modified catheter revealed the presence of AgNPs (8-21 nm size). The modified catheter exhibited antibiofilm property with a value of 90.8%, 90.2%, 89.8%, and 84% against *Staphylococcus haemolyticus* and different strains of *S. epidermidis*, respectively. TEM analysis confirmed morphological changes in bacterial cell wall after treatment with the modified catheter compared to a urinary catheter without AgNPs.

The literature reports the antimicrobial effect of AgNPs as free particles (Lok et al., 2007; Mansouri & Ghader, 2009; Rojas-Andrade et al., 2015) and adhered to a surface, such as in medical devices and catheters (Neethu et al., 2020; R. Thomas et al., 2015). The mechanism of action of AgNPs in these two approaches is similar and based on their attachment to the cell wall, diffusion to the intracellular matrix, release of Ag^+ ions, generation of ROS species, and reaction with DNA components that leads to cell death (Ogunsona et al., 2020; Salomoni et al.,

2017). **Table 2** describes the different synthesis methods and the resulting shape and size of AgNPs. The antimicrobial activity and tested microorganisms are also included.

Table 2. Synthesis methods of AgNPs, characteristics, and antimicrobial activity.

Route	Synthesis method*	Size and shape	Microorganisms and antimicrobial activity (MIC/MBC/D)**	Reference
Chemical	AgNO ₃ /NaBH ₄ /PVP/sodium citrate	5 - 100 nm Triangular (95%) Wire-like structure (5%)	NE	(Sun et al., 2003)
Chemical	AgNO ₃ /sodium citrate/ PVP/H ₂ O ₂ /NaBH ₄	31 ± 7 nm Triangular	NE	(Métraux & Mirkin, 2005)
Chemical	AgNO ₃ /sodium citrate/NaBH ₄ /light irradiation	40 - 110nm Triangular	NE	(Jia et al., 2006)
Chemical	AgNO ₃ /NaBH ₄ /sodium citrate/nitrogen/BSA	62 ± 18 nm Spherical	Ag-sensitive <i>E. coli</i> MIC: 2 nM Ag-resistant <i>E. coli</i> MIC: > 80 nM	(Lok et al., 2007)
Chemical	AgNO ₃ /hydrazine/sodium citrate	94 ± 8 nm Spherical, hexagonal, triangular	NE	(Mansouri & Ghader, 2009)
Chemical	AgNO ₃ /NaBH ₄ /sodium citrate/nitrogen/blue LEDs	4.76 ± 3.88 nm Spherical 10 - 40 nm Triangular nanoprisms after irradiation	<i>E. coli</i> MIC: 5.4 µg mL ⁻¹ (spherical) MIC: 4.9 µg mL ⁻¹ (triangular)	(Rojas-Andrade et al., 2015)
Green	AgNO ₃ /heparin	10 - 28nm Isotropic	NE	(Huang & Yang, 2004)
Green	AgNO ₃ /starch	22.85 ± 12.94 nm Spherical, pentagonal prism	NE	(Vigneshwaran et al., 2006)
Green	AgNO ₃ /tea and coffee extract	5 - 100 nm Spherical	NE	(Nadagouda & Varma, 2008)
Green	AgNO ₃ /starch/glucose	10 nm Spherical	NE	(Tai et al., 2008)
Biological	<i>A. terreus</i> /AgNO ₃	1-20 nm Spherical	<i>S. aureus</i> D: 16 ± 1 mm <i>P. aeruginosa</i> D: 12 ± 1 mm <i>E. coli</i> D: 13 ± 1 mm <i>C. albicans</i> D: 16 ± 1 mm <i>Candida krusei</i> D: 14 ± 2 mm <i>Candida parapsilosis</i> D: 13 ± 1 mm <i>Candida tropicalis</i> D: 14 ± 1 mm	(G. Li et al., 2012)

Green	Chitosan (DD > 85%)/silver and platinum plates/nitrogen/UV irradiation	2 - 16 nm Spherical	<i>B. thuringiensis</i> D: 47 mm <i>P. aeruginosa</i> D: 55 mm	(Reicha et al., 2012)
Green	Sugar/AgNO ₃ /PEG/nitrogen	11.23 ± 7.91 nm Spherical	<i>S. typhimurium</i> D: 11.51 ± 0.43 mm <i>S. aureus</i> D: 13.64 ± 0.29 mm	(Shameli et al., 2012)
Biological	AgNO ₃ / <i>Aspergillus tamarri</i> , <i>Aspergillus niger</i> , <i>Penicillium ochrochloron</i> (isolated from <i>Potentilla fulgens</i> L.)	3.5 ± 3 nm (<i>A. tamarri</i>) 8.7 ± 6 nm (<i>A. niger</i>) 7.7 ± 4.3 nm (<i>P. ochrochloron</i>) Spherical	NE	(Devi & Joshi, 2015)
Green	AgNO ₃ /dopamine	30 - 50 nm Spherical	<i>S. aureus</i> D: 2.0 - 3.5 mm	(J. Deng et al., 2015)
Green	AgNO ₃ /chitosan (DD 75-85%, MW 310 kDa)/ammonia water/nitric acid	10 ± 5.4 nm Spherical	<i>E. coli</i> MIC: 2.48 µg mL ⁻¹ MBC: 4.96 µg mL ⁻¹ <i>S. aureus</i> MIC: 4.96 µg mL ⁻¹ MBC: 9.92 µg mL ⁻¹ <i>C. albicans</i> MIC: 2.48 µg mL ⁻¹ MBC: 4.96 µg mL ⁻¹	(Biao et al., 2017)
Biological	<i>Ocimum gratissimum</i> /AgNO ₃ /PEG/BSA	20 ± 5 nm (<i>O. gratissimum</i>) 50 ± 10 nm (PEG) 40 ± 10 nm (BSA) Triangular	NE	(B. Das, Tripathy, et al., 2017)
Biological	<i>A. terreus</i> (isolated from <i>C. procera</i>)/AgNO ₃	16.54 nm Oval and spherical	<i>P. aeruginosa</i> D: 14.33 ± 0.58 mm <i>S. marcescens</i> D: 15.33 ± 0.58 mm <i>S. flexneri</i> D: 14.67 ± 0.58 mm <i>S. typhi</i> D: 16.67 ± 0.58 mm <i>E. coli</i> D: 15.67 ± 0.58 mm <i>P. mirabilis</i> D: 14.67 ± 0.58 mm <i>K. pneumoniae</i> D: 13.67 ± 0.58 mm <i>E. faecalis</i> D: 15.00 ± 1.00 mm <i>S. aureus</i> D: 15.67 ± 0.58 mm <i>E. coli</i> (MDR) D: 14.67 ± 0.58 mm <i>K. pneumoniae</i> (MDR) D: 13.33 ± 0.58 mm <i>P. aeruginosa</i> (MDR) D: 15.33 ± 0.58 mm	(Rani et al., 2017)

Biological	AgNO ₃ / <i>P. polonicum</i> (isolated from <i>C. antennina</i>)	0 - 55 nm Spherical and polyhedral	<i>S. typhi</i> MIC: 7.81 µg mL ⁻¹ MBC: 15.62 µg mL ⁻¹ D: 24.6 ± 0.8 mm	(Neethu et al., 2018)
Green	Ag ₂ C ₂ O ₄ /tea extract/chitin/UV irradiation	50 nm Triangular	<i>S. aureus</i> D: 19 - 21 mm <i>P. aeruginosa</i> D: 18 - 21 mm <i>A. baumannii</i>	(Saha et al., 2019)
Biological	<i>P. polonicum</i> /AgNO ₃ /polydopamine	10 - 15 nm Spherical	MIC: 15.6 µg mL ⁻¹ MBC: 31.2 µg mL ⁻¹ D: 23.9 ± 0.8 mm	(Neethu et al., 2020)
Chemical	AgNO ₃ /acetic acid	10 - 35 nm Spherical	<i>P. aeruginosa</i> MIC: 76 µg mL ⁻¹	(Rajivgandhi et al., 2019)
Biological	AgNO ₃ / <i>Myristica fragrans</i> extract	31.31 nm Spherical, hexagonal, triangular, rod	<i>B. subtilis</i> D: 11 mm <i>S. aureus</i> D: 13 mm <i>E. coli</i> D: 15 mm <i>P. aeruginosa</i> D: 21 mm	(Sasidharan et al., 2020)
Green	<i>Streptomyces</i> strain RB7AG inoculum/AgNO ₃ /Chitosan	NE	(Biofilm inhibition) <i>E. coli</i> : 33% (Biofilm inhibition) <i>S. aureus</i> : 26.5%	(Behera et al., 2025)

*AgNO₃ (silver nitrate), NaBH₄ (sodium borohydride), PVP (polyvinylpyrrolidone), BSA (bovine serum albumin), DD (degree of deacetylation), LED (light-emitting diodes), PEG (polyethylene glycol), Ag₂C₂O₄ (silver oxalate).

**MIC (minimum inhibitory concentration), MBC (minimum bactericidal concentration), D (inhibition zone diameter), NE (not evaluated), MDR (multidrug-resistant).

2.4 Chitosan-Silver Nanoparticles

Several studies have applied CS as a particle-forming polymer and surface coating material for polymeric, lipid, and metal-based nanoparticles and nanocomposites (Frank et al., 2020). Also, metal-based nanoparticles, such as gold, copper, zinc, and Ag have received increased interest in the clinical scenario due to their antimicrobial activity (Mohandas et al., 2018). The small size and large surface area of NPs facilitate their permeation through cell membranes and enhance their biological activity (Oryan et al., 2018). In this sense, CS incorporated with AgNPs (CS-AgNPs) has been investigated in biomedical and pharmaceutical areas because of their strong antimicrobial properties against pathogenic microorganisms and MDR bacteria (Akmaz et al., 2013; Lima et al., 2017; Rodríguez-Argüelles et al., 2011; Senthilkumar et al., 2019; Shah et al., 2019; Shao et al., 2017).

2.4.1 Synthesis methods

Different methods can be employed to produce CS-AgNPs depending on the ability of CS to act as a reducing agent and capping or stabilizing agents (**Figure 5**). The most used method is based on the mixture of a CS solution into previously synthesized AgNPs (Espinosa-Cristóbal et al., 2015; Liang et al., 2019). In this case, CS act as a capping agent, forming a shell and coating the AgNPs (Frank et al., 2020). CS is considered a suitable capping agent due to the presence of two reactive functional groups (NH_2 and OH) with a strong affinity to metal ions that facilitate the interaction of CS to metals (Begum et al., 2021; Nate et al., 2018). In CS-AgNPs, the metal AgNPs chelate the lone pair electrons provided by oxygen and nitrogen atoms of CS to disperse the AgNPs in CS (Niu et al., 2020). Alternatively, a CS solution can be added to an AgNO_3 solution when producing AgNPs (Hajji et al., 2019; Oryan et al., 2018). In this method, CS acts as a reducing agent of Ag^+ ions, and a redox reaction is believed to occur between the amino groups of CS and AgNO_3 . Polymers containing amino groups, can reduce metal ions. In the reaction, the nitrogen atom may lose one electron to form its oxidized form, and Ag^+ acquires the electron to become Ag^0 (Biao et al., 2017). This mechanism can be evidenced, for example, in the FTIR spectrum of CS-AgNPs by a displacement of absorption bands in the region of approximately 1600 cm^{-1} related to the NH_2 and CONH_2 groups of CS, indicating the attachment of Ag to nitrogen atoms (Venkatesham et al., 2014).

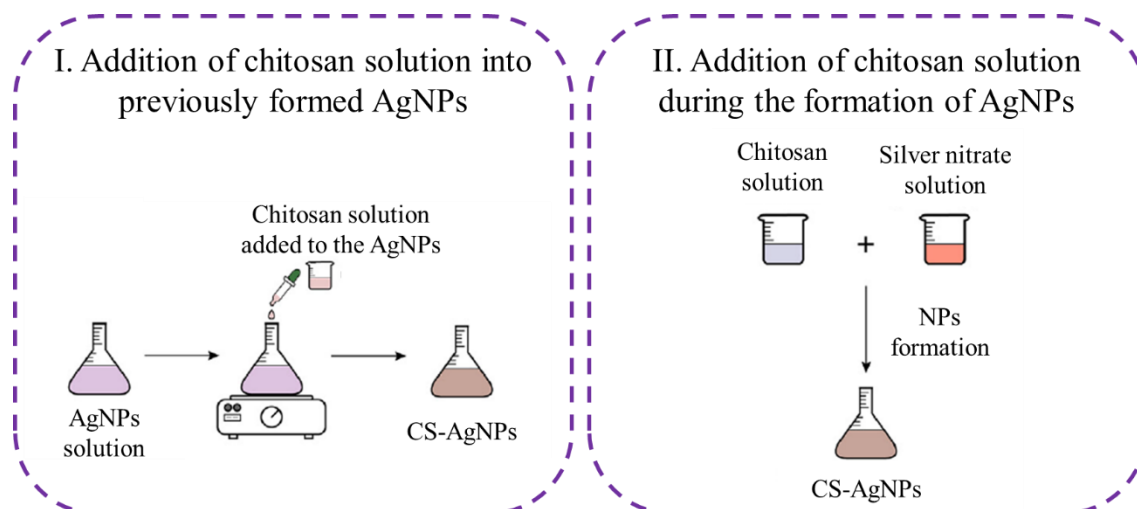


Figure 5. Main approaches to produce CS-AgNPs. Source: adapted from Frank et al. (2020).

Some techniques used to prepare AgNPs have been previously described, including the reduction of Ag^+ by chemical or biological methods. Aiming to produce CS-AgNPs by a green route, AgNPs were synthesized using ginger extract (*Zingiber officinale*) as a surfactant and ascorbic acid as a reducing agent (Holubnycha et al., 2018). The extract was obtained by mixing chopped ginger in a water-ethanol solution (1:1 ratio) and then combined with the acid ascorbic solution. This mixture was added to the aqueous solution of AgNO_3 . CS with DD of 82% was solubilized in 2% v/v acetic acid solution and incorporated into the AgNPs solution. The CS-AgNPs were spherical in shape with diameters between 10 and 12 nm. Another environmentally friendly method for the synthesis of CS-AgNPs is the use of *Talinum portulacifolium* leaf extract, a medicinal plant belonging to the Portulacaceae family, as a reducing agent (Senthilkumar et al., 2019). The AgNPs were prepared by incubating the plant extract and the AgNO_3 solution. Then, CS was solubilized in acetic acid solution and mixed with the AgNPs under magnetic stirring. The resulting CS-AgNPs were predominantly uniform with spherical and hexagonal shapes in the size range of 3.24 to 44.80 nm. The presence of AgNPs in the synthesized CS-AgNPs was confirmed by UV-Vis spectrophotometry at 387 nm (Holubnycha et al., 2018) and 419 nm (Senthilkumar et al., 2019), attributed to the characteristic SPR bands of AgNPs. Also, the XRD analysis evidenced the formation of crystalline materials with an FCC configuration, while the FTIR spectra showed characteristic N-H and O-H vibration bands that are typical of Ag and CS materials.

CS-AgNPs can be synthesized using TPP as a polyanion to agglutinate CS units and electrostatically attract Ag^+ ions inside the CS NPs, where they were reduced by the terminal glucosamine units (deacetylated units) of CS, forming stable CS-AgNPs (Rodríguez-Argüelles et al., 2011). TPP aqueous solution was added to the CS solution (DD 85%) in acetic acid 2%,

and the resulting solution was incorporated into the AgNO_3 aqueous solution. The CS-AgNPs presented oval and spherical shapes with an average hydrodynamic diameter of 78 ± 19 nm with small embedded AgNPs with 0.93 to 1.7 nm size.

CS-AgNPs were prepared by chemical reduction during the synthesis of AgNPs with a CS solution (Dananjaya et al., 2017). The AgNO_3 solution was added to the CS solution, used as a capping agent, and mixed with a Sodium borohydride (NaBH_4) solution that chemically reduced Ag^+ . The CS-AgNPs were spherical and the average size of embedded AgNPs, determined by TEM analysis, varied from 2 to 18 nm. The presence of AgNPs was confirmed by the characteristic plasmon band at 415 nm (UV-vis absorption spectra) and the FCC lattice (XRD diffractogram).

Similarly, CS-AgNPs were synthesized by chemical reduction of AgNO_3 using NaBH_4 as a reducing agent and CS as a capping agent (Lima et al., 2017). The UV-vis absorption spectra monitored the formation of CS-AgNPs. The plasmon absorption band, characteristic of AgNPs, was observed at 400 nm. The absorption bands of NH_2 and CONH_2 groups in CS shifted to different values in the FTIR spectrum of CS-AgNPs, indicating the binding of AgNPs to an N-H bond of CS. The CS-AgNPs presented an average diameter of 15 nm in TEM images.

During the green synthesis of CS-AgNPs, CS was used as both capping and reducing agents in alkaline pH (Nate et al., 2018). The amino groups of CS were activated using ammonia at pH 8, facilitating the binding of amino groups to Ag atoms. The method consisted of mixing an aqueous solution of AgNO_3 with a CS solution (1.0 and 2.0% w/v) under a nitrogen atmosphere. This solution was centrifuged and washed with acetone. The synthesis with 1 and 2% w/v CS resulted in spherical particles with average diameters of 2 and 6 nm, respectively. The XRD pattern evidenced the FCC structure of AgNPs. The FTIR spectra of CS-AgNPs gave a broad peak at 3327 cm^{-1} (N-H and O-H stretching), indicating a prevalence of the O-H group as the N-H group was binding to the Ag^0 , along with the disappearance of the band at about 1600 cm^{-1} (NH_2 bending). These results confirmed the formation of CS-AgNPs.

Rajivgandhi et al. reported the synthesis of CS-AgNPs using acetic acid (organic acid) as a reducing agent and CS as a stabilizing agent (Rajivgandhi et al., 2019). In this method, 100 mL of a CS solution (DD 75%, 0.7% w/v in 0.1 M acetic acid) was continuously stirred for 12 h. Then, 40 mL of AgNO_3 solution (0.05 M) was added, and the mixture was heated to $90\text{ }^\circ\text{C}$ until the color change, indicating the formation of CS-AgNPs. The AgNPs formed spherical aggregates surrounded by CS in a size range of 6 to 18 nm. The absorption peaks at ~ 3464 and $\sim 1643\text{ cm}^{-1}$ in FTIR spectra provided information on the interaction between AgNPs and the amino groups of CS.

CS-AgNPs were synthesized by adding different concentrations of AgNO₃ solution (0.02, 0.04, and 0.06 M) and NaOH solution (0.3 M) to an aqueous solution of CS (DD > 75%) at 95 °C (Akmaz et al., 2013). CS was used as a capping agent and mild reducing agent in the presence of NaOH at high temperatures. AgNPs were well dispersed in the CS matrix with average diameters ranging from 3 to 8 nm depended on the AgNO₃ concentration. The characteristic absorption peak, measured by UV-vis spectrophotometry, at 413 nm indicated the formation of AgNPs. The FTIR analysis revealed characteristic bands of OH and NH₂ groups commonly found in the spectra of CS-AgNPs. The XRD pattern of pure CS exhibited a characteristic peak at $2\theta = 20^\circ$, while that of CS-AgNPs showed another peak at 38° , corresponding to the (111) crystal plane of AgNPs, thus characterizing the crystalline structure of the material.

A simple route to produce CS-AgNPs employing CS and thymol as reducing and capping agents, respectively, has been reported (Manukumar et al., 2017). This synthesis was performed by dissolving 0.5 g of CS in 2% v/v acetic acid solution and 0.5 g of AgNO₃ in deionized water. The resulting solution was mixed and kept in an autoclave at 120 °C for 1 h. Then, 0.5 g of thymol was added to the solution and sonicated for 3 h. The thymol-loaded CS-AgNPs were characterized by UV-vis spectroscopy, FTIR, Dynamic Light Scattering (DLS), SEM, and XRD. An intense peak at 490 nm indicated the formation of AgNPs embedded in the CS matrix with a predominant spherical shape and an average diameter of 28.94 nm.

A composite material consisted of AgNPs, CS, and alginate was synthesized for biomedical purposes (Bilal et al., 2017). The biosynthesis of AgNPs was achieved by reducing Ag⁺ ions using the methanolic extract of *Euphorbia helioscopia*, while CS and alginate were used as capping agents. The AgNPs were incorporated into a sodium alginate solution, and this mixture was added dropwise into a CS-calcium chloride dispersion through a syringe needle to generate spherical beads of approximately 2 mm diameter. A characteristic absorption peak at 420 nm, belonging to the SPR phenomenon, confirmed the formation of AgNPs. TEM images revealed the spherical shape of AgNPs with diameters ranging from 50 to 70 nm.

2.4.2 Antimicrobial activity

The mechanism of bacterial growth inhibition by CS-AgNPs is still not clearly elucidated. Some studies have indicated that the strong bactericidal effect is attributed to the affinity of AgNPs with active groups on microbial surfaces. This interaction results in the release of Ag⁺ ions and generation of ROS that damage cell walls, modify the metabolic pathways, including the DNA replication and cell division (Asghar et al., 2020; Das et al., 2017;

Rajivgandhi et al., 2019). CS can react with both the cell wall and the external membrane of gram-positive and gram-negative bacteria (Asghar et al., 2020). The positively charged amino groups in CS and NCS interact with negatively charged components in bacterial cell wall, such as lipopolysaccharides and cell surface proteins, causing the disruption of cell wall and membranes, leakage of proteinaceous compounds, and other intracellular constituents from the microorganisms (Goy et al., 2009; Niu et al., 2020). Another mechanism is associated with the interaction between CS and cellular DNA, inhibiting the transcription of DNA, RNA, and protein synthesis, culminating with cell death (Shah et al., 2019). The CS-AgNPs also accumulate on the membrane surface and ion channels, being transported to the intracellular matrix by porins or endocytosis (Bondarenko et al., 2018; S. Kim & Choi, 2012; Milić et al., 2015). The proposed mechanism of action of CS-AgNPs against bacteria is illustrated in **Figure 6**.

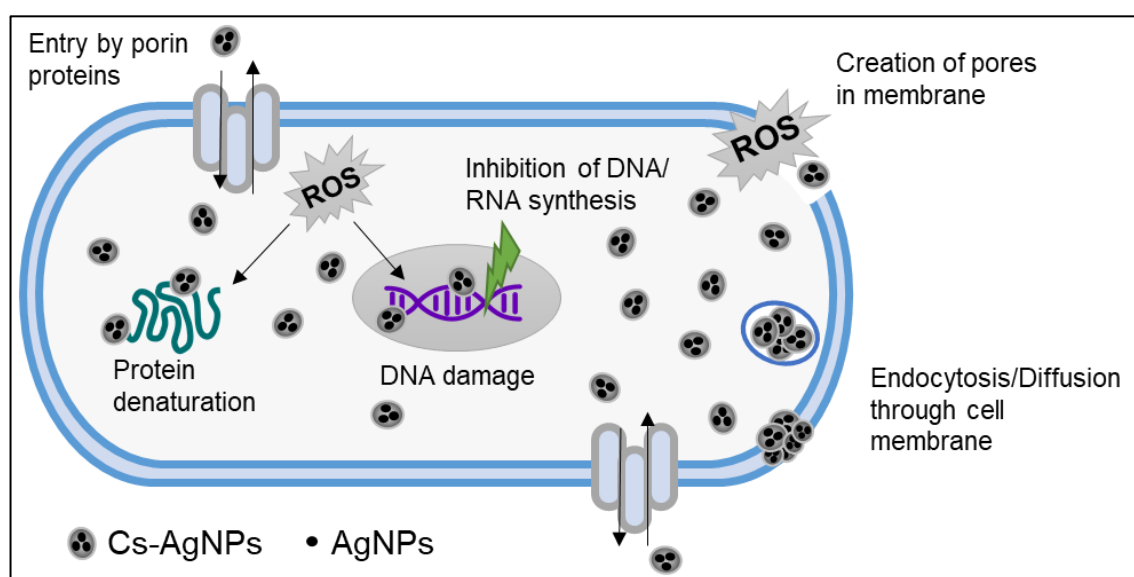


Figure 6. Schematic model of the antimicrobial mechanism of Cs-AgNPs. Source: Polinarski et al. (2021).

Gram-negative bacteria *P. aeruginosa* are commonly associated with hospital infections. The antimicrobial activity of Cs-AgNPs against ESBL-producing *P. aeruginosa* presented 92% of inhibition with a MIC of $50 \mu\text{g mL}^{-1}$ that was higher than AgNPs ($80 \mu\text{g mL}^{-1}$). This result was attributed to a synergistic effect between AgNPs and CS, as CS can control the release of Ag^+ ions and prolong the antimicrobial effect over time (Rajivgandhi et al., 2019).

Other studies have also reported the synergism between AgNPs and CS, resulting in improved antimicrobial activity compared to pure CS or AgNPs. The antimicrobial activity of

CS-AgNPs was evaluated against gram-positive bacteria (*S. aureus* and *E. faecalis*), gram-negative bacteria (*K. pneumoniae* and *P. aeruginosa*), and fungi (*C. albicans* and *Cryptococcus neoformans*). The antibacterial and antifungal effects were assayed with CS-AgNPs containing 1 and 2% w/v CS. The respective MIC values were: 0.4 and 1.56 mg mL⁻¹ (*E. faecalis*), 1.56 and 3.13 mg mL⁻¹ (*P. aeruginosa*), and 0.20 mg mL⁻¹ (*C. albicans* and *C. neoformans*). The synthesized Cs-AgNPs were more effective in inhibiting bacterial and fungal growth than pure CS and positive controls (neomycin and amphotericin B) (Nate et al., 2018). Likewise, the antibacterial effect of CS-AgNPs showed better results than pure CS and AgNPs against MRSA strains, with a MIC of 1.2 µg mL⁻¹ (Holubnycha et al., 2018). The maximum inhibition halo of 20 and 15 mm against *S. marcescens* and *E. coli*, respectively, was obtained for CS-AgNPs at the concentration of 50 µL (Senthilkumar et al., 2019).

CS-AgNPs were tested against fungi (*Candida glabrata* and *Saccharomyces cerevisiae*), gram-negative bacteria (*E. coli*, *K. pneumoniae*, and *Salmonella* spp.), and gram-positive bacteria (*S. aureus* and *B. cereus*). The antimicrobial activity, expressed in MIC, was 5 µg mL⁻¹ for fungi and ranged from 1.3 to 2.5 µg mL⁻¹ for gram-positive and gram-negative bacteria (Rodríguez-Argüelles et al., 2011). Similarly, the antifungal effect of CS-AgNPs against *Fusarium oxysporum* was higher than CS, with MIC values of 100 and 400 µg mL⁻¹, respectively (Dananjaya et al., 2017).

The antimicrobial properties of CS-AgNPs synthesized with different concentrations of AgNO₃ (0.02, 0.04, and 0.06 M) were evaluated against *E. coli*, *A. baumannii*, *S. aureus*, *E. faecalis*, *P. aeruginosa*, and *S. pneumoniae* (Akmaz et al., 2013). The CS-AgNPs presented a higher antibacterial effect than pure CS against all tested strains, and their efficiency was dependent on the AgNO₃ concentration. The lowest minimum bactericidal concentration (MBC) value (< 25 ppm) was found for *P. aeruginosa*.

The antimicrobial activity of CS-AgNPs was assessed against resistant bacteria gram-positive MRSA and gram-negative ESBL-producing *E. coli* and *K. pneumoniae* (Lima et al., 2017). The CS-AgNPs induced a potent effect against all tested microorganisms at MICs of 1.69 µg mL⁻¹ (MRSA and *E. coli*) and 3.38 µg mL⁻¹ (*K. pneumoniae*). These values were lower than the MICs of pure CS and AgNO₃ solutions and were attributed to the synergism between CS and AgNPs. CS stabilizes and prevents the agglomeration of AgNPs, also inducing positive surface charges and enhancing their binding to the negative charges on the cell wall.

Thymol-loaded CS-AgNPs showed antimicrobial activity comparable to the antibiotic streptomycin at 100 µg mL⁻¹. The maximum inhibition zones were 10.08, 10.00, 11.23 mm

against *S. aureus*, *S. epidermidis*, *S. haemolyticus*, and 9.28, 9.33, 12.03 mm against *S. typhimurium*, *P. aeruginosa*, and *S. flexneri*, respectively (Manukumar et al., 2017).

The antibacterial activity of CS-alginate-AgNPs was verified against *S. aureus*, *P. aeruginosa*, *K. pneumoniae*, *A. baumannii*, *Morganella morganii*, and *Haemophilus influenza*. These particles presented a significant log reduction compared to the initial bacterial count, especially at higher chitosan-alginate ratios of 2:1 and 2:2. The antibacterial mechanism of CS-alginate-AgNPs was related to the synergistic effect of the composite material that caused membrane disruption, ROS generation, and DNA damage (Bilal et al., 2017).

AgNPs coated with catechol-conjugated CS exhibited antibacterial activity against *S. aureus* and *E. coli* (X. Huang et al., 2017). The authors reported that gram-positive bacteria were killed by disorganization of the cell wall and leakage of cytoplasmic content, while a modification in membrane permeability induced by adsorption of catechol-conjugated CS-coated AgNPs was the primary mechanism of action in gram-negative bacteria. Catechol can be oxidized to benzoquinone that has antimicrobial properties (Amini, 2019; Lana et al., 2006; Magdziak et al., 2002).

Sámano-Valencia et al. evaluated the bactericidal efficiency of CS hydrogels with AgNPs, chlorhexidine, and gallic acid (Sámano-Valencia et al., 2013). AgNPs were spherical with 7 nm size. The CS gel with AgNPs presented an inhibition halo of 10.27 ± 2.13 mm against *Streptococcus mutans*. The CS-AgNPs hydrogel released Ag^+ ions during at least two weeks with a bactericidal activity comparable to the antibiotic chlorhexidine.

The antibiofilm activity of CS hydrogels loaded with AgNPs and ampicillin were tested against bacterial strains from clinical isolates associated with CVCs infections (Lopez-Carrizales et al., 2020). The hydrogels inhibited the biofilm formation of carbapenem-resistant *A. baumannii* (Log_{10} reduction of 10 ± 0.01), vancomycin-resistant *Enterococcus faecium* (Log_{10} reduction of 8.9 ± 0.02), oxacillin-resistant *S. epidermidis* (Log_{10} reduction of 7.8 ± 0.13), and β -lactam-resistant *Enterobacter cloacae* (Log_{10} reduction of 9.9 ± 0.11). These results showed a promising application of AgNPs-loaded CS hydrogels to prevent sepsis and thrombosis in medical devices.

The increased microbial inhibition of the nanocomposite CS-AgNPs, compared to NCS and AgNPs alone, results from the synergistic effect between CS and Ag, making this material an excellent candidate to combat and prevent biofilm formation in medical devices (Asghar et al., 2020; Niu et al., 2020). The antimicrobial activity of CS-AgNPs can be dependent on the release of Ag ions from AgNPs. However, few studies report prolonged results of Ag^+ release. Also, there is a lack of studies addressing the application of CS-AgNPs on the surface of

medical devices to prevent biofilm formation. These factors represent a challenge for the development of medical devices coated with CS-AgNPs because the release of Ag^+ ions should be maintained over the period of application within an effective concentration to kill bacteria without compromising the cytotoxicity (Neoh et al., 2017).

The antimicrobial effect of CS-AgNPs and its correlation with the synthesis methods and NPs properties are listed in **Table 3**.

Table 3. Synthesis methods of CS-AgNPs, characteristics, and antimicrobial activity.

Material*	Route	Synthesis method**	Particle size***	Microorganisms and antimicrobial activity (MIC/MBC/D/%)****	Reference
CS-AgNPs	Chemical	Chitosan (DD 85%)/TPP/AgNO ₃	CS-AgNPs: 78 ± 19 nm AgNPs: 0.93 - 1.7 nm	<i>C. glabrata</i> MIC: 5 µg mL ⁻¹ <i>S. cerevisiae</i> MIC: 5 µg mL ⁻¹ <i>E. coli</i> MIC: 1.3 µg mL ⁻¹ <i>K. pneumoniae</i> MIC: 2.5 µg mL ⁻¹ <i>Salmonella</i> spp. MIC: 2.5 µg mL ⁻¹ <i>S. aureus</i> MIC: 2.5 µg mL ⁻¹ <i>B. cereus</i> MIC: 1.3 µg mL ⁻¹	(Rodríguez-Argüelles et al., 2011)
CS-AgNPs	Green	<i>T. portulacifolium</i> extract/AgNO ₃ /chitosan (DD: 75-58%)	3.24 - 44.80 nm	<i>E. coli</i> D: 15 mm <i>S. marcescens</i> D: 20 mm <i>E. faecalis</i> MIC: 0.4 - 1.64 µg mL ⁻¹	(Senthilkumar et al., 2019)
CS-AgNPs	Green	AgNO ₃ (0.1 M)/chitosan (0.5, 1.0, 2.0% v/v)/nitrogen/acetone	0.2 - 14 nm	<i>P. aeruginosa</i> MIC: 1.53 - 3.13 µg mL ⁻¹ <i>C. albicans</i> MIC: 0.2 - 1.5 µg mL ⁻¹ <i>C. neoformans</i> MIC: 0.20 µg mL ⁻¹	(Nate et al., 2018)
CS-AgNPs + CTAB	Green	Ginger extract/ascorbic acid/AgNO ₃	4 - 34 nm	<i>S. aureus</i> MIC: 3.3 µg mL ⁻¹	(Holubnycha et al., 2018)
CS-AgNPs	Chemical	Chitosan (310 kDa, DD 75%)/acetic acid/AgNO ₃	6 - 18 nm (embedded AgNPs)	<i>P. aeruginosa</i> MIC: 50 µg mL ⁻¹	(Rajivgandhi et al., 2019)
CS-AgNPs	Chemical	Chitosan/AgNO ₃ /NaBH ₄ /glycerol/water	10 - 100 nm	<i>S. aureus</i> D: 27 mm <i>P. aeruginosa</i> D: 23.33 mm MRSA D: 15.33 mm	(Shah et al., 2019)
CS-AgNPs	Chemical	Chitosan/acetic acid/NaOH/AgNO ₃	20 - 59 nm	NE	(Anusuya & Banu, 2016)
CS gel-AgNPs	Chemical	AgNO ₃ /gallic acid/NaOH/chitosan/acetic acid/glycerol	7 nm (embedded AgNPs)	<i>Streptococcus mutans</i> D: 10.27 mm	(Sámano-Valencia et al., 2013)
CS-AgNPs-GO	Chemical	Chitosan/AgNO ₃ /NaBH ₄ /graphite	10 - 30 nm (embedded AgNPs)	<i>S. aureus</i> MIC: 1.09 µg mL ⁻¹	(Marta et al., 2015)
CS-AgNPs	Chemical	Chitosan (DD 75%)/AgNO ₃ /NaOH	3 - 8 nm	<i>S. pneumoniae</i> : MBC: 50 - 200 ppm <i>A. baumannii</i> MBC: 25 - 100 ppm <i>E. coli</i> MBC: 50 - 200 ppm <i>P. aeruginosa</i> MBC: <25 - 100 ppm <i>E. faecalis</i> MBC: 25 - 100 ppm	(Akmaz et al., 2013)

CS NF-AgNPs	Electrospinning	Chitosan (DD 90%, MW 200-400 kDa)/PEO/glutaraldehyde/AgNO ₃	168 - 185 nm	<i>S. aureus</i> MBC: 25 - 100 ppm <i>Porphyromonas gingivalis</i> D: 12 - 16 mm <i>Fusobacterium nucleatum</i> D: 13 - 20 mm	(Shao et al., 2017)
CS-AgNPs	Chemical	AgNO ₃ /NaBH ₄ /chitosan	14.9 ± 7.5 nm	<i>S. aureus</i> MIC: 1.69 µg mL ⁻¹ <i>E. coli</i> MIC: 1.69 µg mL ⁻¹ <i>K. pneumoniae</i> MIC: 3.38 µg mL ⁻¹	(Lima et al., 2017)
Thymol-CS-AgNPs	Chemical	Chitosan/AgNO ₃ /thymol	28.94 nm	<i>S. aureus</i> D: 10.08 mm <i>S. epidermidis</i> D: 10 mm <i>S. haemolyticus</i> D: 11.23 mm <i>S. typhimurium</i> D: 9.28 mm <i>P. aeruginosa</i> D: 9.33 mm <i>S. flexneri</i> D: 12.03 mm	(Manukumar et al., 2017)
CS-AgNPs	Chemical	Chitosan (DD 75-85%)/AgNO ₃	7.01 - 33.09 nm	<i>S. aureus</i> : 100% <i>P. aeruginosa</i> : 100%	(Luna-Hernández et al., 2017)
CS-AgNPs	Chemical	AgNO ₃ /NaBH ₄ /chitosan	18 nm	<i>P. oxysporum</i> MIC: 3.38 µg mL ⁻¹	(Dananjaya et al., 2017)
CS-Ag-Ms	Chemical	AgNO ₃ /glutaraldehyde/PVP/chitosan	264 ± 5.6 nm	<i>E. coli</i> : 80 - 90% <i>Penicillium citrinum</i> : 60 - 90% <i>S. cerevisiae</i> : 80 - 98% <i>S. aureus</i> D: 18 - 21 mm <i>B. cereus</i> D: 11 - 13 mm	(Liang et al., 2019)
CS-AgNPs	Chemical	Chitosan (DD 75%)/polyvinyl acetate/AgNO ₃	190 - 200 nm	<i>Micrococcus luteus</i> D: 17 - 20 mm <i>Salmonella enterica</i> D: 11 - 17 mm <i>E. coli</i> D: 11 - 15 mm <i>S. typhimurium</i> D: 9 - 10 mm <i>K. pneumoniae</i> D: 16 - 17 mm	(Hajji et al., 2019)
CS-AgNPs	Chemical	AgNO ₃ /NaBH ₄ /chitosan	15 nm	NE	(Oryan et al., 2018)
CS-AgNPs	Green	<i>Saccharum officinarum</i> /AgNO ₃ /chitosan	10 - 60 nm (embedded AgNPs)	<i>Streptococcus faecalis</i> D: 10.6 mm <i>B. subtilis</i> D: 13.5 mm <i>Klebsella planticola</i> D: 13.2 mm <i>P. aeruginosa</i> D: 15 mm	(Paulkumar et al., 2017)
CS-AgNPs	Green	Pineapple crown extract/AgNO ₃ /chitosan	10 - 60 nm	<i>E. coli</i> D: 12.2 mm <i>E. coli</i> : 99.68% <i>S. aureus</i> : 98%	(Shahid-ul-Islam et al., 2019)

CS NF-AgNP	Electrospinning	Chitosan (DD 90%, MW 200-400 kDa)/PEO/AgNO ₃	200 nm	<i>S. aureus</i> : H = 16 - 17 mm	(Shao et al., 2019)
CS-AgNPs	Chemical	Chitosan (DD 88%)/methanol/benzaldehyde/HCl/ethanol/AgNO ₃	10 - 25 nm (embedded AgNPs)	<i>E. faecalis</i> MIC: 0.24 µg mL ⁻¹ <i>S. epidermidis</i> MIC: 0.12 - 0.24 µg mL ⁻¹ <i>E. coli</i> MIC: 0.49 - 6.50 µg mL ⁻¹ <i>E. coli</i> D: 7.8 mm <i>S. aureus</i> D: 8.2 mm	(Elmehbad & Mohamed, 2020)
CS-AgNPs					
CS-RB-AgNPs-GO-0.5	Green/chemical	Chitosan (DD 75-85%, LMW)/ AgNO ₃ (4 mM); Graphene Oxide (0.5 – 1.5wt%)/ RT-APM (Room Temperature Atmospheric Pressure Microplasma)/helium gas	NI	<i>E. coli</i> D: 8.2 mm <i>S. aureus</i> D: 8.8 mm	(Su et al., 2021)
CS-RB-AgNPs-GO-1.5				<i>E. coli</i> D: 8.1 mm <i>S. aureus</i> D: 9.1 mm	
Bcp*C@AgNPs	Green/Chemical	Chitosan (0.25 g)/AgNO ₃ (0.25)/ 0.25 g of (4-(4-methoxybenzoyl) piperazine-1-yl) (2,3-dihydrobenzo[b][1, 4] dioxin-3-yl) methanone which was synthesized from 1-(1,4-benzodioxane-2-carbonyl) piperazine (1) and phenyl isocyanate (2).	34.2 nm	<i>Staphylococcus aureus</i> (MRSA) D: 14.20±0.04 <i>Bacillus cereus</i> D: 6.40±0.03 <i>Enterobacter faecalis</i> D: 4.98±0.04 <i>Escherichia coli</i> D: 5.96±0.01 <i>Salmonella typhimurium</i> D: 5.80±0.01 <i>Shigella flexneri</i> D: 6.82±0.03	(Karthik et al., 2021)
CS-Ag	Green	<i>Streptomyces</i> strain RB7AG inoculum/AgNO ₃ /Chitosan	65 nm	<i>E. coli</i> : 70% <i>S. aureus</i> : 50.5%	(Behera et al., 2025)

*CS (chitosan), AgNPs (silver nanoparticles), CTAB (cetrimonium bromide), GO (graphene oxide), NF (nanofiber), PVP (polyvinylpyrrolidone); Bcp*C@AgNPs (benzodioxane coupled piperazine decorated chitosan silver nanoparticle) .

**DD (degree of deacetylation), TPP (sodium tripolyphosphate), AgNO₃ (silver nitrate), NaBH₄ (sodium borohydride), NaOH (sodium hydroxide), PEO (polyethylene oxide); LMW (low molecular weight).

*** NI: Not informed

****MIC (minimum inhibitory concentration), MBC (minimum bactericidal concentration), D (inhibition zone diameter), NE (not evaluated), MRSA (methicillin-resistant *S. aureus*).

As presented in this review, CS, NCS and AgNPs have been widely studied as alternative antimicrobial agents. The CS-AgNPs possess strong antimicrobial effects against reference and multidrug-resistant strains of gram-positive and gram-negative bacteria and fungi due to a synergistic effect between CS and Ag combined in a nanomaterial. The literature reports that NPs greater than 10 nm can accumulate on the cell wall of bacteria, compromising their permeability and efficacy. Also, NPs smaller than 10 nm are easily transported and incorporated into the bacterial cell, damaging intracellular mechanisms, including DNA replication, leading to cell death (Holubnycha et al., 2018). However, the physicochemical properties of Cs-AgNPs, which can also be dependent on the synthesis methods and type of materials, are important parameters when designing new antimicrobial materials, as they can influence the resulting bactericidal effect.

New antimicrobial materials have been investigated worldwide as a strategy to prevent bacterial biofilm formation in medical devices, such as catheters, probes, and dressings, as a complementary treatment or targeting a complete substitution of antibiotics. Several bacterial strains have shown resistance to antibiotics and other antimicrobial agents. CS, NCS and AgNPs have been widely used in pharmaceutical and biomedical areas due to their strong antimicrobial properties. The combined and synergistic effects of CSNPs and AgNPs in a nanocomposite CS-AgNPs provide a potential antimicrobial nanomaterial to prevent infections caused by pathogens resistant to commonly used antibiotics. Although Cs-AgNPs show great promise as materials for medical devices, future efforts should focus on addressing key aspects to optimize their use in biomedical applications. These include understanding the mechanisms behind the sustained release of Ag^+ ions, particularly on coated surfaces like CVCs, to ensure effective antimicrobial concentrations with minimal toxicity; enhancing the surface coverage of CS-AgNPs on medical devices to promote robust antimicrobial action and prevent biofilm formation without posing risks to patients; and developing or refining green, environmentally friendly, cost-effective synthesis methods to produce CS-AgNPs with strong antimicrobial properties.

2.4.3 Toxicity of CS-AgNPs

Even though CS-AgNPs are promising candidates to fight bacterial adhesion and biofilm formation, there are still some concerns related to their toxicity. To assure they safe use in humans, understanding their biocompatibility and non-toxic effects are fundamental. The characteristics are primarily determined by the surface properties of the material, which are

assessed by evaluating the intensity of any adverse host response (Ghasemi et al., 2025). CS and its derivatives are widely used by the industries, including medicine, biomedicine, pharmacy, among others. Because of that, there are numerous data on CS being used in therapeutics and medical treatments, suggesting a safe profile from in vivo studies in rats, mice and even in humans (Kean & Thanou, 2010; Koumentakou et al., 2024; Zoe et al., 2023).

Despite decades of use, the toxicity of AgNPs remains ambiguous and continues to be a topic of discussion. Depending on the synthesis approach, AgNPs can exhibit certain levels of toxicity, particularly when fabricated with chemical reducing agents (e.g., sodium borohydride). The Lowest Observed Adverse Effect Level (LOAEL) for silver nanoparticles AgNPs refers to the lowest dose at which adverse effects are first observed in a given system. Studies have shown that long-term exposure to AgNPs can lead to renal ultrastructural damage, renal inflammation, and altered expression of cell survival factors, contributing to necrotic cell death in the kidneys (Nie et al., 2023). These toxic effects are dose-dependent, but even doses of AgNPs below the LOAEL, when administered repeatedly over a long period, can still cause significant damage and pathological changes in affected organs. In this way, minimizing exposure to AgNPs and carefully controlling their dosage is crucial to preventing toxicity, especially in everyday life. In this regard, the green synthesis of AgNPs, using natural reducing agents such as plant extracts (e.g., green tea, aloe vera, or curcumin) or biopolymers like chitosan, can offer a safer alternative by potentially reducing their toxicity while maintaining their desired properties (Chauke et al., 2025; S. Thomas et al., 2024).

Ghasemi et al. (2025) synthesized AgNPs and CS-AgNPs through a green synthesis approach using *Ferula gummosa Boiss* gum extract. The synthesized nanoparticles were evaluated for their potential as antimicrobial, antioxidant, and anticancer agents. The cytotoxicity of both nanoparticle types was assessed via MTT and hemolysis assays on normal and cancer cell lines. The results demonstrated significant antibacterial activity against *Staphylococcus aureus* and *Bacillus subtilis*. Additionally, the antioxidant assays showed great free radical scavenging activity, with CS-AgNPs displaying superior antioxidant properties. Hemolysis assays indicated low hemolytic activity for both AgNPs and CS-AgNPs. Moreover, the MTT assay showed a significant cytotoxic effect of the AgNPs and CS-AgNPs on the MCF-7 breast cancer cell line, suggesting promising potential for pharmaceutical applications.

CHAPTER 3: ARTICLE 1

Effect of chitosan and other reducing agents on the synthesis and antimicrobial activity of silver nanoparticles for antimicrobial coatings

Marcos Antonio Polinarski^{a,b,c,d}, Rayssa Cristina Souza^e, Juliana Bernardi Wenzel^e, Phuong Nguyen-Tri^{a,b}, Helton José Alves^{c,d}

^a Laboratory of Advanced Materials for Energy and Environment, Université Du Québec à Trois-Rivières (UQTR), 3351, Boul. des Forges, C.P. 500, Trois-Rivières, Québec, G9A 5H7, Canada.

^b Department of Chemistry, Biochemistry and Physics, Université du Québec à Trois-Rivières (UQTR), 3351 Bd des Forges, Trois-Rivières, QC G8Z 4M3, Canada.

^c Renewable Materials and Energy Laboratory (LABMATER), Federal University of Paraná (UFPR – Setor Palotina), R. Pioneiro, 2153, 85950-000, Palotina, PR, Brazil.

^d Postgraduate Program in Environmental Engineer and Technology, Federal University of Paraná (UFPR – Setor Palotina), R. Pioneiro, 2153, 85950-000, Palotina, PR, Brazil.

^e Medicine Course – Toledo Campus, Federal University of Paraná, Rodovia PR 182, S/N, Km 320/321, CP 2028, Toledo-PR, 85919-899 Brazil.

Abstract

Due to the rise of multidrug-resistant bacteria there is an increasing global demand for the development of novel antimicrobial materials, particularly in the medical field where infection control is important. In this sense, AgNPs have emerged as a promising alternative, due to their antimicrobial activity, and have been extensively studied for different applications, such as wound dressings and coatings for medical devices. This study investigated the use of various reducing agents, including TPP, heparin, glucose, NCS, and CS combined with different AgNO₃ proportions in the synthesis of AgNPs. The nanoparticles were characterized by DLS, SEM, UV-Vis spectroscopy, and energy-dispersive X-ray spectroscopy (EDS), and their antimicrobial and antibiofilm activity was tested against *S. aureus*. Significant differences in NPs morphology and antimicrobial activity were observed based on the choice of reducing agent and the AgNO₃ concentration. Among the reducing agents, CS stood out due to its dual role as a reducing and stabilizing agent. The sample synthesized with CS and the lowest amount of AgNO₃ showed a high inhibition zone and effective biofilm prevention. In contrast, samples synthesized with higher concentrations of AgNO₃ displayed larger particle sizes and reduced antimicrobial effectiveness. The results suggested that the use of CS as both reducing and stabilizing agent, increased AgNPs antimicrobial properties, making the synthesized particles a promising candidate for the development of antimicrobial coatings in medical devices.

Keywords: nanotechnology; bacterial infections; coating; biofilm inhibition; chitosan.

3.1 Introduction

Medical devices, such as CVCs, are widely used in hospital procedures for hemodynamic monitoring, drug delivery, parenteral nutrition, phlebotomy and long-term intravenous therapies (Buonsenso et al., 2022; Torres et al., 2024). Despite their essential role, medical devices can also serve as entry points for microorganisms, which significantly increasing the risk of bacterial and hospital-acquired infections (Polinarski et al., 2021). Catheter-related bloodstream infections (CRBSIs) and catheter-associated urinary tract infections (CAUTIs) are among the major complications associated with the use of medical devices. More than 75% of hospital-acquired urinary tract infections (UTIs) are related to catheter use, with CAUTIs representing one of the most frequent nosocomial infections that contribute to high morbidity and mortality rates worldwide (L. Liu et al., 2024).

There are four main pathways by which the catheter may contribute to infections: (1) the tip of the catheter and the surrounding skin tract may become colonized by normal microbiota from the skin; (2) the lumen of the catheter can become contaminated; (3) an infection in another part of the body may spread to the catheter through the bloodstream; and (4) the catheter lumen may be contaminated by an infusate (Puplampu et al., 2024). Gram-positive bacteria, such as *S. epidermidis* and *S. aureus*, and gram-negative bacteria such as *Pseudomonas aeruginosa* and *Klebsiella pneumoniae*, along with fungal pathogens like *Candida albicans* are among the leading contributors to CRBSIs (Buonsenso et al., 2022; W. Li et al., 2024; Puplampu et al., 2024).

The colonization these pathogens on catheter surfaces leads biofilm formation. Biofilms are communities of cells encased within an exopolymeric matrix, attached to a surface and they are known for their resistance to antimicrobial treatments and host immune defenses, making infections particularly difficult to treat (Paharik & Horswill, 2016). In this way, nanotechnology has emerged as a promising alternative by integrating antimicrobial agents, such as AgNPs, into medical devices coatings to inhibit bacterial adhesion, biofilm formation, and reduce the risk of hospital-acquired infections.

Ag is a well-known metal due to its optical, electrical, catalytic, and antimicrobial properties, especially in the form of AgNPs and their related nanocomposites (Polinarski et al., 2021). These materials offer significant advantages, including strong antibacterial activity, biocompatibility, and the ability to be easily coated on various surfaces to combat different

pathogens (Dridi et al., 2024). Their antimicrobial action primarily stems from the release of Ag^+ ions, which inhibit respiratory enzymes in bacterial and fungal cells (Sklyar et al., 2023).

There are several protocols to synthesize AgNPs, with the most common methods involving chemical approaches by the reduction of Ag^+ ions to Ag^0 using organic or inorganic reducing agents, such as sodium citrate ($\text{Na}_3\text{C}_6\text{H}_5\text{O}_7$) or sodium borohydride (NaBH_4) (Polinarski et al., 2021). However, there is a growing interest in green synthesis methods, which are environmentally friendly alternatives that avoid the use of toxic chemicals. These methods utilize natural reducing agents, such as polymers, monosaccharides and polysaccharides, which offer a sustainable approach to producing AgNPs (Jiang et al., 2023).

Tripolyphosphate (TPP), a commonly used cross-linker, plays a significant role in nanoparticle synthesis by acting as a stabilizing agent. TPP is known for its ability to interact with positively charged polymers, such as CS, to enhance the structural stability of nanoparticles, facilitating their uniform formation and size control (Rodríguez-Argüelles et al., 2011). Heparin (HP), a naturally occurring polysaccharide, composed of (1,4)-linked hexosamine and uronic acid units, is an intravenous anticoagulant and can act as both a reducing and stabilizing agent in the biosynthesis of metallic NPs (Huang & Yang, 2004; Jiang et al., 2023). Glucose (Glc), a monosaccharide, is also frequently used in green synthesis approaches as a mild reducing agent, in association with CS (Abdelgawad et al., 2014).

CS, a biopolymer derived from chitin, has garnered significant attention due to its biocompatibility and natural antimicrobial properties. In the synthesis of AgNPs, CS acts as both reducing and stabilizing agent, enhancing their antimicrobial properties through its synergistic effect with Ag (Polinarski et al., 2021). These compounds not only contribute to the synthesis of nanoparticles but also add functional properties, making the resulting nanocomposites highly effective for preventing microbial contamination and biofilm formation.

Therefore, this study aimed to explore different synthesis methods for AgNPs using various reducing agents, including TPP, HP, Glc, and CS, to identify which offers the most effective antimicrobial performance and possesses attractive characteristics for application as an antimicrobial agent in the medical field. The synthesized AgNPs were characterized by DLS, SEM, UV-Vis spectroscopy, and EDS to evaluate their particle size, morphology, and optical properties. Furthermore, their antimicrobial activity was assessed to identify the most promising formulations for preventing microbial contamination and biofilm formation. Based on the synergistic properties between CS and AgNPs, it is hypothesized that CS used as both a reducing and stabilizing agent will result in AgNPs with enhanced antimicrobial and antibiofilm activity, compared to other reducing agents.

3.2 Material and Methods

3.2.1 Synthesis of Silver Nanoparticles (AgNPs)

The literature presents several protocols to synthesize AgNPs, in which, most of them are based on physical or chemical methods, using different reducing agents, such as CS, TPP, NaBH₄, Glc and HP (Abdelgawad et al., 2014; Anjugam et al., 2018; Huang & Yaung., 2004; Rodríguez-Argüelles et al., 2011). This study employed different methods for synthesizing AgNPs, that included the use of different reducing agents, following different protocols suggested by the literature with modifications. The schematic representation of the syntheses is presented in **Figure 7**.

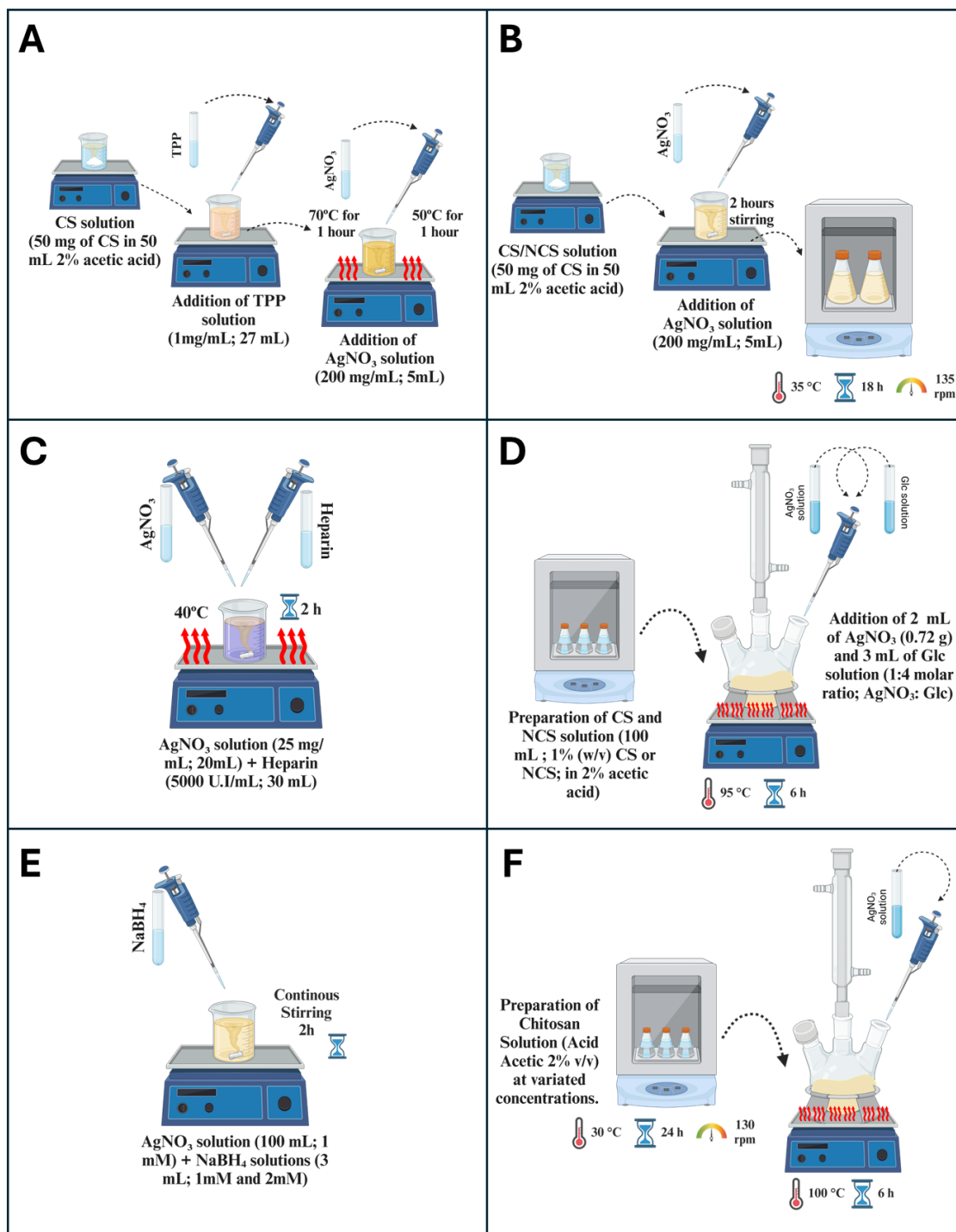


Figure 7. Schematic representation of the different methods used for the synthesis of AgNPs. A) represents the procedures for the Chitosan-TPP mediated Synthesis; B) represents the Chitosan and Nanochitosan-based synthesis; C) represents the Heparin-mediated synthesis; D) represents the Chitosan/Nanochitosan-Glucose Synthesis; E) represents Sodium Borohydride Reduction Synthesis; F) represents the Synthesis of AgNPs with variation in the amount of chitosan and AgNO₃.

3.2.1.1 Chitosan-TPP mediated Synthesis

The synthesis was adapted from the methodology proposed by Rodríguez-Arguelles et al. (2011). Briefly, 50 mg of CS (90% DD; 173 kDa) was dissolved in 50 mL of 2% acetic acid under magnetic stirring until complete dissolution. Then, 27 mL of a TPP solution (1mg/mL) was added dropwise to the CS solution and stirred for an additional 40 minutes. Subsequently, the solution was heated to 70°C, and 5 mL of a AgNO₃ solution (200 mg/mL) was added dropwise while maintaining continuous stirring. After one hour, the temperature decreased to 50°C and stirring continued for an additional hour. The final solution was maintained under agitation at 135 rpm and 35°C for 18 hours. The resultant sample was labeled as CS-TPP-Ag.

3.2.1.2 Chitosan and Nanochitosan-based synthesis

CS (90% DD, 180 kDa) and NCS (75% DD, 18 kDa) were used as both reducing and stabilizing agents. Briefly, a 50 mL CS solution (50 mg in 2% acetic acid) was prepared under magnetic stirring (450 rpm) at room temperature (25°C). After fully dissolved, 5 mL of an aqueous AgNO₃ solution (200 mg/mL) was added dropwise, and stirring was continued for an additional 2 hours. The mixture was then transferred to an incubator at 35°C with stirring at 135 rpm for 18 hours. The same procedure was performed with NCS. The resulting samples were labeled CS-Ag and NCS-Ag, respectively.

3.2.1.3 Heparin-mediated synthesis

This synthesis was carried out following the procedures proposed by Huang and Yang, with modifications, with heparin as reducing agent (Huang & Yaung, 2004). In this way, a 20 mL AgNO₃ (25mg/mL) solution was added to a 150.000 UI heparin solution. The mixture was heated to 40 °C and kept under magnetic stirring for 2 hours. A color change was observed in the solution from transparent to dark purplish. The resulting sample was labelled HP-Ag.

3.2.1.4 Chitosan/Nanochitosan-Glucose Synthesis

AgNPs were synthesized via chemical reduction of AgNO₃ using Glc as the reducing agent and CS (90% DD, 180 kDa) and NCS (75% DD, 18 kDa) as the stabilizing agent, following a modified version of the methodology proposed by Abdelgawad et al. (2014)(Abdelgawad et al., 2014). A 100 mL solution of 1% (w/v) CS or NCS in 2% acetic acid was heated to 95 °C under stirring. Separately, 0.72 g of AgNO₃ was dissolved in 2 mL ultrapure water and added dropwise to the polymer solution. A 3 mL glucose solution was then added at a 1:4 molar ratio (AgNO₃:Glc). The reaction mixture was maintained at 95 °C with continuous

stirring for a total of 6 hours. The resulting samples were labelled as CS-Glc-Ag and NC-Glc-Ag.

3.2.1.5 Sodium Borohydride Reduction Synthesis

Two syntheses using NaBH_4 were performed to evaluate the efficacy of alternative approaches against the conventional technique. The methodology consisted in preparing a 100 mL AgNO_3 1 mM solution under magnetic stirring followed by the addition of NaBH_4 solutions (1mM and 2mM). Then, the mixture was stirred for 2 hours at room temperature (Anjugam et al., 2018). A color change from transparent to light yellow was observed, indicating the formation of AgNPs. The resultant samples were named NaBH_4 -Ag 1:1 and NaBH_4 -Ag 2:1.

3.2.1.6 Synthesis of AgNPs with variation in the amount of chitosan

An adapted version of the methodology proposed by Rodriguez-Argueles et al. (2011) was used, with modifications in the amounts of AgNO_3 and CS, in the absence of TPP. In this protocol, the AgNO_3 amount was fixed at 200 mg, while CS amounts varied (50, 100, 150, 200, and 250 mg). Briefly, a 50 mL solution of 2% acetic acid containing CS (DD 95%, MM: 173 kDa) was stirred at 130 rpm and 30°C for 24 hours. The solution was transferred to a three-neck flask and heated to 100°C under reflux using an ultrathermostatic bath. Then, 5 mL of an AgNO_3 solution was added dropwise, and the mixture was maintained at 100°C for 6 hours. Subsequently, the mixture was cooled to ambient temperature and stored in darkness. The samples were named CS50Ag200, CS100Ag200, CS150Ag200, CS200Ag200, and CS250Ag200.

3.2.1.7 Synthesis of AgNPs with variation in the amount of AgNO_3

The same protocol from the previous section was followed, but the CS amount was fixed at 150 mg, while different AgNO_3 masses (75, 150, 250, 500, 1000, and 1500 mg) were used. The resulting samples were labeled as CS150Ag75, CS150Ag150, CS150Ag250, CS150Ag500, CS150Ag1000, and CS150Ag1500.

3.2.2 Characterizations

Following synthesis, all AgNPs were thoroughly characterized using multiple analytical techniques. Dynamic Light Scattering (DLS, Nanoptic 90, BETTERSIZER) was employed to determine the hydrodynamic diameter of the nanoparticles. UV-Visible Spectroscopy (Cary 60 UV-Vis, Agilent) was utilized to assess the optical properties of the AgNPs by analyzing their Surface Plasmon Resonance (SPR) peak position, intensity, and shape, which are indicative of

nanoparticle size, aggregation state, and concentration. Scanning Electron Microscopy (SEM, Vega3, TESCAN) was conducted to visualize the morphological characteristics of the nanoparticles, allowing for the evaluation of shape, surface texture, and particle aggregation. Additionally, Energy Dispersive X-ray Spectroscopy (EDS, OXFORD) was performed to confirm the elemental composition.

3.2.3 Antimicrobial Assays

All synthesized AgNPs were submitted to antimicrobial testing to verify their potential in inhibiting bacteria growth, against *S. aureus* (ATCC 6538). The antimicrobial analysis was divided into two different steps: agar diffusion method and antibiofilm testing.

3.2.3.1 Agar diffusion method

Pure *S. aureus* strains were cultured in Mueller-Hinton (MH) broth, and the bacterial suspensions were standardized to a turbidity of 0.5 McFarland, corresponding to approximately 1.5×10^8 CFU/mL. Sterile paper disks were impregnated with 10 μ L of each AgNP solution. Subsequently, 100 μ L of the standardized bacterial suspension was evenly spread on MH agar plates, and the prepared disks were carefully placed on the agar surface. The plates were then incubated at 37°C for 18-24 hours, after which the diameter of the inhibition zones around each disk was measured in millimeters.

3.2.3.2 Antibiofilm Activity Test

An antibiofilm activity test was conducted for the sample who had the highest inhibitory activity. The bacterial strain *S. aureus* (ATCC 6538) was standardized to a 0.5 McFarland turbidity standard (approximately 1.5×10^8 CFU/mL) and incubated in Mueller-Hinton (MH) broth for 24 hours at $37 \pm 2^\circ\text{C}$. Polyurethane central venous catheter (CVC) segments were used as the surface for biofilm formation. In 96-well microtiter plates, 20 μ L of the bacterial inoculum, 100 μ L of Mueller-Hinton Broth (MHB), and 100 μ L of the AgNPs solution were added, followed by the placement of the catheter segments into the wells. A second method was employed to assess biofilm inhibition, in which the catheter segments were pre-treated by immersion in AgNP solution for 30 minutes, then transferred into the 96-well microtiter plate containing 20 μ L of the bacterial suspension and 100 μ L of MHB. The plates were incubated for five days at $37 \pm 2^\circ\text{C}$. SEM analysis was used to observe biofilm formation and bacteria.

3.3 Results and Discussion

3.3.1 Particle Size Distribution

The DLS results (**Figure 8**) of AgNPs synthesized under different conditions showed variations in their hydrodynamic size. The samples were prepared with various concentrations of AgNO_3 and CS, as well as variations with other stabilizers such as TPP, HP, Glc, NCS and NaBH_4 .

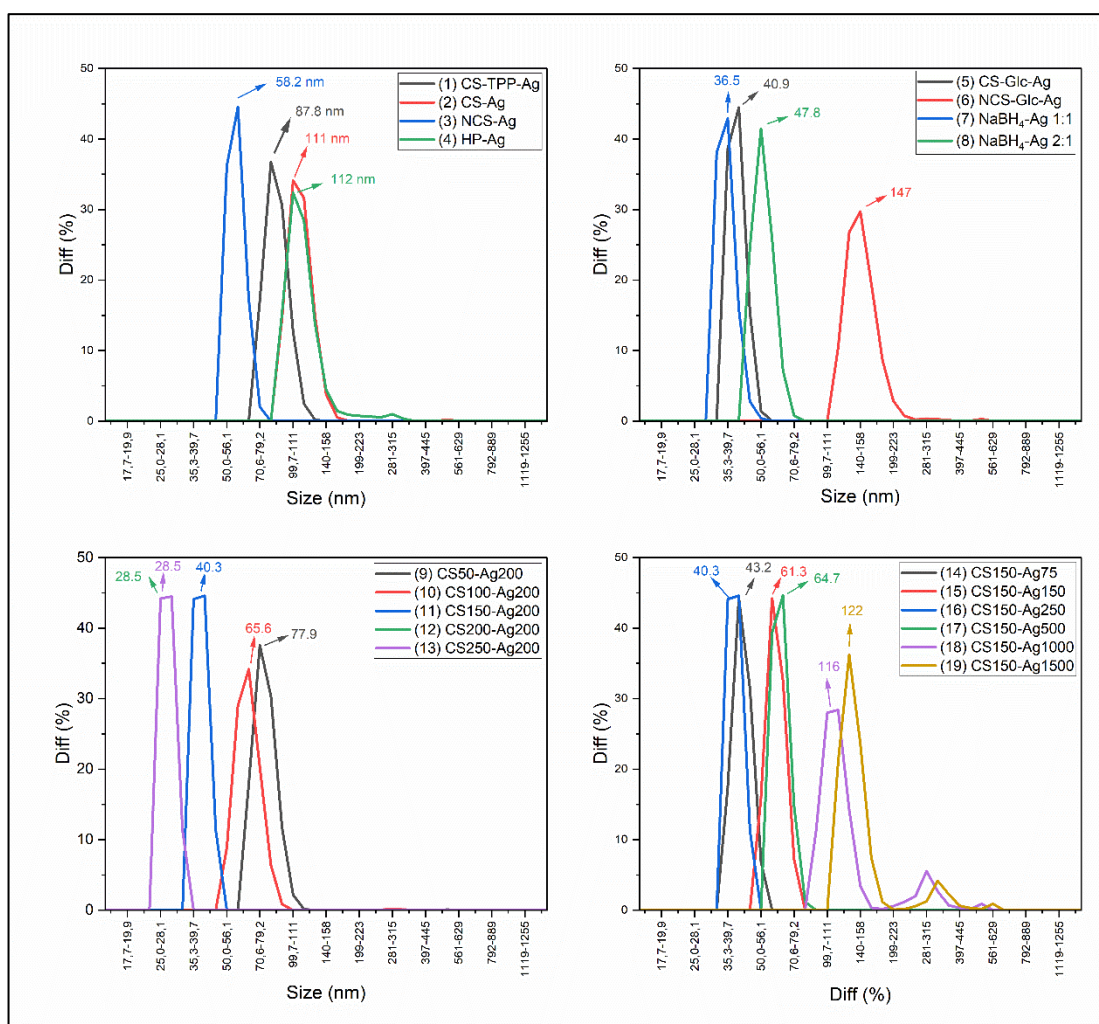


Figure 8. Particle size distribution of AgNPs synthesized using different methods measured by DLS in number distribution mode.

The sample CS-TPP-Ag resulted in a particle size of 87.8 nm. It is believed that TPP played a significant role in controlling the growth and stabilization of AgNPs, yielding particles of moderate size (Rodríguez-Argüelles et al., 2011). The presence of TPP likely enhanced particle uniformity by acting as a polyanionic template, attracting Ag^+ ions and assisting in the controlled reduction and nucleation process. Sample CS-Ag was synthesized using CS as both

the reducing and stabilizing agent. The DLS results showed an average particle size of 111 nm, which is larger than that of CS-TPP-Ag. The sample synthesized with NCS (75% DD, 18 kDa), resulted in particles of 58.2 nm. The heparin-mediated synthesis, corresponding to sample HP-Ag, resulted in particles with a hydrodynamic size of 112 nm, similar to the CS-Ag sample. Heparin is a large polysaccharide with numerous functional groups, and in this synthesis, it acted as both a reducing and stabilizing agent (Huang & Yaung., 2004).

CS-Glc-Ag presented a relatively small particle size of 40.9 nm, which reflects the stabilizing effect of CS when combined with Glc that led for controlled reduction and particle formation (Abdelgawad et al., 2014). However, NCS-Glc-Ag, synthesized with NCS, resulted in particles with an average size of 147 nm. While NCS has a smaller molecular weight and larger surface area, which in other syntheses has been associated with smaller particle sizes, in the presence of glucose, it appears to promote a greater degree of aggregation, leading to the formation of larger nanoparticles. In contrast, the samples synthesized with NaBH_4 as reducing agent, NaBH_4 -Ag 1:1 and NaBH_4 -Ag 2:1, presented an average particle size of 38.5 and 47.8 nm respectively. The small particles size is due to the strong reducing power of NaBH_4 , which leads to rapid AgNPs nucleation. However, the uncontrolled reduction and lack of stabilizing polymers may contribute to less consistent particle formation and possible aggregation over time.

The DLS of samples synthesized with CS and a fixed mass of AgNO_3 (200 mg) demonstrated the efficiency of CS as a reducing agent, once all samples presented a particle size distribution below 100 nm. The sample CS50-Ag200 exhibited a hydrodynamic size of 77.9 nm, whereas CS100-Ag200 showed a size of 65.6 nm. Doubling the CS mass in the synthesis resulted in a noticeable reduction in nanoparticle size in suspension. Further increases in CS concentration led to even smaller particle sizes, as observed in samples CS150-Ag200 (40.3 nm), CS200-Ag200 (28.5 nm), and CS250-Ag200 (28.5 nm).

The DLS analysis of samples CS150-Ag75, CS150-Ag150, CS150-Ag250, CS150-Ag500, CS150-Ag1000, and CS150-Ag1500 showed variations in particle size, as the amount of AgNO_3 increased. CS150-Ag75 and CS150-Ag250 exhibit the smallest particle sizes (43.2 nm and 40.3 nm, respectively), which suggests that lower AgNO_3 concentrations favor the formation of smaller nanoparticles, where the limited availability of Ag^+ allows for controlled nucleation and growth. In contrast, samples CS150-Ag150 and CS150-Ag500 display relatively similar sizes (61.3 nm and 64.7 nm). At higher concentrations of AgNO_3 , an increase in particle size was noticed. Sample CS150-Ag1000 showed an average size of 116 nm, while sample

CS150-Ag1500 presented particles of around 122 nm. This suggests that an excess of Ag^+ significantly promotes nanoparticle growth.

Overall, the DLS analysis showed that all synthesized samples presented nanoparticles distribution with a hydrodynamic size distribution below 150 nm. Among the samples, the ones synthesized with only CS and AgNO_3 stands out, as they favored the production of smaller particles, while requiring a smaller number of materials during the synthesis. Additionally, as a natural biopolymer, CS facilitates film formation, enhancing AgNPs antimicrobial properties due to its synergistic effect which is highly beneficial for coating applications (Polinarski et al., 2021). Furthermore, the use of CS stands out as an efficient and sustainable strategy, contributing to the development of multifunctional coatings that combine enhanced adhesion and antimicrobial activity (Polinarski et al., 2024).

3.3.2 Optical Properties and Plasmonic Behavior

The UV–Vis absorption spectrums of all synthesized AgNPs solutions are shown in **Figure 9**. The primary peak in the range of 400-500 nm corresponds to the surface plasmon resonance (SPR) band of AgNPs (Lalegani & Seyyed Ebrahimi, 2020).

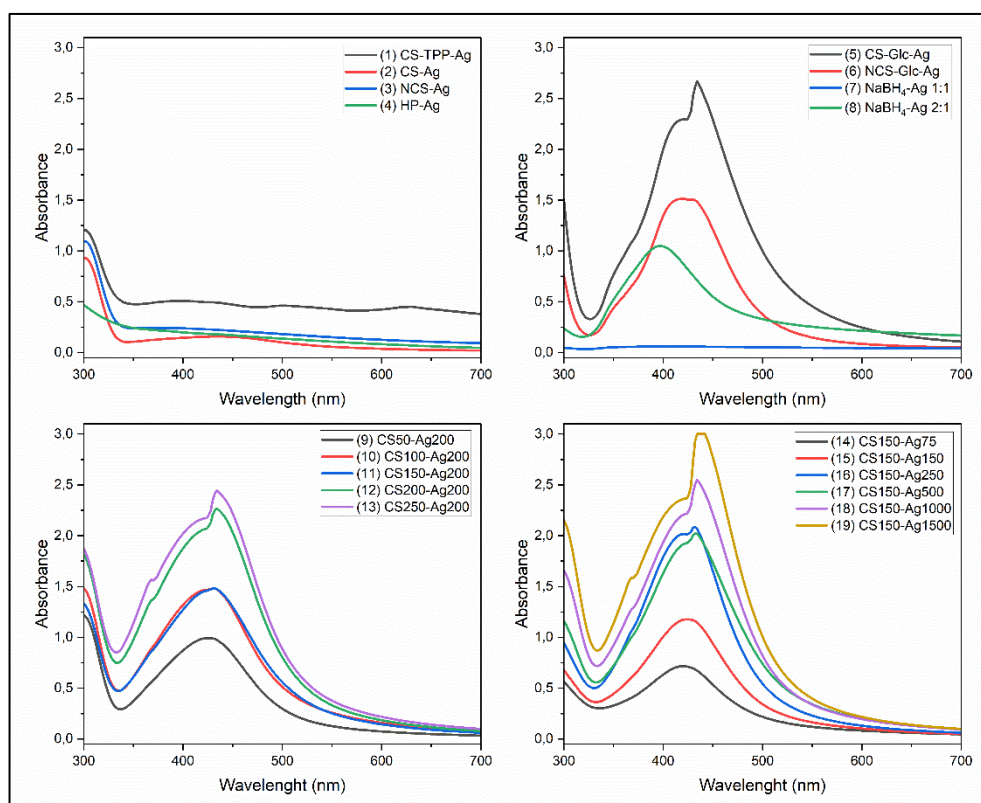


Figure 9. UV-Vis absorption spectra of AgNPs synthesized by various methods.

The UV-Vis spectra for the samples CS-TPP-Ag, CS-Ag, NCS-Ag, and HP-Ag, did not show characteristic SPR peaks, which are typically expected for AgNPs. The absence of SPR peaks may be due to several factors, including particle aggregation, size distribution, and morphology, which could shift the SPR to longer wavelengths beyond the measured range (H. Y. Kim et al., 2014; S. H. Lee & Jun, 2019). For instance, larger or anisotropic particles, such as the triangular shapes observed in CS-Ag (**Figure 10, B**), could shift the SPR towards longer wavelengths, potentially into the near-infrared region depending on the degree of anisotropy and size (S. H. Lee & Jun, 2019). Similarly, highly dispersed or irregularly shaped particles, as seen in sample NCS-Ag (**Figure 10, C**), may not produce well-defined SPR peaks due to broadening or suppression of the resonance signal. Additionally, the overall concentration of nanoparticles in the solutions could have been insufficient to produce a detectable SPR signal in the visible range.

Despite the absence of an SPR peak, the DLS results and the coloration of the nanoparticle solutions suggest the formation of AgNPs. This indicates that while the nanoparticles were successfully synthesized, their optical properties were altered in a way that prevented typical SPR detection. A similar study using CS and TPP as stabilizers also reported the formation of AgNPs confirmed by DLS and microscopy, but no UV-Vis analysis was conducted to detect SPR (Rodríguez-Argüelles et al., 2011). This reinforces the possibility that particle morphology, size, or distribution may interfere with SPR detection, even when nanoparticles are present.

The sample CS-Glc-Ag showed a peak at 434 nm with an absorbance of 2.67, and a second peak at 422 nm with an absorbance of 2.29. While the sample NCS-Glc-Ag showed a peak at 420 and 430, with a lower absorbance signal (1.50 and 1.51, respectively). Although the SPR of both samples were very similar, a slight blue shift was observed for NCS-Glc-Ag, with lower absorbance. This difference can be attributed to differences in the physicochemical and optical properties of CS and NCS, associated to the interactions with glucose, which can alter the UV-Vis absorbance characteristics (Guo et al., 2024).

The UV-Vis spectra of NaBH₄-Ag 1:1 and NaBH₄-Ag 2:1 showed SPR peaks at 398 nm and 402 nm, respectively. Shorter SPR wavelengths are typically associated with smaller nanoparticle sizes, which is consistent with the sizes reported by DLS. However, NaBH₄-Ag 1:1 exhibited lower absorbance (0.06), likely reflecting the presence of fewer or less well-dispersed nanoparticles. In contrast, NaBH₄-Ag 2:1 showed a higher absorbance (1.04), suggesting a greater concentration of well-dispersed nanoparticles.

The samples synthesized with varying CS amounts and a fixed amount of AgNO_3 showed a redshift in the main SPR peak, shifting from 426 nm in sample CS50-Ag200 to 434 nm in sample CS250-Ag200, followed by a progressive increase in absorbance intensity (from 0.99 to 2.44). It is possible that increasing CS alters the optical properties of the AgNPs, potentially due to the formation of a denser CS layer around the particles. Although DLS data showed the presence of smaller particles, the thicker CS coating can increase the effective refractive index near the surface of the nanoparticles, leading to redshift even if the core particle size is reduced. The increase in absorbance suggests a higher concentration of AgNPs. Furthermore, the samples CS200-Ag200 and CS250-Ag200, which contain the highest CS concentrations, exhibited an additional peak, potentially indicating the formation of non-spherical AgNPs (Guo et al., 2024).

The samples CS150-Ag75 to CS150-Ag1500, were synthesized varying AgNO_3 content with a fixed CS amount. Similarly to the samples synthesized with fixed AgNO_3 content, the UV-Vis analysis showed a redshift in the main SPR peak, from a wavelength of 420 nm to 468 nm, when increasing the amount of Ag precursor. Sample CS150Ag75 showed a peak at 420 nm with an absorbance of 0.71 suggesting smaller, well-dispersed nanoparticles. This lower absorbance indicates less aggregation and better stability, corroborating the DLS data where this sample exhibits one of the smaller particle sizes. When relating UV-Vis data with DLS, it is possible to suggest that higher amounts of AgNO_3 led to increased polydispersity, larger particle sizes and potentially less stable colloidal systems.

3.3.3 Morphological and Elemental Analysis

The sample CS-TPP-Ag (**Figure 10, A**) exhibited a particular structure, where Ag particles are embedded within a CS matrix, consistent with the findings of Rodríguez-Argüelles et al. (2011), which reported a “pudding with raisins” structure. During the CS-TPP-Ag synthesis, CS acted as a reducing and stabilizing agent, while TPP attracted Ag^+ ions into the CS, enhancing reduction and controlling AgNP size and uniformity (Rodríguez-Argüelles et al., 2011).

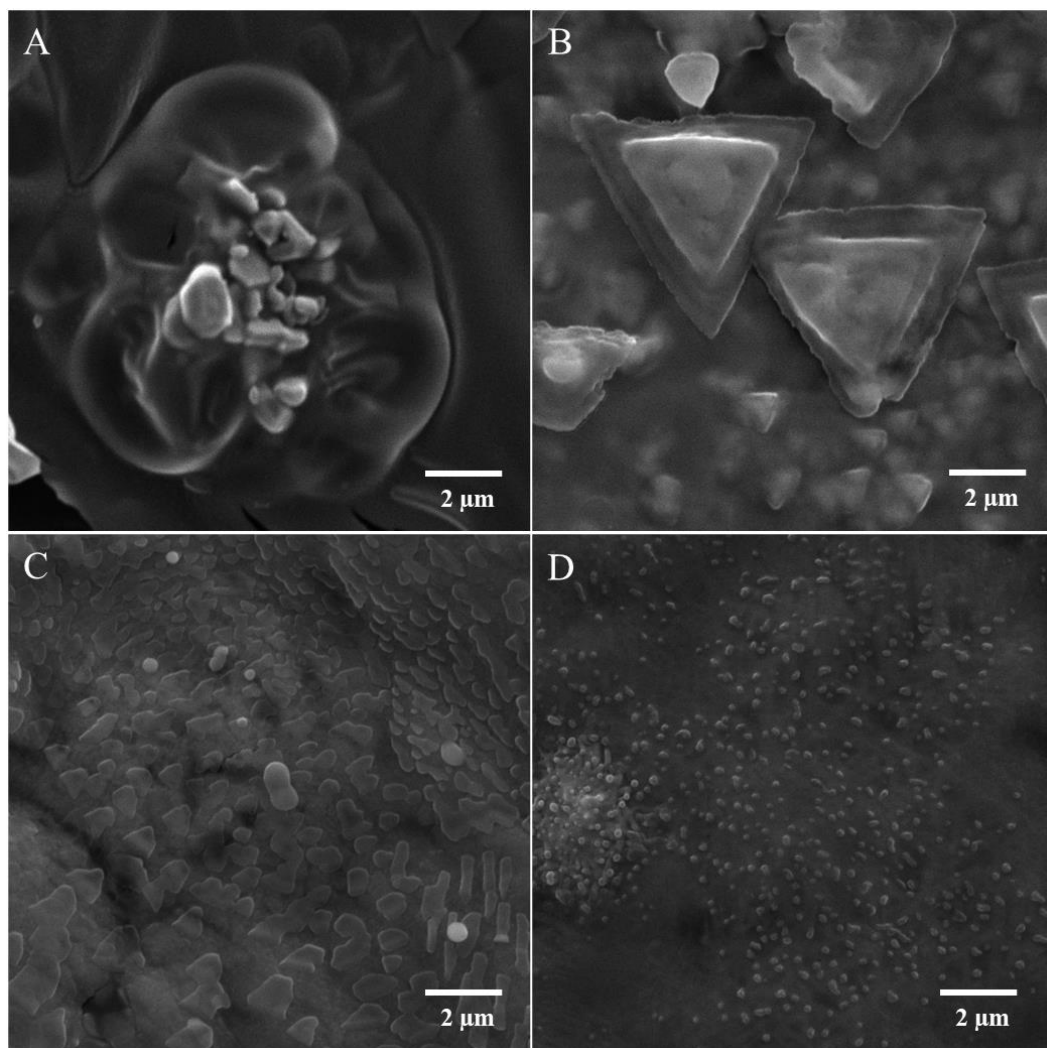


Figure 10. SEM images of samples: A) CS-TPP-Ag, B) CS-Ag, C) NCS-Ag, and D) CS-HP-Ag.

The SEM micrograph of the sample CS-Ag (**Figure 10, B**), synthesized with CS and AgNO_3 at room temperature, showed a diverse morphology, including triangular and irregularly shaped particles. These anisotropic structures suggest that CS may have influenced the directional growth of the particles. The formation of triangular particles, which are known to shift SPR peaks to longer wavelengths, may explain the absence of an SPR peak in the UV-Vis spectrum (Lee & Jun, 2019).

In the sample NCS-Ag (**Figure 10, C**), the SEM micrograph showed the presence of smaller and dispersed particles without distinct shapes, which are consistent with the DLS findings. The SEM micrograph of sample HP-Ag (**Figure 10, D**) showed the presence of small, spherical, and well-dispersed nanoparticles, with some signs of aggregation. The role played by heparin as a reducing agent, possibly supported the formation of uniformly sized particles with low aggregation. However, despite the different morphologies, none of the samples presented in **Figure 10** produced SPR signals.

The morphology of the sample CS-Glc-Ag is presented in **Figure 11, A**. The micrograph showed the presence of Ag particles with spherical morphology with some signs of aggregation. The DLS showed an average particle size of 40.9, while UV-Vis analysis showed the presence of two peaks in the range of 422 and 432 nm, with a high absorbance, which indicates the formation of well-defined particles, potentially spherical. In contrast, the sample NCS-Glc-Ag (**Figure 11, B**), showed a slightly greater tendency to aggregation, which relates to the larger particle size presented in the DLS analysis.

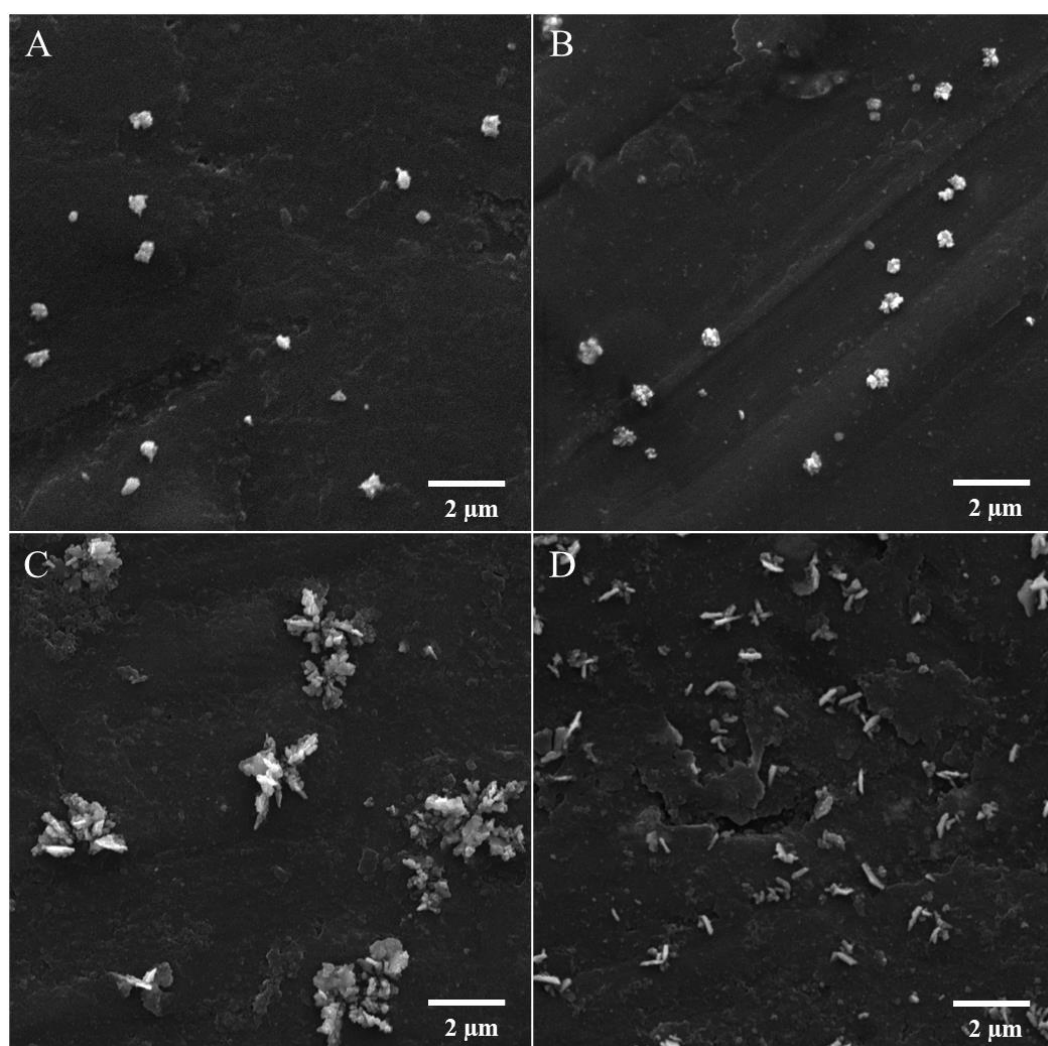


Figure 11. SEM images of samples: A) CS-Glc-Ag, B) NCS-Glc-Ag, C) NaBH₄-Ag 1:1, and D) NaBH₄-Ag 2:1.

The SEM micrograph of sample NaBH₄-Ag 1:1 (**Figure 11, C**) showed larger and aggregated structures, suggesting that the lower concentration of NaBH₄ led to rapid but less controlled reduction of Ag, promoting particle agglomeration. At the same time, sample NaBH₄-Ag 2:1 (**Figure 11, D**) presented smaller and more dispersed particles. The discrepancy

between the DLS data and SEM observations for NaBH₄-Ag 1:1 can be explained due to the nature of the DLS measurement. DLS often detects smaller individual particles in solutions, even if these particles are part of larger aggregates observed in SEM. It is possible that some particle fragmentation occurs in solution or that the aggregation seen in SEM is less prominent when in solution. The UV-Vis data further supports these findings. The sample NaBH₄-Ag 1:1 showed a peak at 402 nm and absorbance at 0.06, indicating fewer or weakly dispersed particles, while the sample NaBH₄-Ag 2:1 showed a peak at 398 nm and absorbance at 1.04, suggesting better dispersion and higher concentration of AgNPs.

The morphology of samples synthesized with a fixed amount of AgNO₃ and varying amounts of CS is shown in **Figure 12**. A total of five syntheses were carried out with CS amounts ranging from 50 to 250 mg, in 50 mg increments between each sample. The samples CS50-Ag200, CS100-Ag200 and CS200-Ag200 (**Figure 12, A, B and D**) exhibited the presence of a dendritic structure, with several ramifications. Those dendritic structures were also observed by Kumar-Krishnan et al. (2015) when analyzing the morphology of CS/Ag⁺ films (Kumar-Krishnan et al., 2015). It is well established in the literature that CS is capable of adsorbing Ag⁺ through mechanisms such as ion exchange and chelation. The amino and hydroxyl groups in CS facilitate the interaction with Ag⁺, while also serving as capping agents to stabilize the particles (Zienkiewicz-Strzałka et al., 2020). As a result, during the initial stages of reduction, clusters of Ag⁺ and Ag⁰ are formed. These clusters subsequently grow and assemble into dendritic structures due to electrostatic attractions between the carboxyl (–COO) and protonated amine (–NH₃) groups of CS (Kumar-Krishnan et al., 2015). Over time, the Ag⁺ clusters are progressively reduced to form Ag⁰, meaning that the dendritic structures contain both metallic Ag and Ag ions at different stages of reduction.

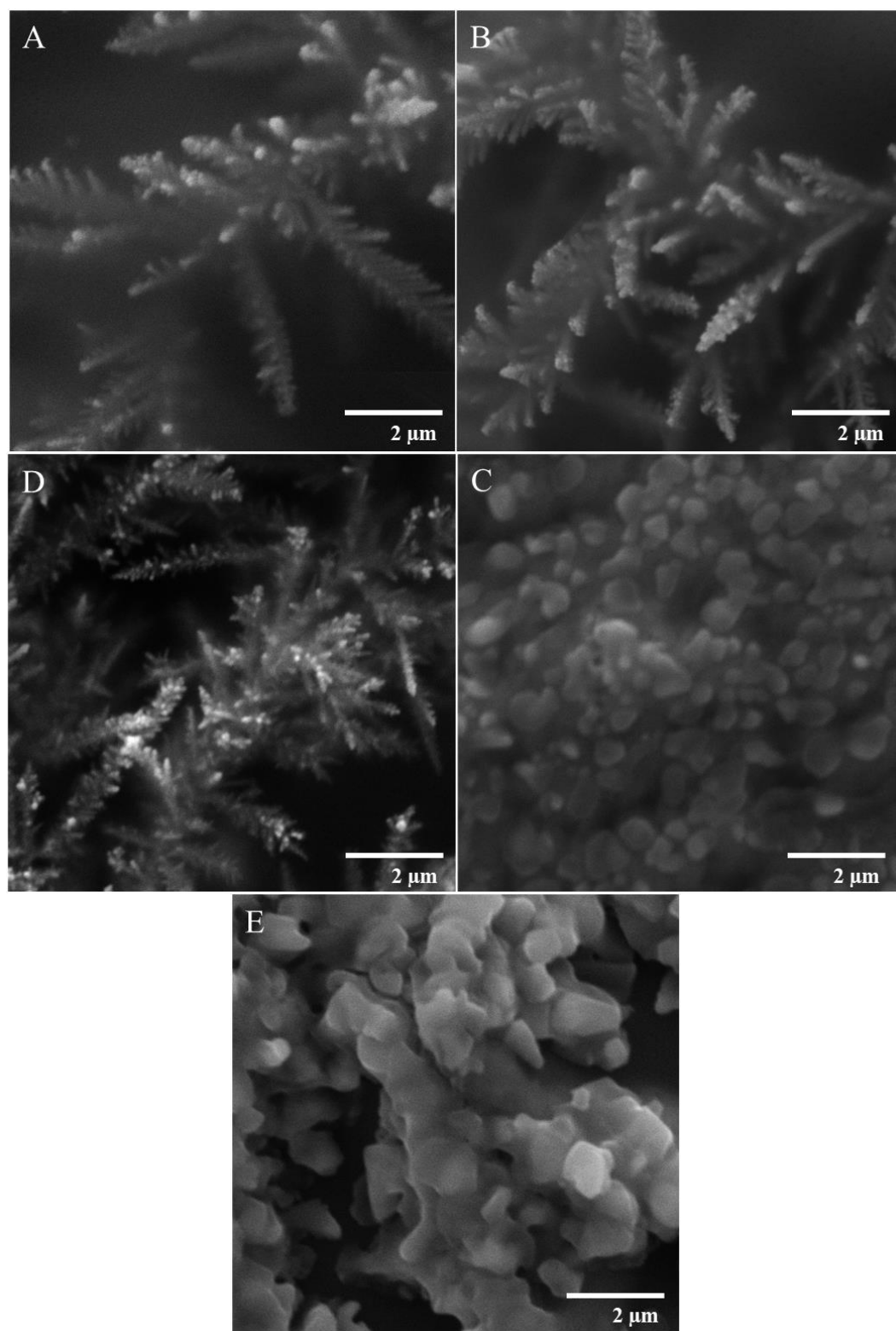


Figure 12. SEM images of AgNPs synthesized with a fixed AgNO_3 concentration (200 mg) and varying CS amounts: A) CS50-Ag200, B) CS100-Ag200, C) CS150-Ag200, D) CS200-Ag200, and E) CS250-Ag200.

The morphology of the samples prepared from the synthesis with a fixed amount of CS (150 mg) and different amounts of AgNO_3 are shown in **Figure 13**. Overall, DLS results pointed out that minor quantities of AgNO_3 resulted in smaller particles. On the other hand,

increasing the content of the Ag precursor, resulted in different SPR peaks with different absorbances, where the samples with higher amounts of AgNO_3 tended to show higher absorbances and double peaks suggesting high presence of AgNPs and agglomeration. When relating those results with the micrographs, it is evident that the samples CS150-Ag1000 and CS150-Ag1500 present strong signs of agglomeration without distinct shapes. The considerable difference in the CS and AgNO_3 ratio likely led to the formation of large aggregates with non-defined shapes.

The morphology of the sample CS150-Ag75 (**Figure 13, A**) suggests the presence of small, potentially spherical Ag particles embedded in a larger structure, which appears to resemble a dendritic structure in its initial growth stage. This sample was prepared with the smallest amount of AgNO_3 , and according to DLS analysis, resulted in AgNPs with an average size of 43.2 nm. In the SEM micrograph, it is possible to notice the presence of very small particles, which correlates with the DLS findings. Additionally, the UV-Vis spectrum showed an absorption peak at 420 nm, which is characteristic of small, spherical AgNPs. The relatively low absorbance value at 0.71 also supports the presence of a moderate concentration of small AgNPs. Thus, at a lower concentration of AgNO_3 , allowed the growth of small AgNPs forming primarily small clusters rather than fully developed dendritic structures.

The sample CS150-Ag150 (**Figure 13, B**) exhibited more aggregated and irregular structures compared to the previous sample, suggesting the presence of larger Ag particles. This observation is consistent with the findings from DLS and UV-Vis analysis, which reported an average particle size of 61.3 nm and an absorption peak at 424 nm, indicating the formation of larger AgNPs. In contrast, the samples CS150-Ag250 and CS150-Ag500 (**Figures 13, C and D**) exhibited well-defined dendritic structures and dendritic flowerlike structure, like those observed in **Figure 12** and the ones reported by Kumar-Krishnam and collaborators (Kumar-Krishnan et al., 2015). Although the synthesis method was the same for the samples in **Figures 12 and 13**, the variation in the ratio of CS to AgNO_3 significantly affected the morphology of the Ag particles.

The samples CS150-Ag1000 and CS150-Ag1500 (**Figure 13, E and F**) showed significant change in their morphological structure compared to the previous samples. The dendritic structure is not present, instead, there is the presence of particles with different shapes and sizes, with strong signs of aggregation. At higher concentrations of AgNO_3 , the nucleation and growth of Ag particles seem to favor the formation of larger and compact aggregates, rather than organized structures.

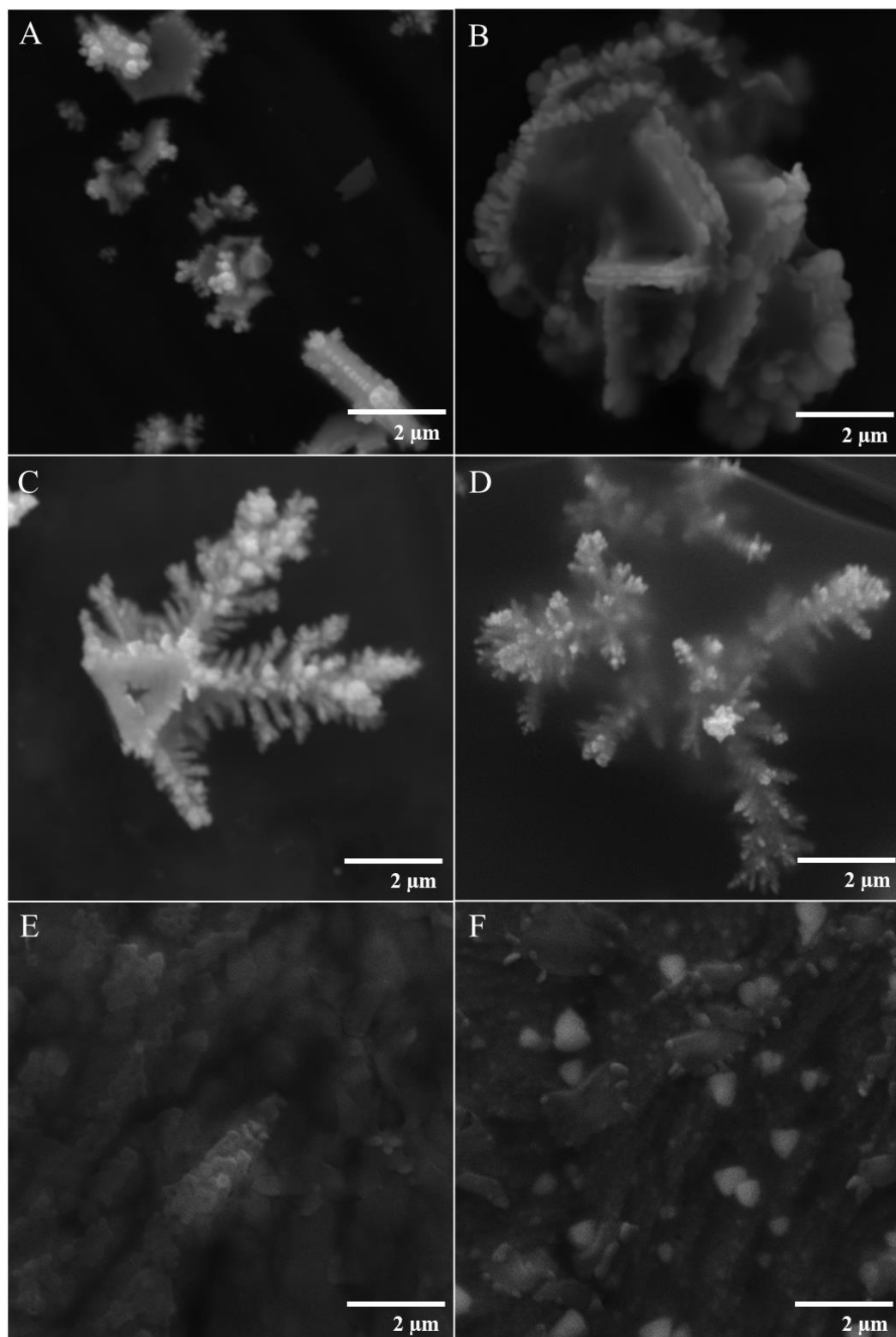


Figure 13. SEM images of AgNPs synthesized with a fixed CS concentration (150 mg) and varying AgNO_3 amounts: A) CS150-Ag75, B) CS150-Ag150, C) CS150-Ag250, D) CS150-Ag500, E) CS150-Ag1000 and F) CS150-Ag1500.

The EDS analysis (**Table 4**) shows the variations in the elemental composition across the different samples. It is important to note that the EDS results were reported in weight %,

representing the relative proportion of each element's weight compared to the total detected elements in the sample (i.e, the EDS does not provide absolute amounts of Ag but rather its relative proportion among other present elements).

Table 4. Elemental composition (weight %) of different samples obtained by EDS analysis.

Samples	Elements Weight (%)					
	C	O	Ag	N	Na	S
CS-TPP-Ag	5.66	43.93	35.7	13.58	1.22	-
CS-Ag	3.83	26.88	49.56	19.73	-	-
NCS-Ag	3.19	9.57	68.75	8.49	-	-
CS-HP-Ag	5.55	17.82	69.24	-	5.25	2.14
CS-Glc-Ag	39.82	36.13	24.04	-	-	-
NCS-Glc-Ag	27.49	39.29	24.04	-	-	-
NaBH ₄ -Ag 1:1	13.12	42.73	44.15	-	-	-
NaBH ₄ -Ag2:1	29.44	39.51	31.05	-	-	-
CS50-Ag200	2.6	65.39	24.73	7.27	-	-
CS100-Ag200	3.11	57.32	33.62	5.95	-	-
CS150-Ag200	4.9	24.11	51.33	19.65	-	-
CS200-Ag200	8.19	50.72	37.29	3.8	-	-
CS250-Ag200	5.41	26.99	44.86	22.75	-	-
CS150-Ag75	11.71	31.27	48.77	8.25	-	-
CS150-Ag150	11.83	37	39.12	12.04	-	-
CS150-Ag250	7.78	38.34	49	4.88	-	-
CS150-Ag500	7.78	43.85	46.75	1.62	-	-
CS150-Ag1000	0.96	29.73	48.2	21.12	-	-
CS150-Ag1500	2.61	30.44	42.09	24.86	-	-

The samples CS-Ag and NCS-Ag showed high Ag (49.56% and 68.75%, respectively) and N levels, which are related to the presence of CS and NCS. The sample CS-TPP-Ag contained less Ag (35.7%) and a minor amount of Na, associated with the presence of TPP. Meanwhile, the sample HP-Ag showed 69.24% of Ag, along with trace amounts of Na and S, originating from heparin. The samples reduced with glucose, CS-Glc-Ag and NCS-Glc-Ag, exhibited similar compositions, with around 24% of Ag, reflecting the interaction between glucose and the polymers.

Regarding the samples synthesized with a fixed AgNO₃ content and varying CS amounts (CS50-Ag200 to CS250-Ag200), the EDS analysis showed Ag values ranging from 24.73% to 51.33%, with different percentages of C, O and N, related to the use of CS as reducing and stabilizing agent. Although the amount of CS increased from 50 mg to 250 mg,

the changes in elemental composition were not strictly proportional. This may be due to the saturation in the ability of CS to stabilize the nanoparticles or the formation of thicker CS layers around the particles, affecting the relative detection of elements like Ag in the EDS analysis. Interestingly, some samples exhibited higher Ag content than others, despite the variation in CS amounts. This suggests that there might be optimal proportions between CS and AgNO₃ that enhance the reduction of Ag⁺ to Ag⁰.

In the samples prepared with a fixed amount of CS and varying amounts of AgNO₃ (CS150-Ag75 to CS150-Ag1500), EDS analysis showed that Ag content ranged from 39.12% to 49%. As the concentration of AgNO₃ increased, the C content generally decreased, indicating that the AgNO₃ to CS ratio significantly influences the surface chemistry of the nanoparticles. However, although the elemental analysis showed a decrease in the relative percentage of Ag (from 48.77% in CS150-Ag75 to 42.09% in CS150-Ag1500), this does not necessarily indicate a lower absolute amount of Ag. The UV-Vis analysis further supports these observations. As the AgNO₃ content increased, the absorbance of the SPR peak also increased, indicating the formation of more AgNPs. The higher availability of Ag⁺ ions in samples with higher AgNO₃ concentrations resulted in a stronger SPR signal, reflecting the greater presence of AgNPs. EDS reflects the relative proportions of the elements, and the increase in other components (such as C and O) from CS may have contributed to the relatively lower detected % of Ag.

Notably, the sample CS150-Ag75, despite having the lowest amount of AgNO₃, exhibited one of the highest relative Ag contents (48.77%), comparable to samples synthesized with higher AgNO₃ concentrations. This does not imply that the absolute amount of Ag in this sample was higher; instead, the lower proportions of other elements, such as carbon and O from CS, may have contributed to the increased relative Ag content detected by EDS. Moreover, the effective stabilization by CS may have contributed to the formation of smaller and more dispersed nanoparticles, as suggested by UV-Vis analysis, leading to a higher surface area of Ag being detected in relation to other components.

The CS150-Ag75 sample demonstrated a combination of advantageous properties. The UV-Vis spectrum revealed a distinct SPR peak at 420 nm with an absorbance of 0.71, indicating the presence of small, well-dispersed nanoparticles. This finding aligns with the DLS analysis, which confirmed smaller particle sizes (43.2 nm). Regarding morphology, although early-stage dendritic features were observed, it was also possible to identify small and spherical particles. The Ag content (48.77%) determined by EDS, along with the N content (11.71%), suggests that the CS provided effective stabilization of the AgNPs without excessive polymer coating. These

results indicate that, among all the samples, CS150-Ag75 demonstrated the best balance between particle size, dispersion, and stability.

3.3.4 Antimicrobial Activity and Biofilm Inhibition of Synthesized AgNPs

The results of the antimicrobial inhibition test against *S. aureus* (ATCC 6538) are illustrated in **Figure 14** showing the diameters of the inhibition zones formed around the synthesized samples. Notably, only 10 μ L of each colloidal solution was used for the test, and overall, the inhibition zones varied from 5.93 to 9.58 mm, except for the sample NCS-Glc-Ag, which exhibited no inhibition against the pathogen. The variations in inhibition zones highlight the influence of synthesis conditions, selection of stabilizers and reducing agents, and the concentration ratios on the antimicrobial properties of the AgNPs.

The sample CS-TPP-Ag, which showed particles embedded in a CS matrix, exhibited an inhibition zone of 8.5 mm. The antimicrobial activity of the CS-Ag sample, synthesized without TPP and at room temperature, was comparable to that of CS-TPP-Ag, with an inhibition zone of 8.64 mm. The samples NCS-Ag and HP-Ag, on the other hand, exhibited inhibition zones of 7.16 mm and 7.75 mm, respectively. Although the synthesis with TPP, NCS and HP demonstrated antimicrobial activity, the sample CS-Ag stood out. Its better antimicrobial activity could be attributed to its triangular-shaped particles.

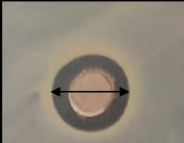
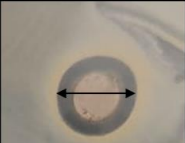
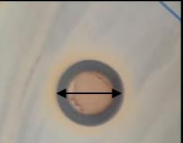

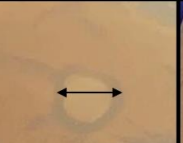
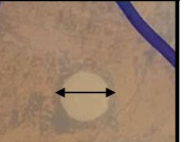
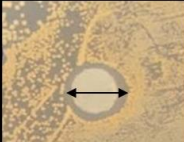



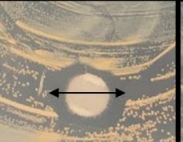

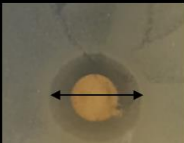
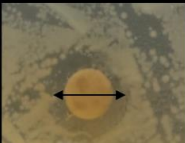
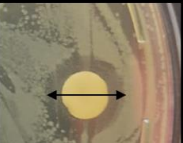


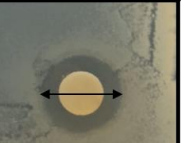
<i>S. aureus</i>					
CS-TPP-Ag	CS-Ag	NCS-Ag	HP-Ag	CS-Glc-Ag	NaBH ₄ -Ag 1:1
 8.50 mm	 8.64 mm	 7.16 mm	 7.75 mm	 7.43 mm	 5.93 mm
NaBH ₄ -Ag 2:1	CS50-Ag200	CS100-Ag200	CS150-Ag200	CS200-Ag200	CS250-Ag200
 6.33 mm	 7.13 mm	 7.71 mm	 7.90 mm	 7.73 mm	 8.36 mm
CS150-Ag75	CS150-Ag150	CS150-Ag250	CS150-Ag500	CS150-Ag1000	CS150-Ag1500
 9.52 mm	 8.04 mm	 8.32 mm	 8.63 mm	 9.06 mm	 9.58 mm

Figure 14. Inhibition Zone of all synthesized AgNPs solutions against *S. aureus*.

The literature reported that the antimicrobial effectiveness of AgNPs can be influenced by their shape, and faceted structures, like triangular, are likely to have higher antibacterial properties (Polinarski et al., 2021). However, this cannot be considered an absolute statement. For instance, while some research found cubic and icosahedral shapes to be more effective against *E. coli* than triangular or spherical nanoparticles (El-Zahry et al., 2015; Hong et al., 2016), other studies reported that triangular and spherical shapes demonstrated superior antimicrobial performance compared to other morphologies (Kim et al., 2017; Pal et al., 2007).

The sample CS-Glc-Ag exhibited an inhibition zone of 7.43 mm, while the NCS-Glc-Ag did not show any antimicrobial activity. Additionally, the NCS-Ag sample demonstrated lower antimicrobial effectiveness compared to CS-Ag. Clearly, the use of NCS did not enhance the antimicrobial properties of the material. These findings suggest that the combination of NCS with glucose may have impacted the antimicrobial mechanisms, even though the presence of AgNPs was confirmed by UV-Vis analysis. The samples NaBH₄ 1:1 and NaBH₄ 2:1 resulted in AgNPs with average sizes of 38.5 nm and 47.8 nm, respectively. Despite the small particle sizes reported by DLS, their antimicrobial activity (5.93 mm and 6.33 mm, respectively) was lower than that of all the other samples that exhibited inhibition zones.

The inhibition zone of the samples prepared with 200 mg of AgNO₃, and varying amounts of CS ranged from 7.13 to 8.36 mm. In general, as the amount of CS increased, antimicrobial activity also improved. The sample CS50-Ag200 exhibited an inhibition zone of 7.13 mm, with a particle size of 77.9 nm, and SEM images showed dendritic structures. For the sample CS100-Ag200, the inhibition zone increased to 7.71 mm, and the average particle size was reduced to 65.5 nm, while dendritic formations remained present. The sample CS200-Ag200, which had the smallest particle size (28.5 nm) and also presented dendritic structures, showed an inhibition zone of 7.73 mm. In contrast, samples CS150-Ag200 and CS250-Ag200 exhibited irregular structures with non-defined shapes and strong signs of aggregation. Despite this, their antimicrobial activity was higher, with inhibition zones of 7.90 mm and 8.36 mm, respectively.

The samples synthesized with a fixed amount of CS (150 mg) and varying concentrations of AgNO₃ showed inhibition zones ranging from 8.04 to 9.58 mm. The CS150-Ag75 sample, which had the smallest particle size (43.2 nm), exhibited a high inhibition zone of 9.52 mm. SEM analysis revealed small, potentially spherical Ag particles embedded within a dendritic structure. Interestingly, when the AgNO₃ concentration increased to 150 mg in the CS150-Ag150 sample, the inhibition zone decreased to 8.04 mm. Despite the higher Ag concentration, the antimicrobial activity of CS150-Ag150 was lower than that of CS150-Ag75.

Except for sample CS150-Ag75, a general pattern of increasing antimicrobial activity was observed with higher AgNO₃ concentrations.

While the CS150-Ag1500 sample showed the largest inhibition zone (9.58 mm), its high AgNO₃ content potentially increases synthesis costs. Additionally, in biomedical applications, elevated Ag concentrations can raise safety concerns due to potential cytotoxic effects. As highlighted by Zhang et al. (2014), AgNPs can induce oxidative stress and ROS generation, leading to cytotoxicity and genotoxicity in human cells (T. Zhang et al., 2014). On the other hand, the CS150-Ag75 sample achieved a nearly equivalent antimicrobial effect, with an inhibition zone of 9.52 mm, using the lower AgNO₃ concentration (75 mg). This reduction in Ag content lowers synthesis costs and minimizes the risk of Ag-induced toxicity, making CS150-Ag75 a more cost-effective and safer option for applications requiring biocompatibility. The use of CS as a stabilizing agent may also contribute to reducing the potential toxicity of AgNPs by providing a biocompatible coating (C. Liao et al., 2019; T. Zhang et al., 2014). Nevertheless, further studies are required to confirm its safety and validate its potential for biomedical use.

Due to its antimicrobial performance and favorable characteristics observed during physicochemical characterization, the sample CS150-Ag75 sample was submitted to an antibiofilm assay to evaluate its potential for inhibiting biofilm growth. To align with the goal of developing an alternative antimicrobial agent for biomedical applications, polyurethane central venous catheter (CVC) segments were used as the surface for biofilm formation. The findings are demonstrated in **Figure 15**.

The surface of the CVC is typically smooth and uniform, with no visible irregularities or signs of microbial attachment (**Figure 15, A**). However, after five days of exposure to an *S. aureus* suspension, a dense biofilm was formed on the CVC surface, as it can be seen in **Figure 15, B**. When the CVC was exposed to bacterial suspension for five days in the presence of the CS150-Ag75 solution (**Figure 15, C**) the presence of a few *S. aureus* colonies was noted, with signs of potential disruption of the bacterial cell walls, indicating cell death. The micrograph of the CVC segment immersed in the CS150-Ag75 solution prior to biofilm growth also showed minimal bacterial colonization (**Figure 15, D**). This pre-treatment appeared to modify the CVC surface due to the adhesion of a CS and AgNPs layer, preventing bacterial adhesion and biofilm development.

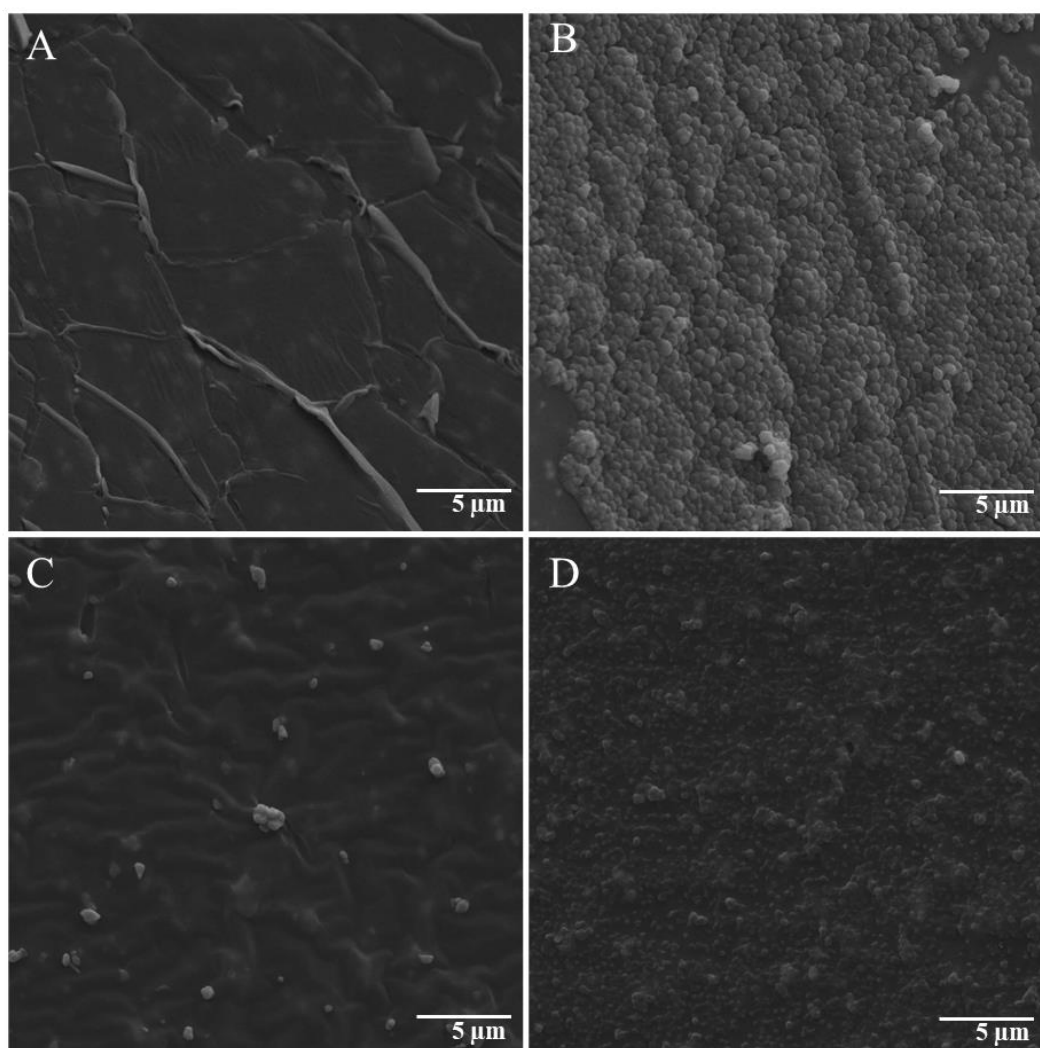


Figure 15. SEM micrographs of CVC specimens under different conditions: (A) CVC without bacterial exposure, serving as a control; (B) CVC after five days of exposure to *S. aureus* bacterial suspension; (C) CVC exposed to *S. aureus* bacterial suspension for five days in the presence of the CS150-Ag75 solution; (D) CVC pre-treated by immersion in the CS150-Ag75 solution prior to five days of exposure to *S. aureus* bacterial suspension.

The ability of sample CS150-Ag75 to inhibit bacterial adhesion and biofilm formation highlights its potential as an effective alternative to conventional antimicrobial treatments, particularly for use in medical device coatings. CS enhances the biocompatibility of AgNPs by stabilizing the nanoparticles, limiting Ag^+ release, and reducing cytotoxicity through its protective barrier properties (C. Liao et al., 2019). However, the long-term safety of AgNPs, especially regarding cytotoxic effects, still requires further evaluation (T. Zhang et al., 2014).

To better understand the antimicrobial effects of the synthesized AgNPs, particularly the **CS150-Ag75** sample, it is important to examine the key mechanisms by which AgNPs act against bacteria. These nanoparticles disrupt bacterial cells through several pathways, including membrane destabilization, ROS generation, and the release of Ag^+ . In this study, the higher

antimicrobial efficacy observed in the sample CS150-Ag75, can be attributed to the larger surface area of these particles, facilitating the release of Ag^+ and enhancing interaction with the bacterial cell wall. CS, used as a stabilizer, not only improves the dispersion of AgNPs but may also enhance the antimicrobial effect due to its inherent antimicrobial properties, creating a synergistic effect between CS and AgNPs (Polinarski et al., 2021). While the detailed mechanism was not directly investigated, it is possible to suggest that the combined action of Ag ion release, cell membrane disruption, and oxidative stress contributes to the observed results.

3.4 Partial Conclusions

In summary, this study synthesized and characterized different AgNPs prepared by a broad range of methodologies proposed in the literature, using different reducing agents, aiming to evaluate their potential as alternatives for combating bacteria. Among the reducing agents, the samples prepared with CS demonstrated superior antimicrobial results. The CS150-Ag75 sample, synthesized with a lower concentration of AgNO_3 , exhibited a nearly equivalent inhibition zone to samples with higher Ag concentrations, highlighting that reduced Ag content can still lead to strong antimicrobial performance. While particle size and shape are often critical in determining antimicrobial activity, this study did not establish a clear correlation between smaller nanoparticle sizes and increased activity, suggesting that multiple factors, such as nanoparticle shape, choice of reducing agent, and synthesis conditions, contribute to the overall effectiveness. The balance between AgNO_3 and CS, as seen in the CS150-Ag75 sample, led to the most promising results, demonstrating efficient biofilm inhibition and antibacterial properties against *S. aureus*. However, further comprehensive testing is necessary to ensure the long-term safety and biocompatibility of this formulation, particularly for use in biomedical applications.

CHAPTER 4: ARTICLE 2

The content of this section has been previously published in *Materials Today Communication* (<https://doi.org/10.1016/j.mtcomm.2024.109987>).

In-situ growth of Ag nanoparticles embedded in chitosan coating for potent antimicrobial activity

Marcos Antonio Polinarski^{a,b,c,d}, Nhu-Nang Vu^{a,b}, Safa Ladhari^a, Cédrik Boisvert^{a,b}, Simon Barnabé^b, Juliana Bernardi Wenzel^e, Helton José Alves^{c,d}, Phuong Nguyen-Tri^{a,b}

^a Laboratory of Advanced Materials for Energy and Environment, Université Du Québec à Trois-Rivières (UQTR), 3351, Boul. des Forges, C.P. 500, Trois-Rivières, Québec, G9A 5H7, Canada.

^b Department of Chemistry, Biochemistry and Physics, Université du Québec à Trois-Rivières (UQTR), 3351 Bd des Forges, Trois-Rivières, QC G8Z 4M3, Canada.

^c Renewable Materials and Energy Laboratory (LABMATER), Federal University of Paraná (UFPR – Setor Palotina), R. Pioneiro, 2153, 85950-000, Palotina, PR, Brazil.

^d Postgraduate Program in Environmental Engineer and Technology, Federal University of Paraná (UFPR – Setor Palotina), R. Pioneiro, 2153, 85950-000, Palotina, PR, Brazil.

^e Medicine Course – Toledo Campus, Federal University of Paraná, Rodovia PR 182, S/N, Km 320/321, CP 2028, Toledo-PR, 85919-899 Brazil.

Abstract

Developing highly antimicrobial coatings is an important strategy to control the risk of pathogen colonization and biofilm formation, especially in indwelling and implantable medical devices. This work presents a facile and practical approach to preparing potent antimicrobial coatings based on the CS-Ag composite. The synthesis is conducted by simply stirring a CS solution with different amounts of Ag at room temperature, and the composite is applied as a coating on a polystyrene (PS) surface. In-situ reduction of Ag⁺ ions to metallic Ag (Ag⁰) during the coating process leads to AgNPs forming into Ag rods half-embedded into the CS film and half-exposed on the coating surface. This distinctive structure promotes effective antibacterial action through the Ag⁺ release and photocatalytic activity of AgNPs. The coatings exhibit potent antimicrobial activity with 99.89% efficiency against *Escherichia coli* after 90 minutes and 100% against *Staphylococcus epidermidis* after 30 minutes under LED light irradiation. These coatings also display high stability with an insignificant decrease in the antibacterial activity after three times of reutilization. The newly synthesized formulations can be considered a promising alternative for antimicrobial coatings to avoid biofilm formation and for coating materials with various applications, especially in the biomedical field.

Keywords: nanoparticles, antimicrobial, biomedical, biomaterials, coatings.

4.1 Introduction

Healthcare-associated infections (HCAIs) are illnesses acquired by patients while receiving medical care within a healthcare facility. These infections can result from contact with contaminated surfaces, ingestion of contaminated food, or exposure to aerosol droplets from other patients. HCAIs represent a significant global burden, contributing substantially to morbidity and mortality rates (Bonilla-Gameros et al., 2020). In clinical treatment of bacterial infections, overuse of conventional antibiotics has increased bacterial drug resistance, making it highly necessary to develop new antibiotics and alternatives to combat MDR strains (Song et al., 2021). Furthermore, according to the World Health Organization (WHO), infections related to drug-resistant pathogens have shown a solid connection to the increase in the death rate associated with pandemic and epidemic diseases (C. G. A. Das et al., 2020). Developing new and effective materials capable of preventing bacterial contamination is thus urgently needed.

There has been an increasing emphasis on developing green materials in the most diverse fields, especially in the biomedical area, focusing on synthesizing biobased polymers for antimicrobial applications (Ladhari et al., 2023). In that regard, CS emerges as a promising alternative for being a nature-derived biopolymer due to its abundance, reasonable price, and unique physicochemical properties (e.g., biodegradability, biocompatibility, antimicrobial and antioxidant activity, low immunogenicity, nontoxicity) (Seidi et al., 2021; Yousefzadeh et al., 2024). As a cationic polymer, CS has distinctive characteristics, such as cell transfection, biological adhesion, anti-inflammatory, and antimicrobial properties, that can be enhanced when combined with other materials (Gao & Wu, 2022). In the biomedical field, CS has been widely explored as a particle-forming polymer and surface coating, especially in medical devices (Frank et al., 2020; Lamprou et al., 2019). Owing to abundant functional groups, CS induces strong interaction with metal ions and nanoparticles (NPs), conferring the ability to form composites with advanced properties (Babamoradi et al., 2022; Zienkiewicz-Strzałka et al., 2020).

Ag-based materials, prominently AgNPs, are well-known for their optical, electrical, catalytic, and, exceptionally, antimicrobial properties while having low toxicity. For this reason, these NPs have been widely used in various applications such as wound dressing, water disinfection, antiseptic spraying, and coating (Chernousova & Epple, 2013; C. G. A. Das et al., 2020; Joardar et al., 2021; Logambal et al., 2023). AgNPs can attach to the bacterial cell

membrane to alter their natural permeability, and the NPs can bind to respiratory enzymes and/or penetrate the cell membrane to interact with the DNA (X. Du et al., 2021).

In the last few years, the combination of CS and Ag has emerged as one of the effective strategies for preparing potent antimicrobial materials (Kumar-Krishnan et al., 2015; Mirajkar et al., 2021). The antimicrobial properties of CS-Ag composites were reported to be significantly enhanced compared to AgNPs or CS alone due to a synergistic effect of these components (Mirajkar et al., 2021; Polinarski et al., 2021). Precisely, CS controls the release of Ag^+ ions and promotes a prolonged effect as a function of time. Moreover, the CS macromolecules may induce a positive charge to the AgNP outer side, increasing their attaching to the negative charges of the bacteria cell surface.

There are different kinds to develop CS-Ag composites, where two methodologies stand out: (1) the addition of CS solution into previously prepared Ag-NPs; and (2) CS addition during the AgNPs formation (Frank et al., 2020). The literature reported different CS-Ag composites with antimicrobial properties for application in the pharmaceutical, biomedical, and food fields (Frank et al., 2020; Mishra et al., 2015; Perepelkin et al., 2023). However, in most cases, the composite is formed by AgNPs previously synthesized, which can affect their stability and efficacy for extended periods. Besides that, the costs for some metal precursors, the origin of the reducing agents, the high temperatures used during synthesis, and the environmental and health issues associated with their application and disposal configure the drawbacks of those materials (Frank et al., 2020; Freitas et al., 2022; Iqbal et al., 2023; Mohamed & Madian, 2020).

The synthesis of AgNPs by conventional chemical methods can result in the deposition of toxic residues on their surface, leading to limited use in biomedical applications. Eco-friendly synthesis methods are, thus, an alternative approach to preparing those materials. CS-coated metallic nanoparticles have demonstrated desirable characteristics to the biomedical and pharmaceutical industries, such as biodegradability, ease of preparation, and biocompatibility (Jiang et al., 2023; Mohamed & Madian, 2020).

This work presents a facile method for a two-step green synthesis of a CS-Ag composite using AgNO_3 as a Ag precursor and CS as both a reducing and stabilizing agent for coating purposes. The in-situ reduction of Ag ions during the coating preparation process led to the formation of AgNPs with antimicrobial properties. The formed composite was applied as a coating on polystyrene surfaces, and their morphology, physical-chemical characteristics, and antimicrobial and antibiofilm properties were investigated. The interaction of CS with Ag promotes the reduction of Ag^+ , leads to in-situ growth of AgNPs, and enhances the coating's

antimicrobial properties, making it a promising material to prevent biofilm formation and bacterial infection to protect human health.

4.2 Material and Methods

4.2.1 Materials

CS (deacetylation degree: 95%; molecular weight: 173 kDa) was produced by the Laboratory of Materials and Renewable Energy (LABMATER, Federal University of Paraná, Palotina, Brazil) (Alves et al., 2019). Silver Nitrate (AgNO_3) solution (0.1 M) was purchased from Honeywell (Germany). Glacial Acetic Acid (CH_3COOH) solution (99.7%) was purchased from Fisher Chemical (USA). Tryptic Soy Agar (TSA) and Tryptic Soy Broth (TSB) were purchased from Sigma-Aldrich. *E. coli* (ATCC 11229) and *S. epidermidis* (ATCC 12228) bacteria cultures were purchased from Cedarlane (Canada).

4.2.2 Synthesis of chitosan-silver composite

The synthesis was conducted via a two-step process. First, a CS solution was prepared at a final concentration of 1mg.mL^{-1} (w/v) by dissolving 50mg of CS powder in a 2% (v/v) aqueous solution of acetic acid. The solution was vigorously stirred at 420 rpm for 12 hours at 30°C . Then, different volumes of silver nitrate (AgNO_3) solution were added to the CS solution at the Ag^+ concentrations of 5%, 10%, 20%, and 50% (wt% of CS) and kept under continuous stirring in the dark for 6 hours at room temperature. The samples were assigned as CS-Ag-5%, CS-Ag-10%, CS-Ag-20%, and CS-Ag-50%, according to the used percentage of Ag^+ . After that, the prepared CS-Ag composite solution was stored in the dark for further applications and characterization. Details of the prepared formulations are shown in **Table 5**.

Table 5. Description of CS-Silver composites: CS and silver ions amount, and coating methodology.

Samples	Chitosan (mg.mL^{-1})	Ag^+ (wt%)	Coating Method	Number of coatings
CS-Ag-5%	1	5	Drop	1
CS-Ag-10%	1	10	Drop	1
CS-Ag-20%	1	20	Drop	1
CS-Ag-50%	1	50	Drop	1

4.2.3 Preparation and coating of the plastic samples

PS is one of the most used plastics (labware, sample storage, disposable medical products, diagnostic devices, medical packaging, etc.). In this work, it was coated with a CS-

Ag composite using different methodologies. Before coating, PS pieces were cut in 1x1cm and submitted to surface modification with plasma treatment to modify their wettability and improve the coating distribution on their surface. Plasma was performed in a PE-50-Venus Plasma Etcher vacuum chamber (working pressure at 40mTorr by injecting oxygen (O₂) at 10 sccm under vacuum, with an RF power of 80 W for 1 min). The coating was carried out using two methodologies: (1) drop technique and (2) dip-coating (**Figure 16**). Different volumes (50, 75, and 100 μ L) of sample CS-Ag-20% were taken with an automatic volumetric pipette and placed on a PS surface for the drop technique. For the dip coating, a volume of the sample was placed in a sterilized glass beaker, and PS specimens were dipped one by one into the solution for no longer than 3 minutes. After the coating, all the samples were dried overnight at room temperature in the dark. Samples with 1, 2, and 3 coating layers were prepared. Details of coated samples are shown in **Table 6**.

Table 6. PS samples were coated with CS-Ag-20% composite using different coating methodologies.

Sample	Volume (μ L)	Number of layers	Coating Method	Ag quantity (mg/cm^2)
Drop-50	50	N/A	Drop-Coating	8.4 ± 0.2
Drop-75	75	N/A		15.8 ± 0.4
Drop-100	100	N/A		16.4 ± 0.5
Dip-1L	-	1	Dip-Coating	7.7 ± 0.2
Dip-2L	-	2		8.6 ± 0.2
Dip-3L	-	3		9.4 ± 0.3

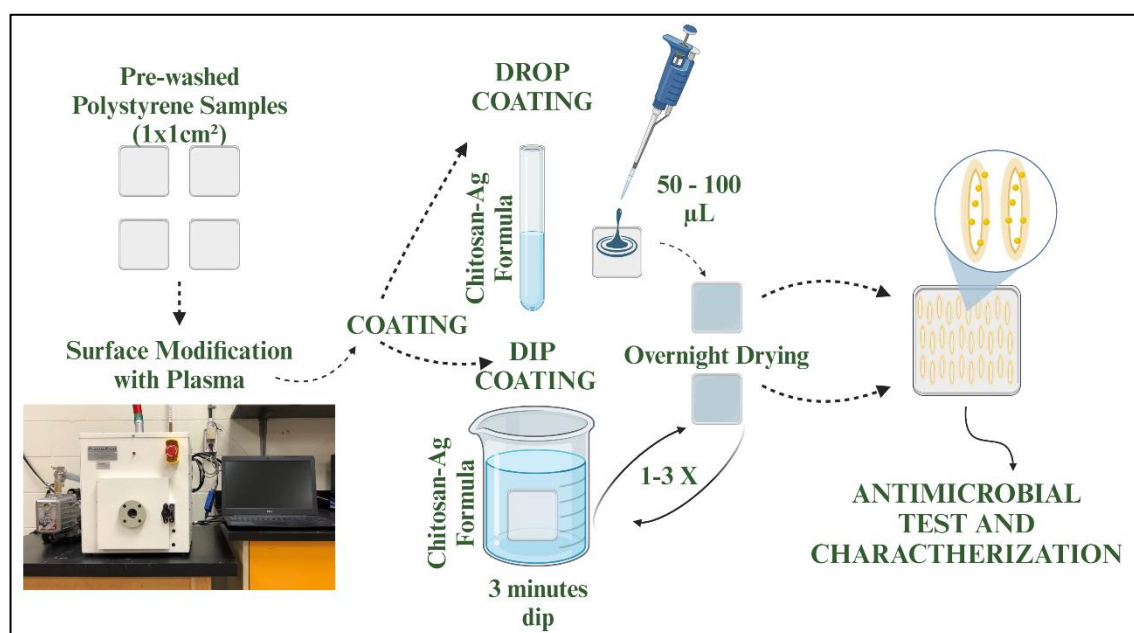


Figure 16. Illustration of the applied coating methods on the surface of PS pieces using CS-Ag composite.

4.2.4 Characterizations

The morphological features of the prepared coatings were obtained by scanning electron microscopy (SEM, Hitachi, and Tescan). Elemental mappings were performed using energy-dispersive X-ray spectroscopy (EDS, FEI Quanta 440 – OXFORD Instruments) to elucidate the coating's chemical composition. The identification of CS functional groups on the coating surface was evaluated by Fourier-transform infrared spectroscopy (FTIR, ATR mode) recorded on an infrared spectrophotometer (FTS 45). Surface roughness was measured on a VK-X1000 3D laser confocal microscope. The static water contact angle (WCA) was determined with a Theta Flex optical tensiometer (Attension). X-ray photoelectron spectroscopy (XPS) surveys and high-resolution (HR) elemental XPS spectra were collected using a photoelectron spectrometer (Kratos Axis-Ultra) with Al K α radiation. Ag quantification of coated samples was measured using an inductively coupled plasma optical emission spectrometry (ICP–OES) spectrometer (PerkinElmer Optima 4300 DV). Detailed information about sample preparation before ICP-OES analysis is available in supplementary information.

4.2.5 Antibacterial assays

PS samples coated with different volumes of CS-Ag composite had their antibacterial activity tested against *E. coli* and *S. epidermidis* by the agar diffusion method and the spread plate method. A third assay was performed to evaluate the bacteria's ability to biofilm formation and the CS-Ag coating potential to inhibit it. Before the tests, cultures of *E. coli* and *S. epidermidis* were prepared according to the method described in our research group's previous work with modifications (Vu et al., 2022). Bacterial stock solution was added to TSB broth and incubated for 24 h. After that, the bacterial suspensions were adjusted to the 0.5 MacFarland standard (1.5×10^8 CFU/mL).

4.2.5.1 Agar diffusion method

For the agar diffusion method, 100 μ L of the adjusted bacterial suspension was spread onto a nutrient agar medium (TSA) included in Petri dishes of 9 cm diameter. Then, 1x1 cm PS samples coated with 100 μ L of the CS-Ag composite (with 5%, 10%, 20%, and 50% of Ag on its composition), pure CS, pure AgNO₃, and an uncoated sample were placed faced down on the TSA Petri dishes and incubated at 35°C for 24 hours. After that, the diameter of the zones around the samples, where bacterial growth was inhibited, was measured (Vu et al., 2022).

4.2.5.2 Spread plate technique for colony counting

The antibacterial efficacy of prepared CS-Ag composite was evaluated against *S. epidermidis* and *E. coli* using the spread plate technique agar plate test (K. Ma et al., 2022). Bacterial suspensions were adjusted for 1.5×10^5 CFU/mL and 100 μ L of the bacterial suspensions were placed on top of the CS-Ag-coated samples and then stored in two aseptic conditions under the dark and light for 15-120 min at a temperature of 30°C. For the condition under the light, the samples were placed in a photochemical reactor equipped with 16 LED cool white lamps (LuzChem 16-LED Photoreactor, 64W). In contrast, the samples were placed in a conventional bacterial incubator for dark conditions. After, the samples were washed with 2mL saline solution (NaCl 0.9%) and vortexed for 8 seconds. 100 μ L of the washed solution was taken, spread onto a TSA agar plate, and incubated for 24 hours at 35°C, followed by colony counting. For the reusability test, coated samples were washed with 2 mL of saline solution, vortex for 10 seconds in ethanol, air-dried, and submitted to the same test three times, adapted from (Herigstad et al., 2001).

4.2.5.3 Evaluation of Biofilm Formation

A biofilm formation assay was performed following the methodology proposed by Mulla et al. (2016) with modifications. Coated and uncoated PS pieces were put in growth media inoculated with *E. coli* and *S. epidermidis* (1.5×10^8 CFU/mL) and incubated for five days at 37°C (Mulla et al., 2016). The coated and uncoated PS samples were submitted to the fixation and dehydration processes (Bates et al., 2021). Scanning electron microscopy (SEM) analysis was used to observe biofilm formation and bacteria.

4.3 Results and Discussion

4.3.1 Preliminary evaluation of chitosan-silver coatings

In total, four different syntheses were prepared. Initially, all synthesized formulations were used to coat the PS pieces, followed by morphological observation using the SEM technique and antimicrobial tests. For all the samples, it was possible to observe the formation of Ag rods with different lengths and widths (**Figure 17**). The surface of sample CS-Ag-5% (**Figure 17, A**) presented a heterogenous distribution of Ag rods, with sizes ranging from 3 to 75 μ m. For the CS-Ag-10% (**Figure 17, B**), a dendritic structure with several different ramification sizes mixed with Ag rods was observed. The sample CS-Ag-20% (**Figure 17, C**) showed a uniform distribution of Ag rods, with sizes ranging from 7 to 11 μ m. Sample CS-Ag-

50% (**Figure 17, D**) shows a heterogenous distribution, with Ag rods of different sizes and lengths.

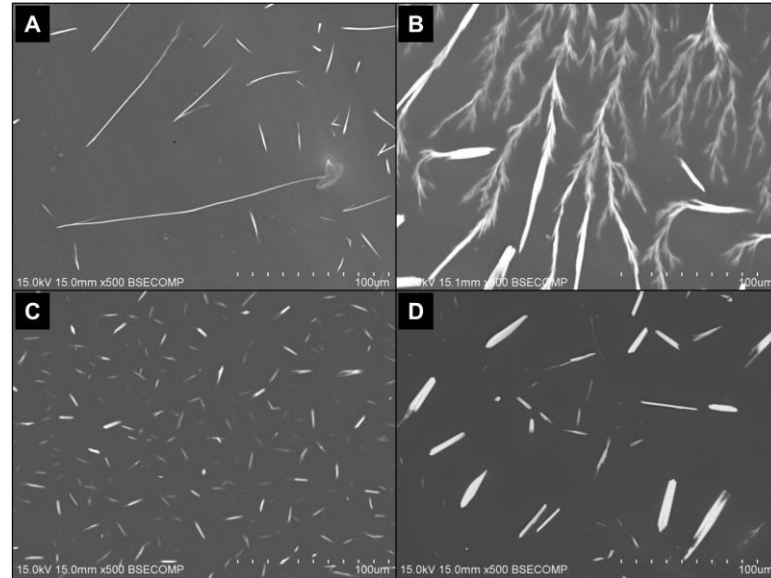


Figure 17. Scanning Electron Microscopy micrographs of PS pieces coated with CS-Ag composite, where (A) corresponds to sample CS-Ag-5%, (B) to CS-Ag-10%, (C) to CS-Ag-20%, and (D) to CS-Ag-50%.

The elemental mapping images showed clear signals of Ag, C, O, and N (**Figure 18**) for all samples. Notably, the Ag signals are distributed majorly in the same place where rods are present, indicating that the rods visualized on SEM micrographs are constituted by Ag. The amino and hydroxyl groups in CS allow the interaction with Ag ions and act as capping sites for particle stabilization (Zienkiewicz-Strzałka et al., 2020). Because of this, in the initial stage of reduction, clusters of Ag^+ ions and Ag metal particles can be formed, grow, and assembly into dendritic structures due to electrostatic attraction between $-\text{COO}^-$ and $-\text{NH}_3^+$ groups of CS with Ag^+ ions (Kumar-Krishnan et al., 2015).

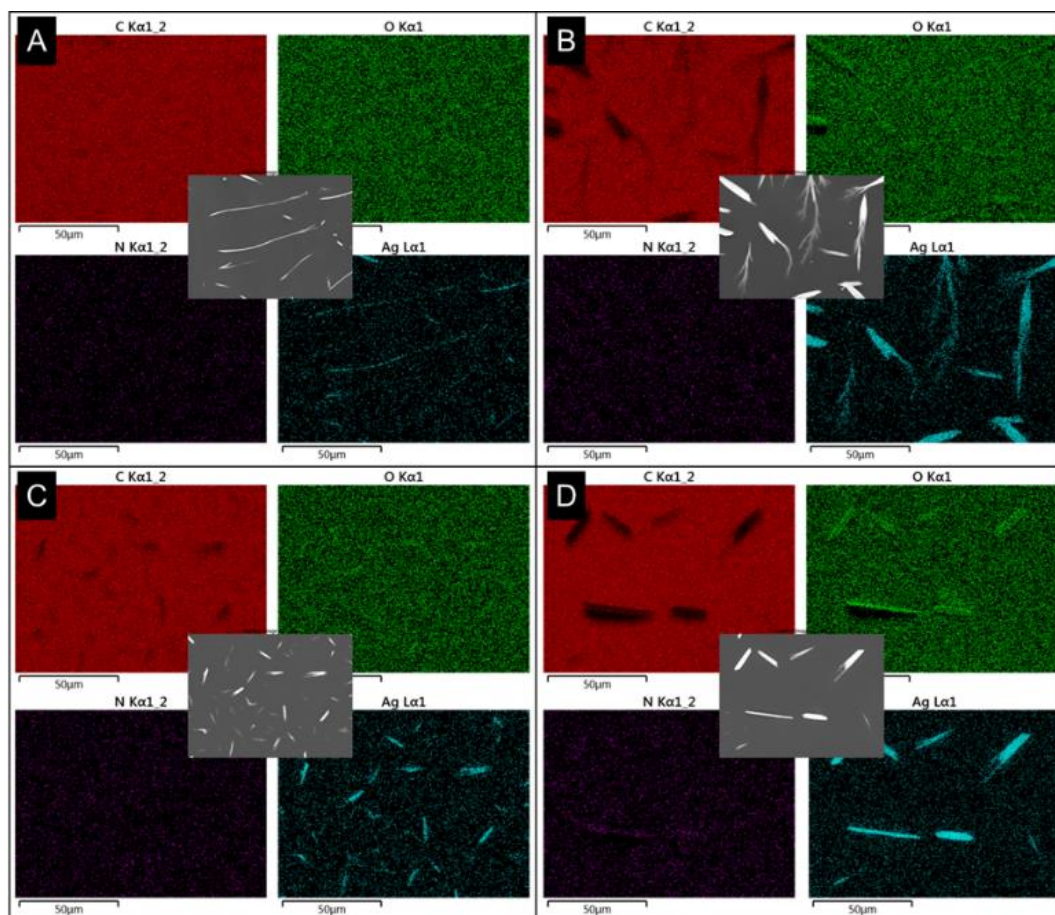


Figure 18. SEM and elemental mapping image (C, O, N, and Ag) of (A) CS-Ag-5%, (B) CS-Ag-10%, (C) CS-Ag-20%, and (D) CS-Ag-20%.

A preliminary antimicrobial test was conducted to verify the antibacterial properties of the coatings prepared with CS-Ag composites. The tests were carried out using the agar diffusion method, and the results obtained demonstrate a prominent inhibition zone for samples CS-Ag-20% and CS-Ag-50% (**Figure 19**). Those samples induced a clear inhibition zone against *E. coli*, with diameters of 12.7 mm and 13 mm, and against *S. epidermidis*, with 14 mm and 17 mm diameters. No inhibition zone was found for the samples coated only with CS and AgNO₃.

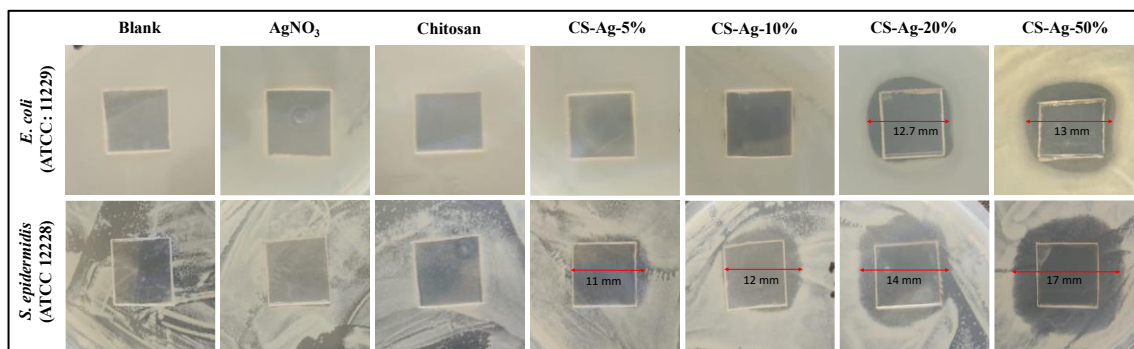


Figure 19. Inhibition Zone of uncoated PS pieces (Blank) and PS pieces coated with pure AgNO₃, Chitosan, and CS-Ag composite against *E. coli* and *S. epidermidis*.

CS-Ag-20% and CS-Ag-50% had promising antibacterial properties, showing clear inhibition zones for gram-positive and gram-negative bacteria. However, when evaluating the morphology of the coatings, sample CS-Ag-20% had a better Ag rod distribution, representing a higher surface area that is desirable when coating surfaces (Polinarski et al., 2021). For this reason, the following analysis focuses on coatings fabricated using the formulation CS-Ag-20%.

4.3.2 Characteristics

The morphology of samples prepared by the dip coating technique (**Figure 20**) showed a similar structure as the one coated by the drop technique (**Figure 17**), where it is possible to notice the presence of Ag rods. When the CS-Ag-20% is applied on the PS surface, the CS amino (-NH₂) and hydroxyl (-OH) groups lead to the reduction of Ag ions (Ag⁺) present in the solution. This process forms Ag atoms (Ag⁰) stabilized by the CS polymer. The reduced Ag atoms interact with each other forming clusters. During the drying process, those clusters grow into elongated structures, facilitated by CS molecules, which serve as a stabilizing agent. CS interacts with the Ag atoms through its functional groups and helps to control the morphology and growth of the Ag rods within the coating (Z. Chen et al., 2013; Kulikouskaya et al., 2022; Tran et al., 2010).

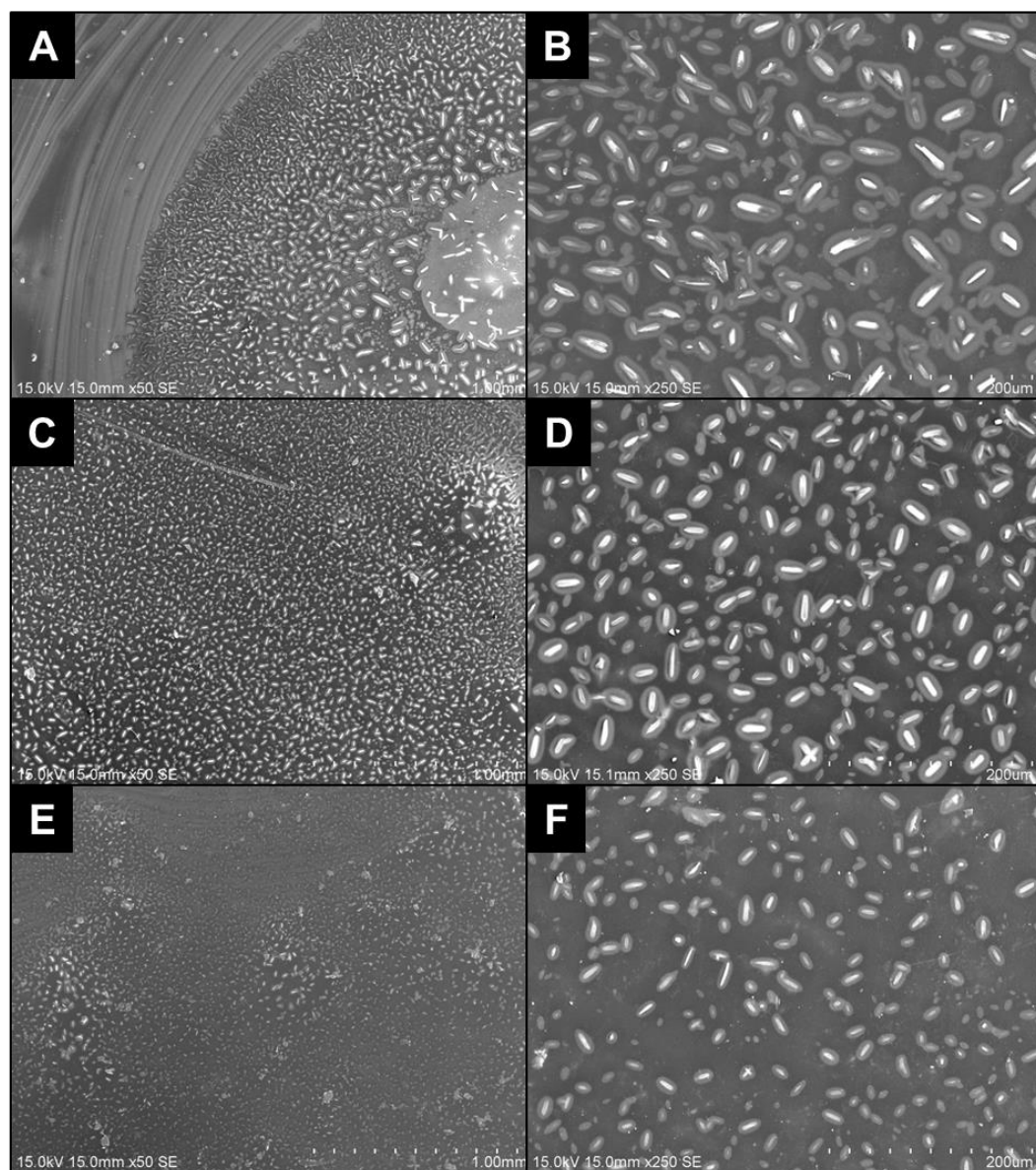


Figure 20. Scanning electron microscopy micrographs of samples prepared by the dip-coating technique, where (A-B) correspond to sample with 1 coating layer, (C-D) 2 coating layers, and (E-F) 3 coating layers.

SEM was employed to carefully verify the morphology of samples Drop-100 and DIP-2L due to their good distribution on the PS substrate (**Figures 21, A, and B**). Remarkably, the micrographs reveal the presence of uniform coatings enveloping the PS substrate, regardless of the employed coating methodology. Additionally, these images depict the presence of Ag rods distributed uniformly across the surface. Upon higher magnifications, it becomes evident that these Ag-rod structures are formed by the assemblage of AgNPs with various sizes, which all exhibit a spherical morphology. These observations confirm the role of CS as not only a reducing agent for Ag ions but also a stabilizing agent. The stabilizing properties of CS facilitated the growth of well-organized Ag rods formed by spherical AgNPs. This stabilization

was achieved through electrostatic repulsion, provided by the protonated amino groups of CS, and chemical interactions between the hydroxyl and amino groups of CS and the Ag^+ ions, preventing aggregation and ensuring the formation of stable, well-defined nanostructures.

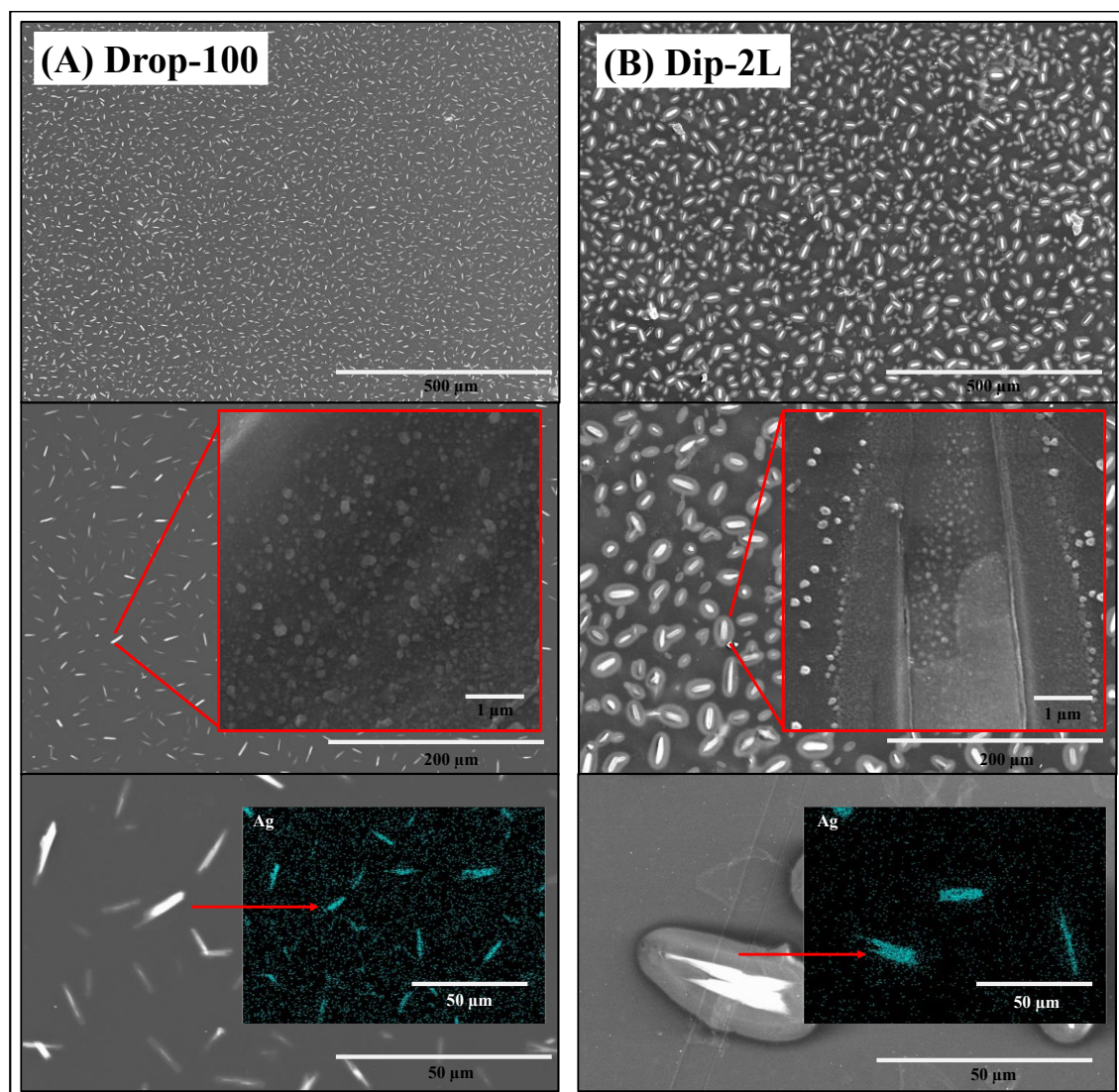


Figure 21. Scanning electron microscopy micrographs of CS-Ag-20% of the coating overview, silver rods and AgNPs, and EDS mapping of Ag, where (A) correspond to sample Drop-100 and (B) sample Dip-2L in different magnifications.

The XPS technique was applied for samples Drop-100 and Dip-2L, revealing the presence of N, C, O (related to CS), and Ag (**Figure 22, A and B**). The high-resolution $\text{Ag}3d$ spectra (**Figure 22, C and D**) showed the presence of Ag in three different chemical states: Ag^0 , $\text{Ag}^+/\text{AgNO}_3$, and Ag_2O , where the intensity of the absorption peak is proportional to the concentration of the substance (Zhao et al., 2022). The 3d HRXPS spectra of coated PS surfaces give rise to two well-resolved peaks at binding energy values of 368.1 and 374.1 eV, which are assigned to $\text{Ag } 3d_{5/2}$ and $\text{Ag } 3d_{3/2}$ of metallic silver (Ag^0) (Nagaraj et al., 2023; Peter et al.,

2023; Sivagami & Asharani, 2023). The two peaks at 369.2 and 375.2 eV can be attributed to Ag 3d_{5/2} and Ag 3d_{3/2}, respectively, which provides evidence for the presence of Ag⁺. In contrast, the low peaks at 367.1 and 373.1 eV (Ag 3d_{5/2} and Ag 3d_{3/2}, respectively) are related to the presence of lower amounts of Ag oxide (Ag₂O) (Ferraria et al., 2012; Reddy et al., 2014).

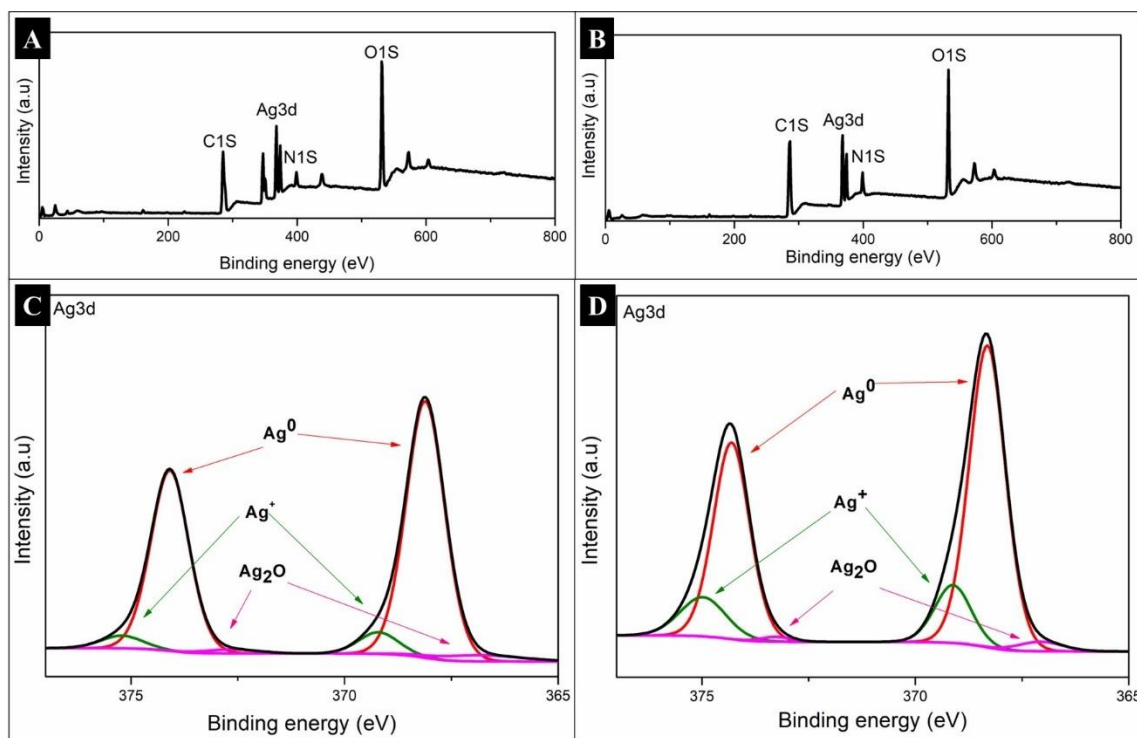


Figure 22. XPS Survey for samples Drop-100 (A) and Dip-2L (B) showing the presence of C, N, O, and Ag. Ag3d spectra for samples Drop-100 (C) and Dip-2L (D).

Although there was no indication of AgNP formation during the CS-Ag composite synthesis, the XPS results showed that the Ag⁺ ions were reduced to Ag by CS, corroborating with SEM images (**Figure 21**). The concentration of acetic acid in CS and temperature plays crucial roles in the reduction procedure, where the higher the temperature and CS concentration, the more significant the nanoparticle formation (Maruthupandy et al., 2019; Tran et al., 2010). In this work, the synthesis was carried out at room temperature without observing AgNP formation. For this reason, the reduction of Ag⁺ ions to Ag⁰ occurred during the coating-drying process.

The preparation of CS-Ag solutions with acetic acid and Ag ions and its subsequent reduction of Ag⁺ to create metal colloids involves two distinct stages: nucleation and growth (Tran et al., 2010). Initially, Ag⁺ ions are reduced to form Ag atoms, which are then stabilized by CS to prevent uncontrolled agglomeration. These stabilized Ag atoms start to cluster together, forming colloidal Ag particles. As the particles grow, CS reduces their surface energy,

aiding in stabilization. Once the particles reach a certain size, they can incorporate additional Ag atoms more easily, marking the conclusion of the nucleation stage and the beginning of the growth phase, which continues primarily through diffusion processes. The early nucleation stage is characterized by higher activation energy compared to the later stages, where Ag particles grow through diffusion processes (Tran et al., 2010; L. Xu et al., 2020).

Besides being directly correlated to composition, roughness, and tissue topography, surface wettability influences the adhesion and proliferation of different cells (Arias Alvarado et al., 2021). When the water contact angle is greater than 90° , the material is considered hydrophobic, and when the angle is lesser, the material is considered hydrophilic. PS is an amorphous polymer with a WCA of about 85° to 97° (Arinda et al., 2019; Zheng et al., 2006). In this work, the WCA for the uncoated PS sample was 82.64° , which aligns with that reported in the literature. For samples coated by the drop method, the found WCA was 65.64° , 79.44° , and 79.72° for Drop-50, Drop-75, and Drop-100, respectively (**Figure 23**). For those coated by the dip-coating method, the WCA were 60.59° , 69.95° , and 69.72° for Dip-1L, Dip-2L, and Dip-3L, respectively.

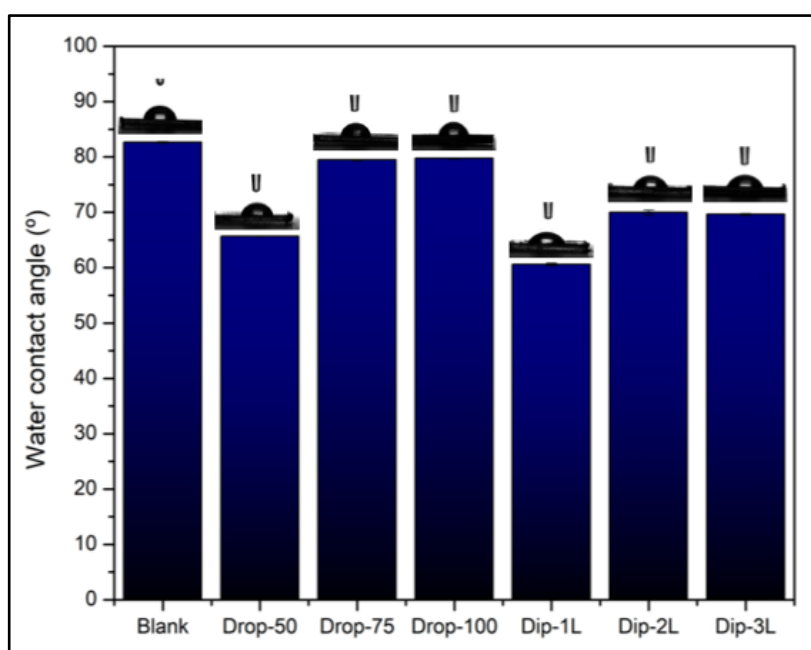


Figure 23. Water contact angle of pure PS sample (Blank) and samples Drop-50, Drop-75, Drop-100, Dip-1L, Dip-2L and Dip-3L.

The surface roughness of Drop-100 and DIP-2L samples was measured using a 3D laser-confocal microscope (**Figure 24**). The surfaces presented some levels of roughness where the Ag rods were present. The surface roughness for Drop-100 was higher than for Dip-2L. This

can be related to the size of the Ag rods, the amount of Ag on the coating surface, and the WCA. According to the Cassie-Baxter model, surface roughness enhances superhydrophobic behavior. Asperities create a solid-liquid and solid-gas interface, preventing liquid penetration and increasing hydrophobicity. Greater rugosity intensifies the Cassie-Baxter state. On hydrophilic surfaces, increased roughness typically leads to a higher contact angle (Nguyen-Tri et al., 2019).

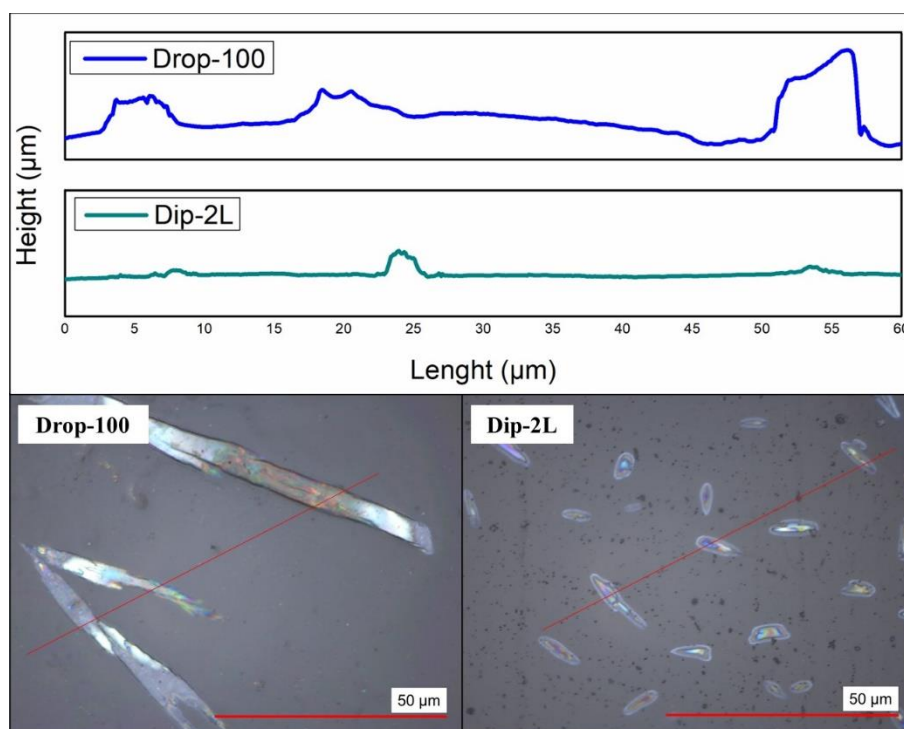


Figure 24. Surface roughness and images of samples DROP-100 and DIP-2L.

When correlating the findings from SEM and 3D-laser confocal microscope, it was possible to notice that some of the Ag rods presented in the coating are half exposed and half embedded in the CS polymeric matrix. This type of structure might enhance the coating's antimicrobial properties and enable a solid fixation of Ag rods to improve the stability of prepared coatings.

The FT-IR spectra showed vibrational bands of functional groups typical of CS (**Figure 25, A**), evidencing its presence in the samples coated with CS-Ag-20%. Typical bands identified in FTIR spectra are: OH axial stretching ($3430\text{--}3485\text{ cm}^{-1}$) overlapped by the NH stretching vibration, C=O axial stretching in secondary amide (1642 cm^{-1}), C–O–C stretching (1076 cm^{-1}) (F. B. Silva et al., 2021; Varma & Vasudevan, 2020). UV-Vis spectra show a prominent absorbance peak at 420 nm (**Figure 25, B**), which represents a strong plasmonic absorption of AgNPs. This result also confirms the formation of AgNPs associated with the

reduction of Ag^+ to Ag^0 by CS. It can be observed that the Drop-100 sample exhibits much stronger light absorption compared to the Dip-2L sample. This is possibly due to the high concentration of AgNPs in the Drop-100 sample. On the other hand, the results obtained from the UV-Vis analysis indicate a strong plasmonic effect of AgNPs that significantly contributes to the antibacterial properties of prepared coatings.

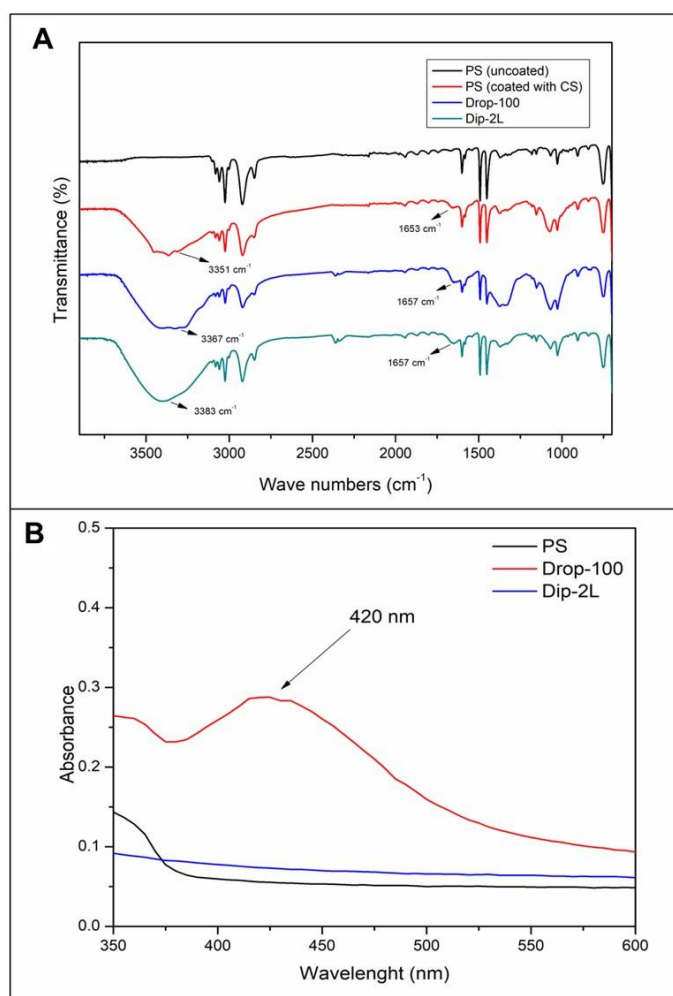


Figure 25. (A) FTIR spectra of uncoated PS, PS coated with chitosan, and samples Drop-100, and Dip-2L. (B) UV-vis spectra of uncoated PS, Drop-100 and Dip-2L

ICP–OES 249 was employed to determine the total quantity of deposited Ag on the PS surface and the results were shown in **Table 6**. As the volume of CS-Ag and the number of coating layers increased, the amount of Ag also rose. For the PS substrate coated by the drop-coating technique, the Ag content was 8.4, 15.8, and 16.4 mg/cm^2 for samples Dip-50, Dip-75, and Dip-100, respectively. Meanwhile, Ag content varied between 7.7 and 9.4 mg/cm^2 for samples prepared by the dip-coating technique. A considerable difference in Ag content was observed between both methods of coating. The Ag content slightly increases as the number of

layers increases for the dip-coating method. Conversely, the Ag quantity doubled its values from the sample coated with 50 μL to the one with 100 μL , which was expected.

Cotton and synthetic fabrics were prepared with Ag-based coatings using commercial colloidal Ag samples, and it was verified that coated fabrics containing higher Ag quantity led to better antimicrobial efficiency (Vu et al., 2022). Considering the antimicrobial application of the coatings, the samples with higher Ag quantities are expected to exhibit higher antimicrobial properties on their surfaces than those with less Ag.

4.3.3 Antimicrobial Properties

A Gram-negative and Gram-positive bacterium, *E. coli* and *S. epidermidis*, were selected as microorganisms to verify the antimicrobial properties of the produced coating, since they are one of the main sources responsible for healthcare-associated infections. The assays were performed under light and dark environments to verify if exposure to visible light can affect its antimicrobial properties. The tests were conducted following contact with different samples, where the bacterial viability, expressed in percentage, indicates the presence of viable bacterial colonies on the coated PS after 120 minutes (*E. coli*) and 30 minutes (*S. epidermidis*) of contact (**Figure 26, A**). The 100% value in the 'Blank' category represents non-coated PS, indicating no antimicrobial effect. For samples prepared using the drop-coating technique with 50, 75, and 100 μL of the CS-Ag-20% formulation, the viability of *E. coli* in dark conditions was 16.93%, 5.29%, and 0%, respectively. Meanwhile, under light conditions, *E. coli* viability was 1.45% for samples Drop-50 and 0% for samples Drop-75 and Drop-100. PS surfaces coated via the dip-coating method exhibited superior efficiency under light conditions, resulting in bacterial viabilities of 6.74%, 2.38%, and 11.24% for samples Dip-1L, Dip-2L, and Dip-3L. While for dark conditions, bacterial viability varied between 32.53% and 34.92%.

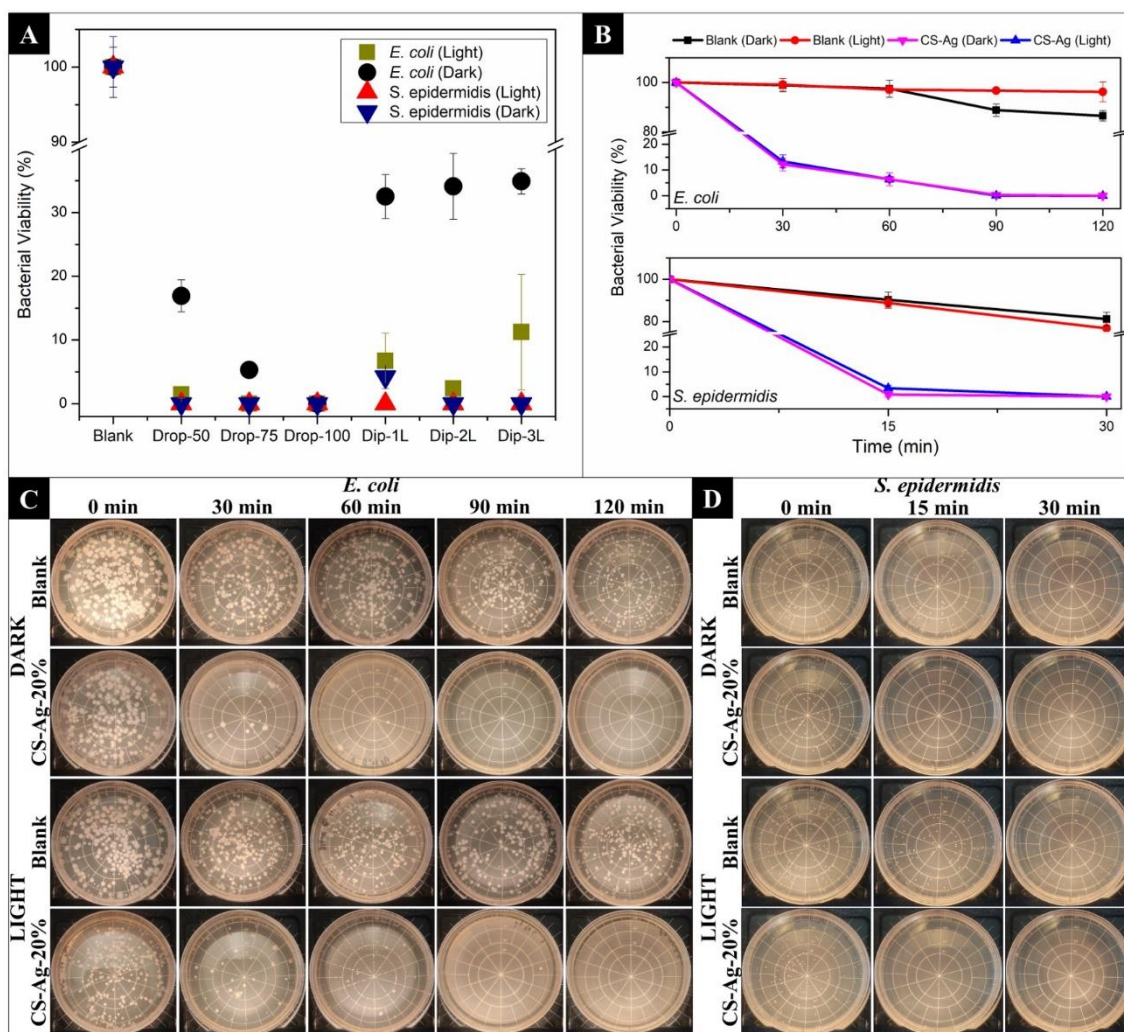


Figure 26. Antibacterial activity against *E. coli* and *S. epidermidis* of CS-Ag-20% coated with different methods on PS surfaces (A). Antibacterial activity of sample DROP-100 against *E. coli* and *S. epidermidis* bacteria over time (B). Agar plates inoculated with *E. coli* (C) and *S. epidermidis* (D) bacterial suspension after contact with the PS samples coated with CS-Ag-20% under light and dark conditions.

Comparing all the samples coated by the dip-coating technique, the one that showed better antimicrobial performance was the DIP-2L, coated with two layers, which is unexpected once the amount of Ag present on the surface was lower than the one coated with three layers. Further investigations are required to understand why the bacterial viability did not increase with the number of coatings once the amount of Ag on the surface was higher in sample DIP-3L than in DIP-1L and DIP-2L. Among all the coated samples, the one prepared with 100 μ L of the CS-Ag-20% formulation by the drop-coating technique was the only one that exhibited no viable *E. coli* cells after 120 minutes of exposure to both light and dark conditions. Similar assays were conducted using the Gram-positive bacterium *S. epidermidis* but with a shorter contact time (30 minutes). The results demonstrated significant antibacterial properties, with no viable bacterial cells after 30 minutes of contact for all samples except Dip-1L, which showed

4.21% viable cells in dark conditions. This indicates the efficiency of the prepared coating in killing gram-positive bacteria in a shorter exposure time.

In the present work, no bacterial viability was found after 120 minutes of white light exposure against *E. coli* and after 30 minutes against *S. epidermidis*. This resulted in an antimicrobial efficiency close to 100%. Furthermore, similar findings were observed under dark conditions, which implies that the prepared coatings could reach good antibacterial efficiency irrespective of the condition. A synergistic effect is observed when combining CS and Ag in a single material. This happens because CS stabilizes and confers a positive charge to Ag surfaces, enhancing their binding to the negative charges at the bacterial cell surface (Lima et al., 2017). It is worth noting that the prepared coatings exhibited enhanced antimicrobial activity under the LED light, as observed in the test against *E. coli* (**Figure 26, A**). This enhancement possibly results from the photocatalytic activity of AgNPs triggered by the light irradiation, which promoted an influential generation of reactive oxygen species (ROS) (e.g., hydroxyl radical ($\bullet\text{OH}$), superoxide radical ($\bullet\text{O}_2^-$) and hydrogen peroxide (H_2O_2)) – potent antibacterial species.

Comparing the presented results, the coating prepared by the drop-coating method with 100 μL (sample Drop-100) showed the most satisfactory results against Gram-positive and Gram-negative bacteria in both dark and light conditions. This led to a new experiment to investigate the kinetics of the antimicrobial mechanism of the coating over time. In the test against *E. coli*, the presence of bacteria was monitored every 30 minutes until no viable cells were left, while for *S. epidermidis*, evaluations were made every 15 minutes (**Figure 26, B**).

When evaluating the antibacterial properties of the coating against *E. coli*, it was observed that 120 minutes of contact time were required to eliminate all viable cells. However, a significant reduction in the number of colonies was noted after just 30 minutes, with a gradual decrease leading to complete bacterial eradication by 120 minutes. In contrast, the coating demonstrated even greater efficacy against *S. epidermidis*, eradicating viable cells within just 30 minutes of contact. **Figure 26** (C and D) shows agar plates inoculated with *E. coli* and *S. epidermidis* bacterial suspensions after contact with the PS samples coated with CS-Ag-20% under light and dark conditions, highlighting the remarkable antimicrobial potential of the coating in eliminating both gram-positive and gram-negative bacteria.

Vaz et al. (2018) verified the antimicrobial properties of a CS coating (low and medium molecular weight) grafted poly(ethylene-alt-maleic anhydride) against *Xylella fastidiosa*. The results indicated 82% and 98% bacteria reduction after four days of incubation for low and medium molecular weight CS, respectively (Vaz et al., 2018). Saidin et al. (2013) used

polydopamine films that underwent metallization with Ag nanoparticles for 12 and 24 hours, after which their antimicrobial efficacy was assessed against *E. coli*. The findings revealed a bactericidal ratio of 32.58% for samples metalized for 12 hours and a substantially improved ratio of 97.88% for those metalized for 24 hours (Saidin et al., 2013). Fan *et al.* (2021) synthesized a CS-AgNPs composites. The short-term antibacterial activity was tested against *S. aureus* and *E. coli*. For *E. coli*, a concentration of 150 µg/mL of CS-AgNPs could kill almost 100% of viable cells within 90 min, while for *S. aureus*, higher concentrations and exposure time were required to obtain a similar results (Fan et al., 2021). When comparing the literature, it is possible to notice that using AgNPs and CS as coating material for antimicrobial purposes is a growing field. However, the synthesis process can be complex and require various materials. In this work, a simple method to synthesize the CS-Ag composite for coatings was proposed, which showed highly efficient antimicrobial properties, capable of eliminating bacteria after just 120 minutes of contact.

4.3.3.1 Reusability test

After the first antimicrobial evaluation (light and dark), the samples were washed with saline water, vortex in an ethanol solution, and air-dried, and the spread plate technique method was applied again to verify if the produced coating could be effective more than once. Based on tests conducted against *E. coli* (**Figure 27, A**), under light conditions, bacterial viability was 13.38% after 30 minutes during the first use. This decreased to 6.41% after 60 minutes, 0.11% after 90 minutes, and no bacterial growth was detected after 120 minutes. A similar pattern was observed during the second use, with bacterial viability gradually decreasing to 0% after 120 minutes. However, the antibacterial properties of the coating declined during the third use. After 30 minutes of light exposure, bacterial viability was 53.60%, and after 120 minutes, it was 10.38%. Under dark conditions, both the first and second use resulted in bacterial viability reaching 0% after 120 minutes of contact with the coating. However, during the third use, bacterial viability was 31.40% after 120 minutes. This indicates a 21.02% difference between light and dark conditions during the third use.

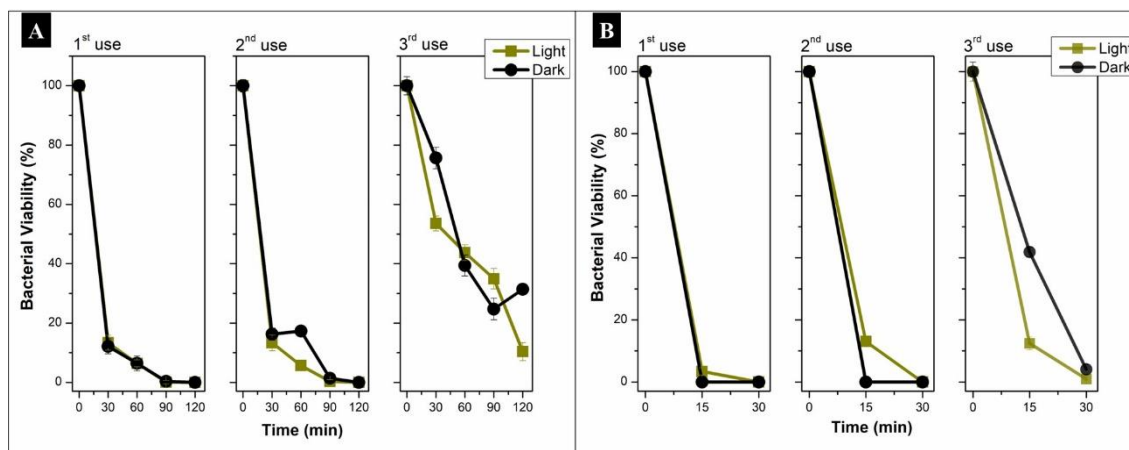


Figure 27. CS-Ag-20% coatings usability test. (A) Bacterial viability of *E. coli* after 1, 2, and 3 uses. (B) Bacterial viability of *S. epidermidis* after 1, 2, and 3 uses.

Regarding the evaluation of the coating against *S. epidermidis* (Figure 27, B), under light conditions, the bacterial viability was 3.39% after 15 minutes during the first use. After 30 minutes, the viability dropped to 0%, indicating high antibacterial properties. In the second use, the results were similar, suggesting that the antibacterial properties of the coating remained consistent over two applications. During the third use, bacterial viability was 12.43% after 15 minutes of light exposure, and 0.95% after 30 minutes. Similarly, in dark conditions, both the first and second use resulted in bacterial viability reaching 0% after 30 minutes. However, in the third use, bacterial viability was 41.86% after 15 minutes and decreased to 4.06% after 30 minutes.

The CS-Ag coating exhibits strong antibacterial properties against both *E. coli* and *S. epidermidis* under light and dark conditions, particularly during the first and second uses. However, its effectiveness diminishes during the third use, especially under dark conditions. While the coating remains more effective against *S. epidermidis* under light exposure, reducing bacterial viability to nearly zero even on the third use, its performance against *E. coli* shows a more significant decline. These results suggest that while the CS-Ag coating is a promising antibacterial agent, its long-term efficacy, particularly under repeated use and in dark conditions, may require longer contact times to eliminate bacteria completely.

The difference in bacterial viability between light and dark conditions is likely related to the distinct mechanisms of ROS generation under light and Ag^+ released under dark. The increased antibacterial activity under light exposure, especially in the third use, can be attributed to the generation of ROS. AgNPs can produce ROS such as hydroxyl radicals, superoxide anions, and hydrogen peroxide when exposed to visible light. These ROS can cause oxidative damage to bacterial cells, enhancing the antimicrobial effect (Kędziora et al., 2018). Ag is one

of the materials that integrate the class of plasmonic photocatalysts studied because of its visible range, resistance to degradation, high stability, and disinfection performance (Cheikhrouhou et al., 2020; Y. Liao et al., 2021). The improved performance of the coating under light suggests that ROS generation plays a crucial role. In the absence of light, the ROS-mediated antibacterial activity is minimized, leading to a reliance on contact killing, which may diminish over time. Under dark conditions, suggests the released of Ag^+ is a significant mechanism. AgNPs can directly interact with bacterial cell membranes, causing structural damage and leading to cell death (Yin et al., 2020). This mechanism does not require light and can explain the initial high antibacterial activity.

The decrease in antibacterial effectiveness in the dark over time and with repeated use could be due to the gradual depletion or inactivation of the active Ag species on the coating surface, reducing its contact killing capability. Ladhari et al. (2024) reported the preparation of polyhydroxybutyrate (PHB) microfiber membranes decorated with photoactive Ag-TiO₂ NPs. The authors observed that the decoration of Ag-TiO₂ nanoparticles strongly enhanced the antibacterial properties of the membranes, particularly under light illumination, due to their photocatalytic activity, which corroborates with the findings in this present study (Ladhari et al., 2024).

The coating morphology might also influence the antimicrobial properties. As previously mentioned, Ag rods containing AgNPs are distributed all over the PS substrate, half-exposed on the surface, and half-embedded into the CS matrix. These embedded Ag rods could imply a slower release of the Ag^+ , making it possible to have a more prolonged antimicrobial effect, while the ones exposed have a quicker release. Conversely, further investigations are needed to understand these antimicrobial mechanism observations and optimize the coating's antibacterial performance. Still, it is believed that after several uses, antimicrobial properties were higher under light irradiation because of the generation of ROS, which is enhanced due to the photocatalytic activity of AgNPs.

4.3.3.2 Biofilm Formation

An assay to evaluate biofilm formation was conducted using sample Drop-100, which was coated with 100 μL of the CS-Ag-20% composite through the drop-coat technique. This assessment targeted the *E. coli* and *S. epidermidis* bacterial strains. As a negative control, an uncoated PS surface was employed, and the presence of bacteria was assessed via SEM. The findings are demonstrated in **Figure 28**. Considering the uncoated PS, it is evident that viable bacterial cells are widespread across the surface, particularly when viewed at lower

magnification. In the case of *E. coli*, no evidence of biofilm formation was observed. However, for *S. epidermidis*, noticeable cell clusters were detected, indicative of biofilm formation. In contrast, the examination of the coated PS surface reveals a significant reduction in bacterial presence. This reduction can be attributed to the antimicrobial properties of the AgNPs and CS presence in the coating, which led to the destruction of bacterial cell walls and, ultimately, their death.

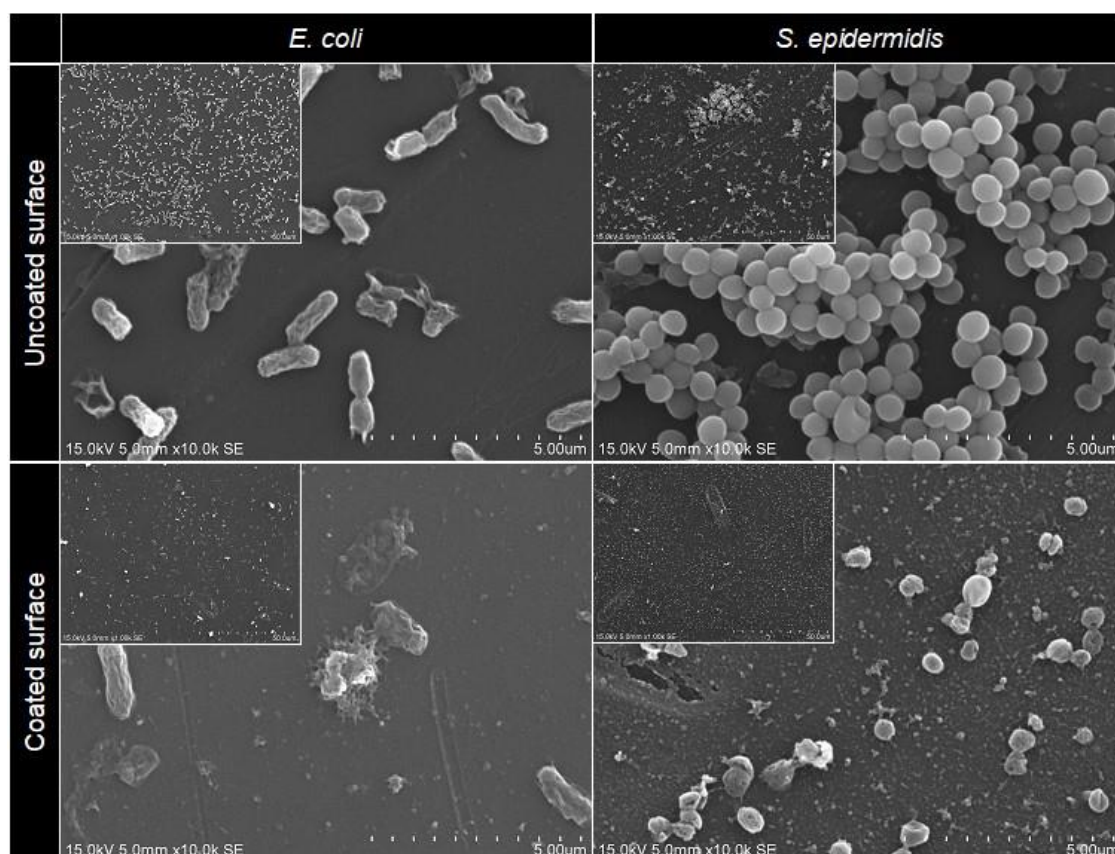


Figure 28. SEM micrographs of uncoated PS and Drop-100 after five days in contact with a bacteria suspension of *E. coli* and *S. epidermidis*.

4.3.3.3 Proposed Antimicrobial Mechanism

The proposed antibacterial mechanism of the CS-Ag composite synthesized in this work is illustrated in **Figure 29**. When bacteria are brought in contact with the prepared coatings, Ag^+ ions are released, causing cell wall damage, which modifies the metabolic pathways and precludes DNA replication and cell division (Asghar et al., 2020; Polinarski et al., 2021; F. Zhang et al., 2020). In this scenario, CS is vital as it reacts with the bacterial cell wall and the cell membrane owing to its positively charged amino groups (Asghar et al., 2020; Sahariah & Másson, 2017). In a non-published assay, the CS-Ag-20% composite showed a more significant bacterial reduction rate than CS and AgNO_3 , confirming their synergistic effect. In this work,

CS-Ag-20% coated in the PS sample with 100 μL exhibited an efficiency of 100% in eliminating the gram-negative and gram-positive bacteria, *E. coli* and *S. epidermidis*, after 120 and 30 minutes of light irradiation, respectively. The samples coated with 50 and 75 μL exhibited an efficiency higher than 95%, suggesting that the synthesized composite can be efficient even in lower amounts. The samples coated by the dip-coating technique also showed a reduction in bacterial population after 120 minutes of illumination.

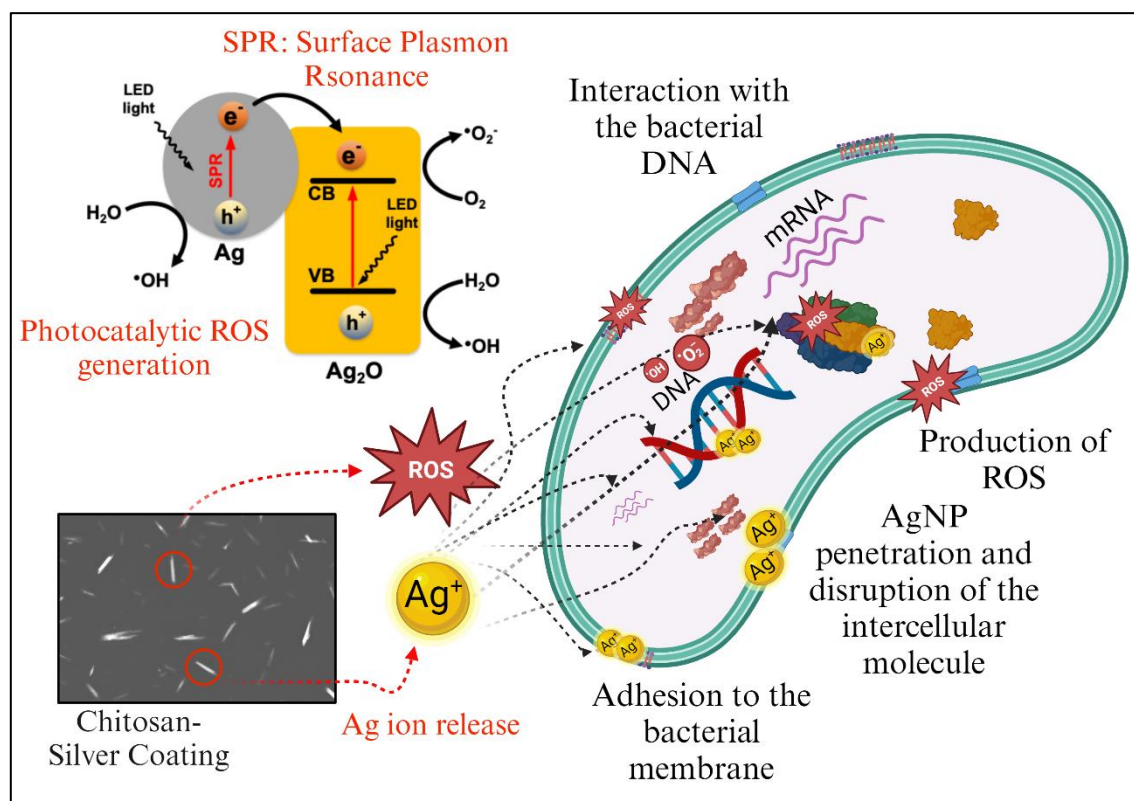


Figure 29. Proposed mechanism of antimicrobial activity on prepared CS-Ag composite coatings.

Notably, the photocatalytic activity of AgNPs significantly promoted the antibacterial activity of prepared coatings under LED light. These NPs have been widely demonstrated to possess excellent surface plasmon resonance (SPR) effect (or plasmonic effect), which enhances their capacity to absorb visible light, as observed in **Figure 25, B**. In particular, this effect makes AgNPs photoactive to generate charge carriers, including electrons (e⁻) and holes (h⁺), which initiate redox reactions with O₂ and H₂O to produce ROS (R. T. P. da Silva et al., 2020). These reactive species cause oxidative stress and damage the cell cytoskeleton, proteins, and nucleic acid oxidation, leading to bacterial cell inactivation and even death (W. Li et al., 2019; Mehata, 2021). Moreover, the formation of Ag₂O, as confirmed by the XPS analysis (**Figure 22**), possibly induces a hybrid composite nanostructure between AgNPs and Ag₂O

(Ag/Ag₂O), which facilitates an efficient charge separation as electrons transfer from AgNPs to Ag₂O while holes remain in these NPs (W. Li et al., 2019). As a result, the ROS generation is strongly promoted, further enhancing the antibacterial activity.

In general, three possible routes stand out for the antibacterial activity of the prepared coatings. The first one is the Ag⁺ ion release, which can bind with transport proteins, leading to proton leakage and an induced collapse of the proton motive force. The second one regards the non-oxidative mechanism, which involves the inactivation of microorganisms by decreasing the critical cellular metabolism without oxidative stress. The last and most attractive one is oxidative stress induction, where different types of ROS are generated upon the photocatalytic activity of AgNPs and, especially, Ag/Ag₂O nanocomposite. When considering the coating morphological structure and the findings presented in this research, it is believed that the antimicrobial mechanisms happen by Ag ion release and ROS generation. Even though further investigations are needed to determine which one plays a dominant role, it is most likely that under light irradiation, the antimicrobial activity happens by ROS generation, while under dark conditions, Ag ion release is the most suitable route. The distinctive structure of the coatings with half-exposed and half-embedded Ag rods induces an effective antimicrobial activity while enhancing its stability.

4.4. Partial Conclusions

In summary, this study presented a two-step method for synthesizing a CS-Ag composite. The simplicity and facility of the synthesis, involving room-temperature stirring of CS with a Ag solution, underscore its potential antibacterial properties when coated on a PS surface. The formulation containing 20% Ag⁺ displayed a uniform distribution featuring Ag rods composed of AgNPs that grew in situ during drying, half-embedded into a CS film. Antimicrobial assays demonstrated a 100% bactericidal rate against *E. coli* and *S. epidermidis* under dark and light conditions. Besides that, the coatings can reduce biofilm formation, and their stability over multiple reutilizations further highlights their durability and reliability. When in contact with the coating, bacteria undergo cell wall damage induced by the release of Ag⁺ ions and/or ROS generation, which, combined with the CS's positive charge amino groups, disrupts metabolic pathways, leading bacteria to death. These newly synthesized formulations hold significant promise as alternatives for antimicrobial coatings, offering potential solutions to combat biofilm formation and providing versatile coating materials, particularly within the biomedical field.

CHAPTER 5: ARTICLE 3

Chitosan and Nanochitosan as dual reducing-stabilizing agents in the synthesis of AgNPs for advanced biomedical applications

Marcos Antonio Polinarski^{a,b,c,d}, Lazaro José Gasparrini^{c,d}, Manuela Nepomuceno Ladeira^e, Juliana Bernardi-Wenzel^e, Phuong Nguyen-Tri^{a,b}, Helton José Alves^{c,d}

^a Laboratory of Advanced Materials for Energy and Environment, Université Du Québec à Trois-Rivières (UQTR), 3351, Boul. des Forges, C.P. 500, Trois-Rivières, Québec, G9A 5H7, Canada.

^b Department of Chemistry, Biochemistry and Physics, Université du Québec à Trois-Rivières (UQTR), 3351 Bd des Forges, Trois-Rivières, QC G8Z 4M3, Canada.

^c Renewable Materials and Energy Laboratory (LABMATER), Federal University of Paraná (UFPR – Setor Palotina), R. Pioneiro, 2153, 85950-000, Palotina, PR, Brazil.

^d Postgraduate Program in Environmental Engineer and Technology, Federal University of Paraná (UFPR – Setor Palotina), R. Pioneiro, 2153, 85950-000, Palotina, PR, Brazil.

^e Medicine Course – Toledo Campus, Federal University of Paraná, Rodovia PR 182, S/N, Km 320/321, CP 2028, Toledo-PR, 85919-899 Brazil.

Abstract

The rise of multidrug-resistant infections, especially those involving biofilms on medical devices, has created an urgent need for alternative antimicrobial coatings. Nanoparticles and natural biopolymers, such as AgNPs and CS are attracting significant attention for their broad-spectrum antimicrobial potential. This work presents a two-step synthesis of AgNPs using CS and NCS as reducing agents, with varying AgNO₃ concentrations. The synthesized AgNP solutions were characterized using UV-Vis spectroscopy, dynamic light scattering (DLS), and transmission electron microscopy (TEM), and their antimicrobial activity was tested against *Escherichia coli* and *Staphylococcus aureus*. Antimicrobial coatings were then applied to the surface of central venous catheters (CVCs), and their morphology and biofilm-inhibiting capacity were assessed using scanning electron microscopy (SEM). The results indicate that both CS and NCS effectively reduced Ag⁺ to Ag⁰, enabling the formation of small, spherical, and potentially semicrystalline AgNPs. Antimicrobial testing revealed that AgNPs synthesized with CS showed a larger inhibition zone against *S. aureus*, while no significant differences were observed among samples tested against *E. coli*. The use of CS and NCS appeared to influence the stabilization and size regulation of AgNPs, though trends were non-linear. Additionally, both CS- and NCS-based AgNP coatings demonstrated antibiofilm activity, suggesting their great potential as antimicrobial coatings for medical device surfaces.

Keywords: nanoparticles, silver, biopolymer, biofilm, antimicrobial.

5.1 Introduction

Controlling the spread of infections caused by bacteria, particularly those associated with multidrug resistance (MDR), is a global health priority (M. Li et al., 2023). The rapid emergence of MDR strains is primarily driven by the improper and excessive use of conventional antibiotics, which leads to infections that are increasingly difficult to treat. MDR bacteria rarely respond to conventional treatments, increasing the risk of pathogen spread, illness, and mortality (Bolaños-Cardet et al., 2024). It has been reported that MDR bacterial infections are the reason for approximately 700,000 deaths worldwide every year. By 2050, MDR bacteria will overtake cancer as the world's leading cause of death, resulting in 10 million deaths and \$100 trillion of economic loss (Bolaños-Cardet et al., 2024; Song et al., 2021).

Nosocomial infections, also known as hospital-acquired infections (HAIs), are particularly concerning within this context. HAIs are infections that patients acquire during treatment in healthcare settings, and they are the sixth leading cause of death in industrialized countries. (Bolaños-Cardet et al., 2024; Low et al., 2021). These infections, which include pneumonia, gastrointestinal infections, surgical site infections, bloodstream infections, and urinary tract infections, often complicate patient outcomes (Ciccacci et al., 2024; Tesini & Dumyati, 2023). Indwelling medical devices, such as central venous catheters (CVCs), are a significant contributor to HAIs because they are prone to bacterial adhesion and biofilm formation (S. Chen et al., 2021; Melariri et al., 2024). Biofilms are an assemblage of microorganisms attached to a surface, enclosed in a self-produced polysaccharide matrix. They shield bacteria from the immune system and antibiotic treatments, making infections difficult to treat, leading to persistent and potentially life-threatening infections (Slettengren et al., 2020; Ul Haq & Krukiewicz, 2023). The pathogens most commonly associated with biofilm formation on medical devices are *E. coli*, *S. aureus*, *K. pneumoniae*, *S. pneumoniae* and *P. aeruginosa* (Canciu et al., 2023; Murray et al., 2022).

Given these challenges, antimicrobial coatings for medical devices, particularly catheters, have emerged as a promising solution. These coatings are designed to prevent bacterial adhesion and growth on device surfaces (He et al., 2024; Ul Haq & Krukiewicz, 2023; Y. Xing et al., 2024). Different materials, including metals, polymers, and organic compounds, have been explored for their antimicrobial properties (Rogala-Wielgus et al., 2024). Among these, CS and AgNPs are receiving significant attention due to their unique physicochemical properties, stability, and strong antimicrobial properties (Polinarski et al., 2024).

CS (β -(1,4)-linked polysaccharide of D-glucosamine), is a biopolymer sourced from the N-deacetylation of chitin (Bach et al., 2022). It has many sensitive functional groups (amino, hydroxyl, and acetamido groups), which confers to the material a high cationic power and unique properties such as its biocompatibility, biodegradability, low toxicity, film-forming ability, and eco-friendliness (Edo et al., 2024; Polinarski et al., 2021). Due to that, CS can be used for a broad range of purposes by the industry for agriculture, pharmaceuticals, food and nutrition, and biomedical applications (Campana et al., 2018). CS exhibits antimicrobial activity against various pathogens, including gram-positive and gram-negative bacteria, and fungi. Its action mechanism includes electrostatic attraction, membrane permeabilization, and enzyme inhibition, depending on the type of microorganism and the characteristics of CS (e.g., molecular weight (Mw) and degree of deacetylation (DD)) (Nasaj et al., 2024). CS functional groups allow strong interactions with metal ions and nanoparticles (e.g., AgNPs), enabling the formation of advanced composites with enhanced antimicrobial properties (Polinarski et al., 2024).

Ag is another material with well-known antimicrobial, optical, and catalytic properties, especially at the nanoscale (B. Du et al., 2024; Obaid et al., 2024; F. B. Silva et al., 2021). AgNPs have a high surface-to-volume ratio, which enhances their antimicrobial efficacy, including against MDR strains (Graziani et al., 2024). Those characteristics make AgNPs particularly valuable in biomedical applications, such as wound dressings, and medical device coatings (Meher et al., 2024). Both CS and AgNPs individually stand out for their remarkable antimicrobial activity and combining them in a single material is a promising strategy to increase antimicrobial effectiveness (Mirajkar et al., 2021; Polinarski et al., 2021).

One possible route to synthesize CS-Ag composites is incorporating a CS solution into previously synthesized AgNPs, however, this method may compromise the long-term stability of the nanoparticles (Polinarski et al., 2024). Alternatively, a CS solution can be added during the synthesis of AgNPs, acting as a capping and/or reducing agent (Ferrerres et al., 2023; Frank et al., 2020). This latter approach is preferable because the stabilizing interactions between the metal and the biopolymer significantly enhance colloidal stability, biocompatibility, and antimicrobial properties, which are desirable characteristics for fabricating antimicrobial coatings.

In this work, CS and NCS with different molecular weights were synthesized from shrimp shells. These biopolymers were then used to produce AgNPs in a simple two-step method, where CS and NCS served as both reducing and stabilizing agents. CS and NCS reduces silver nitrate (AgNO_3) through their functional groups, specifically the amino ($-\text{NH}_2$)

and hydroxyl (-OH) groups, which donate electrons to reduce Ag ions (Ag^+) to metallic Ag (Ag^0). This combination of CS, NCS, and AgNPs is expected to result in a strong antimicrobial material for coating CVCs surfaces in order to prevent biofilm formation. Thus, the present study provides valuable insights into the potential of CS-AgNPs as a promising antimicrobial material, which could significantly enhance the safety and efficacy of medical devices, ultimately contributing to the reduction of HAIs and combating the growing threat of MDR bacteria.

5.2 Material and Methods

5.2.1 Procedures to obtain chitosan

Freshwater shrimp shell, an aquaculture waste, was provided by freshwater shrimp (*Macrobrachium rosenbergii*) producers from western Paraná, Brazil, and used as raw material to produce CS according to the methodology described by Alves et. al. (H. J. Alves et al., 2018) with modifications. Briefly, the process to obtain CS involves the following sequential steps: 1) shrimp's cephalothoraxes washing, cleaning, and drying; 2) ball milling followed by sieving in a 63 μm sieve (230 mesh); 3) demineralization with a 0.55 mol.L^{-1} solution (two washes, 20 minutes each) followed by deproteination with a 0.3 mol.L^{-1} NaOH solution at 80°C and vigorous stirring (two washes, 20 minutes each) to obtain chitin; and 4) deacetylation process of chitin, in a reflux system using a 60% (w/v) NaOH solution at 115°C and 16 hours, resulting in CS.

5.2.2 Procedures to obtain nanochitosan

CS obtained from the previous step was used to produce the NCS through a physical process that involves thermal shock followed by grinding. The methodology for obtaining NCS is protected by patent application number BR 102017022250 (Alves et al., 2019) and was described by Silva et. al. (2021) (Silva et al., 2021) with few modifications. Briefly, it involved the following steps: CS solubilization in an acetic acid solution for 17 h at room temperature; precipitation in 2 M NaOH in a 1:1 ratio (V.V⁻¹) followed by washing until pH 7; drying process by thermal shock (100°C for 10 minutes followed by room temperature for 5 minutes, for 8 hours); grinding in a ball mill for 4.5 hours; and sieving.

5.2.3 Synthesis of silver nanoparticles

CS and NCS obtained from the previous process were used to synthesize AgNPs. The synthesis method was adapted from Tran et al. (2010), Rodríguez-Argüelles et al. (2011), and Rajivgandhi et al. (2019) (Rajivgandhi et al., 2019; Rodríguez-Argüelles et al., 2011; Tran et

al., 2010), where the CS and NCS were used as both reducing and stabilizing agent. CS and NCS solutions were prepared by dissolving 150 mg of the biopolymers in a 50 mL solution of 2% v/v glacial acetic acid. The mixture was continuously stirred at 30°C until complete dissolution of CS and NCS. Subsequently, the solutions were transferred to a three-neck flask, covered with foil to prevent light-induced degradation, and heated under reflux conditions until boiling. Following this, a 5 mL solution of AgNO₃ (75, 37.5, and 25 mg) was added dropwise, with the system maintained at 100°C for 6 hours. Color changes were observed within the first hour, transitioning from colorless to light-yellowish and dark-yellowish, indicating the formation of AgNPs. Finally, the colloidal solutions were cooled to room temperature, stored in sealed Schott glass bottles, wrapped in foil, and refrigerated for future use. Details of the synthesized AgNPs are shown in **Table 7**.

Table 7. Description of the synthesized AgNPs: samples, and amounts of chitosan, nanochitosan, and AgNO₃.

Samples	Chitosan (mg)	Nanochitosan (mg)	AgNO ₃ (mg)	Ratio (w/w)	Ag concentration (mg/mL)
CS-Ag_2	150	-	75	2:1	0.73
CS-Ag_4	150	-	37.5	4:1	0.36
CS-Ag_6	150	-	25	6:1	0.24
NCS-Ag_2	-	150	75	2:1	0.73
NCS-Ag_4	-	150	37.5	4:1	0.36
NCS-Ag_6	-	150	25	6:1	0.24

5.2.4 Preparation of CS-Ag and NCS-Ag NP coatings

Sterile CVC were purchased from Blenta. Before receiving the coating, the catheters were cut into 1cm (length) and submitted to pre-treatment with plasma (Air, 8 kV, 120 kHz, 18 W for 4 minutes), to improve the distribution of the coating over the surface. The CVC pieces were then dip coated by fully immersing the samples into the CS-Ag and NCS-Ag solutions for 5 minutes, airdried in aseptic conditions, and stored until its characterization.

5.2.5 Materials Characterization

The average size of the CS-Ag and NCS-Ag NPs were analyzed using a Dynamic Light Scattering Analyzer (Bettersize, Nanopitc 90). The absorbance was measured in a UV-visible spectrophotometer at a wavelength from 300 to 700 nm. Transmission electron microscopy

analyses of CS-Ag and NCS-Ag NPs were performed with a TECNAI G² F20 instrument FEI operated at 200 kV, with a STEM spot size of 8. Analyses in high-resolution mode (HRTEM) were performed under cryogenic conditions, at liquid N₂ temperature (-178 °C) to avoid CS and NCS decomposition. The morphological features of the coated catheters were obtained by scanning electron microscopy (SEM, Tescan VEGA3 and Hitachi). Elemental mappings were performed using energy-dispersive X-ray spectroscopy (EDS, FEI Quanta 440 – OXFORD Instruments) to elucidate the chemical composition of the coatings.

5.2.6 Antimicrobial Activity

5.2.6.1 Agar Disk Diffusion Method

Pure cultured *Escherichia coli* ATCC 25922 and *Staphylococcus aureus* ATCC 6538 strains were prepared in Mueller-Hinton (MH) agar plates. With a sterile loop, colonies were picked up from pure cultures and suspended in a sterile saline solution. The bacterial suspensions were adjusted to 0.5 McFarland turbidity standard (1.5×10^8 CFU/mL). Sterile paper disks containing 10 μ L of each CS and NCS AgNPs were prepared. Then, 100 μ L of each bacterial suspension was spread into a MH agar plate and the paper disks were placed on the agar. Plates were incubated at 37°C for 18-24 h and the diameter of each zone around the disk, where bacterial growth was inhibited, was measured in millimeters, according to CLSI (CLSI, 2015b).

5.2.6.2 Minimal Inhibitory Concentration

The antibacterial activity of CS-AgNPs and NCS-AgNPs was verified by the MIC test, performed in triplicate, against *E. coli* and *S. aureus*, according to CLSI (CLSI, 2015a). This test provides information about the lowest concentration of the produced antibacterial agent capable of inhibiting bacterial growth. Freshly prepared microbial suspensions (1.5×10^8 CFU/ml) were diluted in sterile saline water until a final concentration of 5×10^5 CFU/mL. Then, CS and NCS AgNPs solutions were tested in dilutions ranging from 100% to 0.05% (v/v). For that, 100 μ L of each dilution was distributed in a 96-well microtiter plate containing 100 μ L of Muller Hinton Broth (MHB) and 20 μ L of bacterial suspension. Two positive controls were prepared, the first with 200 μ L of MHB, and the second with 100 μ L of MHB and 100 μ L of distilled water, both with 20 μ L of bacterial suspension. Negative controls were also prepared. The first with 200 μ L of MHB, with no bacterial suspension, and the second with 100 μ L of ciprofloxacin (50 mg/mL), 100 μ L of MHB, and 20 μ L of bacterial suspension. After that, the samples were incubated for 24 h at 37°C, and then, 10 μ L of 2,3,5-Triphenyltetrazolium

chloride was added in each well and incubated again for 2 h. Finally, the wells with microbial growth turned red, while the ones without microbial presence were colorless.

5.2.6.3 Antibiofilm Activity Test

The antibiofilm activity tests were performed following the methodology proposed by Mulla et al. (2016) and Haney, Timble, and Hancock (2021), with modifications (Haney et al., 2021; Mulla et al., 2016). Polyurethane catheters coated with CS-AgNPs and NCS-AgNPs (2:1 ratio CS/AgNO₃ w/w) were used in this testing. Freshly prepared *E. coli* and *S. aureus* microbial suspensions (1.5×10^8 CFU/ml) were diluted in a 1:15 ratio (v/v). Then, 20 μ L of the diluted bacterial suspension was distributed in a 96-well microtiter plate containing 200 μ L of MHB and the coated catheters, measuring 0.5 cm, were placed on each well. Positive control was prepared with 200 μ L of MHB and 20 μ L of bacterial suspension, with a non-coated catheter. Negative controls were prepared with 200 μ L of MHB, with no bacterial suspension, and the second with 100 μ L of ciprofloxacin (50 mg/mL), 100 μ L of MHB, and 20 μ L of bacterial suspension. After that, samples were incubated for 5 days at 37°C and submitted to fixation and dehydration processes (Bates et al., 2021). Scanning electron microscopy (SEM) analysis was used to observe biofilm formation and bacteria.

5.3 Results and Discussion

5.3.1 Chitosan and Nanochitosan

CS and NCS were successfully synthesized as previously described and the SEM was employed to verify the morphology of the biopolymers. The micrographs (**Figure 30**) showed a clear difference between CS and NCS, both in shape and size. While NCS has a more uniform size distribution, CS presents particles/agglomerates with irregular shapes.

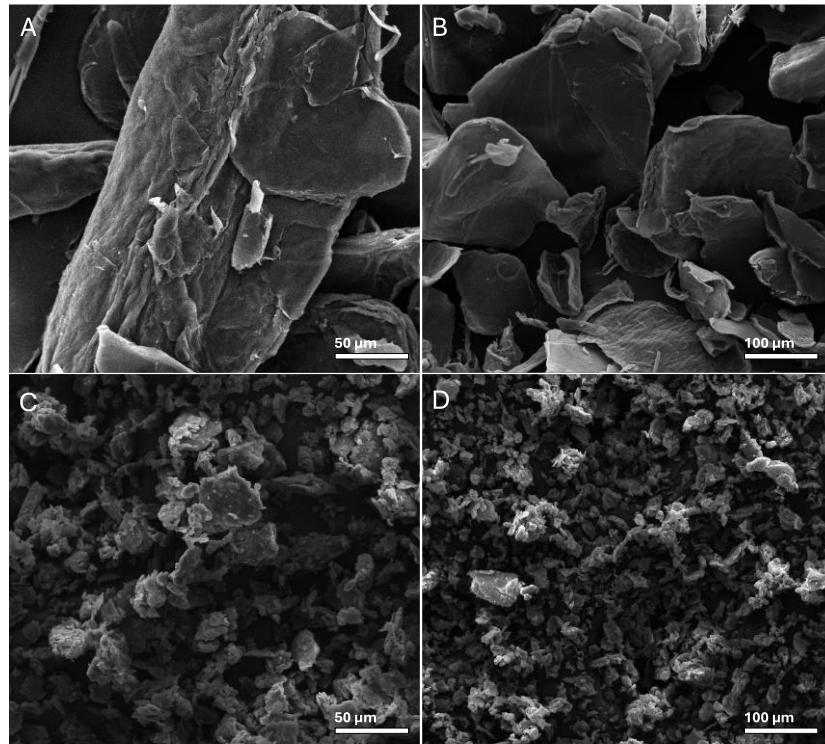


Figure 30. Scanning Electron Microscopy of chitosan at A) 1000x magnification; and B) 500x magnification; and nanochitosan at C) 1000x magnification and D) 500x magnification.

This difference in size is explained by the thermal shock applied during the NCS synthesis, which promotes a reduction in its the Mw, affecting its size. DLS analysis showed that CS has a particle size distribution ranging from 5.61 nm to is 2.5 µm, while for NCS it ranges from 5.61 nm to 158 nm (**Figure 31**). Similar observations were reported by Silva et. al. (2021) (F. B. Silva et al., 2021) and Alves et al. (2021) (H. J. Alves et al., 2021).

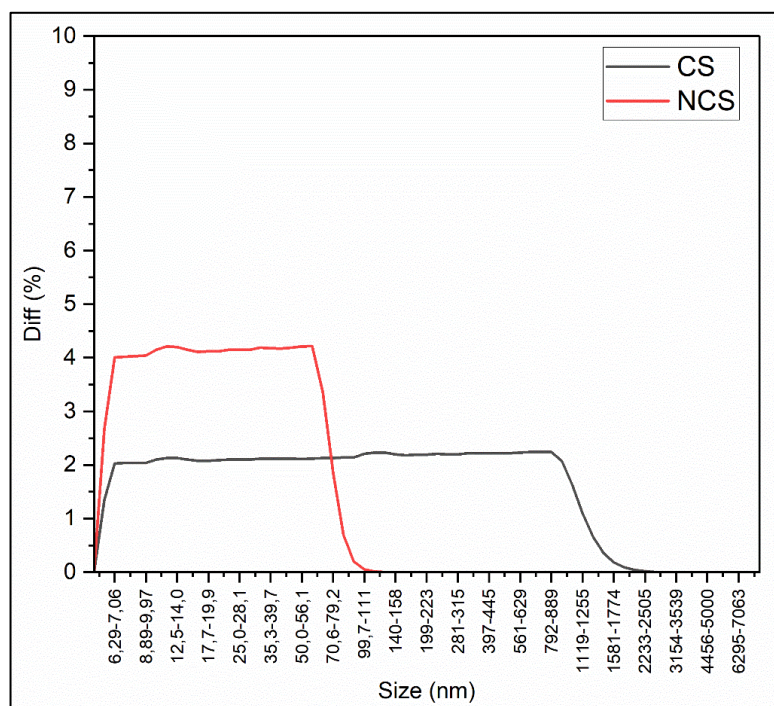


Figure 31. Particle size distribution of CS and NCS measured by DLS in number distribution mode.

The Mw of CS was determined to be 173 kDa, whereas, for the NCS, it was 22 kDa, both with a deacetylation degree (DD) of 95%. The DD and Mw of CS are critical parameters influencing its functionality. For antimicrobial applications, a high DD correlates with enhanced antimicrobial activity, because it augments the number of positively charged amine groups, thereby improving the capacity to bind to negatively charged bacterial cell walls, ultimately leading to the disruption of cell permeability (Campana et al., 2018). Furthermore, low Mw CS has been reported to exhibit greater biological activity, facilitating more effective penetration and interaction with microbial cells, which enhances its bactericidal efficacy (Arantes et al., 2015). Therefore, it is hypothesized that the AgNPs synthesized with NCS will demonstrate greater antimicrobial effectiveness than those synthesized with CS.

5.3.2 Characterization of CS-AgNPs and NCS-AgNPs

5.3.2.1 Optical properties and dynamic light scattering of AgNPs

AgNPs were successfully synthesized using CS and NCS as reducing and stabilizing agents. The formation of the Ag colloidal solutions was first confirmed by observing the presence of opalescence and Tyndall effect using a Laser pointer. The visible scattering of the laser beam through the solution indicated the presence of dispersed NPs, characteristic of colloidal systems, as the light was scattered by the particles in suspension (J. Huang et al., 2021). Then, the formation of AgNPs was monitored by UV–vis spectroscopy and the typical

UV–Vis absorption spectra of the synthesized samples are shown in **Figure 32**. For the AgNPs synthesized with CS the spectrum exhibited the distinctive surface plasmon resonance (SPR) absorption peak located at the wavelengths of 421 nm and 422 nm. In contrast, the samples prepared with NCS the SPR were located at slightly shorter wavelengths, 419 nm and 420 nm, but with higher absorbance. In both cases, UV-Vis results suggest the successful synthesis of AgNPs.

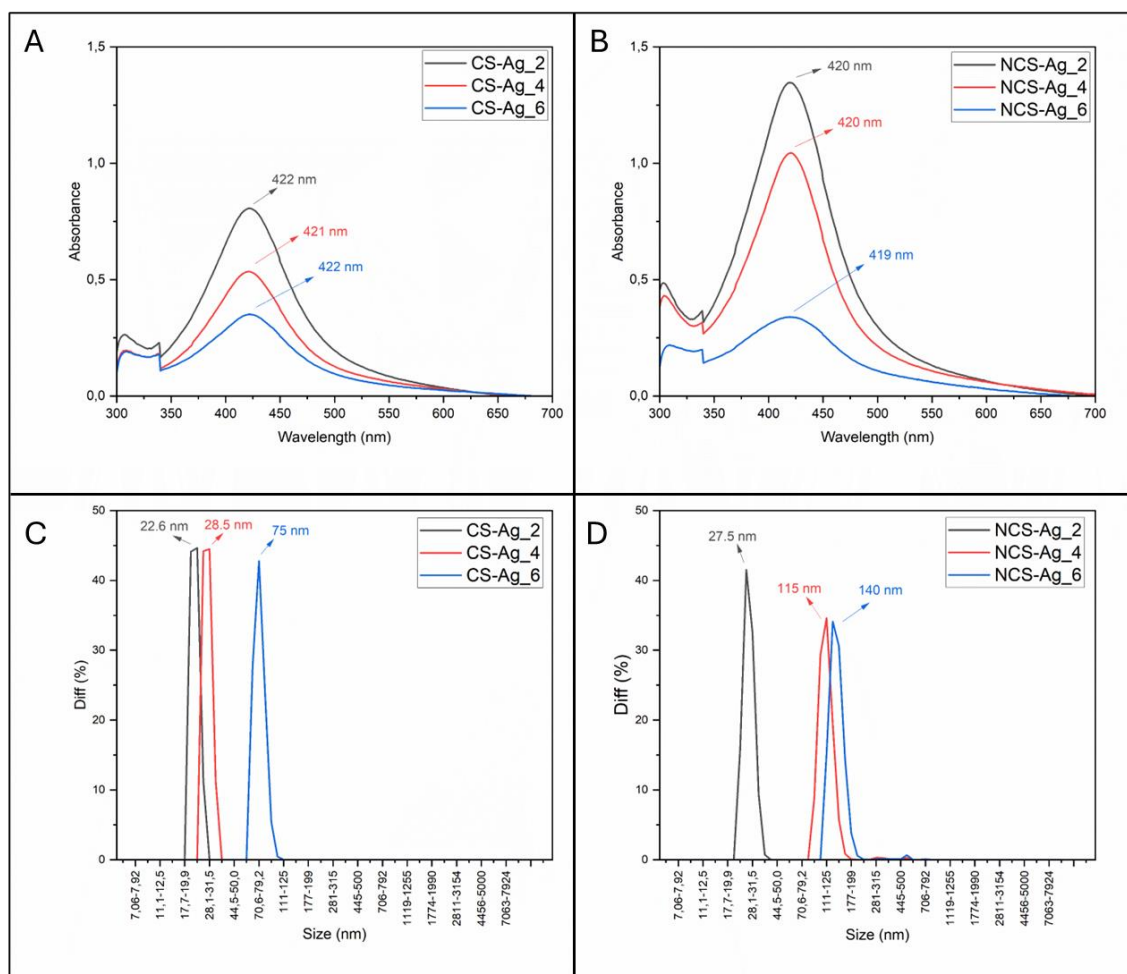


Figure 32. UV-Vis spectra for AgNPs synthesized with (A) chitosan and (B) nanochitosan. Distribution size by dynamic light scattering for AgNPs synthesized with (C) chitosan and (D) nanochitosan.

Both CS and NCS synthesis were performed under the same conditions, with variations in the AgNO_3 :CS/NCS ratios. It was observed that the peak intensity decreased as the ratio increased. The sample CS-Ag_2, synthesized with 75 mg of AgNO_3 , showed an absorbance of 0.8 at a wavelength of 422 nm, while for the samples CS-Ag_4 (37.5 mg of AgNO_3) and CS-Ag_6 (25 mg of AgNO_3), the absorbances observed were 0.53 and 0.35, respectively (**Figure 32, A**). Similar results were observed for the samples synthesized with NCS, where the NCS-

Ag_2, NCS-Ag_4, and NCS-Ag_6 samples resulted in absorbances of 1.34, 1.04, and 0.33, respectively (**Figure 32, B**). However, the sample NCS-Ag_6 exhibited an unexpectedly low absorbance of 0.33 compared to the corresponding CS-Ag_6 sample, which had an absorbance of 0.35. This deviation suggests that, despite the generally higher absorbance values observed for NCS samples, at lower AgNO₃ concentrations the efficiency of NCS as a reducing and stabilizing agent may decrease.

Rajivgandhi et al. (2019) synthesized CS/Ag nanocomposites by reacting 700 mg of CS in 100 mL of acetic acid with 440 mg of AgNO₃ in 40 mL of water at 90°C for 6 hours. UV-Vis characterization revealed a SPR peak at 430 nm, indicating successful synthesis of the CS/Ag nanocomposites (Rajivgandhi et al., 2019). Tran et al. (2010) synthesized AgNPs using CS as a reducing and stabilizing agent. The authors varied the amount of CS with a fixed amount of AgNO₃ (25 mL of 0.1 M solution) and adjusted the temperature from 30°C to 100°C. As results, they observed that the SPR peak around 420 nm was formed only for the synthesis carried out at temperatures above 80°C. Additionally, the authors noted that increasing the concentration of CS led to smaller AgNP sizes due to the dual role of CS in reducing and stabilizing the nanoparticles (Tran et al., 2010). Those results corroborate with the findings in the present work, where similar SPR peaks were observed, further reinforcing the importance of CS as a stabilizing agent in synthesis of AgNPs.

The DLS analysis results showed variations in the size of the AgNPs as in function of the CS/NCS and AgNO₃ concentration ratios. The samples synthesized with CS (**Figure 32, C**) showed a progressive increase in particle size as the AgNO₃ concentration decreased. The sample CS-Ag_2 exhibited the smallest particle size (22.6 nm) with a polydispersity index (PDI) of 0.35, indicating a moderately monodisperse distribution. However, as the AgNO₃ concentration decreased, the particle size increased to 28.5 nm in sample CS-Ag_4 (PDI of 0.41) and 75 nm in sample CS-Ag_6 (PDI of 0.53), suggesting a less uniform dispersion.

The DLS of samples synthesized with NCS (**Figure 32, D**) displayed a similar behavior in terms of nanoparticle size, where the size of the NP increased as the AgNO₃ concentration decreased. The sample NCS-Ag_2 exhibited a particle size of 27.5 nm and the lowest PDI (0.33), demonstrating good dispersion and nanoparticle stability. However, the sample NCS-Ag_4 showed an increase in particle size, reaching 115 nm, but with a PDI of 0.31. Despite its larger size, the distribution remained relatively monodisperse. In the sample NCS-Ag_6, the particle size increased to 140 nm, with a PDI of 0.35. Considering the DLS results, it was observed that while NCS promoted particle stability and apparently uniformity, CS was more

effective in generating smaller nanoparticles, potentially due to its higher molecular weight that influence the reduction and nucleation process more intensely.

5.3.2.2 Structural and morphological analyses of AgNPs

To complement the structural and morphological characterization of the synthesized AgNPs, Transmission Electron Microscopy (TEM) analyses were performed. This technique allows direct observation of the size and shape of the nanoparticles, as well as providing detailed information on their distribution and possible encapsulation by the CS and NCS polymers. The micrograph of the sample CS-Ag_2 (**Figure 33, A**) showed well-dispersed and predominantly spherical nanoparticles, with little agglomeration sites where the AgNPs are possibly embedded in a CS matrix. The average particle size of 9.17 ± 8.03 nm (**Figure 33, B**) indicates successful synthesis of small nanoparticles, with CS acting effectively as both a reducing and stabilizing agent. The HRTEM (**Figure 33, C**) suggests a high degree of crystallinity as evidenced by the visible lattice fringes, which possibly imply the presence of a face-centered cubic (FCC) structure, typical of Ag⁰ (Carbone et al., 2024). Additionally, the selected area electron diffraction (SAED) pattern (**Figure 33, D**) complements the HRTEM findings by exhibiting well-defined diffraction rings with discrete bright spots, indicating a highly crystalline structure with a relatively homogeneous distribution of grain sizes and random orientation of crystalline domains, reinforcing the crystalline nature of the NPs.

In a similar AgNPs synthesis protocol, Rajivgandhi et al. (2019) (Rajivgandhi et al., 2019) observed the presence of a crystalline structure, confirmed by characteristic diffraction peaks corresponding to the (111), (200), (220), and (311) planes, as identified through X-ray diffraction (XRD), which are typical of FCC structure. In the work developed by Tran et al. (2010) (Tran et al., 2010), typical XRD pattern of AgNPs synthesized with CS as reducing agent at 80 °C indicates high crystallinity of AgNPs with the diffraction planes of (1 1 1), (2 0 0), (2 2 0) and (3 1 1) of FCC lattice. In the present study, although XRD analysis was not performed, the results obtained by HRTEM and the SAED pattern indicated the presence of a semicrystalline structure. These findings are consistent with the results reported by Tran et al. (2010) and Rajivgandhi et al. (2019), whose XRD analyses confirmed the same FCC structure in AgNPs synthesized under similar conditions. Their observations strongly support the interpretation of the of FCC crystalline nature of the AgNPs formed in this study.

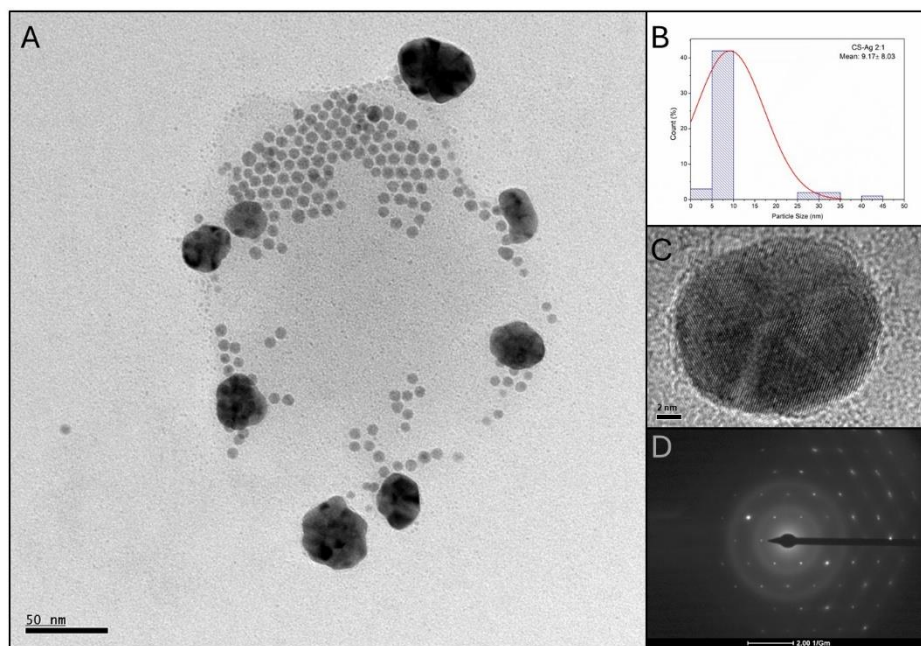


Figure 33. TEM analysis of sample CS-Ag_2, where: (A) TEM micrograph; (B) particle size distribution histogram; (C) HRTEM; (D) SAED pattern.

The TEM analysis of the CS-Ag_4 sample (**Figure 34, A**) revealed a heterogeneous distribution of AgNPs, consistent with the DLS analysis, which reported a PDI of 0.41, suggesting moderate polydispersity. The average particle size observed in the TEM images was 20.41 ± 10.55 nm (**Figure 34, B**). Additionally, the UV-Vis spectra displayed low absorbance, suggesting a reduced formation of AgNPs, which aligns with the lower quantity of nanoparticles observed in the TEM micrographs compared to other samples. The TEM images also revealed the presence of a core-shell structure, clearly visible in the inset of **Figure 34, A**. This structure is attributed to the encapsulation of AgNPs by a CS layer. The core-shell morphology potentially enhances nanoparticle stability and modulates surface properties (Tran et al., 2010). However, the HRTEM image (**Figure 34, C**) showed low presence of lattice fringes, indicating that the AgNPs have a partially crystalline nature. The SAED pattern (**Figure 34, D**), presented homogeneous diffraction rings with fewer intense diffraction spots, suggesting a crystalline structure with potentially lower crystallinity.

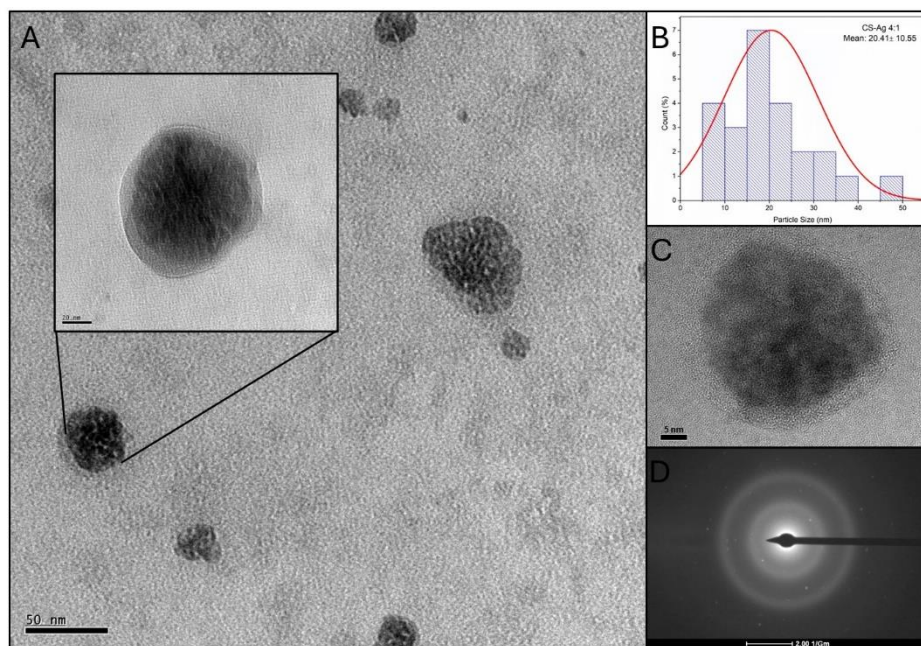


Figure 34. TEM analysis of sample CS-Ag_4, where: (A) TEM micrograph; (B) particle size distribution histogram; (C) HRTEM; (D) SAED pattern.

For the CS-Ag_6 sample, synthesized with 150 mg of CS and 25 mg of AgNO_3 , TEM analysis (**Figure 35, A**) revealed predominantly spherical AgNPs with signs of agglomeration. The histogram (**Figure 35, B**) indicated an average particle size of 14.83 ± 4.08 nm, significantly smaller than the 75 nm size reported by DLS. This discrepancy can be attributed to nanoparticle agglomeration, as DLS measures the hydrodynamic size based on Brownian motion, which tends to overestimate particle size when aggregates are present. The smaller size observed in TEM reflects the actual core dimensions of individual AgNPs, whereas DLS captures the larger, aggregated structures in solution. The HRTEM image (**Figure 35, C**) shows well-defined lattice fringes, suggesting a crystalline nature. The SAED pattern (**Figure 35, D**) shows a series of well-defined diffraction rings, confirming the crystalline nature of the AgNPs. The bright distinct spots overlaid on the rings further suggest the presence of multiple crystalline domains within the NPs, however they are less organized compared to the ones observed in Figure 33. This suggests that the AgNPs exhibit a high degree of crystallinity, even though some agglomeration was observed in the TEM micrographs.

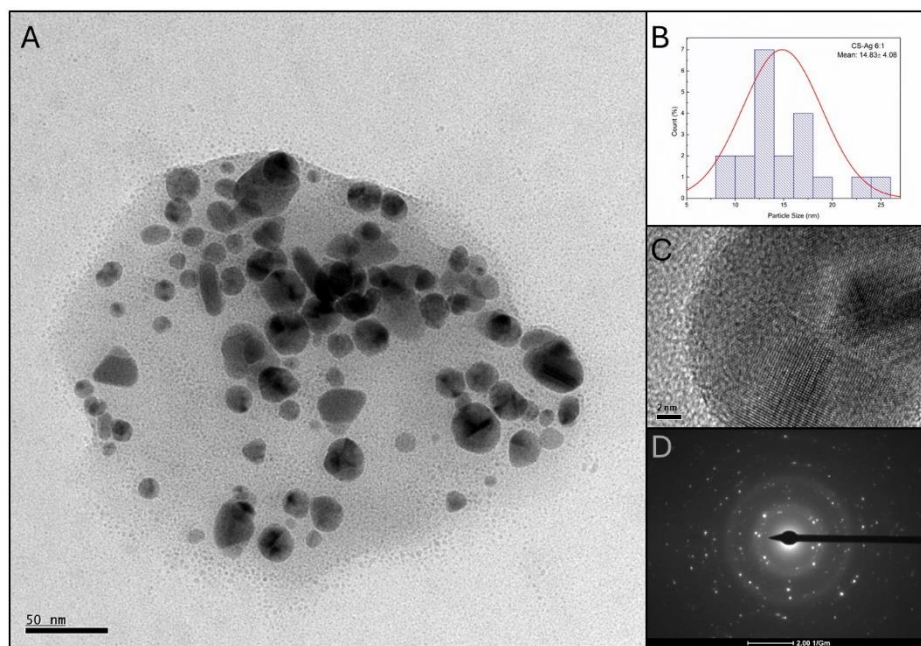


Figure 35. TEM analysis of sample CS-Ag_6, where: (A) TEM micrograph; (B) particle size distribution histogram; (C) HRTEM; (D) SAED pattern.

Regarding the sample NCS-Ag_2, DLS analysis showed a particle size of 27.5 nm and a PDI of 0.33, which initially indicated a relatively uniform size distribution, good colloidal stability and limited agglomeration. However, the TEM analysis (**Figure 36, A**), revealed spherical NPs larger in size with a pronounced tendency to agglomeration, with an average diameter of 58.27 nm. One possible explanation is that the use of NCS as both a reducing and stabilizing agent influences the particle growth dynamics differently than regular CS. NCS has a smaller molecular size and, thus, a greater surface area. In this way, it is possible that it can lead to different interactions and possibly less steric stabilization of the nanoparticles (Kulikouskaya et al., 2022). The HRTEM image (**Figure 36, C**) showed the presence of lattice fringes, but they appear less distinct and more disordered compared to those observed in samples CS-Ag_2 and CS-Ag_6. The SAED pattern (**Figure 36, D**) displayed diffused rings, characteristic of a polycrystalline nature, even though the spots are less sharp than in highly crystalline samples. These findings suggest a mixed phase, possibly combining amorphous and crystalline regions, which aligns with the observations from the HRTEM image.

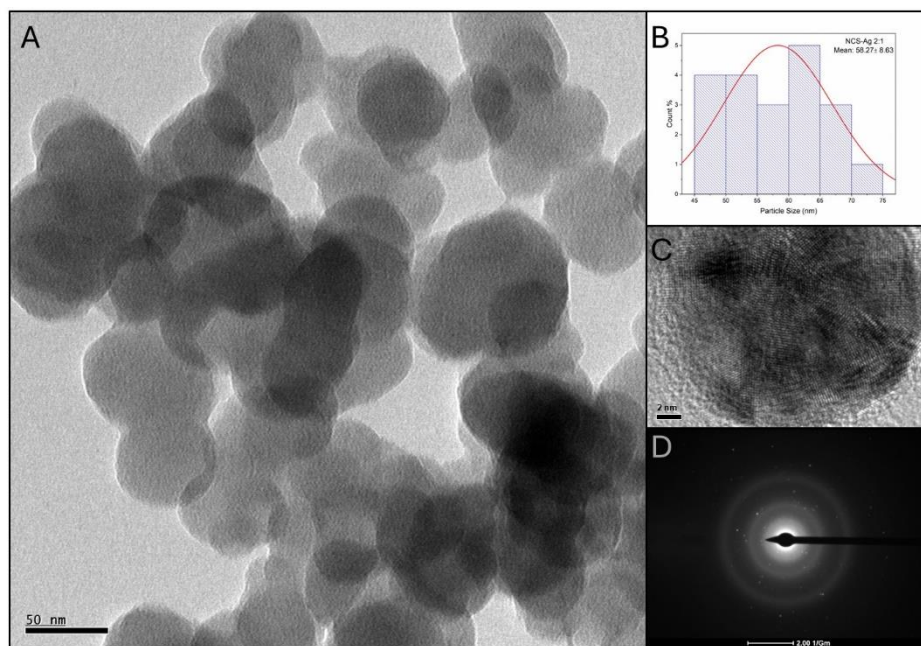


Figure 36. TEM analysis of sample NCS-Ag_2, where: (A) TEM micrograph; (B) particle size distribution histogram; (C) HRTEM; (D) SAED pattern.

Neither the UV-Vis spectra nor DLS analysis of sample NCS-Ag_4 suggested particle agglomeration. However, when analyzing the TEM micrograph (**Figure 37, A**) it is possible to notice the presence of spherical AgNPs with some degree of agglomeration. One possible explanation for this inconsistency is that both UV-Vis and DLS analyses were carried out with the NPs in solution, while TEM was performed on dried samples. During drying, the nanoparticles may come closer together and agglomerate due to van der Waals forces. While DLS suggested an average particle size of 115 nm, TEM revealed an average size of 28.48 ± 4.78 nm (**Figure 37, B**), presenting a relatively narrow size distribution compared to NCS-Ag_2. The HRTEM image and SAED pattern (**Figures 37, C and D**) suggest the polycrystalline nature of the particles, as evidenced by the sharp diffraction rings characteristic of the FCC structure of Ag. Additionally, the presence of very discrete bright spots in the electron diffraction pattern indicates regions with a higher degree of crystallinity within the polycrystalline structure.

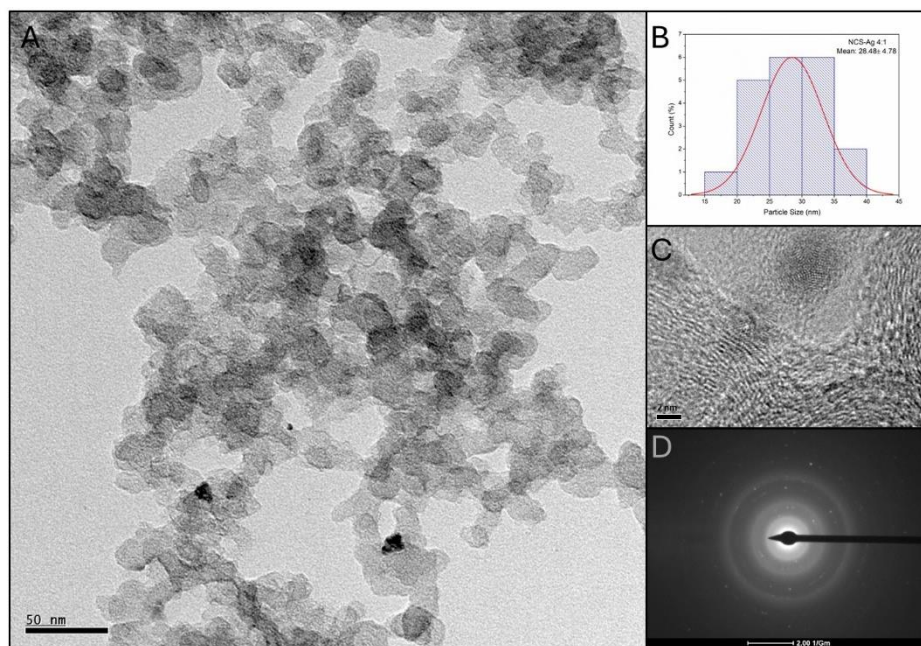


Figure 37. TEM analysis of sample NCS-Ag_4, where: (A) TEM micrograph; (B) particle size distribution histogram; (C) HRTEM; (D) SAED pattern.

The sample NCS-Ag_6, synthesized with 150 mg of NCS and 25 mg of AgNO_3 , resulted in AgNPs with a notably small average size of 6.51 ± 1.34 nm (**Figure 38, B**). The TEM micrograph (**Figure 38, A**) revealed well-dispersed nanoparticles, with minimal aggregation, suggesting efficient stabilization by NCS at the 6:1 ratio. The HRTEM image (**Figure 38, C**) shows the presence of lattice fringes, but only in the center of the particle, implying a polycrystalline structure. In the HRTEM image, it is possible to observe that the small AgNPs exhibit a core-shell structure, similar to what was observed in sample CS-Ag_4 (inset of Figure 34, A), but at a much smaller scale. The shell appears to have an amorphous phase, likely derived from NCS, while the core (AgNP) shows a polycrystalline structure, probably with an FCC arrangement. The SAED pattern (**Figure 38, D**) exhibits smoother, less defined rings, with few intense diffraction spots, indicating a more uniform structure with potentially lower crystallinity or even partial amorphous characteristics. The diffuse nature of the rings suggests that, in the proportions used in this sample, NCS limited particle growth, resulting in smaller particles with lower crystallinity. However, the DLS analysis indicated the presence of much larger particles, which contrasts with the smaller ones observed in the TEM micrographs. This discrepancy may be due to the formation of aggregates or clusters in the colloidal solution, which were detected by DLS but not by TEM.

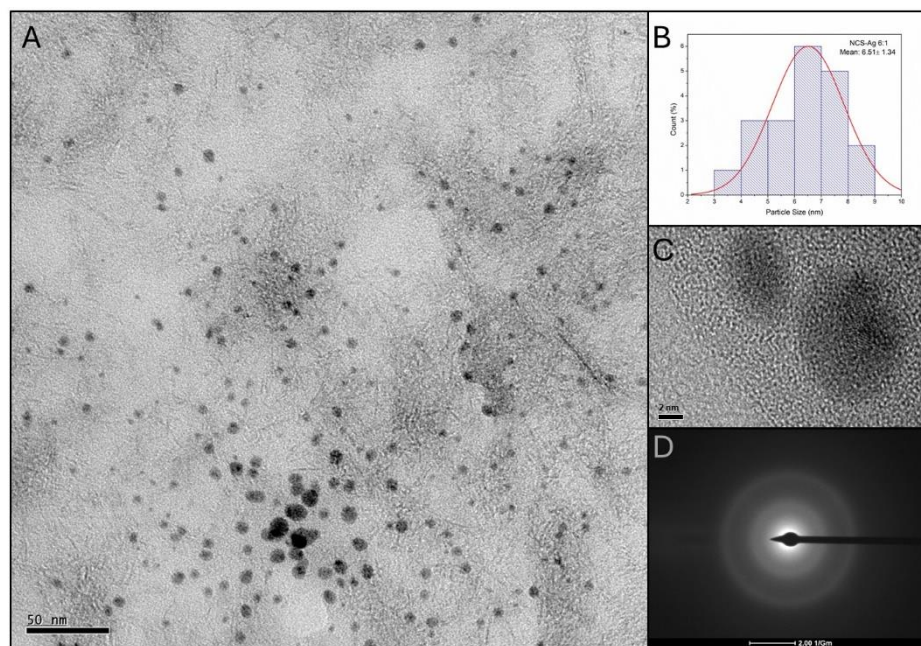


Figure 38. TEM analysis of sample NCS-Ag_6, where: (A) TEM micrograph; (B) particle size distribution histogram; (C) HRTEM; (D) SAED pattern.

This study employed both CS and NCS as reducing and stabilizing agents for the synthesis of AgNPs. The principal difference between the two biopolymers is in their molecular weight (173 kDa for CS and 22 kDa for NCS), which considerably influences the nanoparticle formation process and the stability of the colloidal solutions. The lower molecular weight of NCS results in an elevated surface area-to-mass ratio, which may enhance interactions with silver ions and affect the steric stability of nanoparticles. The morphology and structure of the AgNPs were examined using TEM, HRTEM, and SAED, revealing spherical nanoparticles with a polycrystalline nature across all samples. Notably, core-shell structures were observed in the CS-Ag_4 and NCS-Ag_6 samples, highlighting the stabilizing role of CS and NCS in encapsulating the AgNPs. This encapsulation likely enhances their long-term stability in solutions, as the amorphous shell formed by the biopolymers acts as a protective layer, while the polycrystalline core retains the metallic properties of AgNPs. These findings confirm that CS and NCS function effectively as both reducing and stabilizing agents. Furthermore, variations in molecular weight and the CS/NCS to AgNO_3 ratio significantly influence AgNP nucleation and growth.

5.3.3 Coating morphology

CVC segments underwent plasma treatment to modify the surface in order to enhance coating adherence with CS-AgNPs and NCS-AgNPs. The CVCs were subsequently dip-coated

in CS-Ag and NCS-Ag solutions, air-dried, and subjected to morphological analysis using SEM and EDS. The morphologies of the coating are shown in **Figure 39**.

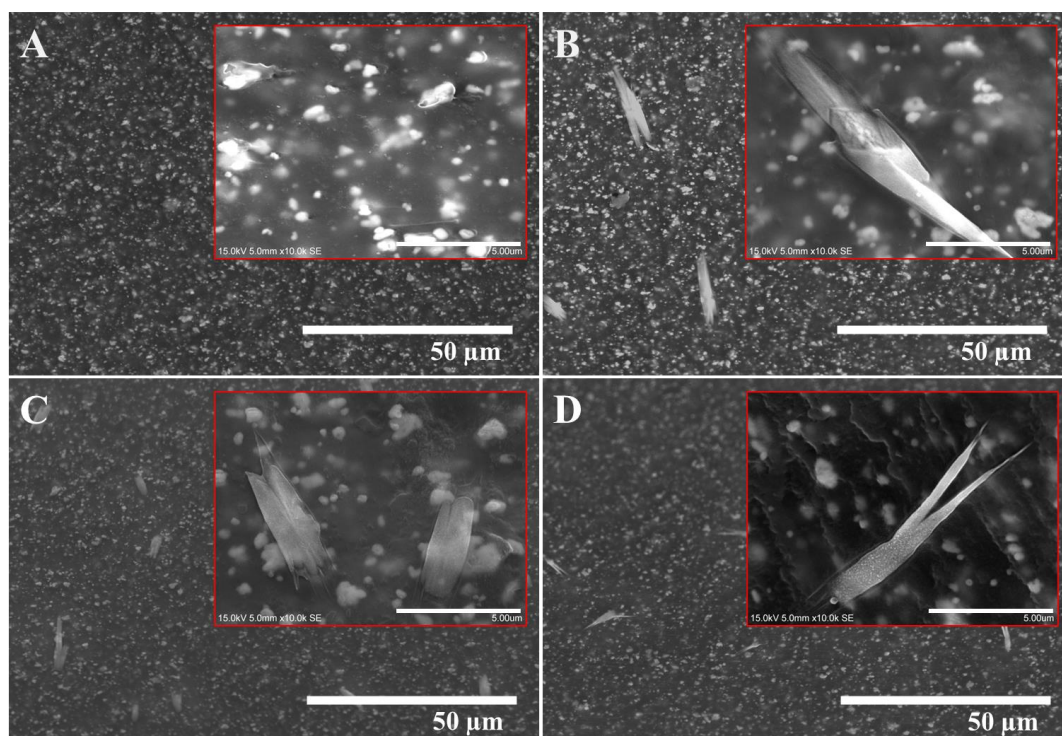


Figure 39. A) Morphology of CVC segment without coating. B) CVC coated with sample CS-Ag_2. C) CVC coated with sample NCS-Ag_4. D) CVC coated with sample NCS-Ag_6.

The SEM image of the control sample (**Figure 39, A**), which is the CVC without coating, shows a relatively smooth and homogenous surface. The EDS analysis detected the presence of Carbon, Oxygen, Nitrogen, Barium, and Sulfur (**Figure 40**), which are elements commonly found in polyurethane catheters. The SEM image of the CVC coated with the sample CS-Ag_2 (**Figure 39, B**), revealed the presence of several elongated structures all over the CVC surface. Those structures were further identified as Ag by EDS analysis (**Figure 41**). The formation of these elongated structures suggests anisotropic growth of Ag, potentially influenced by the interaction between CS and the catheter surface after plasma treatment.

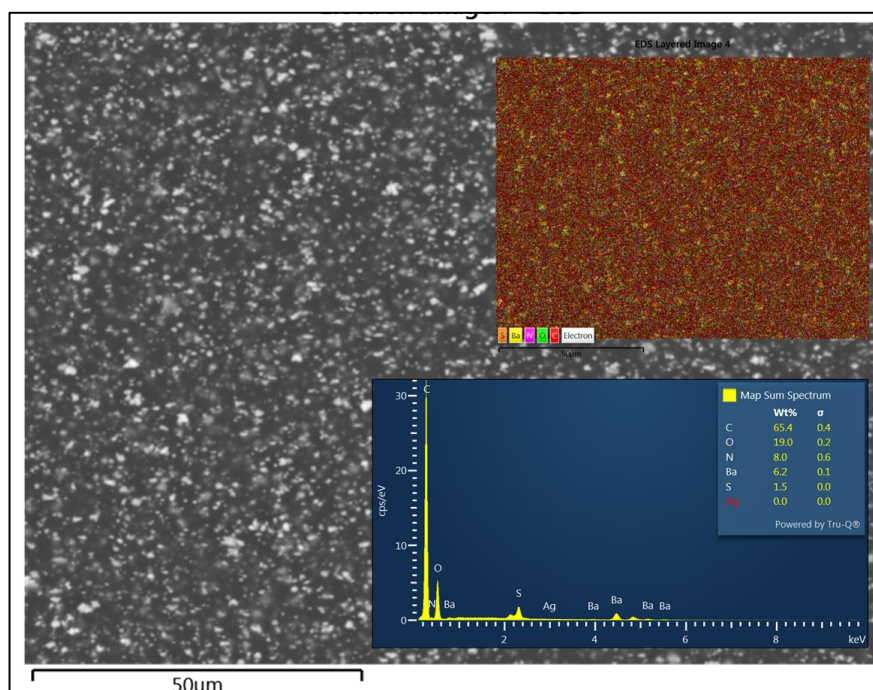


Figure 40. Energy-dispersive X-ray spectroscopy (EDS) analysis and elemental mapping of the surface of pure central venous catheter.

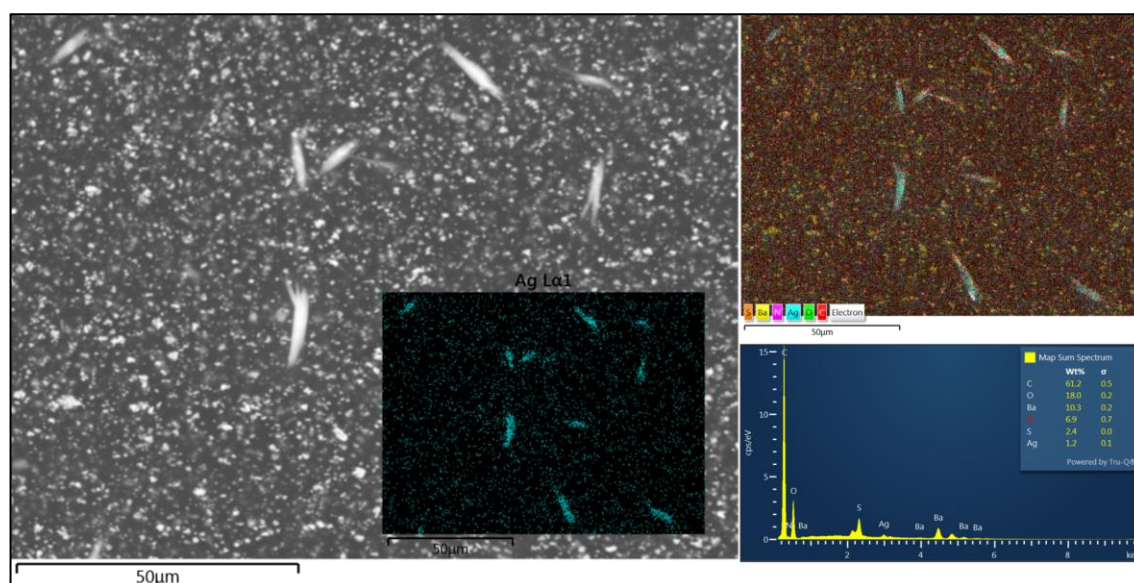


Figure 41. EDS analysis and elemental mapping of the surface of CVC coated with sample CS-Ag₂.

Interestingly, when AgNPs were analyzed separately (not in coating form) via TEM, they appeared as spherical particles. However, after coating, the AgNPs exhibited a different growth pattern, possibly due to interactions with the CVC surface. Similar structures were observed by Polinarski et al. (2024), when they coated polystyrene with a CS-Ag formula. The authors observed that the in-situ reduction of Ag^+ ions to metallic Ag (Ag^0) during the coating process led to the formation of AgNPs that developed into rod-like structures partially

embedded within the CS film (Polinarski et al., 2024). The sample coated with NCS-Ag_4 (**Figure 39, C**) showed similar structure, but with smaller rods over the CVC catheter. Additionally, a thin and almost transparent layer can be observed over the catheter surface, resulting from the NCS coating. This layer was also seen in sample NCS-Ag_2 (**Figure 42**), where the NCS film detached from the CVC surface. In this way, it is possible to affirm these rod-like structures are partially embedded within the NCS film.

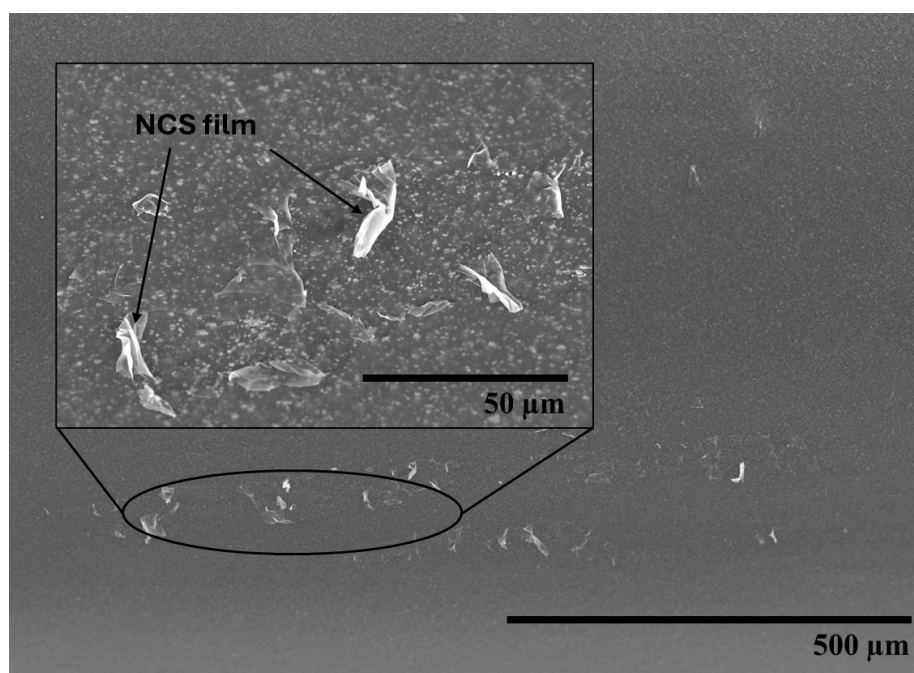


Figure 42. SEM of CVC coated with sample NCS-Ag_2.

Similarly, the sample NCS-Ag_6 also showed this rod-like structure (**Figure 39, D**). It is possible to notice in the inset of **Figure 39D** the presence of small and spherical spots, which are related to the presence of spherical AgNPs. In a previous study, Polinarski et al. (2024) (Polinarski et al., 2024) concluded that these rods are mainly formed by AgNPs. During the CS-Ag and NCS-Ag synthesis, CS and NCS amino and hydroxyl groups lead to the reduction of Ag^+ , forming AgNPs. Upon coating application, during the drying process the reduced Ag particles interact, clustering and subsequently growing into elongated structures. This growth is facilitated by interactions between CS or NCS molecules and Ag, promoting the formation of rod-like structures (Polinarski et al., 2024).

5.3.4 Antimicrobial Activity

5.3.4.1 Agar diffusion method

After synthesizing AgNPs using CS and NCS as reducing agents, their antibacterial effects were evaluated against *E. coli* and *S. aureus*. The bactericidal activity was assessed using the agar diffusion method, applying 10 μ L of each AgNP solution to bacterial cultures with a density of 1.5×10^8 CFU/mL. Inhibition zones, measured in millimeters, are presented in **Figure 43**. All samples effectively inhibited the growth of both *E. coli* and *S. aureus*. Notably, the sample synthesized with regular CS demonstrated superior antimicrobial activity against both strains compared to the NCS sample. Additionally, samples with higher Ag concentrations showed larger inhibition zones for both CS and NCS, while samples with lower Ag concentrations exhibited smaller inhibition zones. Statistical analysis using ANOVA and Tukey's test revealed significant differences in inhibition zones among samples against *S. aureus* ($p < 0.05$), while no significant differences were observed among the samples against *E. coli* ($p = 0.664$) (**Table 8**).

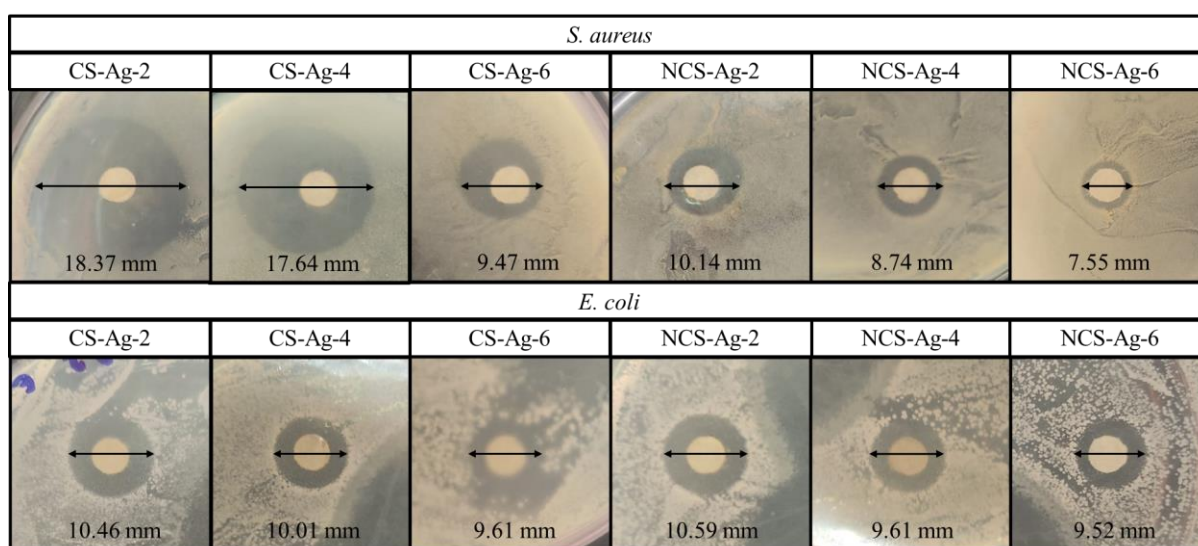


Figure 43. Inhibition Zone of the synthesized AgNPs against *S. aureus* and *E. coli*.

Table 8. ANOVA results for inhibition zones of AgNP samples against *S. aureus* and *E. coli*.

	Source	Sum of Squares	df	F	p-value
<i>S. aureus</i>	Sample	338.03	5	31.09	0.000002
	Residual	26.09	12	-	-
<i>E. coli</i>	Sample	3.26	5	0.654	0.664
	Residual	11.95	12	-	-

Rugaie et al. (2022) synthesized AgNPs synthesized with different stabilizing polymers - polyethylene glycol 6000 (PEG), ethyl cellulose (EC) and polyvinyl pyrrolidone (PVP) - using sodium borohydride as reducing agent and AgNO₃ as Ag precursor. The authors verified the antimicrobial activity against *E. coli* using the agar diffusion method. Bacteria were inoculated on MH agar plates, 5 mm wells were made and the samples were added at a 50 µg mL⁻¹ concentration in these wells. The AgNPs prepared with PVP had a zone of inhibition of 19 mm, while sample prepared with EC and PEG had 17 and 3 mm respectively (Rugaie et al., 2022). In this present study, against *S. aureus*, the samples CS-Ag_2, CS-Ag_4 and CS-Ag_6 resulted in a zone of inhibition of 18.37, 17.64 and 9.47 mm respectively. While the samples NCS-Ag_2, NCS-Ag_4 and NCS-Ag_6 resulted in a zone of inhibition of 10.14, 8.74 and 7.55, respectively.

When comparing the results, the AgNPs synthesized in this study demonstrated effective antimicrobial activity, though generally yielding smaller inhibition zones compared to Rugaie et al. (2022), possibly due to the difference in application doses. While this study used only 10 µL of solution, Rugaie et al. applied 50 µg/mL of AgNPs. Despite this, the samples CS-Ag_2 and CS-Ag_4 samples achieved inhibition zones of 18.37 mm and 17.64 mm against *S. aureus*, closely approaching the performance reported by Rugaie et al. in the sample stabilized by PVP (19 mm). Clearly, the use of different stabilizers impacts antibacterial efficacy. However, the use of CS and NCS appears advantageous due to their dual role as both reducing and stabilizing agents, suggesting that CS might provide stronger antimicrobial support than some synthetic stabilizers like PEG.

Despite using different concentrations of AgNO₃ and types of chitosan (CS and NCS) in the synthesis, no significant differences were observed between the samples tested against *E. coli*, with inhibition zones ranging from 10.59 mm to 9.52 mm. However, it was possible to verify that the action of NCS was higher for this bacterium. CS-Ag_2 and CS-Ag_4 exhibited greater efficacy against *S. aureus*, where significant differences were observed between samples synthesized with CS and NCS. Overall, the synthesized AgNPs showed a larger zone of inhibition against *S. aureus* than *E. coli*.

This happened because *E. coli* is a Gram-negative bacterium and its outer lipopolysaccharide membrane acts as an additional barrier that can hinder the penetration of AgNPs, especially larger ones, which explains the fact that the synthesized AgNPs have better action with NCS. In contrast, *S. aureus*, being Gram-positive bacteria, does not have such an

efficient cell entry selection mechanism, which facilitates the access of AgNPs to interrupt cellular processes (Salimiyan rizi, 2022; Stirk & Van Staden, 2022).

5.3.4.2 Minimal Inhibitory Concentration

The MIC was determined for the AgNP samples synthesized with CS and NCS against *S. aureus* and *E. coli* (**Table 9**). The results highlight differences in antimicrobial performance based on the synthesis conditions, including Ag concentration and particle size.

Table 9. Ag concentration, average particle size (TEM), and antimicrobial activity, as determined by inhibition zone and minimum inhibitory concentration (MIC) against *S. aureus* and *E. coli*.

Sample	Ag concentration (mg/mL)	Average particle size – TEM (nm)	Antimicrobial Testing			
			Inhibition Zone (mm)		MIC (µg/mL)	
			<i>S. aureus</i>	<i>E. coli</i>	<i>S. aureus</i>	<i>E. coli</i>
CS-Ag_2	0.73	9.17 ± 8.03	18.37 ± 1.52	10.46 ± 0.70	0.36	2.84
CS-Ag_4	0.36	20.41 ± 10.55	17.64 ± 2.83	10.01 ± 0.78	0.36	1.40
CS-Ag_6	0.24	14.83 ± 4.08	9.47 ± 1.07	9.61 ± 1.51	1.39	1.87
NCS-Ag_2	0.73	58.27 ± 8.63	10.14 ± 0.91	10.59 ± 0.97	1.82	2.84
NCS-Ag_4	0.36	28.48 ± 4.78	7.74 ± 0.76	9.61 ± 1.21	0.45	2.81
NCS-Ag_6	0.24	6.51 ± 1.34	7.55 ± 0.42	9.52 ± 0.39	1.5	1.87

The samples CS-Ag_2 and CS-Ag_4 exhibited the same MIC of 0.36 µg/mL against *S. aureus*, despite having different Ag concentrations and particle sizes. CS-Ag_2 had the highest Ag concentration (0.73 mg/mL) and the smallest particle size (9.17 ± 8.03 nm), while CS-Ag_4 had a lower Ag concentration (0.36 mg/mL) and a larger particle size (20.41 ± 10.55 nm). This suggests that against *S. aureus*, the antimicrobial performance is not solely dependent on the Ag concentration or particle size but may be influenced by other factors such as nanoparticle stability or the interaction of the AgNPs with the bacterial cell wall.

In contrast, for *E. coli*, CS-Ag_4 demonstrated a lower MIC (1.40 µg/mL) compared to CS-Ag_2 (2.84 µg/mL), despite the smaller particle size and higher Ag concentration of CS-Ag_2. This difference could be due to the complex structure of *E. coli*, a Gram-negative bacterium with an outer membrane that may influence nanoparticle penetration and interaction. The slightly larger particle size of CS-Ag_4 might have resulted in better bacterial interaction or slower Ag ion release, leading to improved efficacy against *E. coli*.

The sample CS-Ag_6, with the lowest Ag concentration (0.24 mg/mL) and an intermediate particle size (14.83 ± 4.08 nm), exhibited MIC values of 1.39 µg/mL against *S.*

aureus and 1.87 µg/mL against *E. coli*. These values are higher than those of CS-Ag_2 and CS-Ag_4 for *S. aureus*, indicating a reduced antimicrobial efficacy at lower Ag concentrations. However, its comparable MIC value for *E. coli* suggests that particle size and Ag concentration may have a different degree of influence on Gram-negative bacteria compared to Gram-positive bacteria.

When analyzing the MIC results for samples synthesized with NCS, it becomes evident that the antimicrobial activity does not follow a linear trend with respect to Ag concentration or particle size. For instance, the sample NCS-Ag_4 demonstrated a notably low MIC value of 0.45 µg/mL against *S. aureus*, while NCS-Ag_2 and NCS-Ag_6 exhibited higher MIC values of 1.82 µg/mL and 1.50 µg/mL, respectively. This non-linear behavior indicates that factors beyond Ag concentration and particle size play a significant role in determining the antimicrobial efficacy of AgNPs.

For example, while NCS-Ag_2 had a three times higher Ag concentration than NCS-Ag_6, the smaller particle size of NCS-Ag_6 (6.51 ± 1.34 nm) likely contributed to its relatively enhanced antimicrobial performance compared to NCS-Ag_2 (58.27 ± 8.63 nm). Interestingly, NCS-Ag_4, despite having a larger particle size (28.48 ± 4.78 nm) than NCS-Ag_6 and a lower Ag concentration than NCS-Ag_2, achieved the lowest MIC value of 0.45 µg/mL against *S. aureus*. This suggests that other factors, such as nanoparticle stability, surface properties, or specific interactions with the bacterial cell wall, may play a crucial role in determining the antimicrobial activity of AgNPs.

In contrast, the MIC results for *E. coli* were consistently higher than those for *S. aureus*. For example, NCS-Ag_4 exhibited an MIC of 2.81 µg/mL against *E. coli* compared to 0.45 µg/mL against *S. aureus*. Similarly, NCS-Ag_6 showed an MIC of 1.87 µg/mL for *E. coli* and 1.50 µg/mL for *S. aureus*. These differences highlight the greater resistance of *E. coli*, a Gram-negative bacterium, likely due to its outer membrane, which acts as an additional barrier to AgNP penetration. In contrast, *S. aureus*, a Gram-positive bacterium, lacks this outer membrane, making it more susceptible to the antimicrobial action of AgNPs.

Additionally, the use of CS promotes a better antimicrobial performance of the synthesized AgNPs in comparison to NCS. The higher molecular weight (Mw) of CS might contribute to better stabilization of the nanoparticles, forming a more robust polymeric network around the AgNPs. These findings underscore the complexity of the antimicrobial mechanisms of AgNPs, suggesting that multiple factors beyond Ag concentration and particle size influence antimicrobial efficacy. For instance, for *S. aureus*, the results suggest a lower dependency on

Ag concentration and particle size, while for *E. coli*, these parameters seem to have a more significant impact on antimicrobial performance.

5.3.4.3 Qualitative antibiofilm assays

CVC segments coated with all synthesized AgNPs were used in assays to determine whether the CS-AgNP and NCS-AgNP coatings could inhibit biofilm formation. This evaluation focused on *S. aureus* and *S. epidermidis* bacterial strains. Uncoated CVC segments served as negative controls, and biofilm formation was assessed via SEM. The results are presented in **Figure 44**. Typically, the surface of CVC is relatively smooth and homogenous, as shown in **Figure 39, A**. However, after 5 days in contact with a *S. aureus* and *E. coli* suspension, a dense biofilm was formed on the catheter surface (**Figures 44 A** and **44 H**, respectively). In contrast, all coated CVCs exhibited antimicrobial activity, with a significant reduction in biofilm formation compared to the uncoated CVC.

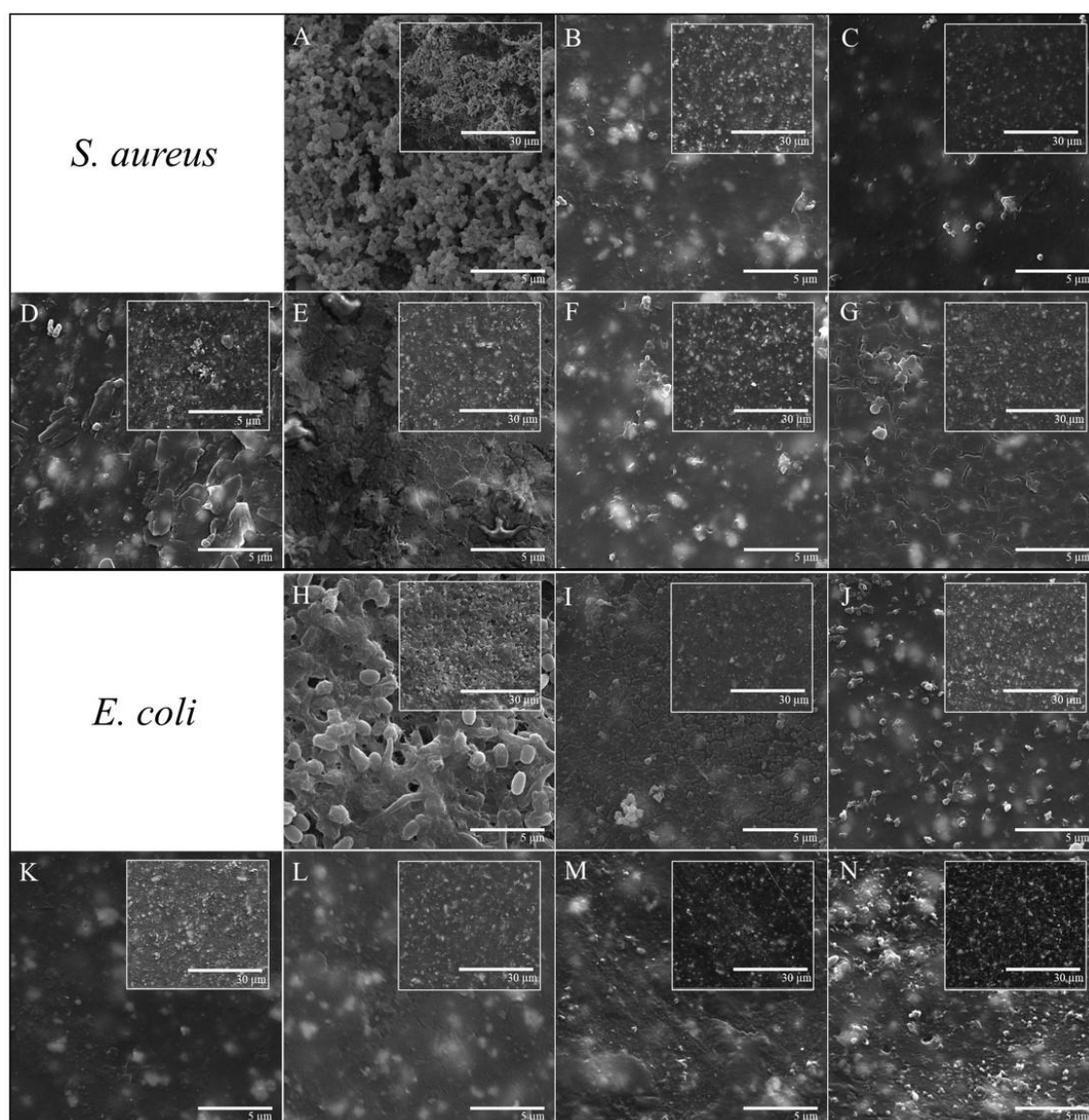


Figure 44. SEM images of CVC segments with and without AgNP coatings (CS-AgNPs and NCS-AgNPs) after incubation with *S. aureus* and *E. coli*. Figures A to G represent the test against *S. aureus*, where A) uncoated CVC; B) CVC coated with CS-Ag_2; C) CS-Ag_4; D) CS-Ag_6; E) NCS-Ag_2; F) NCS-Ag_4; G) NCS-Ag_6. Figure H to N represent the test against *E. coli*, where H) uncoated CVC; I) CVC coated with CS-Ag_2; J) CS-Ag_4; K) CS-Ag_6; L) NCS-Ag_2; M) NCS-Ag_4; and N) NCS-Ag_6.

The samples CS-Ag_2 and CS-Ag_4 exhibited the largest inhibition zones and the lowest MIC against *S. aureus*, demonstrating superior antimicrobial activity. When these samples were used to coat CVC segments, they effectively prevented biofilm formation. As shown in **Figures 44 B** and **C**, the CVC surfaces appear smooth, with only a few isolated bacteria present, and their extracellular matrix visibly disrupted. The sample NCS-Ag_4 presented the lowest MIC among the NCS-Ag and as shown in **Figure 44F**, successfully prevented the formation of biofilm. For the other samples (CS-Ag_6, NCS-Ag_2 and NCS-Ag_6), although biofilm formation was significantly reduced compared to the untreated CVC,

a thinner biofilm layer can still be observed on the surface. The inhibition zone results against *E. coli* exhibited no significant difference among the synthesized samples. However, at the biofilm inhibition assays, the samples CS-Ag_2 (**Figure 44I**) and CS-Ag_6 (**Figure 44K**) showed a notably thinner biofilm layer compared to the uncoated CVC (**Figure 44H**). For the other samples, it was observed isolated microbial colonies with disrupted cell walls.

AgNPs were synthesized using *Spirulina platensis* methanolic extract and had its antibiofilm properties tested against *P. aeruginosa* on urinary catheters (LewisOscar et al., 2021). At a minimum concentration of 10 µg/mL, the AgNPs inhibited 23% of biofilm formation, while at a concentration of 100 µg/mL, inhibition reached 77%. The antibiofilm properties of AgNPs synthesized with *Justicia adhatoda* were tested against a consortium of *E. coli* and *P. aeruginosa* (Francis et al., 2024). The authors reported effective inhibition of bacterial adhesion and biofilm formation, with 85% of biofilm inhibition. In another study, Cai et al. (Cai et al., 2023) synthesized antibacterial AgNPs poly(acrylamide)-chitosan-polyvinylpyrrolidone (AgNPs-PAAm-CS-PVP) composite hydrogel coating on latex urinary catheters. Quantitative analysis revealed that the AgNPs-PAAm-CS-PVP hydrogel-coated surface reduced the number of live, dead, and total adhered bacteria by 92.8%, 90.1%, and 92.3%, respectively.

In this present study, the coated CVC segments demonstrated a strong reduction in biofilm density, which suggests effective antimicrobial activity from the AgNP coatings. In the uncoated CVC samples, the biofilm covered a significant portion of the surface, with densely packed bacterial cells and a prominent extracellular matrix. This extensive biofilm formation highlights the vulnerability of uncoated surfaces to bacterial colonization, especially when exposed to pathogenic strains like *S. aureus* and *E. coli*. In contrast, the coated CVCs showed fewer bacterial cells adhered to the surface, and the extracellular matrix was sparse or absent. This reduction in biofilm not only supports the antimicrobial efficacy of the AgNP coatings but also indicates a potential for these coatings to disrupt the initial adhesion of bacteria, a critical step in biofilm formation (Polinarski et al., 2021). The reduced presence of *S. aureus* and *E. coli* biofilms on the coated surfaces suggests that AgNPs interfere with bacterial growth and adhesion mechanisms, likely through mechanisms such as membrane disruption and generation of reactive oxygen species (ROS).

These results are promising for the use of AgNP coatings in clinical settings, particularly for preventing catheter-related infections. By minimizing biofilm formation, AgNP-coated CVCs may reduce the risk of persistent infections and improve patient outcomes. Further studies could explore the durability of the antimicrobial effects over longer periods and under

varying conditions, as well as the potential for AgNP coatings to prevent biofilms from other clinically relevant bacterial strains. Studies have reported that various materials based on AgNPs, as well as Ag-composites combined with CS and other silver-based substances, have demonstrated broad-spectrum antibacterial properties (Choudhary et al., 2023; X. Du et al., 2021; El-Sheikh, 2024; R. Huang et al., 2024; Le et al., 2024; Mohammed et al., 2023; Nagarajan et al., 2024; Z. Qi et al., 2022; Sangnak et al., 2021; Zhangabay & Berillo, 2023). Their antimicrobial properties hold these materials potential for applications in diverse fields, including agriculture, food, and biomedical sectors. However, their effectiveness can be influenced by the composition and structure of the bacterial cell wall. For example, higher microbial organizations, such as biofilms, are more challenging to combat than planktonic cells (Franco et al., 2022).

In general, the antimicrobial mechanisms of AgNPs are identical for both planktonic and sessile cells and they are based on physical interactions, ion leaching and dissolution, and oxidative stress (Franco et al., 2022). In physical interaction mechanism, the positive charge on AgNPs, especially those stabilized with cationic agents like CS, promotes stronger adhesion to the negatively charged bacterial surface, allowing for better contact and retention on the cell wall (Vanlalveni et al., 2024). This close adherence can disrupt the cell membrane integrity, making it more permeable and allowing AgNPs to bind to cell walls and membranes, thereby changing their permeability, transport activity, and composition. As a result, essential cellular components can leak out, leading to cell dysfunction and ultimately cell death (Vanlalveni et al., 2024).

In the ion leaching and dissolution mechanism, AgNPs release Ag^+ ions that penetrate the bacterial cell and interact with vital cellular components, such as nucleic acids, DNA and RNA. Ag^+ ions have a particular affinity for the phosphate groups, and by binding them, Ag^+ ions disrupt the stability and function of these nucleic acids, hindering essential processes such as DNA replication and RNA transcription (Abada et al., 2024). The antimicrobial mechanisms caused by oxidative stress involves the production of ROS, which includes superoxide (O_2^-), peroxy (RCOO^\cdot), hydroxyl ($^\cdot\text{OH}$), and hydrogen peroxide (H_2O_2). Once produced, these highly reactive molecules that can damage various cellular components and lead to bacterial cell death. The Ag^+ ions released from AgNPs can interact with oxygen and cellular molecules, enhancing ROS production and further contributing to cellular damage (Abada et al., 2024; Franco et al., 2022; Vanlalveni et al., 2024).

Considering the findings presented in this work, it is believed that the antimicrobial mechanism of the CS/NCS-AgNPs likely involves a combination of physical interactions, ion

release, and oxidative stress. Smaller particles may penetrate bacterial cells more effectively and release Ag^+ ions more readily, enhancing intracellular disruption, while larger particles provide a greater surface area for physical interactions with bacterial cell walls. The higher inhibition observed in *S. aureus* compared to *E. coli* may reflect a greater sensitivity of Gram-positive cells to AgNP interactions, possibly due to differences in cell wall structure. Additionally, the great inhibition of biofilm formation highlights the potential of these AgNPs to disrupt both planktonic and sessile cells, suggesting that the material can be considered a promising strategy to antimicrobial coatings.

5.4. Partial Conclusions

This work evaluated the synthesis and antimicrobial efficiency of AgNPs using CS and NCS as reducing and stabilizing agents. The findings revealed that both the choice of CS versus NCS and the CS/NCS- AgNO_3 ratio significantly influenced the structural properties, particle size, and antimicrobial activity of the synthesized materials, though the relationships driving these effects were non-linear. Regarding the antimicrobial applications, all samples demonstrated antimicrobial properties against *S. aureus* and *E. coli*. However, the samples CS-Ag_2 and CS-Ag_4, stood out exhibiting the largest inhibition zones in agar diffusion tests and the lowest MIC values against *S. aureus*. Furthermore, when applied as coatings on CVCs, they significantly inhibited biofilm formation of both gram positive and negative bacteria. The enhanced performance of these samples can be attributed to the synergistic effect of CS within the AgNPs, which not only stabilized the particles but also amplified their antimicrobial activity. These findings contribute to the literature by highlighting the dual role of CS in the synthesis of AgNPs as an effective reducing and stabilizing agent, enhancing antimicrobial properties and indicating its potential for antimicrobial coatings, especially to prevent biofilm formation on medical devices.

5.5 Future Perspectives

Based on the findings highlighted in this present work, the future perspectives to ensure the safety and effectiveness of CS-stabilized AgNP coatings for infection prevention on medical devices involves: the optimization of coating techniques in order to evaluate adhesion, durability and antimicrobial effectiveness under clinical conditions; perform biocompatibility and cytotoxicity testing on human cells, to ensure the safety of these coatings for prolonged contact with human body tissues; to conduct antimicrobial testing with a wider range of

clinically relevant pathogens; and to evaluate the antimicrobial and antibiofilm mechanism of action of the material.

CHAPTER 6: CONCLUSIONS

The objective of this Ph.D. project was to develop potent antimicrobial materials throughout a green route using CS, NCS and AgNPs. In the first study, diverse synthesis was employed using different reducing agents to produce AgNPs, and CS emerged as the most promising reducing agent, yielding small AgNPs with intense surface plasmon resonance peaks and superior antibacterial properties. Different combinations of CS and AgNO₃ concentrations were evaluated, including low CS with high AgNO₃ concentrations and vice versa. It was found that a concentration of 150 mg of chitosan with 75 mg of AgNO₃ resulted in a pronounced antibacterial activity, capable of inhibiting biofilm formation on the surface of central venous catheter.

In the second study, a two-step method for synthesizing a CS-Ag composite was presented. Simply mixing a CS solution at a concentration of 1 mg.mL⁻¹ with 20% (w/w) of Ag⁺ resulted in CS-Ag composite suitable for powerful antimicrobial coating, capable of eliminating bacteria under light and dark conditions. Impressively, the produced coating eliminated 100% of *E. coli* within only after 90 minutes and 100% against *S. epidermidis* after 30 minutes under LED light irradiation. Furthermore, the coating retained excellent antibacterial efficacy even after three cycles of use, making it an ideal candidate for applications requiring durable and extended antimicrobial activity.

Finally, in the third study, CS and NCS with high DD (95%) and different Mw (173 kDa for CS and 22 kDa for NCS) were successfully synthesized using shrimp shells. The freshly prepared biopolymers were used to produce AgNPs using CS and NCS as reducing and stabilizing agents. Considering the findings presented in the first study, the synthesis was conducted with different concentrations of AgNO₃ (75, 37.5 and 25 mg) with a fixed amount of CS/NCS (150 mg). All synthesized AgNPs resulted in good antimicrobial activity against *S. aureus* and *E. coli*. However, the synthesis prepared with CS and AgNO₃ in a 2:1 ratio (w/w) stood out as optimal condition, resulting in small, spherical and crystalline AgNPs with excellent antimicrobial and antibiofilm properties against gram-positive and gram-negative bacteria.

In summary, this Ph.D. project successfully demonstrated the potential of CS-AgNPs and CS-Ag composite as sustainable antimicrobial materials. The findings highlight their significant promise for developing antimicrobial coatings, especially for medical devices. However, in order to advance these materials toward practical applications, some studies are still necessary to address some challenges, such as coating optimization and cytotoxicity and

biocompatibility assays to assure safety for human use. Despite these challenges, this thesis presents valuable contribution to the research field, proving valuable insights into the development of green-synthesized antimicrobial materials with the aim of reducing bacterial infections and preserving human health.

BIBLIOGRAPHY

- Abada, E., Mashraqi, A., Modafer, Y., Al Abboud, M. A., & El-Shabasy, A. (2024). Review green synthesis of silver nanoparticles by using plant extracts and their antimicrobial activity. *Saudi Journal of Biological Sciences*, 31(1), 103877. <https://doi.org/10.1016/J.SJBS.2023.103877>
- Abbasi, E., Milani, M., Aval, S. F., Kouhi, M., Akbarzadeh, A., Nasrabadi, H. T., Nikasa, P., Joo, S. W., Hanifehpour, Y., Nejati-Koshki, K., & Samiei, M. (2014). Silver nanoparticles: Synthesis methods, bio-applications and properties. *Http://Dx.Doi.Org/10.3109/1040841X.2014.912200*, 42(2), 173–180. <https://doi.org/10.3109/1040841X.2014.912200>
- Abdelgawad, A. M., Hudson, S. M., & Rojas, O. J. (2014). Antimicrobial wound dressing nanofiber mats from multicomponent (chitosan/silver-NPs/polyvinyl alcohol) systems. *Carbohydrate Polymers*, 100, 166–178. <https://doi.org/10.1016/J.CARBPOL.2012.12.043>
- Agnihotri, S., Mukherji, S., & Mukherji, S. (2014). Size-controlled silver nanoparticles synthesized over the range 5-100 nm using the same protocol and their antibacterial efficacy. *RSC Advances*, 4(8), 3974–3983. <https://doi.org/10.1039/c3ra44507k>
- Akmaz, S., Dilaver Adgüzel, E., Yasar, M., & Ergüven, O. (2013). The effect of ag content of the chitosan-silver nanoparticle composite material on the structure and antibacterial activity. *Advances in Materials Science and Engineering*, 2013. <https://doi.org/10.1155/2013/690918>
- Alavi, M., & Moradi, M. (2022). Different antibacterial and photocatalyst functions for herbal and bacterial synthesized silver and copper/copper oxide nanoparticles/nanocomposites: A review. *Inorganic Chemistry Communications*, 142, 109590. <https://doi.org/10.1016/J.INOCHE.2022.109590>
- Alqahtani, F., Aleanizy, F., Tahir, E. El, Alhabib, H., Alsaif, R., Shazly, G., Alqahtani, H., Alsarra, I., & Mahdavi, J. (2020). Antibacterial activity of chitosan nanoparticles against pathogenic n. Gonorrhoea. *International Journal of Nanomedicine*, 15, 7877–7887. <https://doi.org/10.2147/IJN.S272736>
- Alqahtani, F. Y., Aleanizy, F. S., Tahir, E. El, Alquadeib, B. T., Alsarra, I. A., Alanazi, J. S., & Abdelhady, H. G. (2019). Preparation, characterization, and antibacterial activity of

- diclofenac-loaded chitosan nanoparticles. *Saudi Pharmaceutical Journal*, 27(1), 82–87. <https://doi.org/10.1016/j.jsps.2018.08.001>
- ALVES, H. J., ALVES, M. K. A., MUNIZ, G. I. B., & ELLENDERSEN, L. D. S. N. (2019). *Processamento de exoesqueleto de crustáceos para obtenção de nanoquitosana* (Patent 102017022250–0). República Federativa do Brasil.
- Alves, H. J., Furman, M., Kugelmeier, C. L., De Oliveira, C. R., Bach, V. R., Lupatini, K. N., Neves, A. C., & Arantes, M. K. (2017). Effect of shrimp shells milling on the molar mass of chitosan. *Polímeros*, 27(1), 41–47. <https://doi.org/10.1590/0104-1428.2354>
- Alves, H. J., Gasparini, L. J., Silva, F. E. B., Cacicano, L., de Muniz, G. I. B., Ballester, E. L. C., Cremonez, P. A., & Arantes, M. K. (2021). Alternative methods for the pilot-scale production and characterization of chitosan nanoparticles. *Environmental Science and Pollution Research*, 28(9), 10977–10987. <https://doi.org/10.1007/S11356-020-11343-5/FIGURES/8>
- Alves, H. J., Vieceli, M., Alves, C., Muñoz, G. I. B., de Oliveira, C. L. P., Feroldi, M., & Arantes, M. K. (2018). Chitosan Depolymerization and Nanochitosan Production Using a Single Physical Procedure. *Journal of Polymers and the Environment*, 26(9), 3913–3923. <https://doi.org/10.1007/S10924-018-1267-7>
- Alves, P., Gomes, L. C., Vorobii, M., Rodriguez-Emmenegger, C., & Mergulhão, F. J. (2020). The potential advantages of using a poly(HPMA) brush in urinary catheters: effects on biofilm cells and architecture. *Colloids and Surfaces B: Biointerfaces*, 191, 110976. <https://doi.org/10.1016/J.COLSURFB.2020.110976>
- Amini, S. M. (2019). Preparation of antimicrobial metallic nanoparticles with bioactive compounds. *Materials Science and Engineering: C*, 103, 109809. <https://doi.org/10.1016/J.MSEC.2019.109809>
- Anjugam, M., Vaseeharan, B., Iswarya, A., Divya, M., Prabhu, N. M., & Sankaranarayanan, K. (2018). Biological synthesis of silver nanoparticles using β -1, 3 glucan binding protein and their antibacterial, antibiofilm and cytotoxic potential. *Microbial Pathogenesis*, 115, 31–40. <https://doi.org/10.1016/J.MICPATH.2017.12.003>
- Ansari-Asl, Z., Shahvali, Z., Sacourbaravi, R., Hoveizi, E., & Darabpour, E. (2022). Cu(II) metal-organic framework@Polydimethylsiloxane nanocomposite sponges coated by chitosan for antibacterial and tissue engineering applications. *Microporous and Mesoporous Materials*, 336, 111866. <https://doi.org/10.1016/J.MICROMESO.2022.111866>

- Antonino, R. S. C. M. D. Q., Fook, B. R. P. L., Lima, V. A. D. O., Rached, R. Í. D. F., Lima, E. P. N., Lima, R. J. D. S., Covas, C. A. P., & Fook, M. V. L. (2017). Preparation and Characterization of Chitosan Obtained from Shells of Shrimp (*Litopenaeus vannamei* Boone). *Marine Drugs* 2017, Vol. 15, Page 141, 15(5), 141. <https://doi.org/10.3390/MD15050141>
- Antsiferova, A., Kopaeva, M., & Kashkarov, P. (2018). Effects of Prolonged Silver Nanoparticle Exposure on the Contextual Cognition and Behavior of Mammals. *Materials*, 11(4). <https://doi.org/10.3390/MA11040558>
- Anusuya, S., & Banu, K. N. (2016). Silver-chitosan nanoparticles induced biochemical variations of chickpea (*Cicer arietinum* L.). *Biocatalysis and Agricultural Biotechnology*, 8, 39–44. <https://doi.org/10.1016/j.bcab.2016.08.005>
- Arantes, M. K., Kugelmeier, C. L., Cardozo-Filho, L., Monteiro, M. R., Oliveira, C. R., & Alves, H. J. (2015). Influence of the drying route on the depolymerization and properties of chitosan. *Polymer Engineering and Science*, 55(9), 1969–1976. <https://doi.org/10.1002/PEN.24038>
- Arias Alvarado, F., Iriarte, M. R., Jordan Mariño, F., Quijano-Guauque, S., Pérez, L. D., Baena, Y., & García-Guerrero, C. (2021). Experimental Solution of Chitosan and Nanochitosan on Wettability in Root Dentine: In Vitro Model Prior Regenerative Endodontics. *International Journal of Biomaterials*, 2021. <https://doi.org/10.1155/2021/8772706>
- Arinda, P. S., Santjojo, D. J. D. H., Masrurah, M., & Sakti, S. P. (2019). Stability of Polystyrene Film Surface Wettability Modified Using Oxygen Plasma. *Materials Today: Proceedings*, 13, 24–29. <https://doi.org/10.1016/J.MATPR.2019.03.181>
- Asghar, M. A., Yousuf, R. I., Shoaib, M. H., & Asghar, M. A. (2020). Antibacterial, anticoagulant and cytotoxic evaluation of biocompatible nanocomposite of chitosan loaded green synthesized bioinspired silver nanoparticles. *International Journal of Biological Macromolecules*, 160, 934–943. <https://doi.org/10.1016/J.IJBIOMAC.2020.05.197>
- Azadpour, A., Hajrasouliha, S., & Khaleghi, S. (2022). Green synthesized-silver nanoparticles coated with targeted chitosan nanoparticles for smart drug delivery. *Journal of Drug Delivery Science and Technology*, 74, 103554. <https://doi.org/10.1016/J.JDDST.2022.103554>
- Babamoradi, J., Ghorbani-Vaghei, R., & Alavinia, S. (2022). Click synthesis of 1,2,3-triazoles using copper iodide nanoparticles anchored poly(sulfonamide-thiazole) modified layered

- double hydroxides/chitosan nanocomposite. *International Journal of Biological Macromolecules*, 209, 1542–1552. <https://doi.org/10.1016/J.IJBIOMAC.2022.04.140>
- Bach, V. R., Zempulski, D. A., Oliveira, L. G., Polinarski, M. A., Parussolo Tonin, A. P., Meurer, E. C., Cardozo-Filho, L., & Alves, H. J. (2022). Green synthesis of NiO nanoparticles and application in production of renewable H₂ from bioethanol. *International Journal of Hydrogen Energy*, 47(60), 25229–25244. <https://doi.org/10.1016/J.IJHYDENE.2022.05.264>
- Bates, I. I. C., Carrillo, I. B. S., Germain, H., Loranger, É., & Chabot, B. (2021). Antibacterial electrospun chitosan-PEO/TEMPO-oxidized cellulose composite for water filtration. *Journal of Environmental Chemical Engineering*, 9(5), 106204. <https://doi.org/10.1016/J.JECE.2021.106204>
- Beck, B. H., Yildirim-Aksoy, M., Shoemaker, C. A., Fuller, S. A., & Peatman, E. (2019). Antimicrobial activity of the biopolymer chitosan against *Streptococcus iniae*. *Journal of Fish Diseases*, 42(3), 371–377. <https://doi.org/10.1111/JFD.12938>
- Begum, S., Yuhana, N. Y., Md Saleh, N., Kamarudin, N. H. N., & Sulong, A. B. (2021). Review of chitosan composite as a heavy metal adsorbent: Material preparation and properties. *Carbohydrate Polymers*, 259, 117613. <https://doi.org/10.1016/J.CARBPOL.2021.117613>
- Behera, S. S., Majumdar, A. G., Gullani, H., Roy, A. L., Dash, A. K., Behera, P. K., Parwez, Z., Giri, S., Mohanty, P. S., & Ray, L. (2025). Green synthesis of silver-chitosan nanocomposite exhibits promising antibiofilm properties against pathogenic bacteria *Escherichia coli* and *Staphylococcus aureus*. *The Microbe*, 6, 100264. <https://doi.org/10.1016/J.MICROB.2025.100264>
- Bernardi, F., Zadinelo, I. V., Alves, H. J., Meurer, F., & dos Santos, L. D. (2018). Chitins and chitosans for the removal of total ammonia of aquaculture effluents. *Aquaculture*, 483, 203–212. <https://doi.org/10.1016/J.AQUACULTURE.2017.10.027>
- Bezerra, A. M. (2011). *Síntese e avaliações físico-químicas e biológicas de derivados de quitosana de alta e baixa massa molecular* [Biblioteca Digital de Teses e Dissertações da Universidade de São Paulo]. <https://doi.org/10.11606/D.9.2011.tde-22042013-105019>
- Biao, L., Tan, S., Wang, Y., Guo, X., Fu, Y., Xu, F., Zu, Y., & Liu, Z. (2017). Synthesis, characterization and antibacterial study on the chitosan-functionalized Ag nanoparticles. *Materials Science and Engineering: C*, 76, 73–80. <https://doi.org/10.1016/J.MSEC.2017.02.154>
- Bilal, M., Rasheed, T., Iqbal, H. M. N., Li, C., Hu, H., & Zhang, X. (2017). Development of silver nanoparticles loaded chitosan-alginate constructs with biomedical potentialities.

- International Journal of Biological Macromolecules*, 105, 393–400. <https://doi.org/10.1016/J.IJBIOMAC.2017.07.047>
- Blair, J. M. A., Webber, M. A., Baylay, A. J., Ogbolu, D. O., & Piddock, L. J. V. (2014). Molecular mechanisms of antibiotic resistance. *Nature Reviews Microbiology* 2014 13:1, 13(1), 42–51. <https://doi.org/10.1038/nrmicro3380>
- Bolaños-Cardet, J., Ruiz-Molina, D., Yuste, V. J., & Suárez-García, S. (2024). Bioinspired phenol-based coatings for medical fabrics against antimicrobial resistance. *Chemical Engineering Journal*, 481, 148674. <https://doi.org/10.1016/J.CEJ.2024.148674>
- Bondarenko, O. M., Sihtmäe, M., Kuzmičiova, J., Ragelienė, L., Kahru, A., & Daugelavičius, R. (2018). Plasma membrane is the target of rapid antibacterial action of silver nanoparticles in escherichia coli and Pseudomonas aeruginosa. *International Journal of Nanomedicine*, 13, 6779–6790. <https://doi.org/10.2147/IJN.S177163>
- Bonilla-Gameros, L., Chevallier, P., Sarkissian, A., & Mantovani, D. (2020). Silver-based antibacterial strategies for healthcare-associated infections: Processes, challenges, and regulations. An integrated review. *Nanomedicine: Nanotechnology, Biology and Medicine*, 24, 102142. <https://doi.org/10.1016/J.NANO.2019.102142>
- Buonsenso, D., Salerno, G., Soderò, G., Mariani, F., Pisapia, L., Gelormini, C., Di Nardo, M., Valentini, P., Scoppettuolo, G., & Biasucci, D. G. (2022). Catheter salvage strategies in children with central venous catheter-related or -associated bloodstream infections: a systematic review and meta-analysis. *Journal of Hospital Infection*, 125, 1–20. <https://doi.org/10.1016/J.JHIN.2022.03.010>
- Cai, Y., Yang, H., Li, J., Gu, R., Dong, Y., Zhao, Q., Chen, Y., Li, Y., & Wang, R. (2023). Antibacterial AgNPs-PAAm-CS-PVP nanocomposite hydrogel coating for urinary catheters. *European Polymer Journal*, 196, 112260. <https://doi.org/10.1016/J.EURPOLYMJ.2023.112260>
- Campana, R., Biondo, F., Mastrotto, F., Baffone, W., & Casettari, L. (2018). Chitosans as new tools against biofilms formation on the surface of silicone urinary catheters. *International Journal of Biological Macromolecules*, 118, 2193–2200. <https://doi.org/10.1016/J.IJBIOMAC.2018.07.088>
- Campana, R., Casettari, L., Ciandrini, E., Illum, L., & Baffone, W. (2017). Chitosans inhibit the growth and the adhesion of Klebsiella pneumoniae and Escherichia coli clinical isolates on urinary catheters. *International Journal of Antimicrobial Agents*, 50(2), 135–141. <https://doi.org/10.1016/j.ijantimicag.2017.03.031>

- Canciu, A., Cernat, A., Tertis, M., Graur, F., & Cristea, C. (2023). Tackling the issue of healthcare associated infections through point-of-care devices. *TrAC Trends in Analytical Chemistry*, 161, 116983. <https://doi.org/10.1016/J.TRAC.2023.116983>
- Carbone, G. G., Manno, D., Serra, A., Buccolieri, A., Cennamo, S., Aziz, M. R., Gabriele, A., & Calcagnile, L. (2024). Green synthesis and characterization of AgNPs/CDs hybrid system for enhanced oxidation resistance at physiological concentration of H₂O₂. *Journal of Molecular Structure*, 1318, 139195. <https://doi.org/10.1016/J.MOLSTRUC.2024.139195>
- Chauke, N. M., Munonde, T. S., & Mketi, N. (2025). A critical review of the anti-biofouling properties of biogenic-based silver nanoparticles (AgNPs) embedded on polymer membranes for wastewater treatment. *Journal of Industrial and Engineering Chemistry*. <https://doi.org/10.1016/J.JIEC.2025.02.012>
- Cheikhrouhou, W., Ferraria, A. M., Botelho do Rego, A. M., Ferreira Machado, I., Vieira Ferreira, L. F., & Boufi, S. (2020). Cotton fabrics decorated with nanostructured Ag/AgX (X:Cl,Br) as reusable solar light-mediated bactericides: A comparative study. *Colloids and Surfaces B: Biointerfaces*, 196, 111342. <https://doi.org/10.1016/J.COLSURFB.2020.111342>
- Chen, S., O'Malley, M., & Chopra, V. (2021). How common are indwelling devices in hospitalized adults? A contemporary point prevalence study in a tertiary care hospital. *American Journal of Infection Control*, 49(2), 194–197. <https://doi.org/10.1016/J.AJIC.2020.06.205>
- Chen, Z., Zhang, X., Cao, H., & Huang, Y. (2013). Chitosan-capped silver nanoparticles as a highly selective colorimetric probe for visual detection of aromatic ortho-trihydroxy phenols. *Analyst*, 138(8), 2343–2349. <https://doi.org/10.1039/C3AN36905F>
- Chernousova, S., & Epple, M. (2013). Silver as Antibacterial Agent: Ion, Nanoparticle, and Metal. *Angewandte Chemie International Edition*, 52(6), 1636–1653. <https://doi.org/10.1002/ANIE.201205923>
- Chien, R. C., Yen, M. T., & Mau, J. L. (2016). Antimicrobial and antitumor activities of chitosan from shiitake stipes, compared to commercial chitosan from crab shells. *Carbohydrate Polymers*, 138, 259–264. <https://doi.org/10.1016/J.CARBPOL.2015.11.061>
- Choudhary, P., Ramalingam, B., & Das, S. K. (2023). Rational design of antimicrobial peptide conjugated graphene-silver nanoparticle loaded chitosan wound dressing. *International*

- Journal of Biological Macromolecules*, 246, 125347.
<https://doi.org/10.1016/J.IJBIOMAC.2023.125347>
- Ciccacci, F., De Santo, C., Mosconi, C., Orlando, S., Carestia, M., Guarente, L., Liotta, G., Palombi, L., & Emberti Gialloreti, L. (2024). Not only COVID-19: a systematic review of anti-COVID-19 measures and their effect on healthcare-associated infections. *Journal of Hospital Infection*, 147, 133–145. <https://doi.org/10.1016/J.JHIN.2024.02.008>
- CLSI. (2015a). *Methods for dilution antimicrobial susceptibility test for bacteria that grow aerobically. Approved standard, 10th ed. CLSI document M7-A10. 10th ed.* .
- CLSI. (2015b). *Performance standards for antimicrobial disk susceptibility tests. Approved standard, 12th ed. CLSI document M02-A12.*
- Costa, E. M., Silva, S., Pina, C., Tavaría, F. K., & Pintado, M. M. (2012). Evaluation and insights into chitosan antimicrobial activity against anaerobic oral pathogens. *Anaerobe*, 18(3), 305–309. <https://doi.org/10.1016/J.ANAEROBE.2012.04.009>
- Costa, E. M., Silva, S., Veiga, M., Tavaría, F. K., & Pintado, M. M. (2018). Exploring chitosan nanoparticles as effective inhibitors of antibiotic resistant skin microorganisms – From in vitro to ex vitro testing. *Carbohydrate Polymers*, 201, 340–346. <https://doi.org/10.1016/j.carbpol.2018.08.083>
- Costa, E. M., Silva, S., Vicente, S., Neto, C., Castro, P. M., Veiga, M., Madureira, R., Tavaría, F., & Pintado, M. M. (2017). Chitosan nanoparticles as alternative anti-staphylococci agents: Bactericidal, antibiofilm and antiadhesive effects. *Materials Science and Engineering C*, 79, 221–226. <https://doi.org/10.1016/j.msec.2017.05.047>
- Costerton, J. W., Stewart, P. S., & Greenberg, E. P. (1999). Bacterial biofilms: A common cause of persistent infections. *Science*, 284(5418), 1318–1322. <https://doi.org/10.1126/science.284.5418.1318>
- da Silva, R. T. P., Petri, M. V., Valencia, E. Y., Camargo, P. H. C., de Torresi, S. I. C., & Spira, B. (2020). Visible light plasmon excitation of silver nanoparticles against antibiotic-resistant *Pseudomonas aeruginosa*. *Photodiagnosis and Photodynamic Therapy*, 31, 101908. <https://doi.org/10.1016/J.PDPDT.2020.101908>
- Dananjaya, S. H. S., Erandani, W. K. C. U., Kim, C. H., Nikapitiya, C., Lee, J., & De Zoysa, M. (2017). Comparative study on antifungal activities of chitosan nanoparticles and chitosan silver nano composites against *Fusarium oxysporum* species complex. *International Journal of Biological Macromolecules*, 105, 478–488. <https://doi.org/10.1016/J.IJBIOMAC.2017.07.056>

- Darabpour, E., Kashef, N., & Mashayekhan, S. (2016). Chitosan nanoparticles enhance the efficiency of methylene blue-mediated antimicrobial photodynamic inactivation of bacterial biofilms: An in vitro study. *Photodiagnosis and Photodynamic Therapy*, 14, 211–217. <https://doi.org/10.1016/j.pdpdt.2016.04.009>
- Das, B., Dash, S. K., Mandal, D., Ghosh, T., Chattopadhyay, S., Tripathy, S., Das, S., Dey, S. K., Das, D., & Roy, S. (2017). Green synthesized silver nanoparticles destroy multidrug resistant bacteria via reactive oxygen species mediated membrane damage. *Arabian Journal of Chemistry*, 10(6), 862–876. <https://doi.org/10.1016/J.ARABJC.2015.08.008>
- Das, B., Tripathy, S., Adhikary, J., Chattopadhyay, S., Mandal, D., Dash, S. K., Das, S., Dey, A., Dey, S. K., Das, D., & Roy, S. (2017). Surface modification minimizes the toxicity of silver nanoparticles: an in vitro and in vivo study. *Journal of Biological Inorganic Chemistry*, 22(6), 893–918. <https://doi.org/10.1007/s00775-017-1468-x>
- Das, C. G. A., Kumar, V. G., Dhas, T. S., Karthick, V., Govindaraju, K., Joselin, J. M., & Baalamurugan, J. (2020). Antibacterial activity of silver nanoparticles (biosynthesis): A short review on recent advances. *Biocatalysis and Agricultural Biotechnology*, 27, 101593. <https://doi.org/10.1016/J.BCAB.2020.101593>
- deFarias, B. S., Grundmann, D. D. R., Rizzi, F. Z., Martins, N. S. S., Sant'Anna Cadaval Junior, T. R., & de Almeida Pinto, L. A. (2019). Production of low molecular weight chitosan by acid and oxidative pathways: Effect on physicochemical properties. *Food Research International*, 123, 88–94. <https://doi.org/10.1016/j.foodres.2019.04.051>
- Deng, J., Wu, K., Yang, Y., Zhang, Y., & Lin, C. (2015). Antimicrobial activity and cytocompatibility of silver nanoparticles coated catheters via a biomimetic surface functionalization strategy. *International Journal of Nanomedicine*, 10(1), 7241. <https://doi.org/10.2147/IJN.S92307>
- Deng, Q., Wang, X., Shao, M., Fang, L., Zhao, X., Xu, J., & Wang, X. (2022). Synthesis of chitosan-modified magnetic metal-organic framework and its adsorption of Congo red and antibacterial activity. *Microporous and Mesoporous Materials*, 342, 112042. <https://doi.org/10.1016/J.MICROMESO.2022.112042>
- Devi, L., & Joshi, S. (2015). Ultrastructures of silver nanoparticles biosynthesized using endophytic fungi. *Journal of Microscopy and Ultrastructure*, 3(1), 29. <https://doi.org/10.1016/j.jmau.2014.10.004>
- Dimopoulos, G., Kollef, M. H., & Cohen, J. (2016). In 2035, will all bacteria be multiresistant? Yes. *Intensive Care Medicine*, 42(12), 2014–2016. <https://doi.org/10.1007/S00134-016-4310-Y/TABLES/1>

- Divya, K., & Jisha, M. S. (2017). Chitosan nanoparticles preparation and applications. *Environmental Chemistry Letters* 2017 16:1, 16(1), 101–112. <https://doi.org/10.1007/S10311-017-0670-Y>
- Dridi, D., Vu, N. N., Singh, J., Eesaee, M., Saidi, A., Elkoun, S., & Nguyen-Tri, P. (2024). Recent advances on engineering of silver related nanocomposites toward antibacterial applications. *Nano-Structures & Nano-Objects*, 38, 101195. <https://doi.org/10.1016/J.NANOSO.2024.101195>
- Du, B., Pan, L., Zheng, M., Zhang, B., & Hu, Y. (2024). Preparation of AgNPs/oregano essential oil composite film and its antibacterial application in the conservation of paper relics. *Inorganic Chemistry Communications*, 160, 112008. <https://doi.org/10.1016/J.INOCHE.2023.112008>
- Du, X., Jiang, H., Guo, X., Chen, L., & Kang, T. (2021). Synthesis of ferrocene/chitosan-AgNPs films and application in plasmonic color-switching and antimicrobial materials. *Reactive and Functional Polymers*, 169, 105061. <https://doi.org/10.1016/J.REACTFUNCTPOLYM.2021.105061>
- Durán, N., Rolim, W. R., Durán, M., Fávaro, W. J., & Seabra, A. B. (2019). Nanotoxicology of silver nanoparticles: Toxicity in animals and humans. *Quimica Nova*, 42(2), 206–213. <https://doi.org/10.21577/0100-4042.20170318>
- Ebrahimi, A., Jafferli, H., Habibian, S., & Lotfalian, S. (2018). Evaluation of anti biofilm and antibiotic potentiation activities of silver nanoparticles against some nosocomial pathogens. *Iranian Journal of Pharmaceutical Sciences*, 14(2), 7–14. <https://doi.org/10.22034/IJPS.2018.33684>
- Edo, G. I., Yousif, E., & Al-Mashhadani, M. H. (2024). Modified chitosan: Insight on biomedical and industrial applications. *International Journal of Biological Macromolecules*, 275, 133526. <https://doi.org/10.1016/J.IJBIOMAC.2024.133526>
- Elmehbad, N. Y., & Mohamed, N. A. (2020). Designing, preparation and evaluation of the antimicrobial activity of biomaterials based on chitosan modified with silver nanoparticles. *International Journal of Biological Macromolecules*, 151, 92–103. <https://doi.org/10.1016/j.ijbiomac.2020.01.298>
- El-Sheikh, M. A. (2024). Synthesis of a novel carboxymethyl chitosan-silver - ginger nanocomposite, characterization, and antimicrobial efficacy. *Carbohydrate Polymer Technologies and Applications*, 8, 100561. <https://doi.org/10.1016/J.CARPTA.2024.100561>

- El-Zahry, M. R., Mahmoud, A., Refaat, I. H., Mohamed, H. A., Bohlmann, H., & Lendl, B. (2015). Antibacterial effect of various shapes of silver nanoparticles monitored by SERS. *Talanta*, 138, 183–189. <https://doi.org/10.1016/J.TALANTA.2015.02.022>
- Engels, S., & O’Born, R. J. (2022). Realizing the potential of humic acid recovery in Norway through chitosan treatment of drinking water. *Procedia CIRP*, 105, 177–182. <https://doi.org/10.1016/J.PROCIR.2022.02.031>
- Espinosa-Cristóbal, L. F., Martínez-Castañón, G. A., Loyola-Rodríguez, J. P., Niño-Martínez, N., Ruiz, F., Zavala-Alonso, N. V., Lara, R. H., & Reyes-López, S. Y. (2015). Bovine Serum Albumin and Chitosan Coated Silver Nanoparticles and Its Antimicrobial Activity against Oral and Nonoral Bacteria. *Journal of Nanomaterials*, 2015(1), 420853. <https://doi.org/10.1155/2015/420853>
- Fafliora, E., Bampalis, V. G., Lazarou, N., Mantzouranis, G., Anastassiou, E. D., Spiliopoulou, I., & Christofidou, M. (2014). Bacterial contamination of medical devices in a Greek emergency department: Impact of physicians’ cleaning habits. *American Journal of Infection Control*, 42(7), 807–809. <https://doi.org/10.1016/J.AJIC.2014.03.017>
- Fahim, M., Shahzaib, A., Nishat, N., Jahan, A., Bhat, T. A., & Inam, A. (2024). Green synthesis of silver nanoparticles: A comprehensive review of methods, influencing factors, and applications. *JCIS Open*, 16, 100125. <https://doi.org/10.1016/J.JCISO.2024.100125>
- Fair, R. J., & Tor, Y. (2014). Antibiotics and bacterial resistance in the 21st century. *Perspectives in Medicinal Chemistry*, 6, 25–64. https://doi.org/10.4137/PMC.S14459/ASSET/IMAGES/LARGE/10.4137_PMC.S14459-FIG20.JPEG
- Fan, M., Si, J., Xu, X., Chen, L., Chen, J., Yang, C., Zhu, J., Wu, L., Tian, J., Chen, X., Mou, X., & Cai, X. (2021). A versatile chitosan nanogel capable of generating AgNPs in-situ and long-acting slow-release of Ag⁺ for highly efficient antibacterial. *Carbohydrate Polymers*, 257, 117636. <https://doi.org/10.1016/J.CARBPOL.2021.117636>
- Farhangi Ghaleh Joughi, N., Farahpour, M. R., Mohammadi, M., Jafarirad, S., & Mahmazi, S. (2022). Investigation on the antibacterial properties and rapid infected wound healing activity of silver/laterite/chitosan nanocomposites. *Journal of Industrial and Engineering Chemistry*, 111, 64–75. <https://doi.org/10.1016/J.JIEC.2022.03.034>
- Felipe, V., Breser, M. L., Bohl, L. P., Rodrigues da Silva, E., Morgante, C. A., Correa, S. G., & Porporatto, C. (2019). Chitosan disrupts biofilm formation and promotes biofilm eradication in Staphylococcus species isolated from bovine mastitis. *International Journal*

- of *Biological Macromolecules*, 126, 60–67.
<https://doi.org/10.1016/j.ijbiomac.2018.12.159>
- Ferraria, A. M., Carapeto, A. P., & Botelho Do Rego, A. M. (2012). X-ray photoelectron spectroscopy: Silver salts revisited. *Vacuum*, 86(12), 1988–1991.
<https://doi.org/10.1016/J.VACUUM.2012.05.031>
- Ferreres, G., Ivanova, K., Torrent-Burgués, J., & Tzanov, T. (2023). Multimodal silver-chitosan-acylase nanoparticles inhibit bacterial growth and biofilm formation by Gram-negative *Pseudomonas aeruginosa* bacterium. *Journal of Colloid and Interface Science*, 646, 576–586. <https://doi.org/10.1016/J.JCIS.2023.04.184>
- Flemming, H. C., Wingender, J., Szewzyk, U., Steinberg, P., Rice, S. A., & Kjelleberg, S. (2016). Biofilms: an emergent form of bacterial life. *Nature Reviews Microbiology*, 14(9), 563–575. <https://doi.org/10.1038/nrmicro.2016.94>
- Francis, A. L., Namasivayam, S. K. R., & Samrat, K. (2024). Potential of silver nanoparticles synthesized from *Justicia adhatoda* metabolites for inhibiting biofilm on urinary catheters. *Microbial Pathogenesis*, 196, 106957. <https://doi.org/10.1016/J.MICPATH.2024.106957>
- Franco, D., Calabrese, G., Guglielmino, S. P. P., & Conoci, S. (2022). Metal-Based Nanoparticles: Antibacterial Mechanisms and Biomedical Application. *Microorganisms* 2022, Vol. 10, Page 1778, 10(9), 1778.
<https://doi.org/10.3390/MICROORGANISMS10091778>
- Frank, L. A., Onzi, G. R., Morawski, A. S., Pohlmann, A. R., Guterres, S. S., & Contri, R. V. (2020). Chitosan as a coating material for nanoparticles intended for biomedical applications. *Reactive and Functional Polymers*, 147, 104459.
<https://doi.org/10.1016/J.REACTFUNCTPOLYM.2019.104459>
- Freitas, E. D., Bataglioli, R. A., Oshodi, J., & Beppu, M. M. (2022). Antimicrobial peptides and their potential application in antiviral coating agents. *Colloids and Surfaces B: Biointerfaces*, 217, 112693. <https://doi.org/10.1016/J.COLSURFB.2022.112693>
- Gadkari, R. R., Suwalka, S., Yogi, M. R., Ali, W., Das, A., & Alagirusamy, R. (2019). Green synthesis of chitosan-cinnamaldehyde cross-linked nanoparticles: Characterization and antibacterial activity. *Carbohydrate Polymers*, 226, 115298.
<https://doi.org/10.1016/j.carbpol.2019.115298>
- Gao, Y., & Wu, Y. (2022). Recent advances of chitosan-based nanoparticles for biomedical and biotechnological applications. *International Journal of Biological Macromolecules*, 203, 379–388. <https://doi.org/10.1016/J.IJBIOMAC.2022.01.162>

- Geng, Y., Xue, H., Zhang, Z., Panayi, A. C., Knoedler, S., Zhou, W., Mi, B., & Liu, G. (2023). Recent advances in carboxymethyl chitosan-based materials for biomedical applications. *Carbohydrate Polymers*, 305, 120555. <https://doi.org/10.1016/J.CARBPOL.2023.120555>
- Ghasemi, M., Govahi, M., & Litkahi, H. R. (2025). Green synthesis of silver nanoparticles (AgNPs) and chitosan-coated silver nanoparticles (CS-AgNPs) using *Ferula gummosa* Boiss. gum extract: A green nano drug for potential applications in medicine. *International Journal of Biological Macromolecules*, 291, 138619. <https://doi.org/10.1016/J.IJBIOMAC.2024.138619>
- Goy, R. C., De Britto, D., & Assis, O. B. G. (2009). A review of the antimicrobial activity of chitosan. *Polímeros*, 19(3), 241–247. <https://doi.org/10.1590/S0104-14282009000300013>
- Graziani, G., Ghezzi, D., Boi, M., Baldini, N., Sassoni, E., Cappelletti, M., Fedrizzi, G., Maglio, M., Salamanna, F., Tschon, M., Martini, L., Zaffagnini, S., Fini, M., & Sartori, M. (2024). Ionized jet deposition of silver nanostructured coatings: Assessment of chemico-physical and biological behavior for application in orthopedics. *Biomaterials Advances*, 159, 213815. <https://doi.org/10.1016/J.BIOADV.2024.213815>
- Guggenbichler, J. P., Böswald, M., Lugauer, S., & Krall, T. (1999). A new technology of microdispersed silver in polyurethane induces antimicrobial activity in central venous catheters. *Infection*, 27(SUPPL. 1), S16–S23. <https://doi.org/10.1007/BF02561612>
- Guo, Y., Qiao, D., Zhao, S., Zhang, B., & Xie, F. (2024). Advanced functional chitosan-based nanocomposite materials for performance-demanding applications. *Progress in Polymer Science*, 157, 101872. <https://doi.org/10.1016/J.PROGPOLYMSCI.2024.101872>
- Hadidi, M., Pouramin, S., Adinepour, F., Haghani, S., & Jafari, S. M. (2020). Chitosan nanoparticles loaded with clove essential oil: Characterization, antioxidant and antibacterial activities. *Carbohydrate Polymers*, 236, 116075. <https://doi.org/10.1016/j.carbpol.2020.116075>
- Hajji, S., Khedir, S. Ben, Hamza-Mnif, I., Hamdi, M., Jedidi, I., Kallel, R., Boufi, S., & Nasri, M. (2019). Biomedical potential of chitosan-silver nanoparticles with special reference to antioxidant, antibacterial, hemolytic and in vivo cutaneous wound healing effects. *Biochimica et Biophysica Acta (BBA) - General Subjects*, 1863(1), 241–254. <https://doi.org/10.1016/J.BBAGEN.2018.10.010>
- Hamed, I., Özogul, F., & Regenstein, J. M. (2016). Industrial applications of crustacean by-products (chitin, chitosan, and chitooligosaccharides): A review. *Trends in Food Science & Technology*, 48, 40–50. <https://doi.org/10.1016/J.TIFS.2015.11.007>

- Haney, E. F., Trimble, M. J., & Hancock, R. E. W. (2021). Microtiter plate assays to assess antibiofilm activity against bacteria. *Nature Protocols* 2021 16:5, 16(5), 2615–2632. <https://doi.org/10.1038/s41596-021-00515-3>
- Hasan, K. M. F., Xiaoyi, L., Shaoqin, Z., Horváth, P. G., Bak, M., Bejő, L., Sipos, G., & Alpár, T. (2022). Functional silver nanoparticles synthesis from sustainable point of view: 2000 to 2023 – A review on game changing materials. *Heliyon*, 8(12), e12322. <https://doi.org/10.1016/J.HELİYON.2022.E12322>
- He, G., Li, H., Zhao, Z., Liu, Q., Yu, J., Ji, Z., Ning, X., & Ning, F. (2024). Antifouling coatings based on the synergistic action of biogenic antimicrobial agents and low surface energy silicone resins and their application to marine aquaculture nets. *Progress in Organic Coatings*, 195, 108656. <https://doi.org/10.1016/J.PORGOAT.2024.108656>
- Herigstad, B., Hamilton, M., & Heersink, J. (2001). How to optimize the drop plate method for enumerating bacteria. *Journal of Microbiological Methods*, 44(2), 121–129. [https://doi.org/10.1016/S0167-7012\(00\)00241-4](https://doi.org/10.1016/S0167-7012(00)00241-4)
- Hofer, U. (2018). The cost of antimicrobial resistance. *Nature Reviews Microbiology* 2018 17:1, 17(1), 3–3. <https://doi.org/10.1038/s41579-018-0125-x>
- Holubnycha, V., Kalinkevich, O., Ivashchenko, O., & Pogoriellov, M. (2018). Antibacterial Activity of In Situ Prepared Chitosan/Silver Nanoparticles Solution Against Methicillin-Resistant Strains of Staphylococcus aureus. *Nanoscale Research Letters*, 13(1), 1–8. <https://doi.org/10.1186/S11671-018-2482-9/FIGURES/2>
- Hong, X., Wen, J., Xiong, X., & Hu, Y. (2016). Shape effect on the antibacterial activity of silver nanoparticles synthesized via a microwave-assisted method. *Environmental Science and Pollution Research*, 23(5), 4489–4497. <https://doi.org/10.1007/S11356-015-5668-Z/FIGURES/7>
- Hu, B., Guo, Y., Li, H., Liu, X., Fu, Y., & Ding, F. (2021). Recent advances in chitosan-based layer-by-layer biomaterials and their biomedical applications. *Carbohydrate Polymers*, 271, 118427. <https://doi.org/10.1016/J.CARBPOL.2021.118427>
- Hu, G., Jin, W., Zhang, W., Wu, K., He, J., Zhang, Y., Chen, Q., & Zhang, W. (2018). Surfactant-assisted shape separation from silver nanoparticles prepared by a seed-mediated method. *Colloids and Surfaces A: Physicochemical and Engineering Aspects*, 540, 136–142. <https://doi.org/10.1016/j.colsurfa.2017.12.071>
- Huang, H., & Yang, X. (2004). Synthesis of polysaccharide-stabilized gold and silver nanoparticles: a green method. *Carbohydrate Research*, 339(15), 2627–2631. <https://doi.org/10.1016/J.CARRES.2004.08.005>

- Huang, J., Mo, X., Fu, H., Sun, Y., Gao, Q., Chen, X., Zou, J., Yuan, Y., Nie, J., & Zhang, Y. (2021). Tyndall-effect-enhanced supersensitive naked-eye determination of mercury (II) ions with silver nanoparticles. *Sensors and Actuators B: Chemical*, 344, 130218. <https://doi.org/10.1016/J.SNB.2021.130218>
- Huang, R., Huang, X., Zhang, Q., Fan, J., Zhang, Z., & Huang, J. (2024). Humidity-responsive pectin/AgNPs/ZnO composite films with high antimicrobial and UV-proof functions. *International Journal of Biological Macromolecules*, 279, 135075. <https://doi.org/10.1016/J.IJBIOMAC.2024.135075>
- Huang, X., Bao, X., Liu, Y., Wang, Z., & Hu, Q. (2017). Catechol-Functional Chitosan/Silver Nanoparticle Composite as a Highly Effective Antibacterial Agent with Species-Specific Mechanisms. *Scientific Reports* 2017 7:1, 7(1), 1–10. <https://doi.org/10.1038/s41598-017-02008-4>
- Huq, T., Khan, A., Brown, D., Dhayagude, N., He, Z., & Ni, Y. (2022). Sources, production and commercial applications of fungal chitosan: A review. *Journal of Bioresources and Bioproducts*, 7(2), 85–98. <https://doi.org/10.1016/J.JOBAB.2022.01.002>
- Ing, L. Y., Zin, N. M., Sarwar, A., & Katas, H. (2012). Antifungal activity of chitosan nanoparticles and correlation with their physical properties. *International Journal of Biomaterials*. <https://doi.org/10.1155/2012/632698>
- Iqbal, Y., Ahmed, I., Irfan, M. F., Chatha, S. A. S., Zubair, M., & Ullah, A. (2023). Recent advances in chitosan-based materials; The synthesis, modifications and biomedical applications. *Carbohydrate Polymers*, 321, 121318. <https://doi.org/10.1016/J.CARBPOL.2023.121318>
- Issahaku, I., Tetteh, I. K., & Tetteh, A. Y. (2023). Chitosan and chitosan derivatives: Recent advancements in production and applications in environmental remediation. *Environmental Advances*, 11, 100351. <https://doi.org/10.1016/J.ENVADV.2023.100351>
- Jia, H., Xu, W., An, J., Li, D., & Zhao, B. (2006). A simple method to synthesize triangular silver nanoparticles by light irradiation. *Spectrochimica Acta - Part A: Molecular and Biomolecular Spectroscopy*, 64(4), 956–960. <https://doi.org/10.1016/j.saa.2005.09.004>
- Jiang, M., Althomali, R. H., Ansari, S. A., Saleh, E. A. M., Gupta, J., Kambarov, K. D., Alsaab, H. O., Alwaily, E. R., Hussien, B. M., Mustafa, Y. F., Narmani, A., & Farhood, B. (2023). Advances in preparation, biomedical, and pharmaceutical applications of chitosan-based gold, silver, and magnetic nanoparticles: A review. *International Journal of Biological Macromolecules*, 251, 126390. <https://doi.org/10.1016/J.IJBIOMAC.2023.126390>

- Joardar, S., Adams, M. L., Biswas, R., Deodhar, G. V., Metzger, K. E., Deweese, K., Davidson, M., Richards, R. M., Trewyn, B. G., & Biswas, P. (2021). Direct synthesis of silver nanoparticles modified spherical mesoporous silica as efficient antibacterial materials. *Microporous and Mesoporous Materials*, 313, 110824. <https://doi.org/10.1016/J.MICROMESO.2020.110824>
- Kandi, V., & Kandi, S. (2015). Antimicrobial properties of nanomolecules: potential candidates as antibiotics in the era of multi-drug resistance. *Epidemiology and Health*, 37, e2015020. <https://doi.org/10.4178/EPIH/E2015020>
- Karthik, C. S., Chethana, M. H., Manukumar, H. M., Ananda, A. P., Sandeep, S., Nagashree, S., Mallesha, L., Mallu, P., Jayanth, H. S., & Dayananda, B. P. (2021). Synthesis and characterization of chitosan silver nanoparticle decorated with benzodioxane coupled piperazine as an effective anti-biofilm agent against MRSA: A validation of molecular docking and dynamics. *International Journal of Biological Macromolecules*, 181, 540–551. <https://doi.org/10.1016/J.IJBIOMAC.2021.03.119>
- Kasaai, M. R., Arul, J., & Charlet, G. (2013). Fragmentation of chitosan by acids. *The Scientific World Journal*, 2013. <https://doi.org/10.1155/2013/508540>
- Kean, T., & Thanou, M. (2010). Biodegradation, biodistribution and toxicity of chitosan. *Advanced Drug Delivery Reviews*, 62(1), 3–11. <https://doi.org/10.1016/J.ADDR.2009.09.004>
- Kędziora, A., Speruda, M., Krzyżewska, E., Rybka, J., Łukowiak, A., & Bugła-Płoskońska, G. (2018). Similarities and Differences between Silver Ions and Silver in Nanoforms as Antibacterial Agents. *International Journal of Molecular Sciences*, 19(2). <https://doi.org/10.3390/IJMS19020444>
- Khan, A. U., Qutob, M., Gacem, A., Rafatullah, Mohd., Yadav, K. K., Kumar, P., Bhutto, J. K., Rahman, M., Bansoid, S., Eltayeb, L. B., Malik, N., Ali, M. A., Alreshidi, M. A., & Alam, M. W. (2024). Investigation of a broad diversity of nanoparticles, including their processes, as well as toxicity testing in diverse organs and systems. *Toxicology*, 153985. <https://doi.org/10.1016/J.TOX.2024.153985>
- Kim, D. H., Park, J. C., Jeon, G. E., Kim, C. S., & Seo, J. H. (2017). Effect of the size and shape of silver nanoparticles on bacterial growth and metabolism by monitoring optical density and fluorescence intensity. *Biotechnology and Bioprocess Engineering*, 22(2), 210–217. <https://doi.org/10.1007/S12257-016-0641-3/METRICS>
- Kim, H. Y., Rho, W. Y., Lee, H. Y., Park, Y. S., & Suh, J. S. (2014). Aggregation effect of silver nanoparticles on the energy conversion efficiency of the surface plasmon-enhanced

- dye-sensitized solar cells. *Solar Energy*, 109(1), 61–69.
<https://doi.org/10.1016/J.SOLENER.2014.08.019>
- Kim, S., & Choi, I. H. (2012). Phagocytosis and Endocytosis of Silver Nanoparticles Induce Interleukin-8 Production in Human Macrophages. *Yonsei Medical Journal*, 53(3), 654.
<https://doi.org/10.3349/YMJ.2012.53.3.654>
- Kou, S. (Gabriel), Peters, L. M., & Mucalo, M. R. (2021). Chitosan: A review of sources and preparation methods. *International Journal of Biological Macromolecules*, 169, 85–94.
<https://doi.org/10.1016/J.IJBIOMAC.2020.12.005>
- Koumentakou, I., Meretoudi, A., Emmanouil, C., & Kyzas, G. Z. (2024). Environmental toxicity and biodegradation of chitosan derivatives: A comprehensive review. *Journal of Industrial and Engineering Chemistry*. <https://doi.org/10.1016/J.JIEC.2024.11.027>
- Krajewska, B., Wydro, P., & Jańczyk, A. (2011). Probing the modes of antibacterial activity of chitosan. Effects of pH and molecular weight on chitosan interactions with membrane lipids in Langmuir films. *Biomacromolecules*, 12(11), 4144–4152.
https://doi.org/10.1021/BM2012295/ASSET/IMAGES/MEDIUM/BM-2011-012295_0007.GIF
- Kulikouskaya, V., Hileuskaya, K., Kraskouski, A., Kozerozhets, I., Stepanova, E., Kuzminski, I., You, L., & Agabekov, V. (2022). Chitosan-capped silver nanoparticles: A comprehensive study of polymer molecular weight effect on the reaction kinetic, physicochemical properties, and synergetic antibacterial potential. *SPE Polymers*, 3(2), 77–90. <https://doi.org/10.1002/PLS2.10069>
- Kumar, S., Mukherjee, A., & Dutta, J. (2020). Chitosan based nanocomposite films and coatings: Emerging antimicrobial food packaging alternatives. *Trends in Food Science & Technology*, 97, 196–209. <https://doi.org/10.1016/J.TIFS.2020.01.002>
- Kumari, S., Tiyyagura, H. R., Pottathara, Y. B., Sadasivuni, K. K., Ponnammma, D., Douglas, T. E. L., Skirtach, A. G., & Mohan, M. K. (2021). Surface functionalization of chitosan as a coating material for orthopaedic applications: A comprehensive review. *Carbohydrate Polymers*, 255, 117487. <https://doi.org/10.1016/J.CARBPOL.2020.117487>
- Kumar-Krishnan, S., Prokhorov, E., Hernández-Iturriaga, M., Mota-Morales, J. D., Vázquez-Lepe, M., Kovalenko, Y., Sanchez, I. C., & Luna-Bárcenas, G. (2015). Chitosan/silver nanocomposites: Synergistic antibacterial action of silver nanoparticles and silver ions. *European Polymer Journal*, 67, 242–251.
<https://doi.org/10.1016/J.EURPOLYMJ.2015.03.066>

- Ladhari, S., Vu, N. N., Boisvert, C., Polinarski, M. A., Venne, C., Saidi, A., Barnabe, S., & Nguyen-Tri, P. (2024). Biodegradable polyhydroxybutyrate microfiber membranes decorated with photoactive Ag-TiO₂ nanoparticles for enhanced antibacterial and anti-biofouling activities. *Journal of Applied Polymer Science*, 141(29), e55660. <https://doi.org/10.1002/APP.55660>
- Ladhari, S., Vu, N. N., Boisvert, C., Saidi, A., & Nguyen-Tri, P. (2023). Recent Development of Polyhydroxyalkanoates (PHA)-Based Materials for Antibacterial Applications: A Review. *ACS Applied Bio Materials*, 6(4), 1398–1430. https://doi.org/10.1021/ACSABM.3C00078/ASSET/IMAGES/MEDIUM/MT3C00078_0010.GIF
- Lalegani, Z., & Seyyed Ebrahimi, S. A. (2020). Optimization of synthesis for shape and size controlled silver nanoparticles using response surface methodology. *Colloids and Surfaces A: Physicochemical and Engineering Aspects*, 595, 124647. <https://doi.org/10.1016/J.COLSURFA.2020.124647>
- Lamprou, D. A., Scoutaris, N., Ross, S. A., & Douroumis, D. (2019). Polymeric Coatings and Their Fabrication for Medical Devices. *Encyclopedia of Biomedical Engineering*, 1–3, 177–187. <https://doi.org/10.1016/B978-0-12-801238-3.99869-6>
- Lana, E. J. L., Carazza, F., & Takahashi, J. A. (2006). Antibacterial evaluation of 1,4-benzoquinone derivatives. *Journal of Agricultural and Food Chemistry*, 54(6), 2053–2056. <https://doi.org/10.1021/JF052407Z/ASSET/IMAGES/LARGE/JF052407ZF00001.JPEG>
- Lara, H. H., Ayala-Núñez, N. V., del Turrent, L. C. I., & Padilla, C. R. (2010). Bactericidal effect of silver nanoparticles against multidrug-resistant bacteria. *World Journal of Microbiology and Biotechnology*, 26(4), 615–621. <https://doi.org/10.1007/S11274-009-0211-3/FIGURES/3>
- Le, A. T., Ha, H. A., Al-Ansari, M. M., Elankathirselvan, K., & Al-Humaid, L. A. (2024). Aristolochia bracteolata flower extract based phytosynthesis and characterization of AgNPs: Antimicrobial, antidiabetic, and antioxidant activities potential assessment. *Environmental Research*, 251, 118729. <https://doi.org/10.1016/J.ENVRES.2024.118729>
- Lee, P. C., & Meisel, D. (1982). Adsorption and surface-enhanced Raman of dyes on silver and gold sols. *Journal of Physical Chemistry*, 86(17), 3391–3395. <https://doi.org/10.1021/j100214a025>

- Lee, S. H., & Jun, B. H. (2019). Silver Nanoparticles: Synthesis and Application for Nanomedicine. *International Journal of Molecular Sciences*, 20(4). <https://doi.org/10.3390/IJMS20040865>
- LewisOscar, F., Nithya, C., Vismaya, S., Arunkumar, M., Pugazhendhi, A., Nguyen-Tri, P., Alharbi, S. A., Alharbi, N. S., & Thajuddin, N. (2021). In vitro analysis of green fabricated silver nanoparticles (AgNPs) against *Pseudomonas aeruginosa* PA14 biofilm formation, their application on urinary catheter. *Progress in Organic Coatings*, 151, 106058. <https://doi.org/10.1016/J.PORGCOAT.2020.106058>
- Li, G., He, D., Qian, Y., Guan, B., Gao, S., Cui, Y., Yokoyama, K., & Wang, L. (2012). Fungus-mediated green synthesis of silver nanoparticles using *aspergillus terreus*. *International Journal of Molecular Sciences*, 13(1), 466–476. <https://doi.org/10.3390/ijms13010466>
- Li, J., & Zhuang, S. (2020). Antibacterial activity of chitosan and its derivatives and their interaction mechanism with bacteria: Current state and perspectives. *European Polymer Journal*, 138, 109984. <https://doi.org/10.1016/J.EURPOLYMJ.2020.109984>
- Li, M., Liu, Y., Gong, Y., Yan, X., Wang, L., Zheng, W., Ai, H., & Zhao, Y. (2023). Recent advances in nanoantibiotics against multidrug-resistant bacteria. *Nanoscale Advances*, 5(23), 6278–6317. <https://doi.org/10.1039/D3NA00530E>
- Li, Q., Jiang, S., Jia, W., Wang, F., Wang, Z., Cao, X., Shen, X., & Yao, Z. (2022). Novel silver-modified carboxymethyl chitosan antibacterial membranes using environment-friendly polymers. *Chemosphere*, 136059. <https://doi.org/10.1016/J.CHEMOSPHERE.2022.136059>
- Li, W., Cao, J., Du, Y. lu, Wen, Y. di, Luo, W. xiang, & Liu, X. yan. (2024). Risk factors and prediction model construction for peripherally inserted central catheter-related infections. *Heliyon*, 10(8), e29158. <https://doi.org/10.1016/J.HELİYON.2024.E29158>
- Li, W., Song, J., Wang, C., Hao, J., Yang, Y., & Yu, Z. (2019). Facile synthesis of cubic Ag/Ag₂O composites and its shape-dependent photo-catalytic activity examination. *Journal of Materials Science: Materials in Electronics*, 30(6), 5366–5374. <https://doi.org/10.1007/S10854-019-00829-9/FIGURES/14>
- Li, X. fang, Feng, X. qiang, Yang, S., Fu, G. qing, Wang, T. pu, & Su, Z. xing. (2010). Chitosan kills *Escherichia coli* through damage to be of cell membrane mechanism. *Carbohydrate Polymers*, 79(3), 493–499. <https://doi.org/10.1016/J.CARBPOL.2009.07.011>
- Liang, J., Wang, J., Li, S., Xu, L., Wang, R., Chen, R., & Sun, Y. (2019). The size-controllable preparation of chitosan/silver nanoparticle composite microsphere and its antimicrobial

- performance. *Carbohydrate Polymers*, 220, 22–29. <https://doi.org/10.1016/J.CARBPOL.2019.05.048>
- Liao, C., Li, Y., & Tjong, S. C. (2019). Bactericidal and Cytotoxic Properties of Silver Nanoparticles. *International Journal of Molecular Sciences*, 20(2). <https://doi.org/10.3390/IJMS20020449>
- Liao, Y., Wang, J., Song, X., Zhang, G., & Chen, B. (2021). Low-cost and large mass producible phenolic resin for water disinfection and antibacterial coating under weak visible light LED or sunlight irradiation. *Applied Catalysis B: Environmental*, 292, 120189. <https://doi.org/10.1016/J.APCATB.2021.120189>
- Lima, D. D. S., Gullon, B., Cardelle-Cobas, A., Brito, L. M., Rodrigues, K. A. F., Quelemes, P. V., Ramos-Jesus, J., Arcanjo, D. D. R., Plácido, A., Batziou, K., Quaresma, P., Eaton, P., Delerue-Matos, C., Carvalho, F. A. A., Da Silva, D. A., Pintado, M., & Leite, J. R. D. S. A. (2017). Chitosan-based silver nanoparticles: A study of the antibacterial, antileishmanial and cytotoxic effects. *Journal of Bioactive and Compatible Polymers*, 32(4), 397–410. <https://doi.org/10.1177/0883911516681329>
- Liu, H., Du, Y., Wang, X., & Sun, L. (2004). Chitosan kills bacteria through cell membrane damage. *International Journal of Food Microbiology*, 95(2), 147–155. <https://doi.org/10.1016/J.IJFOODMICRO.2004.01.022>
- Liu, L., Xue, B., Niu, M., Chen, L., Yang, Y., Xu, B., & Zhang, L. (2024). Recent advances in anti-infective catheters for preventing catheters associated urinary tract infections. *Chemical Engineering Journal*, 499, 156333. <https://doi.org/10.1016/J.CEJ.2024.156333>
- Liu, Z., Wang, L., Zhao, X., Luo, Y., Zheng, K., & Wu, M. (2022). Highly effective antibacterial AgNPs@hinokitiol grafted chitosan for construction of durable antibacterial fabrics. *International Journal of Biological Macromolecules*, 209, 963–971. <https://doi.org/10.1016/J.IJBIOMAC.2022.04.103>
- Logambal, S., Thilagavathi, T., Chandrasekar, M., Inmozhi, C., Belle Ebanda Kedi, P., Bassyouni, F. A., Uthrakumar, R., Muthukumaran, A., Naveenkumar, S., & Kaviyarasu, K. (2023). Synthesis and antimicrobial activity of silver nanoparticles: Incorporated couroupita guianensis flower petal extract for biomedical applications. *Journal of King Saud University - Science*, 35(1), 102455. <https://doi.org/10.1016/J.JKSUS.2022.102455>
- Lok, C. N., Ho, C. M., Chen, R., He, Q. Y., Yu, W. Y., Sun, H., Tam, P. K. H., Chiu, J. F., & Che, C. M. (2007). Silver nanoparticles: Partial oxidation and antibacterial activities. *Journal of Biological Inorganic Chemistry*, 12(4), 527–534. <https://doi.org/10.1007/S00775-007-0208-Z/TABLES/1>

- Lopez-Carrizales, M., Mendoza-Mendoza, E., Peralta-Rodriguez, R. D., Pérez-Díaz, M. A., Portales-Pérez, D., Magaña-Aquino, M., Aragón-Piña, A., Infante-Martínez, R., Barriga-Castro, E. D., Sánchez-Sánchez, R., Martínez-Castañón, G. A., & Martínez-Gutiérrez, F. (2020). Characterization, antibiofilm and biocompatibility properties of chitosan hydrogels loaded with silver nanoparticles and ampicillin: an alternative protection to central venous catheters. *Colloids and Surfaces B: Biointerfaces*, 196, 111292. <https://doi.org/10.1016/J.COLSURFB.2020.111292>
- Low, J. Le, Kao, P. H. N., Tambyah, P. A., Koh, G. L. E., Ling, H., Kline, K. A., Cheow, W. S., & Leong, S. S. J. (2021). Development of a polymer-based antimicrobial coating for efficacious urinary catheter protection. *Biotechnology Notes*, 2, 1–10. <https://doi.org/10.1016/J.BIOTNO.2020.12.001>
- Luna-Hernández, E., Cruz-Soto, M. E., Padilla-Vaca, F., Mauricio-Sánchez, R. A., Ramirez-Wong, D., Muñoz, R., Granados-López, L., Ovalle-Flores, L. R., Menchaca-Arredondo, J. L., Hernández-Rangel, A., Prokhorov, E., García-Rivas, J. L., España-Sánchez, B. L., & Luna-Bárcenas, G. (2017). Combined antibacterial/tissue regeneration response in thermal burns promoted by functional chitosan/silver nanocomposites. *International Journal of Biological Macromolecules*, 105, 1241–1249. <https://doi.org/10.1016/j.ijbiomac.2017.07.159>
- Lupatini, K. N., Schaffer, J. V., Machado, B., Silva, E. S., Ellendersen, L. S. N., Muniz, G. I. B., Ferracin, R. J., Helton, , & Alves, J. (2018). Development of Chitosan Membranes as a Potential PEMFC Electrolyte. *Journal of Polymers and the Environment*, 26, 2964–2972. <https://doi.org/10.1007/s10924-017-1146-7>
- Ma, K., Zhe, T., Li, F., Zhang, Y., Yu, M., Li, R., & Wang, L. (2022). Sustainable films containing AIE-active berberine-based nanoparticles: A promising antibacterial food packaging. *Food Hydrocolloids*, 123, 107147. <https://doi.org/10.1016/J.FOODHYD.2021.107147>
- Ma, S., Moser, D., Han, F., Leonhard, M., Schneider-Stickler, B., & Tan, Y. (2020). Preparation and antibiofilm studies of curcumin loaded chitosan nanoparticles against polymicrobial biofilms of *Candida albicans* and *Staphylococcus aureus*. *Carbohydrate Polymers*, 241, 116254. <https://doi.org/10.1016/j.carbpol.2020.116254>
- Madureira, A. R., Pereira, A., Castro, P. M., & Pintado, M. (2015). Production of antimicrobial chitosan nanoparticles against food pathogens. *Journal of Food Engineering*, 167, 210–216. <https://doi.org/10.1016/j.jfoodeng.2015.06.010>

- Magdziak, D., Rodriguez, A. A., Van De Water, R. W., & Pettus, T. R. R. (2002). Regioselective oxidation of phenols to o-quinones with o-iodoxybenzoic acid (IBX). *Organic Letters*, 4(2), 285–288. https://doi.org/10.1021/OL017068J/SUPPL_FILE/OL017068J_S1.PDF
- Malik, M., Aamir Iqbal, M., Iqbal, Y., Malik, M., Bakhsh, S., Irfan, S., Ahmad, R., & Pham, P. v. (2022). Biosynthesis of silver nanoparticles for biomedical applications: A mini review. *Inorganic Chemistry Communications*, 145, 109980. <https://doi.org/10.1016/J.INOCHE.2022.109980>
- Mansouri, S. S., & Ghader, S. (2009). Experimental study on effect of different parameters on size and shape of triangular silver nanoparticles prepared by a simple and rapid method in aqueous solution. *Arabian Journal of Chemistry*, 2(1), 47–53. <https://doi.org/10.1016/J.ARABJC.2009.07.004>
- Manukumar, H. M., Umesha, S., & Kumar, H. N. N. (2017). Promising biocidal activity of thymol loaded chitosan silver nanoparticles (T-C@AgNPs) as anti-infective agents against perilous pathogens. *International Journal of Biological Macromolecules*, 102, 1257–1265. <https://doi.org/10.1016/J.IJBIOMAC.2017.05.030>
- Markowska, K., Grudniak, A. M., & Wolska, K. I. (2013). Silver nanoparticles as an alternative strategy against bacterial biofilms. *Acta Biochimica Polonica*, 60(4), 523–530.
- Marta, B., Potara, M., Iliut, M., Jakab, E., Radu, T., Imre-Lucaci, F., Katona, G., Popescu, O., & Astilean, S. (2015). Designing chitosan-silver nanoparticles-graphene oxide nanohybrids with enhanced antibacterial activity against *Staphylococcus aureus*. *Colloids and Surfaces A: Physicochemical and Engineering Aspects*, 487, 113–120. <https://doi.org/10.1016/j.colsurfa.2015.09.046>
- Maruthupandy, M., Rajivgandhi, G., Muneeswaran, T., Vennila, T., Quero, F., & Song, J. M. (2019). Chitosan/silver nanocomposites for colorimetric detection of glucose molecules. *International Journal of Biological Macromolecules*, 121, 822–828. <https://doi.org/10.1016/J.IJBIOMAC.2018.10.063>
- Mathur, P., Jha, S., Ramteke, S., & Jain, N. K. (2018). Pharmaceutical aspects of silver nanoparticles. *Artificial Cells, Nanomedicine, and Biotechnology*, 46(sup1), 115–126. <https://doi.org/10.1080/21691401.2017.1414825>
- Matica, M. A., Aachmann, F. L., Tøndervik, A., Sletta, H., & Ostafe, V. (2019). Chitosan as a Wound Dressing Starting Material: Antimicrobial Properties and Mode of Action. *International Journal of Molecular Sciences*, 20(23). <https://doi.org/10.3390/IJMS20235889>

- Mehata, M. S. (2021). Green route synthesis of silver nanoparticles using plants/ginger extracts with enhanced surface plasmon resonance and degradation of textile dye. *Materials Science and Engineering: B*, 273, 115418. <https://doi.org/10.1016/J.MSEB.2021.115418>
- Meher, A., Tandi, A., Moharana, S., Chakroborty, S., Mohapatra, S. S., Mondal, A., Dey, S., & Chandra, P. (2024). Silver nanoparticle for biomedical applications: A review. *Hybrid Advances*, 6, 100184. <https://doi.org/10.1016/J.HYBADV.2024.100184>
- Melariri, H., Freercks, R., van der Merwe, E., Ham-Baloyi, W. Ten, Oyedele, O., Murphy, R. A., Claasen, C., Etusim, P. E., Achebe, M. O., Offiah, S., & Melariri, P. E. (2024). The burden of hospital-acquired infections (HAI) in sub-Saharan Africa: a systematic review and meta-analysis. *EClinicalMedicine*, 71, 102571. <https://doi.org/10.1016/J.ECLINM.2024.102571>
- Meng, Q., Zhong, S., Wang, J., Gao, Y., & Cui, X. (2023). Advances in chitosan-based microcapsules and their applications. *Carbohydrate Polymers*, 300, 120265. <https://doi.org/10.1016/J.CARBPOL.2022.120265>
- Métraux, G. S., & Mirkin, C. A. (2005). Rapid thermal synthesis of silver nanoprisms with chemically tailorable thickness. *Advanced Materials*, 17(4), 412–415. <https://doi.org/10.1002/adma.200401086>
- Milić, M., Leitinger, G., Pavičić, I., Zebić Avdičević, M., Dobrović, S., Goessler, W., & Vinković Vrček, I. (2015). Cellular uptake and toxicity effects of silver nanoparticles in mammalian kidney cells. *Journal of Applied Toxicology*, 35(6), 581–592. <https://doi.org/10.1002/JAT.3081>
- Mirajkar, S., Rathod, P., Pawar, B., Penna, S., & Dalvi, S. (2021). γ -Irradiated Chitosan Mediates Enhanced Synthesis and Antimicrobial Properties of Chitosan–Silver (Ag) Nanocomposites. *ACS Omega*, 6(50), 34812–34822. https://doi.org/10.1021/ACSOMEGA.1C05358/SUPPL_FILE/AO1C05358_SI_001.PDF
- Mishra, S. K., Ferreira, J. M. F., & Kannan, S. (2015). Mechanically stable antimicrobial chitosan–PVA–silver nanocomposite coatings deposited on titanium implants. *Carbohydrate Polymers*, 121, 37–48. <https://doi.org/10.1016/J.CARBPOL.2014.12.027>
- Młynarczyk-Bonikowska, B., Majewska, A., Malejczyk, M., Młynarczyk, G., & Majewski, S. (2020). Multiresistant *Neisseria gonorrhoeae*: a new threat in second decade of the XXI century. *Medical Microbiology and Immunology*, 209(2), 95–108. <https://doi.org/10.1007/S00430-019-00651-4/TABLES/5>
- Mohamed, N., & Madian, N. G. (2020). Evaluation of the mechanical, physical and antimicrobial properties of chitosan thin films doped with greenly synthesized silver

- nanoparticles. *Materials Today Communications*, 25, 101372. <https://doi.org/10.1016/J.MTCOMM.2020.101372>
- Mohammed, A. M., Hassan, K. T., & Hassan, O. M. (2023). Assessment of antimicrobial activity of chitosan/silver nanoparticles hydrogel and cryogel microspheres. *International Journal of Biological Macromolecules*, 233, 123580. <https://doi.org/10.1016/J.IJBIOMAC.2023.123580>
- Mohandas, A., Deepthi, S., Biswas, R., & Jayakumar, R. (2018). Chitosan based metallic nanocomposite scaffolds as antimicrobial wound dressings. *Bioactive Materials*, 3(3), 267–277. <https://doi.org/10.1016/j.bioactmat.2017.11.003>
- Mulla, S., Kumar, A., Rajdev, S., Mulla, S., Kumar, A., & Rajdev, S. (2016). Comparison of MIC with MBEC Assay for in Vitro Antimicrobial Susceptibility Testing in Biofilm Forming Clinical Bacterial Isolates. *Advances in Microbiology*, 6(2), 73–78. <https://doi.org/10.4236/AIM.2016.62007>
- Müller, R. H., Jacobs, C., & Kayser, O. (2001). Nanosuspensions as particulate drug formulations in therapy: Rationale for development and what we can expect for the future. *Advanced Drug Delivery Reviews*, 47(1), 3–19. [https://doi.org/10.1016/S0169-409X\(00\)00118-6](https://doi.org/10.1016/S0169-409X(00)00118-6)
- Munita, J. M., & Arias, C. A. (2016). Mechanisms of Antibiotic Resistance. *Virulence Mechanisms of Bacterial Pathogens*, 481–511. <https://doi.org/10.1128/9781555819286.CH17>
- Murray, C. J., Ikuta, K. S., Sharara, F., Swetschinski, L., Robles Aguilar, G., Gray, A., Han, C., Bisignano, C., Rao, P., Wool, E., Johnson, S. C., Browne, A. J., Chipeta, M. G., Fell, F., Hackett, S., Haines-Woodhouse, G., Kashef Hamadani, B. H., Kumaran, E. A. P., McManigal, B., ... Naghavi, M. (2022). Global burden of bacterial antimicrobial resistance in 2019: a systematic analysis. *The Lancet*, 399(10325), 629–655. [https://doi.org/10.1016/S0140-6736\(21\)02724-0](https://doi.org/10.1016/S0140-6736(21)02724-0)
- Mutlu, N., Liverani, L., Kurtuldu, F., Galusek, D., & Boccaccini, A. R. (2022). Zinc improves antibacterial, anti-inflammatory and cell motility activity of chitosan for wound healing applications. *International Journal of Biological Macromolecules*, 213, 845–857. <https://doi.org/10.1016/J.IJBIOMAC.2022.05.199>
- Nadagouda, M. N., & Varma, R. S. (2008). Green synthesis of silver and palladium nanoparticles at room temperature using coffee and tea extract. *Green Chemistry*, 10(8), 859–886. <https://doi.org/10.1039/b804703k>

- Nagaraj, K., Thangamuniyandi, P., Kamalesu, S., Dixitkumar, M., Kumar Saini, A., Sharma, S., Naman, J., Priyanshi, J., Uthra, C., Lokhandwala, S., Parekh, N. M., Radha, S., Sakthinathan, S., Chiu, T.-W., & Karuppiyah, C. (2023). Silver nanoparticles using Cassia Alata and its catalytic reduction activities of Rhodamine6G, Methyl orange and methylene blue dyes. *Inorganic Chemistry Communications*, 155, 110985. <https://doi.org/10.1016/J.INOCHE.2023.110985>
- Nagarajan, K., Thamarai, R., Kamaraj, C., Al-Ghanim, K. A., Subramaniam, K., & Malafaia, G. (2024). Green synthesis and evaluation of dual herb-extracted DHM-AgNPs: Antimicrobial efficacy and low ecotoxicity in agricultural and aquatic systems. *Journal of Environmental Management*, 370, 122849. <https://doi.org/10.1016/J.JENVMAN.2024.122849>
- Nasaj, M., Chehelgerdi, M., Asghari, B., Ahmadieh-Yazdi, A., Asgari, M., Kabiri-Samani, S., Sharifi, E., & Arabestani, M. (2024). Factors influencing the antimicrobial mechanism of chitosan action and its derivatives: A review. *International Journal of Biological Macromolecules*, 277, 134321. <https://doi.org/10.1016/J.IJBIOMAC.2024.134321>
- Nate, Z., Moloto, M. J., Mubiayi, P. K., & Sibiya, P. N. (2018). Green synthesis of chitosan capped silver nanoparticles and their antimicrobial activity. *MRS Advances*, 3(42–43), 2505–2517. <https://doi.org/10.1557/ADV.2018.368/METRICS>
- Neethu, S., Midhun, S. J., Radhakrishnan, E. K., & Jyothis, M. (2020). Surface functionalization of central venous catheter with mycofabricated silver nanoparticles and its antibiofilm activity on multidrug resistant *Acinetobacter baumannii*. *Microbial Pathogenesis*, 138, 103832. <https://doi.org/10.1016/j.micpath.2019.103832>
- Neethu, S., Midhun, S. J., Sunil, M. A., Soumya, S., Radhakrishnan, E. K., & Jyothis, M. (2018). Efficient visible light induced synthesis of silver nanoparticles by *Penicillium polonicum* ARA 10 isolated from *Chetomorpha antennina* and its antibacterial efficacy against *Salmonella enterica* serovar Typhimurium. *Journal of Photochemistry and Photobiology B: Biology*, 180, 175–185. <https://doi.org/10.1016/j.jphotobiol.2018.02.005>
- Neoh, K. G., Li, M., Kang, E. T., Chiong, E., & Tambyah, P. A. (2017). Surface modification strategies for combating catheter-related complications: recent advances and challenges. *Journal of Materials Chemistry B*, 5(11), 2045–2067. <https://doi.org/10.1039/C6TB03280J>
- Nguyen-Tri, P., Tran, H. N., Plamondon, C. O., Tuduri, L., Vo, D. V. N., Nanda, S., Mishra, A., Chao, H. P., & Bajpai, A. K. (2019). Recent progress in the preparation, properties and

- applications of superhydrophobic nano-based coatings and surfaces: A review. *Progress in Organic Coatings*, 132, 235–256. <https://doi.org/10.1016/J.PORGCAT.2019.03.042>
- Nie, P., Zhao, Y., & Xu, H. (2023). Synthesis, applications, toxicity and toxicity mechanisms of silver nanoparticles: A review. *Ecotoxicology and Environmental Safety*, 253, 114636. <https://doi.org/10.1016/J.ECOENV.2023.114636>
- Niu, X., Wei, Y., Liu, Q., Yang, B., Ma, N., Li, Z., Zhao, L., Chen, W., & Huang, D. (2020). Silver-loaded microspheres reinforced chitosan scaffolds for skin tissue engineering. *European Polymer Journal*, 134, 109861. <https://doi.org/10.1016/J.EURPOLYMJ.2020.109861>
- Nurani, S. J., Saha, C. K., Khan, Md. A. R., & Sunny, S. M. H. (2015). Silver nanoparticles synthesis, properties, applications and future perspectives: a short review. *IOSR Journal of Electrical and Electronics Engineering*, 10(6), 117–126. <https://doi.org/10.9790/1676-1061117126>
- Nwabike Amitaye, A., Elemike, E. E., Akpeji, H. B., Amitaye, E., Hossain, I., Mbonu, J. I., & Aziza, A. E. (2024). Chitosan: A sustainable biobased material for diverse applications. *Journal of Environmental Chemical Engineering*, 12(4), 113208. <https://doi.org/10.1016/J.JECE.2024.113208>
- Obaid, Z. H., Juda, S. A., Kaizal, A. F., & Mohammed Salman, J. (2024). Biosynthesis of silver nano particles (AgNPs) from blue green algae (*Arthrospira platensis*) and their anti-pathogenic applications. *Journal of King Saud University - Science*, 36(7), 103264. <https://doi.org/10.1016/J.JKSUS.2024.103264>
- O'Callaghan, K. A. M., & Kerry, J. P. (2016). Preparation of low- and medium-molecular weight chitosan nanoparticles and their antimicrobial evaluation against a panel of microorganisms, Including cheese-derived cultures. *Food Control*, 69, 256–261. <https://doi.org/10.1016/j.foodcont.2016.05.005>
- Ogunsona, E. O., Muthuraj, R., Ojogbo, E., Valerio, O., & Mekonnen, T. H. (2020). Engineered nanomaterials for antimicrobial applications: A review. *Applied Materials Today*, 18, 100473. <https://doi.org/10.1016/J.APMT.2019.100473>
- Oryan, A., Alemzadeh, E., Tashkhourian, J., & Nami Ana, S. F. (2018). Topical delivery of chitosan-capped silver nanoparticles speeds up healing in burn wounds: A preclinical study. *Carbohydrate Polymers*, 200, 82–92. <https://doi.org/10.1016/J.CARBPOL.2018.07.077>

- Öztürk, K., Kaplan, M., & Çalış, S. (2024). Effects of nanoparticle size, shape, and zeta potential on drug delivery. *International Journal of Pharmaceutics*, 666, 124799. <https://doi.org/10.1016/J.IJPHARM.2024.124799>
- Paharik, A. E., & Horswill, A. R. (2016). The Staphylococcal Biofilm: Adhesins, Regulation, and Host Response. *Virulence Mechanisms of Bacterial Pathogens*, 529–566. <https://doi.org/10.1128/9781555819286.CH19>
- Pal, S., Tak, Y. K., & Song, J. M. (2007). Does the antibacterial activity of silver nanoparticles depend on the shape of the nanoparticle? A study of the gram-negative bacterium *Escherichia coli*. *Applied and Environmental Microbiology*, 73(6), 1712–1720. <https://doi.org/10.1128/AEM.02218-06/ASSET/6C9C03C4-A4A8-46FD-9451-902F4F8671C3/ASSETS/GRAPHIC/ZAM00607759000008.JPEG>
- Pan, A. D., Zeng, H. Y., Foua, G. B., Alain, C., & Li, Y. Q. (2016). Enzymolysis of chitosan by papain and its kinetics. *Carbohydrate Polymers*, 135, 199–206. <https://doi.org/10.1016/j.carbpol.2015.08.052>
- Panda, P. K., Yang, J. M., & Chang, Y. H. (2021). Preparation and characterization of ferulic acid-modified water soluble chitosan and poly (γ -glutamic acid) polyelectrolyte films through layer-by-layer assembly towards protein adsorption. *International Journal of Biological Macromolecules*, 171, 457–464. <https://doi.org/10.1016/J.IJBIOMAC.2020.12.226>
- Pandit, A., Deshpande, C., Patil, S., Jain, R., & Dandekar, P. (2020). Mechanistic insights into controlled depolymerization of Chitosan using H-Mordenite. *Carbohydrate Polymers*, 230, 115600. <https://doi.org/10.1016/j.carbpol.2019.115600>
- Patil, P., Chavanke, D., & Wagh, M. (2012). A review on ionotropic gelation method: novel approach for controlled gastroretentive gelispheres. *International Journal of Pharmacy and Pharmaceutical Sciences*, 4, 27–32.
- Paulkumar, K., Gnanajobitha, G., Vanaja, M., Pavunraj, M., & Annadurai, G. (2017). Green synthesis of silver nanoparticle and silver based chitosan bionanocomposite using stem extract of *Saccharum officinarum* and assessment of its antibacterial activity. *Advances in Natural Sciences: Nanoscience and Nanotechnology*, 8(3), 9. <https://doi.org/10.1088/2043-6254/aa7232>
- Perepelkin, E. I., Sinolits, M. A., Badun, G. A., Chernysheva, M. G., Anuchina, N. M., Abramchuk, S. S., Levin, E. E., Bakuleva, N. P., Popov, D. A., & Chaschin, I. S. (2023). Composite chitosan-based nanoparticles as a basis for innovative antimicrobial coating for bioprosthesis: Preparation and application using carbonic acid as a “green” self-

- neutralizing solvent. *European Polymer Journal*, 193, 112104. <https://doi.org/10.1016/J.EURPOLYMJ.2023.112104>
- Peter, A., Sadanandan, S., Bindiya, E. S., Mohan, N., Bhat, S. G., & Abhitha, K. (2023). Biofilm inhibition on natural rubber by hydrophilic modification using carboxymethyl chitosan stabilised high energy faceted silver nanoparticles. *Carbohydrate Polymer Technologies and Applications*, 6, 100357. <https://doi.org/10.1016/J.CARPTA.2023.100357>
- Peters, B. M., & Noverra, M. C. (2013). *Candida albicans*-*Staphylococcus aureus* polymicrobial peritonitis modulates host innate immunity. *Infection and Immunity*, 81(6), 2178–2189. <https://doi.org/10.1128/IAI.00265-13>
- Pham, T. D. M., Ziora, Z. M., & Blaskovich, M. A. T. (2019). Quinolone antibiotics. *MedChemComm*, 10(10), 1719–1739. <https://doi.org/10.1039/C9MD00120D>
- Pishbin, F., Mouriño, V., Gilchrist, J. B., McComb, D. W., Kreppel, S., Salih, V., Ryan, M. P., & Boccaccini, A. R. (2013). Single-step electrochemical deposition of antimicrobial orthopaedic coatings based on a bioactive glass/chitosan/nano-silver composite system. *Acta Biomaterialia*, 9(7), 7469–7479. <https://doi.org/10.1016/J.ACTBIO.2013.03.006>
- Polinarski, M. A., B Beal, A. L., B Silva, F. E., Bernardi-Wenzel, J., M Burin, G. R., B de Muniz, G. I., Alves M A Polinarski, H. J., B Beal, A. L., B Silva, F. E., M Burin, G. R., Alves, H. J., Bernardi-Wenzel, J., & B de Muniz, G. I. (2021). New Perspectives of Using Chitosan, Silver, and Chitosan–Silver Nanoparticles against Multidrug-Resistant Bacteria. *Particle & Particle Systems Characterization*, 38(4), 2100009. <https://doi.org/10.1002/PPSC.202100009>
- Polinarski, M. A., Vu, N. N., Ladhari, S., Boisvert, C., Barnabé, S., Wenzel, J. B., Alves, H. J., & Nguyen-Tri, P. (2024). In-situ growth of Ag nanoparticles embedded in chitosan coating for potent antimicrobial activity. *Materials Today Communications*, 40, 109987. <https://doi.org/10.1016/J.MTCOMM.2024.109987>
- Puplampu, P., Opoku-Asare, B., Ganu, V. J., Asafu-Adjaye, O., Asare, A. A., Kyeremateng, I., Opoku-Asare, A., Boima, V., & Sampene-Donkor, E. (2024). Microbial organisms and antibiotic sensitivity patterns in patients with catheter-related bloodstream infections at a tertiary hospital. *Clinical Infection in Practice*, 23, 100365. <https://doi.org/10.1016/J.CLINPR.2024.100365>
- Qi, L., Xu, Z., Jiang, X., Hu, C., & Zou, X. (2004). Preparation and antibacterial activity of chitosan nanoparticles. *Carbohydrate Research*, 339(16), 2693–2700. <https://doi.org/10.1016/j.carres.2004.09.007>

- Qi, Z., Xue, X., Zhou, H., Yuan, H., Li, W., Yang, G., Xie, P., & Wang, C. (2022). The aqueous assembly preparation of OPs-AgNPs with phenols from olive mill wastewater and its mechanism on antimicrobial function study. *Food Chemistry*, 376, 131924. <https://doi.org/10.1016/J.FOODCHEM.2021.131924>
- Quinlivan, E. P., McPartlin, J., Weir, D. G., & Scott, J. (2000). Mechanism of the antimicrobial drug trimethoprim revisited. *The FASEB Journal*, 14(15), 2519–2524. <https://doi.org/10.1096/FJ.99-1037COM>
- Raafat, D., von Barga, K., Haas, A., & Sahl, H. G. (2008). Insights into the mode of action of chitosan as an antibacterial compound. *Applied and Environmental Microbiology*, 74(12), 3764–3773. <https://doi.org/10.1128/AEM.00453-08>
- Rabin, N., Zheng, Y., Opoku-Temeng, C., Du, Y., Bonsu, E., & Sintim, H. O. (2015). Biofilm Formation Mechanisms and Targets for Developing Antibiofilm Agents. *Future Medicinal Chemistry*, 7(4), 493–512. <https://doi.org/10.4155/FMC.15.6>
- Rahman, A., Chowdhury, M. A., & Hossain, N. (2022). Green synthesis of hybrid nanoparticles for biomedical applications: A review. *Applied Surface Science Advances*, 11, 100296. <https://doi.org/10.1016/J.APSADV.2022.100296>
- Rajivgandhi, G., Maruthupandy, M., Veeramani, T., Quero, F., & Li, W. J. (2019). Anti-ESBL investigation of chitosan/silver nanocomposites against carbapenem resistant *Pseudomonas aeruginosa*. *International Journal of Biological Macromolecules*, 132, 1221–1234. <https://doi.org/10.1016/J.IJBIOMAC.2019.03.238>
- Rani, R., Sharma, D., Chaturvedi, M., Yadav, J. P., & Yadav, J. P. (2017). Green synthesis, characterization and antibacterial activity of silver nanoparticles of endophytic fungi *Aspergillus terreus*. *Journal of Nanomedicine and Nanotechnology*, 8(4), 457. <https://doi.org/10.4172/2157-7439.1000457>
- Reddy, P. N., Reddy, M. H. P., Pierson, J. F., & Uthanna, S. (2014). Characterization of Silver Oxide Films Formed by Reactive RF Sputtering at Different Substrate Temperatures. *ISRN Optics*, 2014, 1–7. <https://doi.org/10.1155/2014/684317>
- Reicha, F. M., Sarhan, A., Abdel-Hamid, M. I., & El-Sherbiny, I. M. (2012). Preparation of silver nanoparticles in the presence of chitosan by electrochemical method. *Carbohydrate Polymers*, 89(1), 236–244. <https://doi.org/10.1016/j.carbpol.2012.03.002>
- Rodríguez-Argüelles, M. C., Sieiro, C., Cao, R., & Nasi, L. (2011). Chitosan and silver nanoparticles as pudding with raisins with antimicrobial properties. *Journal of Colloid and Interface Science*, 364(1), 80–84. <https://doi.org/10.1016/J.JCIS.2011.08.006>

- Rogala-Wielgus, D., Majkowska-Marzec, B., & Zieliński, A. (2024). Characteristics of silver-doped carbon nanotube coating destined for medical applications. *Materials Today Communications*, 38, 107712. <https://doi.org/10.1016/J.MTCOMM.2023.107712>
- Rojas-Andrade, M., Cho, A. T., Hu, P., Lee, S. J., Deming, C. P., Sweeney, S. W., Saltikov, C., & Chen, S. (2015). Enhanced antimicrobial activity with faceted silver nanostructures. *Journal of Materials Science*, 50(7), 2849–2858. <https://doi.org/10.1007/S10853-015-8847-X/FIGURES/5>
- Römling, U., Kjelleberg, S., Normark, S., Nyman, L., Uhlin, B. E., & Åkerlund, B. (2014). Microbial biofilm formation: a need to act. *Journal of Internal Medicine*, 276(2), 98–110. <https://doi.org/10.1111/JOIM.12242>
- Rubini, D., Vedha Hari, B. N., & Nithyanand, P. (2021). Chitosan coated catheters alleviates mixed species biofilms of *Staphylococcus epidermidis* and *Candida albicans*. *Carbohydrate Polymers*, 252, 117192. <https://doi.org/10.1016/J.CARBPOL.2020.117192>
- Rugaie, O. Al, Abdellatif, A. A. H., El-Mokhtar, M. A., Sabet, M. A., Abdelfattah, A., Alsharidah, M., Aldubaib, M., Barakat, H., Abudoleh, S. M., Al-Regaiey, K. A., & Tawfeek, H. M. (2022). Retardation of Bacterial Biofilm Formation by Coating Urinary Catheters with Metal Nanoparticle-Stabilized Polymers. *Microorganisms*, 10(7), 1297. <https://doi.org/10.3390/MICROORGANISMS10071297>
- Saha, S., Malik, M. M., & Qureshi, M. S. (2019). Study of synergistic effects of antibiotics and triangular shaped silver nanoparticles, synthesized using UV-light irradiation, on *S. Aureus* and *P. Aeruginosa*. *Materials Today: Proceedings*, 18, 920–927. <https://doi.org/10.1016/j.matpr.2019.06.525>
- Sahariah, P., & Másson, M. (2017). Antimicrobial Chitosan and Chitosan Derivatives: A Review of the Structure-Activity Relationship. *Biomacromolecules*, 18(11), 3846–3868. https://doi.org/10.1021/ACS.BIOMAC.7B01058/SUPPL_FILE/BM7B01058_SI_001.PDF
- Saidin, S., Chevallier, P., Abdul Kadir, M. R., Hermawan, H., & Mantovani, D. (2013). Polydopamine as an intermediate layer for silver and hydroxyapatite immobilisation on metallic biomaterials surface. *Materials Science and Engineering: C*, 33(8), 4715–4724. <https://doi.org/10.1016/J.MSEC.2013.07.026>
- Salimiyan rizi, K. (2022). MXene nanosheets as a novel nanomaterial with antimicrobial applications: A literature review. *Journal of Molecular Structure*, 1262, 132958. <https://doi.org/10.1016/J.MOLSTRUC.2022.132958>

- Salomoni, R., Léo, P., Montemor, A. F., Rinaldi, B. G., & Rodrigues, M. F. A. (2017). Antibacterial effect of silver nanoparticles in *Pseudomonas aeruginosa*. *Nanotechnology, Science and Applications*, 10, 115–121. <https://doi.org/10.2147/NSA.S133415>
- Sámano-Valencia, C., Martinez-Castanon, G. A., Martínez-Martínez, R. E., Loyola-Rodríguez, J. P., Reyes-Macías, J. F., Ortega-Zarzosa, G., & Niño-Martínez, N. (2013). Bactericide efficiency of a combination of chitosan gel with silver nanoparticles. *Materials Letters*, 106, 413–416. <https://doi.org/10.1016/J.MATLET.2013.05.075>
- Samanta, S., Banerjee, J., Das, B., Mandal, J., Chatterjee, S., Ali, K. M., Sinha, S., Giri, B., Ghosh, T., & Dash, S. K. (2022). Antibacterial potency of cytocompatible chitosan-decorated biogenic silver nanoparticles and molecular insights towards cell-particle interaction. *International Journal of Biological Macromolecules*, 219, 919–939. <https://doi.org/10.1016/J.IJBIOMAC.2022.08.050>
- Sangnak, P., Seananud, P., Daniel, P., Ruamcharoen, P., & Phetphaisit, C. W. (2021). Antimicrobial film from PLA/NR-grafted-modified chitosan-chelated-silver ions blend. *Reactive and Functional Polymers*, 169, 105073. <https://doi.org/10.1016/J.REACTFUNCTPOLYM.2021.105073>
- Sasidharan, D., Namitha, T. R., Johnson, S. P., Jose, V., & Mathew, P. (2020). Synthesis of silver and copper oxide nanoparticles using *Myristica fragrans* fruit extract: Antimicrobial and catalytic applications. *Sustainable Chemistry and Pharmacy*, 16, 100255. <https://doi.org/10.1016/j.scp.2020.100255>
- Schwarz, S., Kehrenberg, C., Doublet, B., & Cloeckaert, A. (2004). Molecular basis of bacterial resistance to chloramphenicol and florfenicol. *FEMS Microbiology Reviews*, 28(5), 519–542. <https://doi.org/10.1016/J.FEMSRE.2004.04.001>
- Seidi, F., Khodadadi Yazdi, M., Jouyandeh, M., Dominic, M., Naeim, H., Nezhad, M. N., Bagheri, B., Habibzadeh, S., Zarrintaj, P., Saeb, M. R., & Mozafari, M. (2021). Chitosan-based blends for biomedical applications. *International Journal of Biological Macromolecules*, 183, 1818–1850. <https://doi.org/10.1016/J.IJBIOMAC.2021.05.003>
- Senthilkumar, P., Yaswant, G., Kavitha, S., Chandramohan, E., Kowsalya, G., Vijay, R., Sudhagar, B., & Kumar, D. S. R. S. (2019). Preparation and characterization of hybrid chitosan-silver nanoparticles (Chi-Ag NPs); A potential antibacterial agent. *International Journal of Biological Macromolecules*, 141, 290–298. <https://doi.org/10.1016/J.IJBIOMAC.2019.08.234>
- Severino, R., Ferrari, G., Vu, K. D., Donsì, F., Salmieri, S., & Lacroix, M. (2015). Antimicrobial effects of modified chitosan based coating containing nanoemulsion of

- essential oils, modified atmosphere packaging and gamma irradiation against *Escherichia coli* O157:H7 and *Salmonella* Typhimurium on green beans. *Food Control*, 50, 215–222. <https://doi.org/10.1016/J.FOODCONT.2014.08.029>
- Shah, A., Yameen, M. A., Fatima, N., & Murtaza, G. (2019). Chemical synthesis of chitosan/silver nanocomposites films loaded with moxifloxacin: Their characterization and potential antibacterial activity. *International Journal of Pharmaceutics*, 561, 19–34. <https://doi.org/10.1016/J.IJPHARM.2019.02.029>
- Shahid-ul-Islam, Butola, B. S., & Verma, D. (2019). Facile synthesis of chitosan-silver nanoparticles onto linen for antibacterial activity and free-radical scavenging textiles. *International Journal of Biological Macromolecules*, 133, 1134–1141. <https://doi.org/10.1016/j.ijbiomac.2019.04.186>
- Shameli, K., Ahmad, M. B., Jazayeri, S. D., Shabanzadeh, P., Sangpour, P., Jahangirian, H., & Gharayebi, Y. (2012). Investigation of antibacterial properties silver nanoparticles prepared via green method. *Chemistry Central Journal*, 6(1), 73. <https://doi.org/10.1186/1752-153X-6-73>
- Shao, J., Wang, B., Li, J., Jansen, J. A., Walboomers, X. F., & Yang, F. (2019). Antibacterial effect and wound healing ability of silver nanoparticles incorporation into chitosan-based nanofibrous membranes. *Materials Science and Engineering C*, 98, 1053–1063. <https://doi.org/10.1016/j.msec.2019.01.073>
- Shao, J., Yu, N., Kolwijck, E., Wang, B., Tan, K. W., Jansen, J. A., Walboomers, X. F., & Yang, F. (2017). Biological evaluation of silver nanoparticles incorporated into chitosan-based membranes. *Nanomedicine*, 12(22), 2771–2785. <https://doi.org/10.2217/nnm-2017-0172>
- Sharma, V. K., Yngard, R. A., & Lin, Y. (2009). Silver nanoparticles: green synthesis and their antimicrobial activities. *Advances in Colloid and Interface Science*, 145(1–2), 83–96. <https://doi.org/10.1016/j.cis.2008.09.002>
- Sheng, Z., Guo, A., Wang, J., & Chen, X. (2022). Preparation, physicochemical properties and antimicrobial activity of chitosan from fly pupae. *Heliyon*, 8(10), e11168. <https://doi.org/10.1016/J.HELİYON.2022.E11168>
- Silva, F. B., Gasparini, L. J., Cremonez, P. A., Burin, G. R. M., Machado, B., Polinarski, M. A., Arantes, M. K., & Alves, H. J. (2021). Chitosan preparations with improved fat-binding capacity. *Journal of Applied Polymer Science*, 138(34), 50841. <https://doi.org/10.1002/APP.50841>

- Silva, N. C., Silva, S., Sarmiento, B., & Pintado, M. (2015). Chitosan nanoparticles for daptomycin delivery in ocular treatment of bacterial endophthalmitis. *Drug Delivery*, 22(7), 885–893. <https://doi.org/10.3109/10717544.2013.858195>
- Sivagami, M., & Asharani, I. V. (2023). Catalytic reduction of nitroarenes by *Cucumis maderaspatanus* L. leaves extract mediated silver nanoparticles. *Journal of the Taiwan Institute of Chemical Engineers*, 149, 104981. <https://doi.org/10.1016/J.JTICE.2023.104981>
- Sklyar, A. M., Kalinkevich, O. V., Holubnycha, V. N., Kalinkevich, A. N., Chivanov, V. D., Trofimenko, Y. V., Sofronov, D., Starikov, V., & Danilchenko, S. N. (2023). Easily obtained iodine and silver-iodine doped chitosan for medical and other applications. *Carbohydrate Polymer Technologies and Applications*, 5, 100318. <https://doi.org/10.1016/J.CARPTA.2023.100318>
- Slettengren, M., Mohanty, S., Kamolvit, W., van der Linden, J., & Brauner, A. (2020). Making medical devices safer: impact of plastic and silicone oil on microbial biofilm formation. *Journal of Hospital Infection*, 106(1), 155–162. <https://doi.org/10.1016/J.JHIN.2020.07.011>
- Song, X., Liu, P., Liu, X., Wang, Y., Wei, H., Zhang, J., Yu, L., Yan, X., & He, Z. (2021). Dealing with MDR bacteria and biofilm in the post-antibiotic era: Application of antimicrobial peptides-based nano-formulation. *Materials Science and Engineering: C*, 128, 112318. <https://doi.org/10.1016/J.MSEC.2021.112318>
- Stirk, W. A., & van Staden, J. (2022). Bioprospecting for bioactive compounds in microalgae: Antimicrobial compounds. *Biotechnology Advances*, 59, 107977. <https://doi.org/10.1016/J.BIOTECHADV.2022.107977>
- Su, Z., Sun, D., Zhang, L., He, M., Jiang, Y., Millar, B., Douglas, P., Mariotti, D., Maguire, P., & Sun, D. (2021). Chitosan/Silver Nanoparticle/Graphene Oxide Nanocomposites with Multi-Drug Release, Antimicrobial, and Photothermal Conversion Functions. *Materials (Basel, Switzerland)*, 14(9). <https://doi.org/10.3390/MA14092351>
- Sultan, I., Rahman, S., Jan, A. T., Siddiqui, M. T., Mondal, A. H., & Haq, Q. M. R. (2018). Antibiotics, resistome and resistance mechanisms: A bacterial perspective. *Frontiers in Microbiology*, 9(SEP), 377549. <https://doi.org/10.3389/FMICB.2018.02066/BIBTEX>
- Sun, Y., Mayers, B., & Xia, Y. (2003). Transformation of silver nanospheres into nanobelts and triangular nanoplates through a thermal process. *Nano Letters*, 3(5), 675–679. <https://doi.org/10.1021/nl034140t>

- Tai, C. Y., Wang, Y.-H., & Liu, H.-S. (2008). A green process for preparing silver nanoparticles using spinning disk reactor. *AIChE Journal*, 54(2), 445–452. <https://doi.org/10.1002/aic.11396>
- Tak, Y. K., Pal, S., Naoghare, P. K., Rangasamy, S., & Song, J. M. (2015). Shape-dependent skin penetration of silver nanoparticles: does it really matter? *Scientific Reports*, 5(1), 1–11. <https://doi.org/10.1038/srep16908>
- Tang, S., & Zheng, J. (2018). Antibacterial activity of silver nanoparticles: structural effects. *Advanced Healthcare Materials*, 7(13). <https://doi.org/10.1002/adhm.201701503>
- Tao, Y., Qian, L. H., & Xie, J. (2011). Effect of chitosan on membrane permeability and cell morphology of *Pseudomonas aeruginosa* and *Staphylococcus aureus*. *Carbohydrate Polymers*, 86(2), 969–974. <https://doi.org/10.1016/J.CARBPOL.2011.05.054>
- Teixeira-Santos, R., Lima, M., Gomes, L. C., & Mergulhão, F. J. (2021). Antimicrobial coatings based on chitosan to prevent implant-associated infections: A systematic review. *IScience*, 24(12), 103480. <https://doi.org/10.1016/J.ISCI.2021.103480>
- Tesini, B. L., & Dumyati, G. (2023). Health Care-Associated Infections in Older Adults: Epidemiology and Prevention. *Infectious Disease Clinics of North America*, 37(1), 65–86. <https://doi.org/10.1016/J.IDC.2022.11.004>
- Thomas, R., Soumya, K. R., Mathew, J., & Radhakrishnan, E. K. (2015). Inhibitory effect of silver nanoparticle fabricated urinary catheter on colonization efficiency of Coagulase Negative Staphylococci. *Journal of Photochemistry and Photobiology B: Biology*, 149, 68–77. <https://doi.org/10.1016/J.JPHOTOBIO.2015.04.034>
- Thomas, S., Gonsalves, R. A., Jose, J., Zyoud, S. H., Prasad, A. R., & Garvasis, J. (2024). Plant-based synthesis, characterization approaches, applications and toxicity of silver nanoparticles: A comprehensive review. *Journal of Biotechnology*, 394, 135–149. <https://doi.org/10.1016/J.JBIOTEC.2024.08.009>
- Tipper, D. J. (1985). Mode of action of β -lactam antibiotics. *Pharmacology & Therapeutics*, 27(1), 1–35. [https://doi.org/10.1016/0163-7258\(85\)90062-2](https://doi.org/10.1016/0163-7258(85)90062-2)
- Torres, C. J., Rupp, M. E., & Cawcutt, K. A. (2024). Intravascular Catheter-Related Bloodstream Infections: Contemporary Issues Related to a Persistent Problem. *Infectious Disease Clinics of North America*. <https://doi.org/10.1016/J.IDC.2024.07.002>
- Tran, H. V., Tran, L. D., Ba, C. T., Vu, H. D., Nguyen, T. N., Pham, D. G., & Nguyen, P. X. (2010). Synthesis, characterization, antibacterial and antiproliferative activities of monodisperse chitosan-based silver nanoparticles. *Colloids and Surfaces A:*

- Physicochemical and Engineering Aspects*, 360(1–3), 32–40.
<https://doi.org/10.1016/J.COLSURFA.2010.02.007>
- Turkevich, J., Stevenson, P. C., & Hillier, J. (1951). A study of the nucleation and growth processes in the synthesis of colloidal gold. *Discussions of the Faraday Society*, 11(0), 55–75. <https://doi.org/10.1039/DF9511100055>
- Tyagi, A., Agarwal, S., Leekha, A., & Verma, A. K. (2014). Effect of mass and aspect heterogeneity of chitosan nanoparticles on bactericidal activity. *International Journal of Advanced Research*, 2(8), 357–367.
- Ul Haq, I., & Krukiewicz, K. (2023). Antimicrobial approaches for medical implants coating to prevent implants associated infections: Insights to develop durable antimicrobial implants. *Applied Surface Science Advances*, 18, 100532.
<https://doi.org/10.1016/J.APSADV.2023.100532>
- van Duin, D., & Paterson, D. L. (2016). Multidrug-Resistant Bacteria in the Community: Trends and Lessons Learned. *Infectious Disease Clinics*, 30(2), 377–390.
<https://doi.org/10.1016/J.IDC.2016.02.004>
- Vanlalveni, C., Ralte, V., Zohmingliana, H., Das, S., Anal, J. M. H., Lallianrawna, S., & Rokhum, S. L. (2024). A review of microbes mediated biosynthesis of silver nanoparticles and their enhanced antimicrobial activities. *Heliyon*, 10(11), e32333.
<https://doi.org/10.1016/J.HELİYON.2024.E32333>
- Varma, R., & Vasudevan, S. (2020). Extraction, characterization, and antimicrobial activity of chitosan from horse mussel modiolus modiolus. *ACS Omega*, 5(32), 20224–20230.
https://doi.org/10.1021/ACSOMEGA.0C01903/ASSET/IMAGES/MEDIUM/AO0C01903_M002.GIF
- Vaz, J. M., Taketa, T. B., Hernandez-Montelongo, J., Chevallier, P., Cotta, M. A., Mantovani, D., & Beppu, M. M. (2018). Antibacterial properties of chitosan-based coatings are affected by spacer-length and molecular weight. *Applied Surface Science*, 445, 478–487.
<https://doi.org/10.1016/J.APSUSC.2018.03.110>
- Velkov, T., Thompson, P. E., Nation, R. L., & Li, J. (2010). Structure-activity relationships of polymyxin antibiotics. *Journal of Medicinal Chemistry*, 53(5), 1898–1916.
https://doi.org/10.1021/JM900999H/SUPPL_FILE/JM900999H_SI_001.PDF
- Venkatesham, M., Ayodhya, D., Madhusudhan, A., Veera Babu, N., & Veerabhadram, G. (2014). A novel green one-step synthesis of silver nanoparticles using chitosan: catalytic activity and antimicrobial studies. *Applied Nanoscience (Switzerland)*, 4(1), 113–119.
<https://doi.org/10.1007/S13204-012-0180-Y/FIGURES/8>

- Ventola, C. L. (2015). The Antibiotic Resistance Crisis: Part 1: Causes and Threats. *Pharmacy and Therapeutics*, 40(4), 277. <https://doi.org/Article>
- Vigneshwaran, N., Nachane, R. P., Balasubramanya, R. H., & Varadarajan, P. V. (2006). A novel one-pot “green” synthesis of stable silver nanoparticles using soluble starch. *Carbohydrate Research*, 341(12), 2012–2018. <https://doi.org/10.1016/j.carres.2006.04.042>
- Vorobyova, V., Vasyliiev, G., Uschapovskiy, D., Lyudmyla, K., & Skiba, M. (2022). Green synthesis, characterization of silver nanoparticles for biomedical application and environmental remediation. *Journal of Microbiological Methods*, 193, 106384. <https://doi.org/10.1016/J.MIMET.2021.106384>
- Vu, N. N., Venne, C., Ladhari, S., Saidi, A., Moskovchenko, L., Lai, T. T., Xiao, Y., Barnabe, S., Barbeau, B., & Nguyen-Tri, P. (2022). Rapid Assessment of Biological Activity of Ag-Based Antiviral Coatings for the Treatment of Textile Fabrics Used in Protective Equipment Against Coronavirus. *ACS Applied Bio Materials*, 5(7), 3405–3417. https://doi.org/10.1021/ACSABM.2C00360/ASSET/IMAGES/LARGE/MT2C00360_0008.JPEG
- Wright, G. D. (2011). Molecular mechanisms of antibiotic resistance. *Chemical Communications*, 47(14), 4055–4061. <https://doi.org/10.1039/C0CC05111J>
- Wu, S. (2011). Preparation of water soluble chitosan by hydrolysis with commercial α -amylase containing chitosanase activity. *Food Chemistry*, 128(3), 769–772. <https://doi.org/10.1016/j.foodchem.2011.03.111>
- Xing, K., Chen, X. G., Liu, C. S., Cha, D. S., & Park, H. J. (2009). Oleoyl-chitosan nanoparticles inhibits Escherichia coli and Staphylococcus aureus by damaging the cell membrane and putative binding to extracellular or intracellular targets. *International Journal of Food Microbiology*, 132(2–3), 127–133. <https://doi.org/10.1016/J.IJFOODMICRO.2009.04.013>
- Xing, K., Zhu, X., Peng, X., & Qin, S. (2015). Chitosan antimicrobial and eliciting properties for pest control in agriculture: a review. *Agronomy for Sustainable Development*, 35(2), 569–588. <https://doi.org/10.1007/S13593-014-0252-3/TABLES/3>
- Xing, Y., Lu, L., Li, J., Xu, J., & Zhang, F. (2024). Rosin-based self-healing functionalized composites with two-dimensional polyamide for antimicrobial and anticorrosion coatings. *International Journal of Biological Macromolecules*, 273, 133152. <https://doi.org/10.1016/J.IJBIOMAC.2024.133152>

- Xu, G., Xu, N., Ren, T., Chen, C., Li, J., Ding, L., Chen, Y., Chen, G., Li, Z., & Yu, Y. (2022). Multifunctional chitosan/silver/tannic acid cryogels for hemostasis and wound healing. *International Journal of Biological Macromolecules*, 208, 760–771. <https://doi.org/10.1016/J.IJBIOMAC.2022.03.174>
- Xu, L., Wang, Y. Y., Huang, J., Chen, C. Y., Wang, Z. X., & Xie, H. (2020). Silver nanoparticles: Synthesis, medical applications and biosafety. *Theranostics*, 10(20), 8996. <https://doi.org/10.7150/THNO.45413>
- Yang, X., Jia, M., Li, Z., Ma, Z., Lv, J., Jia, D., He, D., Zeng, R., Luo, G., & Yu, Y. (2022). In-situ synthesis silver nanoparticles in chitosan/Bletilla striata polysaccharide composited microneedles for infected and susceptible wound healing. *International Journal of Biological Macromolecules*, 215, 550–559. <https://doi.org/10.1016/J.IJBIOMAC.2022.06.131>
- Yin, I. X., Zhang, J., Zhao, I. S., Mei, M. L., Li, Q., & Chu, C. H. (2020). The Antibacterial Mechanism of Silver Nanoparticles and Its Application in Dentistry. *International Journal of Nanomedicine*, 15, 2555. <https://doi.org/10.2147/IJN.S246764>
- Yousefzadeh, Y., Izadkhah, V., Sobhanardakani, S., Lorestani, B., & Alavinia, S. (2024). UiO-66-NH₂/guanidine-functionalized chitosan: A new bio-based reusable bifunctional adsorbent for removal of methylene blue from aqueous media. *International Journal of Biological Macromolecules*, 254, 127391. <https://doi.org/10.1016/J.IJBIOMAC.2023.127391>
- Yuan, G., Lv, H., Tang, W., Zhang, X., & Sun, H. (2016). Effect of chitosan coating combined with pomegranate peel extract on the quality of Pacific white shrimp during iced storage. *Food Control*, 59, 818–823. <https://doi.org/10.1016/J.FOODCONT.2015.07.011>
- Yue, W., Yao, P., & Wei, Y. (2009). Influence of ultraviolet-irradiated oxygen on depolymerization of chitosan. *Polymer Degradation and Stability*, 94(5), 851–858. <https://doi.org/10.1016/j.polymdegradstab.2009.01.023>
- Zargar, V., Asghari, M., & Dashti, A. (2015). A Review on Chitin and Chitosan Polymers: Structure, Chemistry, Solubility, Derivatives, and Applications. *ChemBioEng Reviews*, 2(3), 204–226. <https://doi.org/10.1002/CBEN.201400025>
- Zhang, F., Ramachandran, G., Mothana, R. A., Noman, O. M., Alobaid, W. A., Rajivgandhi, G., & Manoharan, N. (2020). Anti-bacterial activity of chitosan loaded plant essential oil against multi drug resistant K. pneumoniae. *Saudi Journal of Biological Sciences*, 27(12), 3449–3455. <https://doi.org/10.1016/J.SJBS.2020.09.025>

- Zhang, G., Li, X., Xu, X., Tang, K., Vu, V. H., Gao, P., Chen, H., Xiong, Y. L., & Sun, Q. (2019). Antimicrobial activities of irradiation-degraded chitosan fragments. *Food Bioscience*, 29, 94–101. <https://doi.org/10.1016/j.fbio.2019.03.011>
- Zhang, T., Wang, L., Chen, Q., & Chen, C. (2014). Cytotoxic Potential of Silver Nanoparticles. *Yonsei Medical Journal*, 55(2), 283. <https://doi.org/10.3349/YMJ.2014.55.2.283>
- Zhangabay, Z., & Berillo, D. (2023). Antimicrobial and antioxidant activity of AgNPs stabilized with Calendula officinalis flower extract. *Results in Surfaces and Interfaces*, 11, 100109. <https://doi.org/10.1016/J.RSURFI.2023.100109>
- Zhao, Z. yuan, Li, P. jun, Xie, R. sheng, Cao, X. ye, Su, D. lin, & Shan, Y. (2022). Biosynthesis of silver nanoparticle composites based on hesperidin and pectin and their synergistic antibacterial mechanism. *International Journal of Biological Macromolecules*, 214, 220–229. <https://doi.org/10.1016/J.IJBIOMAC.2022.06.048>
- Zheng, J., He, A., Li, J., Xu, J., & Han, C. C. (2006). Studies on the controlled morphology and wettability of polystyrene surfaces by electrospinning or electrospraying. *Polymer*, 47(20), 7095–7102. <https://doi.org/10.1016/J.POLYMER.2006.08.019>
- Zienkiewicz-Strzałka, M., Deryło-Marczewska, A., Skorik, Y. A., Petrova, V. A., Choma, A., & Komaniecka, I. (2020). Silver Nanoparticles on Chitosan/Silica Nanofibers: Characterization and Antibacterial Activity. *International Journal of Molecular Sciences*, 21(1). <https://doi.org/10.3390/IJMS21010166>
- Zoe, L. H., David, S. R., & Rajabalaya, R. (2023). Chitosan nanoparticle toxicity: A comprehensive literature review of in vivo and in vitro assessments for medical applications. *Toxicology Reports*, 11, 83–106. <https://doi.org/10.1016/J.TOXREP.2023.06.012>